National Library of Canada
Acquisitions and Bibliographic Services Branch
395 Wellington Street
Ottawa, Ontario
K1A 0N4

Bibliothèque nationale du Canada
Direction des acquisitions et des services bibliographiques
395, rue Wellington
Ottawa (Ontario)
K1A 0N4

Your file Votre référence

Our file Notre référence

NOTICE

The quality of this microform is heavily dependent upon the quality of the original thesis submitted for microfilming. Every effort has been made to ensure the highest quality of reproduction possible.

If pages are missing, contact the university which granted the degree.

Some pages may have indistinct print especially if the original pages were typed with a poor typewriter ribbon or if the university sent us an inferior photocopy.

AVIS

La qualité de cette microforme dépend grandement de la qualité de la thèse soumise au microfilmage. Nous avons tout fait pour assurer une qualité supérieure de reproduction.

S'il manque des pages, veuillez communiquer avec l'université qui a conféré le grade.

La qualité d'impression de certaines pages peut laisser à désirer, surtout si les pages originales ont été dactylographiées à l'aide d'un ruban usé ou si l'université nous a fait parvenir une photocopie de qualité inférieure.

Canada

ISBN 0-612-00598-4

UNIVERSITÉ D'OTTAWA
UNIVERSITY OF OTTAWA

This thesis is dedicated to my parents

谨以此论文献给我的父母

Acknowledgements

First of all, I would like to express my most sincere gratitude to my research supervisor, Dr. C. P. Wilde, who provided me with continuous guidance, help and support throughout the course of this work. Dr. Wilde is especially thanked for spending valuable hours on reading the rough draft of my thesis and giving very good advice and correction concerning many points in this thesis.

The present work can seldom be completed without the assistance of a variety of people. I take this opportunity to thank glass-blowers, Mr. E. Kristoff and Mr. J. Hopkins for fabricating the glass cells utilized in this work, electrician Mr. F. Allard for building the electronic circuits, and machinist Mr. D. Hopkins for some mechanic help.

I also wish to thank all my colleagues in this laboratory, T. Ding, V. Hitimana and D. Pisharodi, for many enjoyable moments we shared.

I wish to acknowledge with thanks the financial support furnished by the University of Ottawa and the Government of Ontario through an assistantship or scholarship, and a Student Award by the Canadian Section of Electrochemical Society in 1993.

Lastly a very special thanks goes to my parents, my wife and my little daughter for their love and understanding all the time.

Contents

List of Figures

limit. At this point, the actual experimental data (recorded at constant offset) fell within a range of only 6ng for curves 1 to 4. Curve 5 was recorded 30 minutes later and differed by 20 ng. Electrode area was 4.62 cm^2.

Figure 66. Cyclic voltammogram and mass response for the oxidation of 0.5 mM formic acid in 0.1 M $HClO_4$. Results for the background electrolyte alone are also shown (dotted line). E_1 = 1.15V, t_1 =120s, E_2 = -0.25V and t_{ads} = 60s. The scan rate was 5 mV/s and the electrode area was 3.82 cm^2. Mass responses are shown exactly as recorded. 222

Figure 67. Details as for Figure 66 except that E_2 was -0.10V and 0.10V for curves 1 and 2 respectively. Electrode area was 4.88 cm^2. The vertical arrow labelled "2" indicates the starting point for the mass for curve 2. 224

Figure 68. Cyclic voltammogram and mass response (upper mass trace) for the oxidation of 9 mM formic acid in 0.1 M $HClO_4$. Results were recorded after a potential profile like that of Figure 66. The second cycle was recorded directly after the first with no pause. The electrode area was 4.88 cm^2 and the scan rate was 5 mV/s. The background mass response only is shown for comparison purposes and is displaced downwards for purposes of clarity. The vertical dotted line is drawn to illustrate the slight shift in the point where irreversible surface oxidation begins when formic acid is present. Point C indicates where the two anodic going mass responses coincide and point D illustrates the mass plateau that follows the step. 226

List of Tables

ABSTRACT

This thesis is concerned with the application of the Electrochemical Quartz Crystal Microbalance (EQCM) technique, which measures mass changes at electrode surfaces with exceptional sensitivity (submonolayer amounts), to the study of adsorption processes in **electrocatalysis.** Systems examined included electro-oxidations of small organic molecules (methanol, formic acid and glucose) at platinum, underpotential deposition (UPD) of metals, and the effect of UPD metal layers on such oxidations.

In the first section of this thesis, the underpotential deposition of lead and bismuth has been investigated at Pt electrodes in perchloric acid. It is shown that the mass changes obtained with the EQCM provide additional, unique information about the UPD process which cannot be obtained from the voltammogram because of the partial overlap of the currents associated with removal and development of UPD deposits with those resulting from the oxidation and reduction of the electrode surface respectively. Large mass changes are seen as the UPD deposits grow and are stripped. In addition, mass responses reveal the adsorption of cationic UPD metal species at potentials positive of the UPD region (i.e. a region where the electrode surface is oxidized). The extent of adsorption of Bi ions was found to be much larger than that of Pb ions. This is presumably due to the adsorption of hydrolysed Bi^{III} species rather than Bi^{3+}, as the adsorption is strongly dependent on the pH of the electrolyte. For both metals (Pb and Bi), the UPD deposits are formed through a combination of discharge of adsorbed species and reduction of metal ions from the electrolyte.

The oxidation of glucose in both acidic and alkaline media as well as the effect of UPD Pb on this oxidation in acid has also been investigated. In acid, the presence of

adsorbates derived from glucose was observed in the hydrogen UPD potential region through the removal of features associated with the presence of adsorbed anions in the background electrolyte. A decrease in mass is seen in this potential region as the electrode becomes covered with poisoning species. In the double-layer region of potential, a mass increase accompanies the oxidative removal of poisoning species from the electrode surface, and is a result of the replacement of adsorbed residues by both anions and fresh reactant. Mass responses also indicate that glucose, or species derived from it, can adsorb on an oxidized Pt electrode surface. In alkaline solution, the influence of glucose on the mass response is less than in acid solution. The mass was found to show an increase in the double-layer region of potential that is similar to that observed in acid solution. At a higher concentration of glucose (0.1M) the mass responses reveal that the onset of oxidation of the electrode surface was shifted positively by several hundred millivolts compared to that in background electrolyte.

In the presence of UPD Pb at Pt in acid, a multiple peak structure in the double layer region of potential was observed in the voltammogram at low glucose concentrations and low UPD coverages because the poison formation cannot be suppressed sufficiently. But it is changed to the more familiar single peak as UPD coverage increases. On the other hand, the presence of glucose is seen, from mass measurements, to have a large effect on changes in UPD Pb coverage in acid media. Some blockage of Pb UPD by glucose, or species derived from it, was revealed by the mass responses recorded during cyclic voltammetry. Deliberate formation of poisons in glucose-containing electrolyte prior to addition of Pb^{2+} ions results in a substantial suppression of UPD coverage especially between -0.1 and 0.1V (SCE). The adsorption of Pb^{2+} cations on an oxidized Pt surface was also found to be suppressed by species derived from glucose.

Finally, the investigation was extended to the oxidation of some simple organic molecules namely methanol and formic acid at Pt in acidic media. It is found that accumulation of strongly adsorbed species at the electrode surface during the oxidation of both organic molecules gives rise to a mass decrease, relative to that of the background electrolyte. The oxidative removal of these adsorbates causes a stepped mass increase. Mass responses also reveal that increasing amounts of methanol or formic acid in the electrolyte cause a shifting of the oxidative removal of strongly adsorbed species to more positive potentials, and a significant suppression of the irreversible oxidation of the electrode surface.

For oxidations of these organic molecules studied in the present work, several common features were revealed as follows:

1. The adsorption of organic molecules at the electrode surface is shown to cause small mass changes (relative to those observed in the background electrolyte alone). This can be attributed to the fact that most organic fragments (for example CO and CHO) have a small molecular weight and, in addition, the adsorption involves displacement of adsorbed water and specifically adsorbed anions (typically ClO_4^-);

2. A mass increase is observed to accompany the oxidative removal of strongly adsorbed species as a result of the transition between a surface that is largely covered with organic adsorbates and one that is largely free from such adsorption;

3. Higher concentrations of organic molecules result in a significant positive shift in the point where irreversible oxidation of the electrode surface begins. This suppression of the initial oxide formation of the surface, where OH is expected to be present, may result from some blockage of surface sites by organic adsorbates, as well as from the rapid consumption of OH in the reaction with the organic molecules or their intermediates.

Publications and Conference Presentations

Some papers which describe the present work have been published:

1. "Chemisorption and oxidation of methanol at polycrystalline Pt in acid solutions", C. P. Wilde and M. Zhang, ***Electrochim. Acta***, 39, 347(1994)
2. "The influence of lead UPD on the oxidation of glucose at platinum electrodes: An Electrochemical Quartz Crystal Microbalance study", C. P. Wilde and M. Zhang, ***Electrochim. Acta***, 38, 2725(1993)
3. " An Electrochemical Quartz Crystal Microbalance study of surface processes at Pt electrodes modified with Bi", C. P. Wilde and M. Zhang, ***Langmuir***, 10, 1600(1994)
4. "Profiles of adsorption during the oxidation of small organic molecules: oxidation of formic acid at polycrystalline Pt in acid solutions", C. P. Wilde and M. Zhang, ***J. Chem. Soc., Faraday Transactions***, 90, 1233(1994)
5. "Oxidation of glucose at electrodeposited platinum electrodes in alkaline solution", C. P. Wilde and M. Zhang, ***J. Chem. Soc., Faraday Transactions***, 89, 385(1993)
6. "Oxidation of glucose at electrodeposited platinum electrodes", C. P. Wilde and M. Zhang, ***J. Electroanal. Chem.***, 340, 241(1992)
7. "In situ probing of the adsorption of Pb^{2+} on oxidised platinum electrodes using an Electrochemical Quartz Crystal Microbalance", C. P. Wilde and M. Zhang, ***J. Electroanal. Chem.***, 338, 359(1992)
8. "Adsorption and underpotential deposition of lead at electrodeposited platinum electrodes", C. P. Wilde and M. Zhang, ***J. Electroanal. Chem.***, 327, 307(1992)

The work described in this thesis was also presented at various conferences:

1. "Adsorption and underpotential deposition of bismuth at platinum electrodes", M. Zhang and C. P. Wilde, Paper 621 presented at the 76th Canadian Chemical Conference, Sherbrooke, Quebec, May 30-June 3, 1993
2. "EQCM studies of ion and neutral molecule adsorption at noble metal electrodes", C. P. Wilde, T. Ding and M. Zhang, Paper 156 presented at the 203rd ACS National Meeting, San Francisco, April 5-10, 1992
3. "Microbalance studies of the role of adsorption in electrocatalysis", C. P. Wilde, M. Zhang and T. Ding, Paper 658 presented at the 75th Canadian Chemical Conference, Edmonton, Alberta, May 31-June 4, 1992
4. "An Electrochemical Quartz Crystal Microbalance study of glucose oxidation at platinum", M. Zhang and C. P. Wilde, Paper 73 presented at the 74th Canadian Chemical Conference, Hamilton, Ontario, June 2-6, 1991
5. "The UPD of Pb at Pt and its influence of the oxidation of glucose", M. Zhang and C. P. Wilde, Paper 731 presented at the 179th Electrochemical Society Meeting, Washington D.C., May 5-10, 1991

Chapter 1

Electrocatalytic Oxidations of Small Organic Molecules

This thesis describes an investigation of electrocatalytic oxidations of several organic molecules (glucose, methanol and formic acid) using the electrochemical quartz crystal microbalance (EQCM) technique. Therefore this chapter presents a description of some general aspects on the electrocatalytic oxidations, such as the effect of the electrocatalytic properties of electrodes, the role of the adsorption of organic molecules in the oxidation process, recent development in the experimental techniques used for the studies of these electrocatalytic oxidations, the effect of metal underpotential deposition (UPD) and some fundamentals of the UPD phenomenon. The principles of the EQCM technique will be presented in Chapter 2.

1.1 INTRODUCTION

Electrocatalysis is defined as the acceleration of an electrode reaction by a substance (generally the electrode) which is not consumed in the overall reaction[1], and electrocatalytic oxidations of small organic molecules have long been a subject of interest because of the possible utilization of species such as methanol and formic acid in fuel cells. Fuel cells have the potential to convert, directly, the chemical energy of fuels into electrical energy with a high energy efficiency (i.e. without the limitation of Carnot's theorem). However, the development of such fuels for commercial applications has been hindered by the electrochemical aspect of the fuel reactions: the electrodes show very poor kinetics for the

oxidations of organic fuels[2-4] principally because of the formation of strongly adsorbing poisons. Thus the overwhelming problem to be overcome remains primarily electrocatalytic and, for this reason, a substantial effort has been devoted to studies of electrocatalysis for the oxidations of small organic molecules and to the development of fuel cells. Electrochemical research on this subject has been covered in several reviews[5-14].

1.1.1 *Electrocatalytic properties of electrodes*

In the area of electrocatalysis, the kinetics of oxidations of small organic molecules have been found to be strongly dependent on the chemical nature and the electronic and geometric structures of the electrode material employed. Thus the electrocatalytic activity of a metal electrode towards a certain reaction differs from metal to metal (e.g. from sp metals to transition metals). Platinum is, in principle, the only sufficiently active catalyst for fuel reactions in acid medium while gold displays a higher catalytic activity towards those fuel reactions in alkaline medium.

However, the catalytic activity of a given metal electrode can easily be varied by several means such as the use of different faces of single crystals, alloying of different metals and modification of the electrode surface by underpotential deposition (UPD) of foreign metals. These aspects will be discussed in more detail later in this Chapter. However, before dealing with those topics, the following section explains the role of adsorption in electrocatalytic processes.

1.1.2 *The role of adsorption in electrocatalysis*

The adsorption of organic molecules on noble metal electrodes plays a vital role in

the overall mechanism of oxidation for small organic molecules. The adsorbed species (which may be reactants, intermediates or products) may determine the reaction pathway (reactive intermediates), the reaction selectivity and the electrocatalytic activity (poisoning intermediates). It is well established that, for simple organic molecules such as methanol, formic acid and glucose, their oxidations on noble metal electrodes proceed via a "dual-pathway" mechanism[11]:

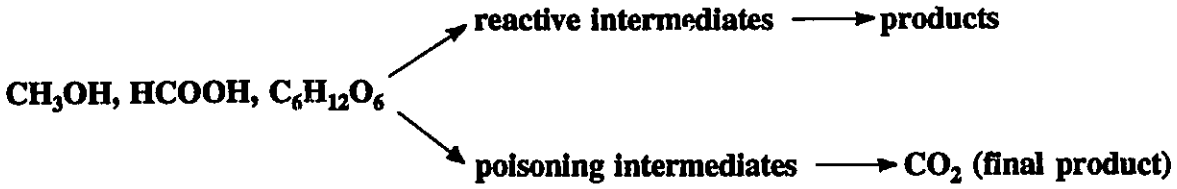

In general, for an electrocatalytic reaction with an oxygenated organic molecule, $C_\alpha H_\beta O_\gamma$, in aqueous solution, a source of oxygen is required to completely oxidize the organic molecule to CO_2, and the overall reaction is complex because several electrons are transferred.

$$C_\alpha H_\beta O_\gamma + (2\alpha - \gamma)\, H_2O \longrightarrow \alpha CO_2 + (4\alpha + \beta - 2\gamma)\, H^+ + (4\alpha + \beta - 2\gamma)\, e \quad (1.1)$$

Thus the reactions proceed through multiple elementary steps and pathways with each step involving no more than one or two electrons. Different adsorbed species can be expected to form due to the interaction of the catalytic surface with electroreactive species. Some of the adsorbed species will be weakly bonded to the surface and will act as reactive intermediates while some will be strongly, perhaps irreversibly, bound and will act as poisoning

intermediates. Strong adsorption leads to the blockage of active sites on the electrode surface and inhibits further electrooxidation. Even the best electrocatalyst, Pt, shows a low activity, since the oxidation currents observed at Pt are much smaller than their diffusion limited values.

It is evident that for a detailed kinetic study on electrocatalytic reactions, the identification of adsorbed species present at the catalytic surface is of paramount importance. This is best achieved by using powerful surface analytical techniques. Spectroscopic methods in particular have shown their ability to give information on the exact nature and structure of the adsorbed species at electrode surfaces. A survey of methods for the study and identification of adsorbates is given below.

1.2 EXPERIMENTAL TECHNIQUES FOR THE IDENTIFICATION OF ADSORBATES AT ELECTRODE SURFACES

1.2.1 *Programmed potential voltammetry*

Most of the methods to be described in this chapter are spectroscopic, but programmed potential voltammetry is one *electrochemical* method that has been used to identify adsorbed species at electrode surfaces. It has been applied by Lamy et.al. to the study of adsorption and oxidation of methanol on poly- and mono-crystalline Pt electrodes[15-17]. In this technique, the organic molecule is adsorbed at a fixed potential (E_{ads}) for various adsorption times (t_{ads}) after pretreatment of the electrode surface. The adsorbed species are then oxidized, using a computer-controlled potential program, at a very high sweep rate (50V/s) to minimize further re-adsorption of the organic molecule in the solution. The calculation takes advantage of the

fact that Pt electrodes adsorb a monolayer of H at certain potentials and that when present on the electrode surface, organic adsorbates will suppress this adsorption. Thus measurements of the charges required to oxidize the adsorbed species (Q_{org}) and to suppress adsorbed hydrogen (Q_H° and Q_H) allow the number of electrons per surface site (N_{eps}) to be calculated. N_{eps} is defined as

$$N_{eps} = Q_{org} / (Q_H^\circ - Q_H) \qquad (1.2)$$

where Q_H° is the charge associated with a full monolayer of adsorbed hydrogen in the background electrolyte alone while Q_H is the charge associated with adsorbed hydrogen in the presence of adsorbed organic species. The nature of the adsorbed species can then be found from the value of N_{eps} as shown in Table 1. The calculation of N_{eps} makes use of the assumption that the adsorption sites for hydrogen and for adsorbed species derived from organic fuels are the same. This assumption is usually feasible for small organic species and has been verified for adsorption of CO[17-19]. However, the disadvantage of this technique is that the determination of N_{eps} is rather difficult and the accuracy of experiments is strongly dependent on the experimental conditions.

Table 1 Possible structures of adsorbed species and corresponding values of N_{eps}

Adsorbed species	- C - H || O	- C ≡ O	≡ C- OH	- C- OH || O	= C = O	≡ C - O
N_{eps}	3	2	1	1	1	0.66

1.2.2 *In-situ IR reflectance spectroscopies*[14,20-24]

In-situ Infrared spectroscopic techniques, which were developed in the early 1980s, can provide the IR vibrational spectra of adsorbed species and thus allow the identification of adsorbed molecules with dipolar groups formed during electrocatalytic reactions of organic molecules. Consequently these methods led to the first unambiguous proof of the presence of adsorbed CO on electrodes during the electrooxidation of species such as methanol, formic acid and glucose[25-27]. Adsorbed CO can occupy one (linearly bound), two (bridge bonded) or three surface sites (multiply bound) and is thought to arise from the dissociative adsorption (dehydrogenation) of the organic species at the electrode. The strength of its adsorption means that it acts as a poison at electrode surfaces.

Although in-situ IR methods have not been employed in the present work, they have been widely used in other studies of electrocatalytic phenomena and so brief descriptions of the different variants of the method are presented here.

1.2.2.1 General experimental details

The successful application of IR methods to studies of the electrode/solution interface became possible because two limitations associated with the measurement of spectra have been overcome in recent years. First, the use of thin layer cells (as shown in Figure 1) avoids the considerable attenuation of the infrared beam by the solution, especially in aqueous solutions which adsorb strongly in broad mid-IR regions. Secondly, signal enhancement techniques have yielded the very high sensitivity needed to detect adsorption by submonolayer coverages of adsorbed species (concentrations as low as 10^{14} to 10^{15} species per cm^2). Two such techniques are discussed below.

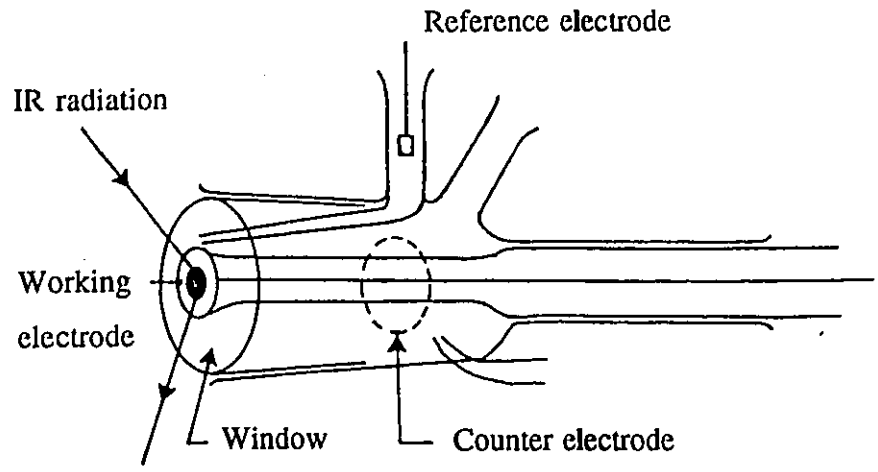

Figure 1. The IR spectroelectrochemical cell (*from Bewick*[22])

1.2.2.2 Signal enhancement techniques

Two types of modulation, light polarization modulation and potential modulation, can be employed to separate the adsorption contributions from solution and from surface bound IR active species. Polarization modulation employs a polarized IR beam and makes use of the so-called "surface selection rule" which holds for infrared reflectance, Raman and UV-visible spectroscopies[28]. In principle, the incident electromagnetic wave has two components of electric field: the p-polarized vector normal to the surface and the s-polarized vector parallel to the surface. Whatever the angle of incidence and the refractive indices of the absorbing media, the s-polarized component is reversed upon reflection (i.e. a phase angle change of 180° occurs) and consequently the resultant of the incident and reflected s-vectors is nearly zero at the surface. However, the phase angle change for the p-polarized component is dependent on the angle of incidence. At certain angles of incidence, the incident and

reflected p-polarized vectors can add at the surface and an enhanced resultant vector can be obtained. Therefore the s-polarized component is always inactive at the electrode surface while the p-polarized component results in an IR activity of adsorbed species with dipoles oscillating perpendicularly to the surface. By modulating the state of light polarization between the p-polarized and s-polarized components, the difference in the resulting intensities of the IR beam can be computed and the obtained spectrum shows absorption bands of species on the surface.

In the case of potential modulation, the electrode potential is changed alternately between two values, a reference (E_1) and a sample potential (E_2), to induce a change in the IR energy absorbed. The spectrum is first collected at the reference potential and then a second spectrum is procured at the sample potential. Thus the resulting change in the IR energy is measured as a relative change in the reflectivity of the electrode

$$\Delta R/R = (R_2 - R_1)/R_1 \tag{1.3}$$

where R_1 and R_2 are the reflectivities at the reference and sample potentials, respectively. For $\Delta R/R \ll 1$, which is usually the case for adsorbed films or thin films, the change in reflectivity $\Delta R/R$ is equivalent to the absorbance change (ΔA).

It is clear that the IR spectra obtained in the case of potential modulation are difference spectra. The change in potential can induce several changes, including migration of ions into or out of the thin layer, adsorption, desorption and faradaic reactions. As a result, the spectra can contain both negative absorption bands from species whose population increases at potential E_2 and positive bands from species present in excess at E_1 compared

to E_2. In addition, when there is a shift of the adsorbate vibrational frequency with potential due to the change of the band strengths of adsorbed species induced by the change of electric field at the interface, a single bipolar band will appear in the spectrum (see Figure 2).

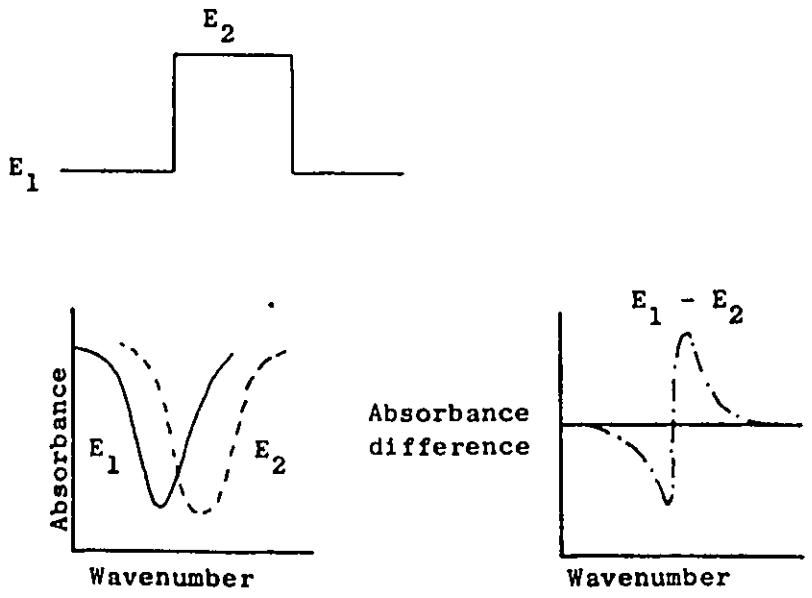

Figure 2. Origin of a bipolar difference band (*from Bewick*[22])

1.2.2.3 Specific IR techniques

Depending on whether a conventional grating spectrometer or a Fourier Transform device is used, several IR techniques have been developed. They are external reflectance infrared spectroscopies and are listed in Table 2.

EMIRS has been widely used to investigate the electrode/electrolyte interface. It consists of applying a square-wave potential modulation to the electrode with an amplitude of 50~500mV at a frequency of 8~25Hz. The absorption bands due to vibrations of adsorbed species can be extracted from the background noise by using phase sensitive detection. This

Table 2 Infrared Reflectance Techniques[14,22]

Type of spectrometer	Signal enhancement technique	Name of techniques	Refs.
Dispersive	electrode potential modulation	Electrochemically Modulated Infrared Reflectance Spectroscopy (EMIRS) (Bewick, 1980)	(24, 29)
	light polarization modulation	Infrared Reflectance Absorption Spectroscopy (IRRAS) (Overend, Russell, 1982)	(30)
	fixed wavelength and repetitive potential sweeps	Linear Potential Sweep Infrared Reflectance Spectroscopy (LPSIRS) (Kunimatsu, 1982)	(31)
Fourier Transform	Difference between sequenced series of interferograms	Subtractively Normalized Infrared Fourier Transform Infrared Reflectance Spectroscopy (SNIFTIRS) (Pons, 1981)	(24, 32)
	light polarization modulation	Potential Difference Alteration IR and Single Potential Alteration IR (PDIRS, SPAIRS) (Weaver, 1986)	(33, 34)
		Polarization Modulated Fourier Transform IR Reflectance Spectroscopy (PMFTIRRAS) (Kunimatsu, Golden, 1984)	(35)

signal, ΔR, is then stored, averaged if necessary, and divided by the electrode reflectivity R in order to obtain the normalized spectrum of the dimensionless differential reflectance ($\Delta R/R$) vs wavenumbers. The main advantage of this technique is that a very high sensitivity can be achieved due to the immense signal to noise discrimination of the phase sensitive detector (absorbance changes as low as 10^{-6} can be detected). On the other hand, there are two major inconveniences associated with this technique, that is, many electrochemical processes may occur in the potential range of the modulation (see above), giving rise to complex spectra, and the accessible wavelength range is narrow as it is limited by the performance of the grating spectrometers designed for EMIRS[24,29].

Using the same equipment for EMIRS, LPSIRS can be performed. This technique, introduced first by Kunimatsu[31], allows the absorbance at a fixed wavelength to be monitored during a potential scan. Repetitive measurements at different wavelengths result in 3-dimensional diagrams ($\Delta R/R$, wavenumber, E), which contain information on the dependence of the spectra on the potential (E).

Moving now to FTIR methods, SNIFTIRS takes advantage of the so-called multiplex character of FTIR and covers the whole spectral range from 5500 to 400cm^{-1} in a single measurement[24,32]. Thus very fast data collection is possible. The data are usually taken as an "interferogram" of intensity of radiation vs the moving mirror position in the interferometer. With the electrode potential being held at each potential for 10s to 100s, short series of interferograms are collected alternately at two given electrode potentials, E_1 and E_2, where the reflectivities are R_1 and R_2. After a subsequent subtraction of the coadded series and then ratioing to R, the spectra $\Delta R/R$ vs wavenumber is obtained using

$$\Delta R/R = (R_2 - R_1)/R_1 = (R_2/R_1 - 1) \qquad (1.4)$$

One advantage of SNIFTIRS over EMIRS is that the former makes more efficient use of the experimental time by measuring all wavelengths simultaneously. In addition, SNIFTIRS is easier to use than EMIRS due to computer facilities in FTIRS. However, it still suffers from difficulty in separating the contribution of adsorbates from the overall signal. Consumption of the species in the thin-layer of solution usually gives rise to strong "negative peaks" in the spectra and thus obscures the observation of the weaker absorption bands of adsorbed species. Such a difficulty is not present in EMIRS because the potential modulation in EMIRS eliminates the non-modulated contribution associated with solution species.

The other Fourier transform variants make use of a modulation between s- and p-polarization of incident light. Single Potential Alteration Infrared Spectroscopy (SPAIRS) involves sampling scans during a potential sweep and then integrating the signals over a certain "working potential range"[34,36]. Polarization Modulated Infrared Reflectance Absorption Spectroscopy (PMFTIRRAS) consists of the recording of the spectral difference between s- and p-polarized infrared light at a set working potential. Thus it is supposed to allow the rejection of solution bands[35]. This technique has a very low signal to noise ratio but also a major drawback: the resulting differential spectra may contain contributions from both the surface species and the solution species in the vicinity of the surface due to anisotropy (the intensity of the reflected infrared beam is different for s- and p-polarized light).

1.2.3 *"On-line" Mass Spectrometry*

Besides IR spectroscopy, mass spectrometry coupled to the electrochemical cell has demonstrated its capability of detecting both reactive intermediates and poisoning

intermediates during the oxidations of small organic molecules[13,37]. Differential Electrochemical Mass Spectrometry (DEMS) and Electrochemical Thermal Desorption Mass Spectrometry (ECTDMS) have successfully been applied to the analyses of adsorbates on electrodes. For instance, with such mass spectrometries, CHO or COH was identified as an adsorbed species in methanol oxidation[38,39].

Bruckenstein and Comeau[40] were the first to develop mass spectrometry coupled to an electrochemical cell for investigating electrochemical reactions. This technique was later improved by Wolter and Heitbaum using a turbo molecular pump system to reduce time response[37], and was subsequently called "Differential Electrochemical Mass Spectrometry" (DEMS). In DEMS, a porous PTFE membrane is fixed to a frit in the inlet of a mass spectrometer. The working electrode (usually a porous noble metal layer) is made by applying a thin layer of a fine metal suspension to the PTFE membrane. Volatile products generated at the electrode surface can traverse the membrane and enter the mass spectrometer to be analyzed. By correlating the mass spectral data with the electrochemical response, DEMS is capable of giving unique information on the nature of the reaction products such as the number of electrons transferred for the formation of products. The oxidations of methanol[38,39,41,42], formic acid[43-46] and glucose[47], etc. have been investigated.

Electrochemical Thermal Desorption Mass Spectrometry (ECTDMS), was recently developed by Wilhelm et al.[48,49] who combined mass spectrometry with thermal desorption. Here, the electrode is emersed from the electrolyte and transferred to the UHV chamber, where the desorption of species on the electrode surface is achieved by heating the electrode, and the desorbing fragments are immediately analyzed by the mass spectrometer. A suitable transfer system, which ensures the exclusion of traces of oxygen during the transfer of the

electrode to the UHV, is required for this ex-situ technique. ECTDMS has been applied to studies of methanol oxidation[48,49].

Finally, it should be noted that when comparing results of mass spectrometries with those of in-situ IR techniques, a disagreement between results obtained with the two techniques may arise because of the different experimental characteristics. It has been suggested that IR spectroscopies are more suitable for detecting strongly bound species such as CO while mass spectrometries can only observe species that may be desorbed from the electrode (i.e. species that are only weakly bonded to the surface such as CHO or COH).

1.2.4 *Other Methods*

Several other methods which are complementary to those described above have also been used in the study of electrocatalysis. The radiotracer method, which uses the labelling of adsorbing species, is very suitable for investigating the behavior of adsorbed species because it can provide direct access to the surface concentration of adsorbed species formed on electrodes. It has been used to study the adsorption and oxidation of glucose at Pt electrodes[50]. In most cases this technique has been employed to study adsorbed intermediates for the oxidation of methanol[39], formic acid[44,51] and glucose[46] etc., in conjunction with other methods such as on-line mass spectrometry and FTIR spectroscopy.

Some ex-situ UHV techniques, such as electron diffraction (LEED)[52,53] and electron spectroscopies (XPS, ESCA)[54,55], have also been used to study the poisoning intermediates formed on electrodes. Since these species are strongly chemisorbed on the electrode, it is possible to get valuable information on the structures of both the electrode and the adsorbate. However, no information on the structure or the composition of the solution side can be

expected from such ex-situ measurements.

"On-line" liquid chromatography has been applied to the analysis of the products accumulated in the solution during prolonged oxidations of small organic molecules, such as methanol[56,57], glucose[58] and gluconic acid[59], etc. It has proven to be a very useful analytical tool for the qualitative and quantitative analyses of mixtures of organic compounds even at concentrations as low as 10^{-6}M.

Finally, the Electrochemical Quartz Crystal Microbalance (EQCM), popularized by Bruckenstein and Shay[60] and Kaufman et al.[61], has been employed in this thesis to study, in-situ, the electrocatalytic oxidation of several small organic molecules (methanol, formic acid and glucose) at Pt electrodes[62-64]. By using an evaporated metal on a quartz wafer as a working electrode, mass changes occurring during oxidation reactions can be measured, with a remarkable sensitivity (a few nanograms), through their effect on the resonant frequency of the quartz crystal (a detailed description of this technique will be given in Chapter 2). The presence of adsorbed species at the electrode surface is found to produce a significant mass change and the mass measurements yield additional, unique information about the nature of adsorbed species formed during the electrocatalytic oxidations.

1.3 VARIATION OF ELECTRODE PROPERTIES

As mentioned earlier, the electrocatalytic activity of an electrode can be altered by several methods. The most widely employed methods include the use of single crystal electrodes, utilization of binary or ternary alloys and modification of the electrode surface by underpotential deposition (UPD) of foreign metals. Such methods will be outlined below.

1.3.1 *Single crystals as electrodes*

By using the low-index faces of single crystals, the geometric and electronic structure of an electrode material can be varied in a known manner, thus providing a unique opportunity to study the effect of the structure of the electrode surface on a variety of organic oxidation reactions. Many interesting features, which are not recognizable with the conventionally-used polycrystalline electrodes, have been revealed. For instance, it is found that each of the three low-index platinum single crystal faces, (100), (110) and (111), behaves differently in the electrooxidation of various organic molecules, such as formic acid[65-70], methanol[71,72] and glucose[73-75]. For the oxidation of simple small molecules (methanol and formic acid), the behavior of the polycrystalline surface can be treated as the weighted contribution of each low-index crystal face with the main contribution coming from the (110) face. Contrarily this is not true for larger molecules (glucose) due to the complexity and variety of the adsorbed species. In the latter case, the low-index single crystal faces are usually more active than the polycrystalline electrode[14].

The structure of the low-index faces can influence the adsorption of the organic molecules through their different local symmetries which may or may not favor the accommodation of a particular structure of the adsorbed species. Thus the low-index faces exhibit different degrees of resistance to poisoning. With small organic molecules, the (110) face becomes rapidly poisoned by the main adsorbed species, CO, as revealed by IR reflectance spectroscopy, and its activity decreases quickly. The (100) face has a moderate resistance to poison formation and the (111) face has the lowest susceptibility to poison formation[76,67]. However, for oxidation of large organic molecules (glucose), the low-index single crystal faces are not as sensitive to poisoning as polycrystalline electrodes and the

(111) is the most active face[73,74]. This is probably due to the presence of different structures of some adsorbed species other than CO (though a small amount of CO has been found). These adsorbed species may demand different geometric arrangements of surface sites for the adsorption.

1.3.2 *Alloys as electrodes*

Another means by which the catalytic activity of electrodes may be modified is alloying of the electrode material, either by simultaneous electrodeposition or by casting. The "alloying" method allows both the geometric and electronic properties of the metal catalyst to be changed. Enhancement of the electrocatalytic oxidation of small organic molecules is often observed with binary alloys such as Pd/Au, Pt/Pd and Pt/Rh at a certain alloy composition. Such "synergistic" effects have been found with the oxidation of formic acid at Pt/Au[77,78], Pt/Rh[79], Pt/Pd[80] and Pd/Au[81] alloy electrodes, and the oxidation of methanol at Pt/Pd[82] and Pt/Rh[83] alloy electrodes. The explanation for the enhancement of activity is similar to those for the catalytic enhancement observed at electrodes modified by sub- or monolayer coverages of foreign metal adatoms (UPD). Briefly, the action of alloys can be interpreted as: modification of the electronic properties of the electrode surface[84]; blocking of poison formation (i.e. "third body mechanism" as first proposed by Conway[77,85]; and promotion of adsorption of oxygen/hydroxyl ions which can participate in the main oxidation reaction[86]. These theories are described in more detail in the following section.

1.3.3 *Modification of the electrode surface by underpotential deposits*

Modification of the electrode surface by foreign metal adatoms can lead to a dramatic

improvement of the catalytic properties of the electrode material. Monolayer or submonolayer arrays of adatoms on the electrode surface can be formed by deposition of the foreign metal ions from the solution at potentials more positive than the Nernst potential for the foreign metal, i.e. by underpotential deposition (UPD) (see the next section for more details). This provides a simple and more convenient means for modification of the electrode properties with specific characteristics for a given process for several reasons. First, the coverage of the adatom layer is easily determined with a high accuracy, and it can be controlled simply by changing the underpotential or the bulk concentration of the metal ions in solution. With respect to the origin of the catalytic effects, there are three proposed explanations for such catalytic effects and each of them will be outlined below.

The first explanation is based on the so-called "third body" mechanism[85] in which the adatoms, distributed across the electrode surface, act as "third bodies" to diminish the probability of adsorbed species coming together to produce a poison. This concept has been used to explain the enhanced electrocatalytic oxidation of formic acid at Pt in the presence of adatoms such as Hg[45,55], Bi[87] and Pb[87,88], and to explain the catalytic effects of adatoms, Pb[88,89], Bi, Ag, As and Cu[89], on the oxidation of methanol at Pt electrode and of Pb, Tl, and Bi adatoms on glucose oxidation at Pt[90,91]. However, an alternative mechanism was proposed to explain catalytic effects of adatoms on the oxidation of formic acid[65,92,93], where the presence of adatoms was conceived to suppress hydrogen adsorption rather than the poison formation because the adsorbed hydrogen is believed to be needed for poison formation. This has been used to account for the catalytic effects of adatoms, Pb, Bi, Tl, Sn and Cu on the oxidation of formic acid at Pt[94-96]. The fact that the catalytic effect was different for each atom was explained in terms of the competitive adsorption of adatoms,

formic acid and its intermediates.

The second explanation for the effect of underpotential deposits is the "bifunctional catalysis" mechanism[97,98]. It is operative with adatoms such as Ge, Sn, Sb, As and Ru that are shown to adsorb oxygen or oxygen-containing species at potentials far more negative than that of Pt itself[99]. It has been suggested that the presence of the adsorbed oxygen-containing species (OH radicals) on the adatoms may assist in the removal (by oxidation) of the formed poisons such as CO and COH to re-generate free active Pt sites for the main oxidation as shown below, where x is the number of platinum sites occupied per CO species.

$$Pt_3COH + 3OH_{ad} \longrightarrow CO_2 + 3Pt + 2H_2O \qquad (1.5)$$

$$Pt_xCO + 2OH_{ad} \longrightarrow CO_2 + xPt + H_2O \qquad (1.6)$$

This concept can explain the catalytic effects of Sn[42,57,100], and Ru[57] on methanol oxidation, and of Pb, As, Sb and Bi on the oxidation of carbon monoxide[101]. Different degrees of enhancement in the catalytic activity have been attributed to different influences of adatoms on the rate of adsorption and on the total amount of OH radicals adsorbed[101].

The third role that adatoms may play is to alter the electronic properties of the electrode. The attached adatoms can cause a perturbation of the work function of the substrate electrode and thus a change in the point of zero charge of the substrate electrode as evidenced by Trasatti[102]. As a result, certain properties such as the activation of free electrode sites[103] and the adsorption properties of the electrode[104], etc. can be modified. The catalytic oxidation of formic acid at Pt in the presence of Pb adatoms[103], and inhibition of poison formation from formic acid by Bi or As adatoms[105] are considered to result from the

electronic effect.

Other proposed mechanisms include the "surface redox" mechanism in which the adatoms act as both an electron acceptor from organic molecules or their intermediates, and electron donator to the electrode. This is the case for the catalytic oxidation of methanol at Pt by Mo adatom[106]. The adsorbed Mo(IV) species is catalytically active and can oxidize methanol directly according to

$$CH_3OH + 6MoO_2 + 18H^+ \rightleftharpoons CO_2 + 6Mo^{3+} + H_2O \qquad (1.7)$$

the Mo^{3+} species formed is then oxidized electrochemically to MoO_2.

Despite the various mechanisms proposed to interpret catalytic effects of different adatoms on certain organic oxidation reactions, the exact mechanism by which an adatom may function is largely dependent on the nature of electrode and the organic molecules. The action of many adatoms can be explained by one of the above mechanisms.

1.4 FUNDAMENTALS OF UNDERPOTENTIAL DEPOSITION OF METALS

As noted above, the presence of UPD adatoms on the electrode surface is seen to yield enhanced currents for the oxidation of certain organic molecules. In order to clarify the effect of UPD adatoms upon these oxidation processes, a more fundamental understanding of the UPD phenomenon is necessary. Therefore some general information on the underpotential deposition of metals is presented in this section.

1.4.1 *The UPD phenomenon*

The underpotential deposition of up to a monolayer of metal on a second metal substrate is a well established phenomenon[107-110]. It refers to an electroreduction of a

metallic ion, M^{z+}, in the so-called underpotential range (ΔE_{UPD}), that is, in a potential region positive to the Nernst reversible equilibrium potential (E_R) of the depositing M^{z+}/M couple[111-114].

$$\Delta E_{UPD} = E_R^{ML} - E_R \tag{1.8}$$

where E_R^{ML} is the standard monolayer equilibrium potential. The value of ΔE_{UPD}, which is sometimes called the underpotential shift[115], may range from a few millivolts to over several hundred millivolts, depending on the strength of the interaction between the depositing metal and the substrate metal. In simpler terms we can describe the UPD phenomenon by referring to a specific system. For example, Pb^{2+} deposits on Pt at a potential more positive than the potential where it would deposit on a Pb electrode.

The UPD phenomenon was first reported by Hevesy in 1912[116], who observed a deviation from the reversible Nernst potential when radioactive metals were deposited onto a Cu substrate. Later Herzfeld[117] gave a formalistic explanation for this phenomenon by assuming that the activity of the depositing metal in the monolayer is less than unity and is a function of coverage (θ). This concept was further extended by Rogers and co-workers[118-120] in the late 1940s and 1950s to explain their results for the deposition of trace amounts of radioactive Ag and Cu on Pt, Au, Pd and Rh substrates. The same treatment was followed by Hassinsky[121,122] in his studies of underpotential deposition. Later, Nicholson investigated the deposition of Ag, Pb and Cu on Pt substrate[123] and Ni on Pt and Au substrates[124]. Mills and Willis were the first to investigate the electrolytic deposition of the first atomic layer of Pb, Tl, Sb and Ni on Au, and Pb on an Ag substrate[125].

The results obtained in these early studies subsequently stimulated the extensive investigations carried out in this field during the past 20 years. The kinetics, thermodynamics

and the structural properties of the UPD layer on poly- and single-crystalline metal substrates have been studied for a number of systems and the progress in the understanding of these subjects is well covered in several review articles[107,109,112,114,126].

1.4.2 *The Thermodynamics of UPD*

Underpotential deposition has usually been described thermodynamically in terms of an activity of less than unity for the deposited metal layer. When considering metal deposition where a metal phase is involved, the activity of the deposit is usually assumed to be constant and set to unity. However, for the charge transfer equilibrium of metal deposition in the underpotential range,

$$M^{z+} + ze \rightleftharpoons M_{ML} \tag{1.9}$$

the activity of the submonolayer should be less than unity and must vary with the surface coverage of the deposited layer. A linear relation between the deposit activity (α) and coverage (θ) is commonly assumed, that is, $\alpha_{ML} = f_{ML}\theta$ for $0 \leq \theta \leq 1$, and $\alpha_{ML} = f_{ML}$ for $\theta \geq 1$ with $f_{ML}=1$. The term, f_{ML}, is the activity coefficient of the deposited layer. Thus the standard monolayer equilibrium potential E_R^{ML} for eq. (1.9) takes the form:

$$E_R^{ML}(\theta) = E_o + (RT/zF)\ln(f_M^{z+}C_M^{z+}/f_{ML}\theta) > E_R \tag{1.10}$$

where f_M^{z+} is the activity coefficient of the metal ion in the electrolyte, and C_M^{z+} the metal ion concentration. This equation yields equilibrium potentials that are always more positive than the corresponding Nernst potential for the bulk phase.

To get a deeper understanding of the underpotential effect, the concept of chemical potential is often used to interpret the thermodynamics of UPD. The existence of the UPD phenomenon signifies a marked difference between the chemical potential of the UPD deposit

(μ_{ML}) and that of the corresponding bulk metal (μ_M). The chemical potentials of the bulk phase and UPD layer can be derived from the equilibrium conditions for the reactions[115]:

$$M^{z+} + ze_{metal} \rightleftharpoons M \tag{1.11}$$

and

$$M^{z+} + ze_{substrate} \rightleftharpoons M_{ML} \tag{1.12}$$

The respective equations for the electrochemical potentials, $\tilde{u} = \mu + ze\varphi$, are

$$\tilde{u}_M{}^{z+} + \tilde{u}_{e(metal)} = \mu_{metal} \tag{1.13}$$

and

$$\tilde{u}_M{}^{z+} + \tilde{u}_{e(substrate)} = \mu_{ML} \tag{1.14}$$

Under the conditions of same solution and the same composition, the values of $\tilde{u}_M{}^{z+}$ in eqs.(1.13) and (1.14) are equal. Thus subtracting eq.(1.13) from eq.(1.14) yields the difference between the chemical potentials of bulk deposit (μ_{metal}) and monolayer (μ_{ML}), that is, $\mu_{ML} - \mu_{metal} = \tilde{u}_{e(substrate)} - \tilde{u}_{e(metal)}$. It is simply the difference in electron energies at potentials necessary to establish the equilibrium conditions for eqs.(1.11) and (1.12):

$$\mu_{ML} - \mu_{metal} = ze[E_R{}^{ML}(\theta) - E_R] = ze\Delta E_{UPD} \tag{1.15}$$

This equation represents a direct measure of the binding energies between a metal adatom on the foreign substrate and this metal atom on a macroscopic sample of itself. The quantity, ΔE_{UPD}, can be determined experimentally from the corresponding I-E curve of the UPD process. Usually the potential difference between bulk and monolayer stripping peaks has

been often chosen as the most suitable value of ΔE_{UPD}[115]. If the monolayer isotherm exhibits multiple peaks such as that of Pb on Au shown in Figure 3, the potential difference between the more anodic peak and the stripping peak is chosen as ΔE_{UPD}.

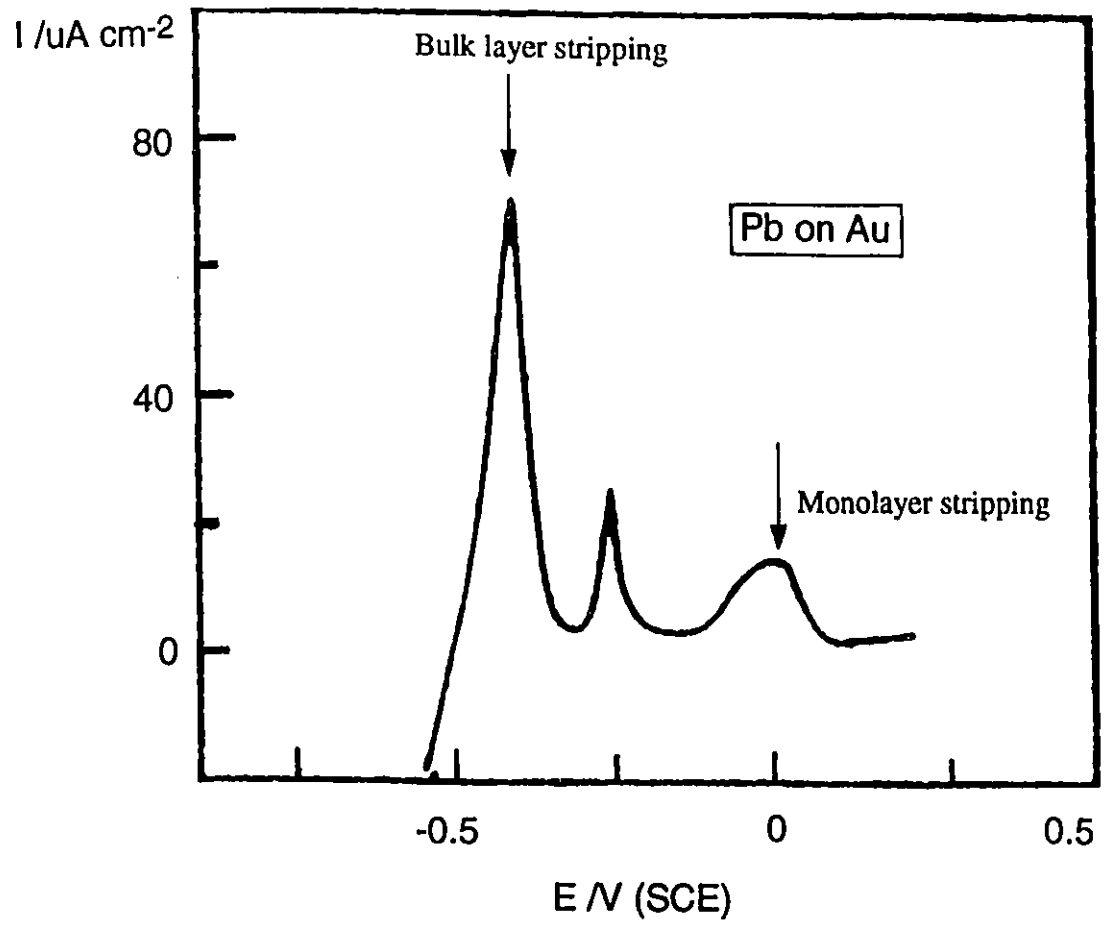

Figure 3. Anodic stripping curve for Pb deposits on Au in 1M $HClO_4$ (pH=3). Scan rate is 20mV/s. (*from Kolb et al.*[115])

1.4.3 *The physical model*

The commonly accepted model for the adatom-substrate bond in the UPD process is

one in which the binding energy of the substrate-deposited metal bond is correlated with the difference of work functions between the substrate and the bulk depositing metal. It is believed that the charge transferred from the adatom to substrate is proportional to the difference in Pauling's electronegativities (χ_M) of the substrate and the adsorbate metal and the difference in electronegativities can be taken as a measure of the polarity of the substrate-adatom bond[114]. It is found empirically that Pauling's electronegativity can be linearly related to the work function (ϕ) of the same bulk metal[127,128], that is,

$$\chi_M = 0.5\phi - \text{constant} \tag{1.16}$$

with a constant value 0.29 for sp-metals and 0.55 for transition metals. Thus the "excess" binding energy, $e\Delta E_{UPD}$, between the deposited metal atom and the substrate metal atom may be correlated to the difference in work function between the bulk substrate and bulk deposited metal by the following equation:

$$e\Delta E_{UPD} = 0.5\Delta\phi \tag{1.17}$$

This correlation has been found to be very satisfactory for about 30 different metal pairs with polycrystalline substrates (see Figure 4). The good linear relation seems to suggest that the covalent part of the adatom-substrate bond is almost the same as that of the bond between the adatom and its own metal surface. However, some departures from eq. (1.17) have been observed for single crystal substrates as reported by Lorenz and co-workers[129], Bewick and Thomas[130] and Schultze and Dickertmann[131]. This indicates that the adsorption energy of UPD is determined not only by the difference in electronegativities expressed as $\Delta\phi$, but also by the lateral interactions between deposited species which are governed by the crystallographic orientation of the substrate.

From the viewpoint of work function, a necessary condition for the UPD to occur

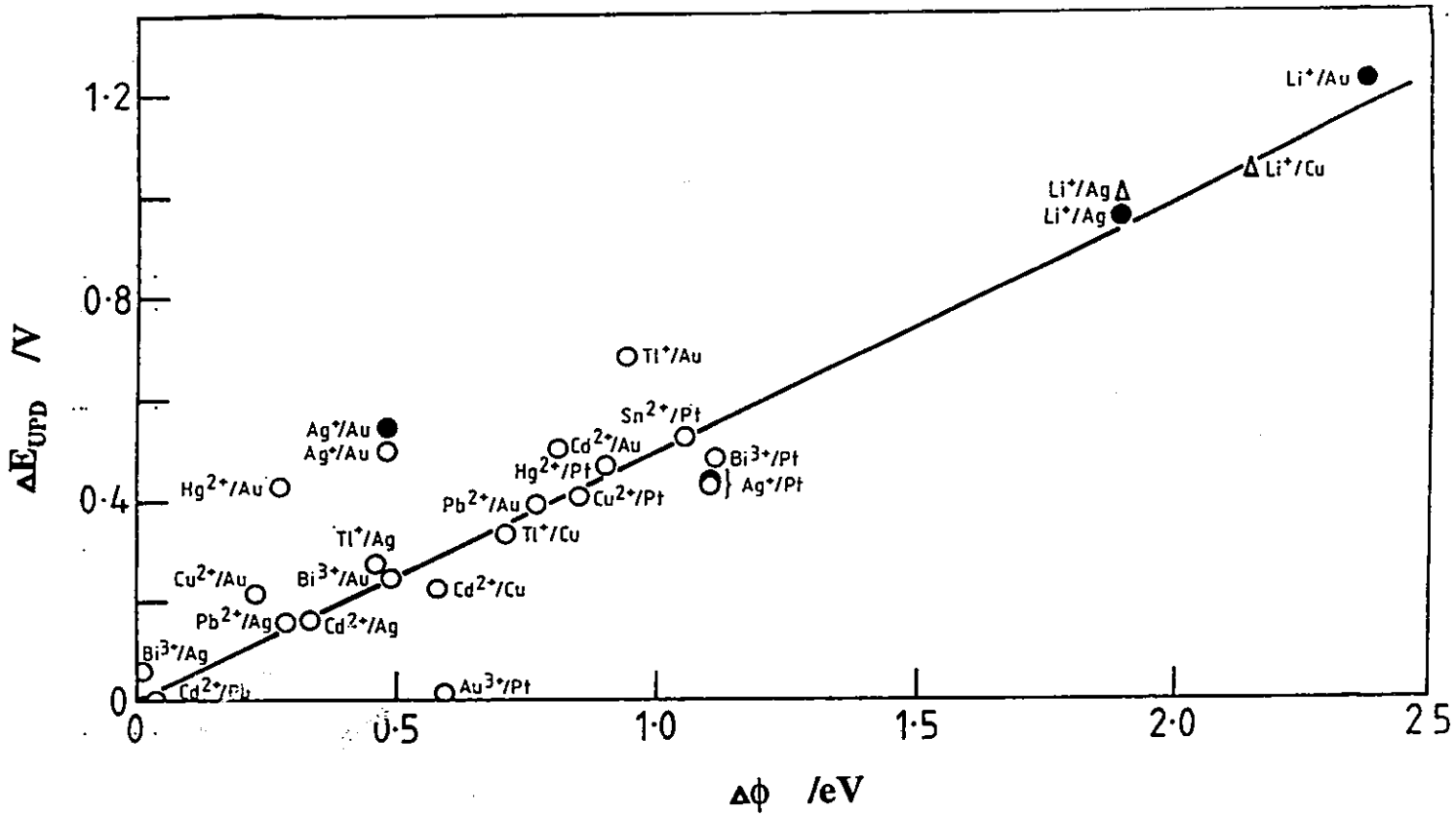

Figure 4. Underpotential shift ΔE_{UPD} between bulk and monolayer stripping peak as a function of $\Delta\phi$, the difference in work function of bulk substrate and bulk adsorbed adatom metal. (○) aqueous solution; (•) acetonitrile and (△) propylene carbonate. (*from Kolb et al.*[115])

seems to be that the work function of the substrate must be larger than that of the deposited metal. Thus the dipole of the adatom-substrate bond usually has a positive end at the adatom because of an electron transfer from the adatom to the substrate.

1.4.4 *The electrosorption valency*

As mentioned earlier, partial charge transfer may occur for some systems due to the difference in the electronegativities of the adsorbate metal and the substrate or, in other words, due to the difference in their Fermi energies. As a result the deposited metal will retain some charge and thus lead to a polar adlayer having a significant surface dipole potential difference[132]. This process can be generally represented by

$$M^{z+} + \gamma e\ (s) \rightleftharpoons M_{UPD}^{(z-\gamma)+}\ (s) \qquad (1.18)$$

where s is the substrate, M^{z+} and M are the dissolved and deposited UPD species and z is the valency of the UPD species in electrolyte. The parameter, γ, is thus referred to as the "electrosorption valency"[133-136]. In the case of excess supporting electrolyte, this parameter is defined thermodynamically by equation (1.19)

$$\gamma = -(1/F)(\partial q_s/\partial \Gamma)_E = (1/F)(\partial \mu_M{}^{z+}/\partial E)_{\Gamma ad} \qquad (1.19)$$

where $\mu_M{}^{z+}$ is the chemical potential of M^{z+} in the supporting electrolyte, E is the electrode potential, q_s is the substrate charge and Γ_{ad} is the surface concentration of the adsorbed metal.

The electrosorption valency, γ, dictates the potential dependence and charge flow during the UPD process in the same manner as z does. It depends on the nature of the deposited metal and substrate, on the electrolyte and on the coverage of adatoms and can be determined experimentally from independent q and Γ measurements using some techniques which enable the separation of the UPD mass flux from the charge flux such as thin-layer

cells, rotating ring-disk electrodes and electrochemical quartz crystal microbalance techniques.

1.4.5 *Effects of co-adsorbed anions*

It has been demonstrated that adsorbed anions can have a remarkable influence on the UPD behavior[112,115,137,138]. Two effects were generally observed for the halide anions: the first one is the decrease of the underpotentials, i.e. the shift of the monolayer cathodic peak to more negative potentials, presumably due to a reduction of the bond strength between the metal adatom and the substrate surface; the second one is an increase of the charge under the monolayer peak resulting from the current contribution from the concomitant halide ion desorption process[112]. As a consequence, a larger value of apparent electrosorption valency is often obtained from an experiment[139]. The effect of anion adsorption was found to increase with increasing specific adsorption in the following order[112,115,140]

$$ClO_4^- < F^- < SO_x^{2-} < Cl^- < Br^- < SCN^- < I^-$$

The halide effect on the UPD at Au substrate has been explained by Schmidt and Wuthrich[141] as a competitive adsorption. They found from their measurements of adsorption isotherms using the thin-layer cell technique that the coverage of the halide adsorption is more than 50% of the monolayer at positive potentials and significantly higher than the expected maximum coverages of 10 - 20% required for simple electrostatic ion adsorption. Therefore they concluded that halide is not adsorbed electrostatically as an ion but forms a compound with the substrate. It is the formation of such a "non-metallic film" that suppresses the metal monolayer formation.

The interesting co-adsorption phenomenon of anions has been observed often. Horanyi et al. reported that the co-adsorption of Cl^- on Pt substrate is favoured by the underpotential

deposition of Cd and Cu[137,142]. Later the same authors found a similar enhancement of HSO_4^- adsorption on Pt by the underpotential deposition of Cu[138]. Conversely, the adsorption of the deposited metal ion, Pb^{2+}, was found to be enhanced by the presence of Cl^- anions in the electrolyte[143].

Besides adsorption effects, the adsorbed anions are likely to induce some changes in the properties of the substrate surface (PZC, work function, its electronegativity, etc.), thus affecting the adatom-substrate bond strength. Such changes may also need to be taken into account in explaining the effects of halide ions on the UPD process.

1.4.6 *Studies with the Electrochemical Quartz Crystal Microbalance technique*

Many experimental techniques have been applied to the studies of UPD process. They include structure-sensitive spectroscopic techniques (X-ray spectroscopic and diffraction techniques[144-153] and Scanning Tunneling and Atomic Force Microscopies[154-157]), specular reflectance methods[112,158-170] and conventional electrochemical techniques such as rotating ring-disk electrode[171-174], thin-layer cell technique[141,175,176] and galvanostatic pulse technique[107,177]. Recently, the EQCM has shown its ability to measure submonolayer quantities of adsorbed species on an electrode surface during the UPD process. As this technique is the one employed throughout the present work, a brief survey of studies performed using this technique is given below. Some studies with other techniques mentioned above can be found in the literature quoted above.

The usefulness of the EQCM for studies of UPD processes derives from its ability to measure mass changes occurring at electrode surfaces. Thus it reveals, alongside the electric current response, the large mass responses arising from the UPD process. In this method, the

change of the resonant frequency of the EQCM is proportional to the added mass of the UPD layer on the electrode surface. The mass change induced by the UPD layer is often so large that the EQCM is relatively insensitive to effects from the solution side such as the change of anion adsorption and the double layer structure during the UPD. Thus the measured mass change represents the mass flux of the UPD process and characteristic quantities such as the coverage and the electrosorption valency for the UPD process can be found from the mass change. Further details of the technique will be presented in Chapter 2.

The first application of the EQCM to a UPD process was demonstrated by Bruckenstein and Swathirajan[178]. These authors measured ex situ the frequency of the EQCM in the dry state before and after the UPD of Pb and Ag on Au substrates. The obtained UPD coverage was in good agreement with that obtained from parallel rotating ring-disk electrode measurements. Later Melroy et al.[179] reported the first in-situ application of the EQCM to a study of the UPD process. They determined the mass change resulting from Pb UPD on Au in 0.1M $HClO_4$ and a value of 2.08±0.10 for the electrosorption valency at complete coverage was found by comparison of the mass gain with the total charge consumed in the UPD region. Deakin and Melroy examined, in more detail, the UPD of Pb, Bi, Cu and Cd on an Au substrate in 0.1M $HClO_4$[180]. The coverage of the UPD layer was determined from the frequency change of the EQCM as a function of potential and the electrosorption valencies were found for Pb (γ=2.0), Bi (γ=2.7), Cu (γ=1.4) and Cd (γ=1.6-2.0). Lakkaraju et al.[181] combined the EQCM with the optical second harmonic generation (SHG) method to investigate the UPD of Cu on Au substrate in 0.5M H_2SO_4. A value of 1.5 for the electrosorption valency was reported, which is comparable to the value obtained in perchlorate media[180]. Similarly the EQCM was employed by Tang and Furtak to study the

UPD of Pb, Cd and Tl on Ag substrate in 0.1M Na_2SO_4 at pH=5[182]. The measured charge and mass data showed a good agreement with the expected values for the UPD of Pb and Cd. A value of 2 for the electrosorption valency was found to be valid for the two UPD metals. An abnormally high charge was observed for Tl^+ and was attributed to charge reorganization in the double layer.

Aside from the above, EQCM experiments can also reveal different aspects of UPD processes such as the adsorption of cations prior to discharge to form the UPD layer[183-185] and ligand expulsion accompanying the UPD process[186-189]. In 0.1M $HClO_4$, adsorption of Pb^{2+} and Bi^{III} species at oxidised Pt substrate surfaces produced significant mass increases and the corresponding formation of UPD layer involves a combination of discharge of these adsorbed cations and the reduction of cations from the electrolyte[183-185]. Ligand expulsion phenomena were observed for the discharge of UPD Pb and Bi at an Ag substrate in 0.1M borate buffer solutions, and the discharge of UPD Pb at Ag in 0.1M NaOH[186-189]. In these systems, a mass increase was initially observed upon addition of Pb^{II} or Bi^{III} to the solutions at potentials positive of the UPD region, which was ascribed to the adsorption of anionic lead or bismuth complexes induced by the positive rational potential of the Ag substrate (the point of zero charge of Ag is very negative and thus the Ag electrode bears a large positive charge at the potentials used). A cathodic scan into the UPD region then resulted in the reduction of the adsorbed anionic species with a mass *decrease* due to the expulsion of ligands from the adsorbed anionic species. However, in more acidic environments where only cationic or neutral Pb^{II} species are present, no adsorption of Pb^{II} species was observed at potentials positive of the UPD region and so the anticipated mass increase was found to accompany the UPD process.

Chapter 2

Fundamentals of The Electrochemical Quartz Crystal Microbalance Technique

2.1 INTRODUCTION

The past few years have seen a rapid development of many novel techniques which enable the in situ detection and monitoring of interfacial phenomena on a microscopic level[190]. One such technique is based on quartz crystal microbalance (QCM) technology. The QCM consists of a thin quartz crystal wafer sandwiched between two metal electrodes that are used to establish an alternating electric field across the crystal, causing the oscillation of the crystal at its resonant frequency. (The top view of a typical QCM electrode is shown in Figure 5). Minute mass changes at the electrode surfaces are then probed through their effect on this resonant frequency. This has provided a powerful approach to examining chemical or electrochemical processes involving monolayer and submonolayer film deposition and dissolution, surface morphology changes and adsorption phenomena. Studies performed using the QCM include the detection of air pollutants (SO_2, H_2S, HCl and CO etc.)[191], the electrosorption of oxides and halides[192-194], electrocatalytic oxidations of organic molecules[62-64], dissolution and oxidation of metals[195-197], underpotential deposition of metals[178,180,182,183,185,198], electrodeposition of conductive polymers and molecular metals[199-203], formation of Langmuir-Blodgett films[204], enzymatic studies[205,206], immunoassay techniques[207,208], and characterization of bulk liquid phase properties such as density,

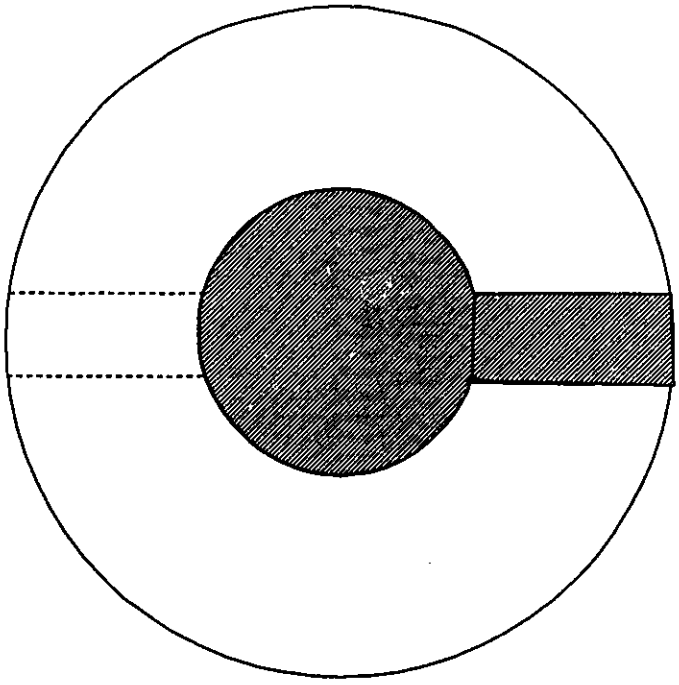

Figure 5. The QCM disk with deposited electrodes

viscosity and conductivity[209,210].

The electrochemical quartz crystal microbalance (EQCM) is an extension of the QCM which was initially used in the gas phase as a mass sensor[211,212]. The terms "EQCM" and "QCM" refer to electrochemical and non-electrochemical applications of QCM technology respectively. Until about 10 years ago it was thought that the QCM device would not function in the liquid phase because of possible oscillation cessation induced by damping effects of the contacting liquid which would have a higher viscosity than a contacting gas. However, successful operation in the liquid environment was demonstrated by Konash and Bastiaans in 1980[213] and Nomura in 1981[214]. Nomura and co-workers[215,216] then further

demonstrated the first in situ application of the QCM to electrochemical measurements in which the concentrations of Cu(II) and Ag(I) in an electrolyte were determined by electrodeposition. Such measurements were accordingly referred to as EQCM measurements.

When used for measuring mass changes at electrode surfaces in situ, one of the EQCM electrodes is used both to provide the alternating electric field which is necessary to drive the oscillation of the crystal and as a working electrode in the electrochemical cell. The other electrode is exposed to air and serves only to complete the oscillation circuit. This configuration allows the measurement of electrochemical parameters, such as potential, current and charge, at the working electrode and the simultaneous measurement of the oscillation frequency of the piezoelectric crystal, from which minute mass changes at the working electrode may be inferred.

In this chapter, a brief view of the physics of the QCM as a mass sensor will be presented and the influence of some factors such as solution viscosity and density on the frequency response of the EQCM will then be outlined. Further details on theoretical aspects of the QCM can be found in several excellent reviews[217-222].

2.2 PHYSICS OF THE QCM AS A MASS SENSOR

2.2.1 *PIEZOELECTRIC EFFECT*

The phenomenon of piezoelectricity was discovered in 1880 by Pierre and Jacques Curie in many substances including natural quartz[223]. They observed that when pressure was applied to some crystals in particular directions, an electric potential was produced between the deformed surfaces of the crystals with the potential being proportional to the applied

pressure. This behavior is referred to as the piezoelectric effect, which is derived from the Greek word "piezein" meaning to press. Only crystals without a center of symmetry possess this property. Shortly after the initial discovery by the Curies, the converse effect in which application of a voltage across these crystals resulted in a corresponding mechanical strain was also verified. This converse piezoelectric effect is the basis of the QCM.

A piezoelectric quartz crystal resonator is a precisely cut wafer taken from a natural or synthetic single crystal of quartz. Figure 6 shows the quartz crystal in its perfect natural form. The piezoelectric effect arises when pressure on a dielectric material deforms the crystal lattice and causes a separation of the centers of gravity of oppositely charged species, which, in turn, gives rise to a dipole moment in each molecule. Similarly the converse piezoelectric effect arises when an electric field applied across the crystal produces a shear

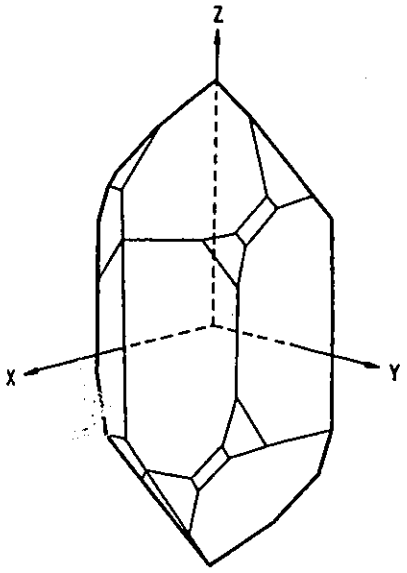

Figure 6. The perfect natural form of a quartz crystal and the assignment of axes (*from Lu and Czanderna*[191])

strain proportional to the applied potential. If an alternating potential is applied instead, vibrational motion occurs within the quartz crystal lattice. Such a process is depicted in Figure 7[221]. Stable oscillation can be attained only at the natural resonant frequency of the crystal and at that frequency the crystal presents a low impedance to the exciting voltage. This crystal is thus called a quartz resonator.

A piezoelectric quartz crystal resonator can vibrate at many modes of resonance, or standing wave patterns at its fundamental resonant frequencies. It can also vibrate at the overtones of each fundamental mode (i.e. odd harmonics). However, the useful mode of

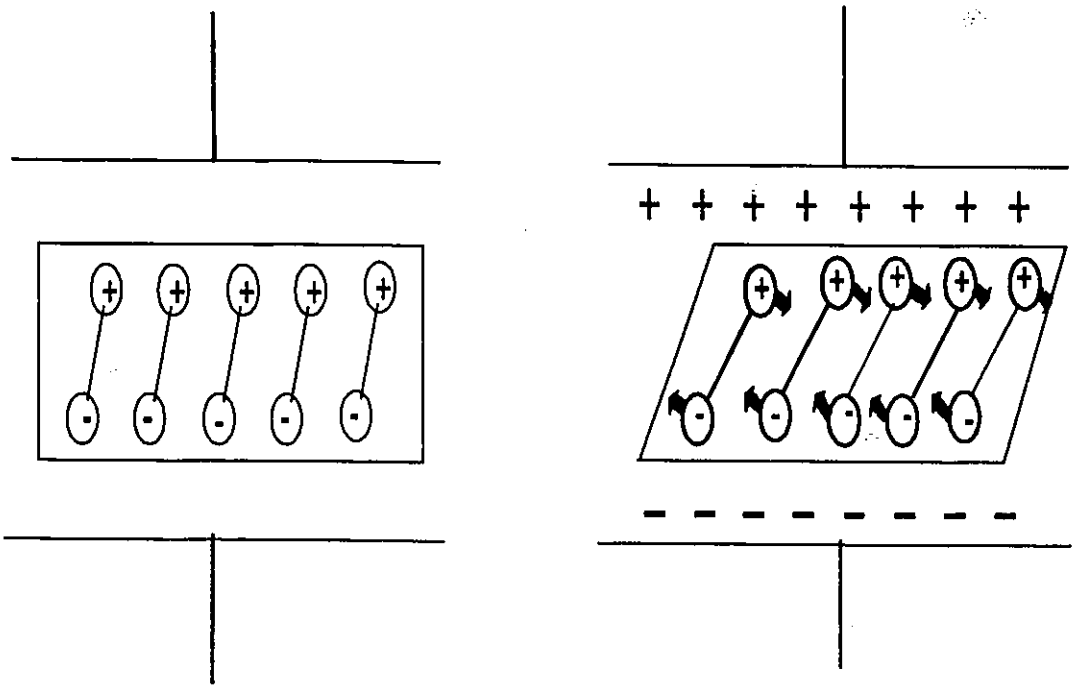

Figure 7. Schematic representation of the converse piezoelectric effect for shear motion. *The electric field induces reorientation of the dipoles of the acentric materials, resulting in a lattice strain and shear deformation of the material. Direction of shear is dependent on the applied potential while the extent of shear depends on the magnitude of the applied potential (from Buttry and Ward[221])*

vibration in the QCM is the high frequency thickness-shear mode which has been shown to be sensitive to the addition or removal of mass at the electrode surface. This kind of vibration is illustrated in Figure 8 for the fundamental mode, where it is evident that the two major surfaces of such a resonator are always antinodal with a node existing in the center of the wafer. This condition corresponds to the establishment of a standing acoustic wave within the bulk of the crystal with the resonant frequency being the frequency of maximum displacement of the crystal surface.

In order for a quartz crystal to oscillate in the thickness-shear mode, the crystal must be cut at specific angles of orientation relative to the principal optical axis. The temperature coefficient and stress coefficient of the resonator are influenced by the angle of cut. Changes in temperature or stress can result in a change in the frequency of the crystal. To minimize

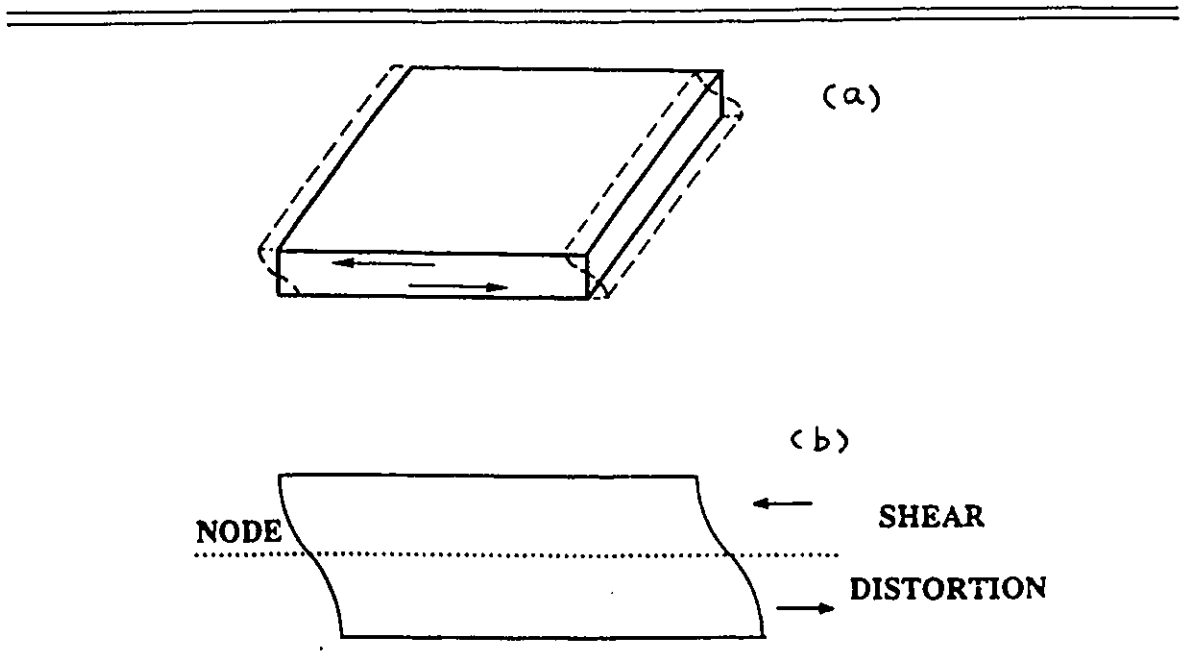

Figure 8. (a) The fundamental thickness-shear motion of vibrations (*from Lu and Czanderna*[191]); (b) Edge view showing shear deformation (*from Buttry*[218])

the effect of temperature, two angles of cut are shown to be ideal for use in QCM technology as they have zero temperature coefficients at room temperature: +35°15'(AT-cut) and -49°00'(BT-cut)(as shown in Figure 9).

2.2.2 *PRINCIPLES OF MASS SENSING*

As mentioned earlier, when a piezoelectric crystal resonator is used as a mass sensor, the mass change is inferred from the change of its resonant frequency. Thus the relationship between the mass and frequency must be known quantitatively. The frequency-to-mass formulae were first developed by Sauerbrey[224,225] based on the simple physical model shown in Figure 10. This treatment was developed for QCM operation in the gas phase. For an AT-cut crystal vibrating in the thickness shear mode, the shear oscillation brings about propagation of a shear wave through the bulk of the crystal, perpendicular to the surfaces of the crystal. The atomic displacements corresponding to this shear motion are thus parallel to the crystal surface. With resonance occurring at the maximum displacement of the crystal surface, the resonant frequency can be related to the thickness of the crystal through the

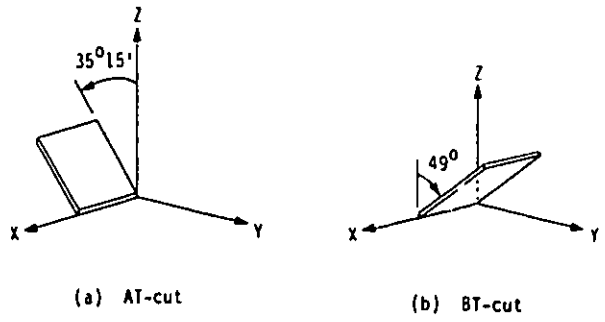

Figure 9. AT- and BT-cut quartz crystal plates (*from Lu and Czanderna*[191])

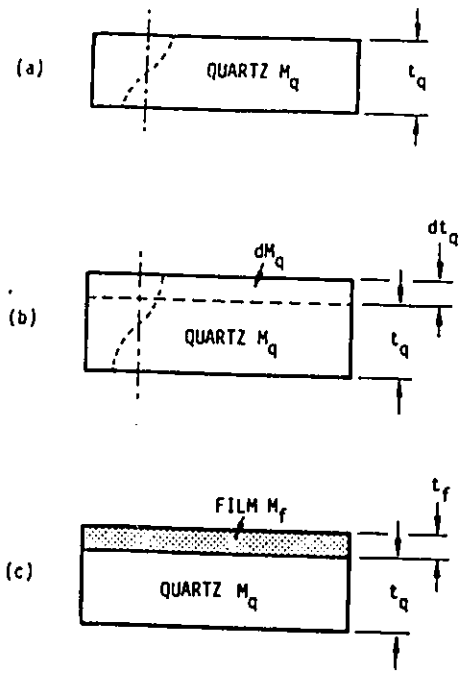

Figure 10. A simplified model of a quartz crystal microbalance. (a) at resonance, the wavelength is equal to half of the quartz plate thickness; (b) an increase in the quartz plate thickness results in a decrease in the resonant frequency (an increase in the wavelength); (c) the mass of a deposited film is treated as an equivalent amount of the quartz mass (*from Lu and Czanderna*[191])

following equation:

$$t_q = \lambda_q/2 \tag{2.1}$$

where t_q is the thickness of the plate and λ_q the wavelength of the shear-mode elastic wave in the thickness direction. In terms of the resonance frequency f_q and the velocity of propagation of the shear wave v_q, (2.1) can be written as

$$f_q\, t_q = v_q/2 \tag{2.2}$$

since

$$\lambda_q\, f_q = v_q \tag{2.3}$$

From (2.2) with appropriate algebraic manipulation, the frequency change (df_q) caused by an infinitesimal change in the crystal thickness, dt_q, is found to be expressed by

$$df_q/f_q = -dt_q/t_q \tag{2.4}$$

The negative sign indicates that an *increase* in the thickness of the quartz crystal plate causes a *decrease* in its resonance frequency.

A relationship exits between density and mass of the crystal which is

$$t_q = M_q/A\rho_q \tag{2.5}$$

where M_q = mass of the quartz plate, A = surface area of the quartz plate, ρ_q = density of the quartz plate ($2.648 gcm^{-3}$). Substituting a differential form of (2.5) into (2.4) yields

$$df_q/f_q = -dM_q/M_q \tag{2.6}$$

Sauerbrey made the assumption that the acoustic properties of the foreign layer are identical to those of quartz and consequently the small mass change due to the foreign layer is treated as tantamount to a mass change of the quartz crystal itself. (2.6) thus becomes

$$df_q/f_q = -dM/M_q \tag{2.7}$$

where dM is an infinitesimal amount of foreign mass uniformly distributed over the crystal surface. If one defines the areal densities m_f and m_q as the mass per unit area for the foreign layer and quartz crystal respectively, (2.7) can be written in the form of

$$df_q/f_q = -m_f/m_q \tag{2.8}$$

For materials with a spatially uniform density, (2.8) can be further arranged to give

$$\Delta f = -2\Delta m f_q^2/\rho_q v_q A \tag{2.9}$$

Since the shear wave velocity v_q is related to the shear modulus of quartz μ_q (2.947×10^{11} $gcm^{-1}s^{-2}$) through the equation:

$$v_q = (\mu_q/\rho_q)^{1/2} \tag{2.10}$$

a final equation, called Sauerbrey's equation, is obtained from (2.9) as given by

$$\Delta f = -2\Delta m f_0^2/A(\mu_q\rho_q)^{1/2} \tag{2.11}$$

where f_0, equivalent to f_q, is the fundamental resonant frequency of the crystal. Substituting values for the constants into (2.11) yields

$$\Delta f = -2.26 \times 10^{-6} f_0^2 \Delta m/A \qquad (2.12)$$

As seen from this Equation, the mass sensitivity is dependent on the square of resonant frequency (f_0). Higher frequency operation of the quartz crystal thus offers the advantage of greater mass sensitivity. However, since f_0 is inversely proportional to t_q, an increase of the fundamental frequency to achieve higher mass sensitivity is limited by the difficulty in handling the extremely thin crystals required. A practical limit is about 15MHz for the fundamental frequency of crystals which can be easily handled (a 15 MHz crystal has a thickness slightly greater than 100μm). It is possible to achieve higher frequency operation by using lower frequency crystals at odd harmonics, but the required circuitry is more complicated[178].

Although the Sauerbrey relationship was derived for QCM operation in gas phase, it is still applicable to the operation in liquids under appropriate conditions. However, another potential difficulty associated with the use of higher frequencies may arise from the viscous damping effect as the solution is more likely to cause the oscillation to cease, depending on the circuitry used. This problem will be described in considerable detail in the next section. As a compromise, suitable frequencies for the oscillations in EQCMs are typically from 1 to 10 Megahertz(MHz). A very high frequency (30MHz) operation was recently reported[226], but more complicated treatments are required for the preparation of the quartz crystal in order to further reduce the thickness of quartz wafer (for example, a chemically milled quartz resonator is etched only in the center to obtain a very thin quartz membrane with a thick outer ring). In the work involved in this thesis, a 10MHz quartz crystal wafer is employed. The mass sensitivity per unit area as calculated from (2.12) is 0.226 $Hzcm^2ng^{-1}$, i.e. 4.42

$ngHz^{-1}cm^{-2}$.

Sauerbrey's theory has been verified for the application of infinitesimally thin overlayers up to a mass load (ΔM) of 2% of the mass (M_q) of unloaded crystal. For higher mass loadings, a more complicated treatment is required and an impedance matching method has been used that compensates for the different acoustic properties of quartz and the foreign overlayers. The detailed description of such a treatment is beyond the scope of this thesis, but it can be found elsewhere[227].

2.2.3 *EQUIVALENT CIRCUIT ANALYSES*

In order to understand the oscillating properties of the QCM it is instructive to consider the quartz resonator in terms of the concept of electrical equivalents. It has been demonstrated that, in addition to the conventional measurements of the resonant frequency of the QCM, the estimation of its electric equivalent circuit parameters can provide unique information on the chemical and physical processes occurring on the QCM.

In general, a quartz resonator in vacuum or air can be represented by an equivalent circuit as shown in Figure 11[191,228]. The motional capacitance C indicates the mechanical elasticity of the vibrating body; the motional inductance L is a measure of the vibrating mass; and the equivalent resistance R corresponds to the total loss of mechanical energy due to internal friction and energy dissipation to the surrounding medium and supporting structures. The shunt capacitance C_0 is an actual lump capacitance due to the electrodes on the quartz resonator and stray capacitance to the supporting structures.

The resonant resistance (R) is often determined by admittance (Y) measurements of the quartz crystal instead of impedance (Z) measurements because the expression for the

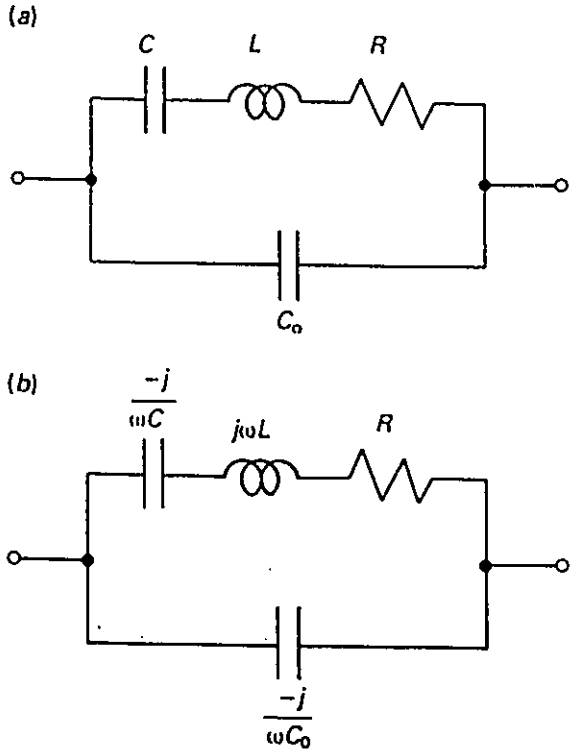

Figure 11. Equivalent circuit of the QCM with (a) parameters and (b) impedances of the circuit elements (*from Thompson et al.*[222])

admittance is much simpler. By definition, Y is the reciprocal of Z. Therefore, if Z is complex, so is Y:

$$Y = G + jB$$

where the conductance, G, is the real part of Y and the susceptance, B, is the imaginary part of Y. For the circuit shown in Figure 11, the admittance is expressed as

$$Y = 1/(R + j\varpi L + 1/j\varpi C) + j\varpi C_0 \qquad (2.13)$$

The quantity, ϖ, is the angular frequency (in rad s^{-1}) and is defined by $\varpi = 2\pi f$ where f is the frequency in Hz. (2.13) can be further separated to form

$$G = R/[R^2 + (\varpi L - 1/\varpi C)^2] \tag{2.14}$$

$$B = -(\varpi L - 1/\varpi C)/[R^2 + (\varpi L - 1/\varpi C)^2] + \varpi C_0 \tag{2.15}$$

From $Z = 1/Y$, the real (R) and imaginary (X) parts of Z in terms of G and B can be written as

$$R = G/(G^2 + B^2) \tag{2.16}$$

$$X = -B/(G^2 + B^2) \tag{2.17}$$

The magnitude of impedance, $|Z|$, and the phase of impedance, θ_Z, are defined as

$$|Z| = \sqrt{R^2 + X^2} \tag{2.18}$$

$$\theta_Z = \tan^{-1} (X/R) \tag{2.19}$$

For an oscillation to occur, two conditions need to be satisfied: i) the phase shift around the oscillating circuit loop should be zero; and ii) the loop gain should be unity. The second condition can be fulfilled by using a proper feedback loop. The first condition is only satisfied when $X/R = 0$ (see (2.19)). Since $-B/G = X/R$ as derived from (2.16) and (2.17), we can see that (2.15) divided by (2.14), with B/G set equal to zero, is a quadratic equation in ϖ and its solution gives the two frequencies of zero phase: i) f_s, called the series resonant frequency, the low frequency of zero phase; and ii) f_p, called the parallel resonant frequency. These two characteristic frequencies are represented in Figure 12 which shows cartesian plots of Z, θ, G and B vs frequency. For typical quartz resonators, $1/LC_0 >> (R/L)^2$ and $C/C_0 << 1$, the two frequencies are generally expressed in the following forms:

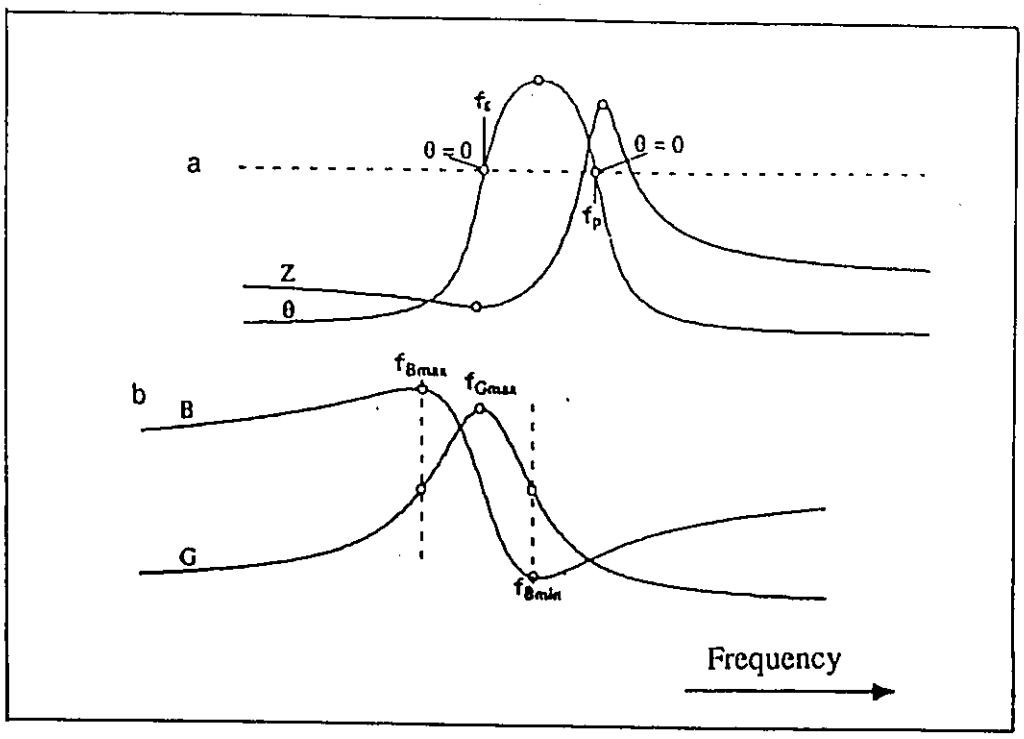

Figure 12. (a) Typical Z - θ plots in the resonance region of an AT-cut quartz resonator; (b) Typical B - G plots in the resonance region of an AT-cut quartz resonator (*from Buttry and Ward*[221])

$$f_s = (2\pi)^{-1} (LC)^{-1/2} \tag{2.20}$$

$$f_p = (2\pi)^{-1} [(LC)^{-1} + (LC_0)^{-1}]^{1/2} \tag{2.21}$$

The oscillation of a quartz crystal resonator can therefore be driven at either the series resonant frequency, f_s, or the parallel resonant frequency, f_p. The most often used oscillators operate at the series resonant frequency because f_s is unaffected by the shunt capacitance C_0 as seen from (2.20).

2.3 VISCOUS COUPLING EFFECTS IN LIQUID

The theoretical treatment presented above has dealt with QCM operation in the gas phase. However for the EQCM the quartz resonator is put in contact with a viscous liquid (an electrolyte) or viscoelastic film, and thus viscous coupling is operative. The consequence is that energy flows out of the quartz into the liquid in the form of acoustic waves as represented in Figure 13. This energy loss is dependent on the properties of the resonator-liquid interface. With the concept of electrical equivalents, the viscous effects induced by addition of foreign layers or immersion in liquid can be easily characterized. An added mass on the surface of the resonator can be considered to affect the inertial mass component which has the electrical equivalent L. Accordingly, the resonance frequency shift resulting from a mass change can be interpreted as a change in the inductance. Additionally, the added liquid

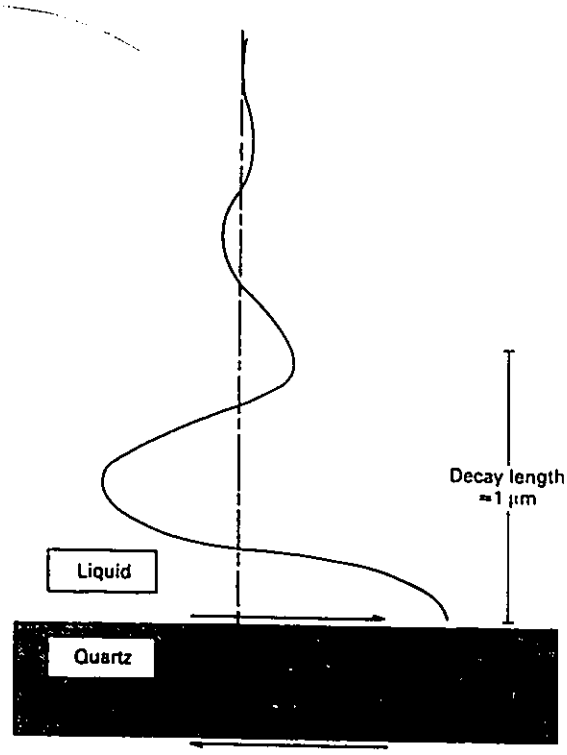

Figure 13. Propagation of the transverse shear wave from the QCM into a liquid (*from Thompson et al.*[222])

corresponds to the introduction of a mechanical impedance which can be expressed as an electrical impedance in Figure 14. Since the liquid is assumed to be viscous, the reactance does not contain a capacitative component that would arise from elastic behavior.

In other popular treatments which were developed by several groups[229-232], similar components in Figure 14 are combined into a single component (i.e. all inductances are combined into one) to give an equivalent circuit in liquid which is identical to that in vacuum or air (Figure 11), but the values of the parameters L, R and C are considered to be altered by the viscous coupling of the QCM to the liquid. It has been proposed that the three parameters L, R and C contain an inductance component for the mass of the solution (coupled by viscous transport), a resistive component due to the strong damping by the solution and a capacitance component due to any elasticity of the solution, respectively. These three parameters can be conveniently determined from the conductance spectrum of the QCM as depicted in Figure 12. In that figure, the frequency showing the maximum value of G ($f_{G_{max}}$)

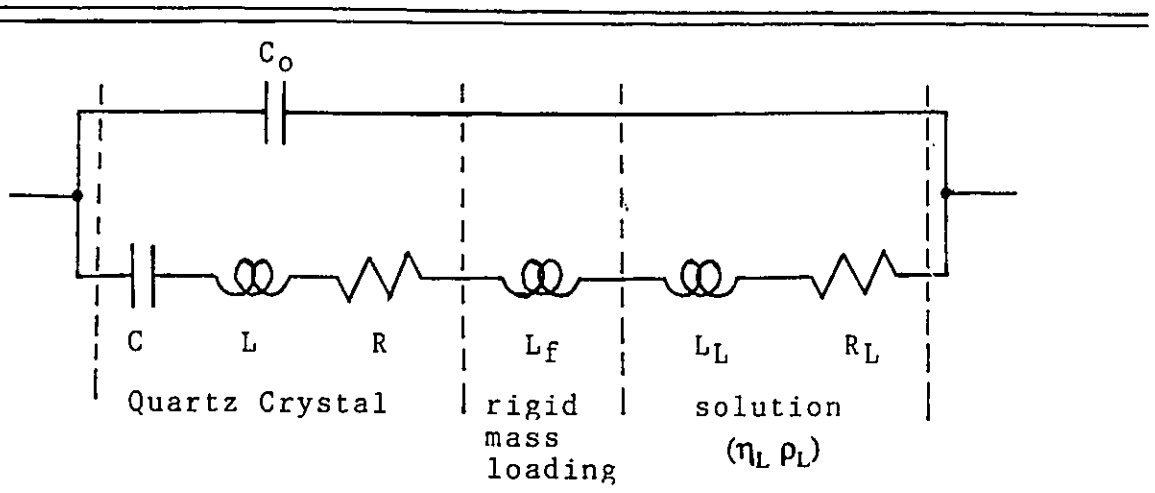

Figure 14. The equivalent circuit representation for an AT-cut quartz resonator with contributions from the mass of a rigid film and the viscosity and density of a liquid in contact with one face of the quartz resonator

is the series resonant frequency, f_s. The frequencies corresponding to the maximum and minimum values of B were represented as f_{Bmax} and f_{Bmin}, respectively. Then values of R, L and C can be derived directly from the following equations[233]:

$$R = 1/G_{max} \tag{2.22}$$

$$R/L = 2\pi (f_{Bmin} - f_{Bmax}) \tag{2.23}$$

$$LC = 1/4\pi^2 f_s^2 \tag{2.24}$$

Several attempts have been made to establish a quantitative connection of the resonant frequency change to the coupling of the resonator to the liquid medium. Muramatsu and co-workers have derived a simple equation for the resonant resistance of the quartz crystal in liquid[234]:

$$R = (2\pi f_0 \rho_L \eta_L)^{1/2} A/k^2 \tag{2.25}$$

where k is the electromechanical coupling factor and ρ_L and η_L are the density and viscosity of the liquid, respectively. In this treatment, the viscous coupling effect is thus reflected by a change of the resonant resistance (R). With the measurements of the impedance of the equivalent circuit, the resonant resistance R can be analyzed and factors such as the viscoelastic properties of the foreign layer and the liquid viscosity etc. can be evaluated through their effects on the resonant resistance[235,236].

In the above treatment, viscous coupling effects are considered to influence the parameters in the equivalent circuit of the quartz resonator. However, these effects can be

treated in another different way. In 1985, two simpler physical models were developed by Bruckenstein and Shay[60] and Kanazawa and Gordon[237]. In the latter authors' model, the quartz crystal is treated as a lossless elastic solid and the liquid as a purely viscous fluid. The viscous coupling of the QCM to the liquid is evaluated in terms of the effects of liquid viscosity η_L and density ρ_L on the frequency. It is assumed that the transverse velocity of the quartz surface is identical with that of the adjacent liquid layer (this is sometimes referred to as the "no slip" condition) and that the transverse displacement of the shear wave decays exponentially in liquid with a characteristic decay length. Thus the contributions of η_L and ρ_L can be incorporated into Sauerbrey's equation ((2.11)) to give

$$\Delta f = -[2f_s^2/(\mu_q\rho_q)^{1/2}]\ \{(\Delta m/A) + (\rho_L\eta_L/4\pi f_s)^{1/2}\} \qquad (2.26)$$

In the absence of a mass change (Δm), the observed frequency will be affected only by the density and viscosity of liquid and (2.26) reduces to

$$\Delta f_L = -f_s^{3/2}(\rho_L\eta_L)^{1/2}/(\pi\rho_q\mu_q)^{1/2} \qquad (2.27)$$

Under ideal conditions, $\rho_L\eta_L$ is constant in typical EQCM experiments and (2.26) reduces to a normal Sauerbrey equation which gives a linear relationship between the added mass Δm and the observed frequency change Δf.

By using dimensional analysis, Bruckenstein and Shay[60] derived a similar, although not identical, relationship which is given by

$$\Delta f_L = -2.26 \times 10^{-6} f_s^{3/2} (\rho_L \eta_L)^{1/2} \qquad (2.28)$$

Both theories predict a frequency decrease of a quartz crystal upon immersion in a liquid medium, but the size of the decrease that they predict is not consistent. For example, for a 10MHz quartz crystal with one face in contact with the liquid, a resulting frequency decrease of ca. 2KHz is predicted by Kanazawa and Gordon's model, which is 3 times lower than that (~7KHz) predicted by Bruckenstein and Shay's model. This discrepancy has not been studied thoroughly and the reason for it remains unclear. Nevertheless, a satisfactory agreement between the prediction of Bruckenstein and Shay theory and our experimental data was observed for a 10MHz quartz resonator.

The general prediction of theoretical models can be examined by admittance measurements of the quartz crystal using impedance or network analyzers. When the EQCM resonator is loaded by viscous coupling to a liquid, its conductance spectrum exhibits a considerable change. Figure 15 shows such a change for a 10MHz crystal both in air (curve A) and in 0.1M NaOH solution at room temperature. A dramatic increase in the width of the resonance and a decrease in the resonant frequencies accompanying the immersion into the liquid are observed. The series frequency f_s, which is close to the frequency of the maximum conductance, shifts down by ca. 7.2KHz which is in reasonable agreement with the predicted value from (2.28).

Of the aforementioned three models, the model proposed by Muramatsu and co-workers differs from the other two in its measurement method. In the former model, the effect of ρ_L and η_L on the resonant resistance of the equivalent circuit is considered. The impedance is then determined from the measurement of a voltage applied across the crystal

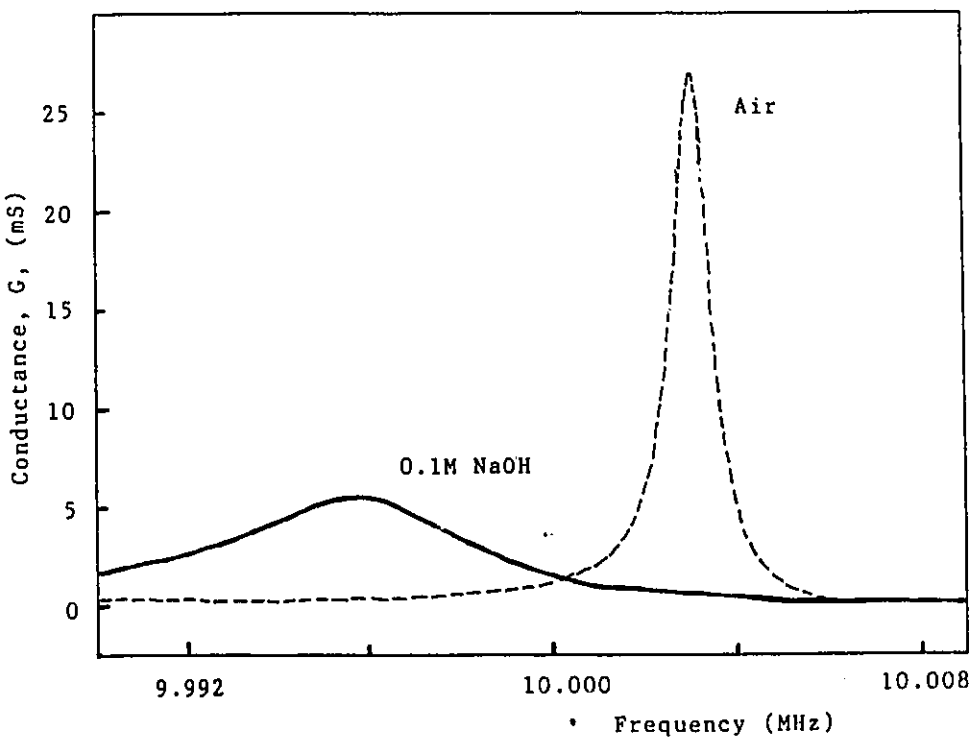

Figure 15. Plots of conductance vs frequency for a 10 MHz AT-cut quartz crystal in air (dashed line) and in 0.1M NaOH (solid line)

and the current flowing through the crystal using an impedance or network analyzer. The crystal does not determine the frequencies of the resonator, but instead the network or impedance analyzer is used to drive the crystal over a small range of frequencies spanning the natural resonance frequency. The impedance is then measured and the equivalent circuit elements may be found. However, in the latter two models, the parameters ρ_L and η_L are treated to be related to the resonant frequency of the resonator. The crystal is part of an oscillator circuit and the crystal itself determines the resonant frequency. The resonator oscillates at the resonance frequency (i.e. the point of the conductance peak as shown in Figure 15) and any viscous coupling effect (ρ_L and η_L) or added foreign mass can cause a

change in the resonance frequency (as represented by a shift of the conductance peak in Figure 15). This is the basis for the commonly used EQCM method and this method has been employed in the present work. The resonant frequency is measured as it changes with addition or removal of mass and frequency changes are related to mass changes through the Sauerbrey equation.

Finally it should be pointed out that the above treatments only take into account the two parameters ρ_L and η_L characteristic of the viscous coupling in liquid and suffer from a lack of consideration of other factors which may govern the frequency response of the quartz resonator in some cases. Such factors include viscoelastic properties, surface roughness and porosity, surface stress and interfacial slippage etc. and will be discussed briefly in the section below.

2.4 NON-IDEAL BEHAVIOR OF THE QCM

A number of factors may result in the departure of the frequency response of QCM from the Sauerbrey equation. In other words, if the crystal is being used as the frequency determining element in a circuit, frequency changes may be observed that are not derived from mass changes but rather result from some of other factors stated above. Care must therefore be taken when interpreting frequency changes solely on the basis of the Sauerbrey equation. If non-ideal behavior is suspected, then the impedance analysis method, described earlier, may be used to elucidate any non-ideal contributions through changes in the equivalent circuit parameters. Examples of such contributions from several factors which have been reported in the literature will be outlined below.

Temperature

The effect of temperature on the resonant frequency of the QCM is mainly reflected in changes of the intrinsic properties ρ_q and μ_q of the QCM with temperature. However, the effect is extremely small for the commonly used AT- and BT-cut QCM resonators (a typical value is around 1Hz per °C depending on the particular cut of the crystal) as the QCM crystals are cut at a specific angle to give a near-zero temperature coefficient at room temperature. When a crystal is immersed in a liquid, larger changes in the frequency of the crystal with temperature are expected due to the coupling of the acoustic shear wave into the liquid. Since the density (ρ_L) and viscosity (η_L) of the solution are functions of temperature, the frequency of the crystal responds to the temperature changes through its relation to the $(\rho_L\eta_L)^{1/2}$ term as shown in eqs. (2.26) and (2.28). Thus for EQCM experiments which may last for long time, the temperature needs to be maintained at a constant value.

Viscoelastic properties

Viscoelastic behavior is frequently encountered in polymer systems where changes in viscoelasticity of the polymer film result from chain entanglement, cross-linking and solvent-induced swelling. In general, the viscoelastic properties of polymer films can be evaluated in terms of their viscosity (η) and shear modulus (μ), and the anomalous frequency change (Δf) is thought to be caused by a substantial change in $\mu\eta$. Polymeric systems will tend to have lower μ values than that of quartz due to their lower stiffness, while having higher η values than that for quartz due to the possibility for viscous loss from translational motion of the chains relative to one other. However, a quantitative correlation of the material properties (i.e. μ and η) of the film with the behavior of the QCM resonator has not yet been

established. It seems that an impedance analysis of the polymer films may help to solve this problem. Mass changes due to viscoelastic effects can be inferred directly from the frequency change (Δf) using the Z-match method[238,239].

Surface roughness and porosity

Roughness and porosity can give rise to large mass loadings due to the liquid trapped within pores at the crystal surface. This effect was reported during the oxidation of Au electrodes in neutral and basic media, in which the observed frequency shift during the oxidation was significantly larger than that expected from oxide formation[240,241]. This was ascribed to water trapped in surface cavities formed during the oxidation/reduction cycle. In other words, oxidation and reduction of the surface caused an increase in the degree of surface roughness (a simplified roughness model is illustrated in Figure 16[240]). This observation demonstrated that, for an unknown process of interest, careful attention must be paid to the interpretation of QCM results.

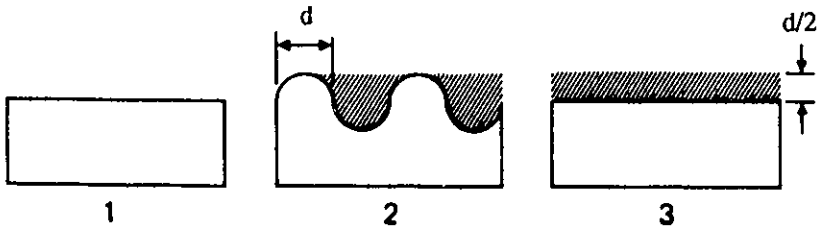

Figure 16. The cross section view of a simplified roughness model. (1) smooth surface; (2) roughened surface assembled of *hemicyclinders* with liquid enclosures (hatched area); (3) equivalent rigidly attached liquid layer on smooth surface. Note that the mass of the metal electrode itself does not change in sketches 1 - 3 (*from Schumacher et al.*[240])

Surface stress

As reported earlier, for typical EQCM experiments, one face of a quartz resonator is immersed in liquid while the opposite face is exposed to air. Thus a stress is produced on the quartz crystal as a result of the hydrostatic pressure exerted by the column of liquid. Heusler et al.[242] examined this stress effect and reported a parabolic relation between the QCM frequency and the hydrostatic pressure according to eq. (2.29)

$$f_o - f_o^{Max} = A(P - P_{Max})^2 \qquad (2.29)$$

where P is the hydrostatic pressure and A is a constant. This relation probably holds true only at higher hydrostatic pressure. At lower pressure, a negligible effect of the hydrostatic pressure on the frequency of the crystal was observed by Bruckenstein and Shay[243], who measured the frequency change after each addition of successive amounts of water to the electrochemical cell to increase the total liquid column height up to 11.2cm. Clearly the role of the hydrostatic pressure in the frequency change needs to be further clarified, but it seems likely that its effect is not very important since the pressure is generally constant throughout a typical EQCM experiment.

Stress effects may also arise from a thick film at the crystal surface. Compressive stresses in metal films on the QCM surface are known to result in a frequency shift which is not related to mass changes, with a decrease in f_s for AT-cut crystals and an increase in f_s for BT-cut ones[244]. Fortunately, the stress coefficients for AT- and BT-cut crystals are nearly equal but are opposite in sign ($K_{AT} = 2.75 \times 10^{-12}$ $cm^2 dyn^{-1}$; $K_{BT} = -2.65 \times 10^{-12} cm^2 dyn^{-1}$). Thus any contributions of stress may be identified using a "double-resonator" technique in which results of the same experiments on both AT- and BT-cut crystals are compared, as demonstrated by Cheek and O'Grady who examined the effect of compressive stress produced

in Pd films upon hydride formation[245]. However, it is likely that stress effects will be important in the QCM experiments for thick films only.

Interfacial slippage

As derived in Section 2.2.2, Sauerbrey's equation makes use of the assumption that the velocity of the shear wave in liquid is identical with that in quartz itself. This implies that the liquid adjacent to the crystal surface should behave as a rigid mass. Thus the "no-slip" condition is ideally required, in which the first layer of the liquid at the crystal surface is tightly bound and does not slip against the metal surface of the electrode during the shear motion of the crystal. If there is slippage, the coupling between the electrode and the adjacent liquid layer will be altered and consequently the decay length of the shear wave and the effective thickness of the liquid layer will be affected.

Several attempts have been made to correlate the slippage effect with some simple physical parameters such as the contact angle of the liquid and the hydrophobicity of the crystal surface[246,247]. However, a quantitative relation between the frequency of the QCM and the slippage effect has not yet been established. It seems that the surface energy plays an important role in determining the extent of slippage at the interface. When a process occurring at the surface produces a hydrophilic/hydrophobic transition, the slippage effect especially needs to be taken into account.

From the preceding discussion, it is evident that, when the EQCM is used to measure actual mass changes, it is desirable to minimize or eliminate possible non-ideal contributions (details on this topic can be found elsewhere[221]). However, frequency changes resulting from

the non-ideal behavior (described above) alone are also of importance and may be indeed useful for some applications such as stress measurement[245] and studies of the viscoelastic properties of hydrodynamic layers[248]. In the present work, only the frequency responses derived from the foreign added mass are measured and the contributions from non-ideal behavior are usually negligible. This is because the species to be studied in the present work are small molecules and thus don't result in significant changes in the viscoelastic properties of the foreign layer formed on the crystal surface. In addition, typical experiments are carried out at a constant temperature and a constant liquid volume. Thus other non-ideal effects such as temperature and surface stress on the frequency are minimized.

Chapter 3

Experimental

In the present work, the electrocatalytic oxidations of methanol, formic acid and glucose have been investigated using the Electrochemical Quartz Crystal Microbalance (EQCM) technique. The principle of this method was introduced in the preceding chapter. In this chapter the instrumental aspects of the technique as well as other aspects of electrochemical experiments involved in the present work will be described.

3.1 Quartz Crystal

Nominal 10.0MHz fundamental AT-cut crystals were employed. The crystals with gold electrodes were purchased from International Crystal Manufacturing Co., Inc., Oklahoma City. Each gold electrode of the crystal was vacuum-deposited by the manufacturer to a thickness of about 900Å, and was finished with 5 micron abrasive (a typical SEM picture for the gold electrode is shown in Figure 17). No adhesive layer was used to facilitate the attachment of the gold layer to the quartz crystal.

3.2 Cells

A four-port Pyrex glass electrochemical cell with an opening at the bottom was used in experiments. Two ports are for the connections of the counter electrode compartment and a Luggin capillary while the other two are for the supply and removal of nitrogen gas. This cell was designed in order to facilitate the attachment of the quartz crystal and to allow the

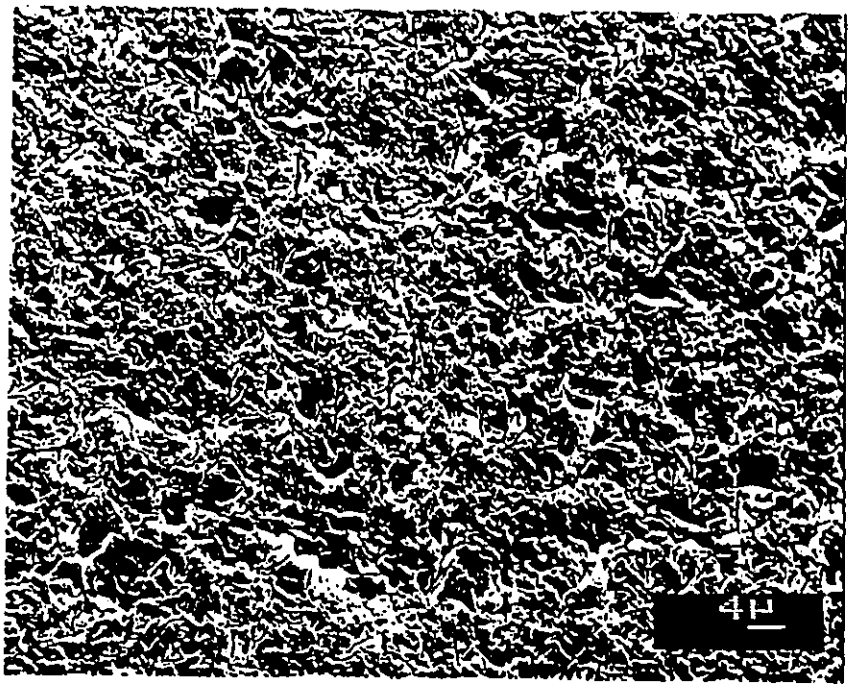

Figure 17. Scanning Electron Micrograph of a gold electrode deposited on the quartz crystal

solution to be degassed easily with nitrogen.

Mounting the quartz crystal to the electrochemical cell is a very important step. Suitable methods should be taken to minimize the influence of the stress (resulting from the mounting) on the absolute frequency of oscillation of the crystal. A simple method was adopted in the present work, i.e. a silicone rubber sealant was used to attach the crystal to the opening of the electrochemical cell as shown in Figure 18. Care was taken to avoid the contact of the sealant with the mass sensitive centre of the crystal electrode. The oscillating circuit board for the EQCM was affixed to the cell using a metal clamp, and rigid leads were used to make the connection of the quartz crystal electrodes to the circuits for control of potential and frequency.

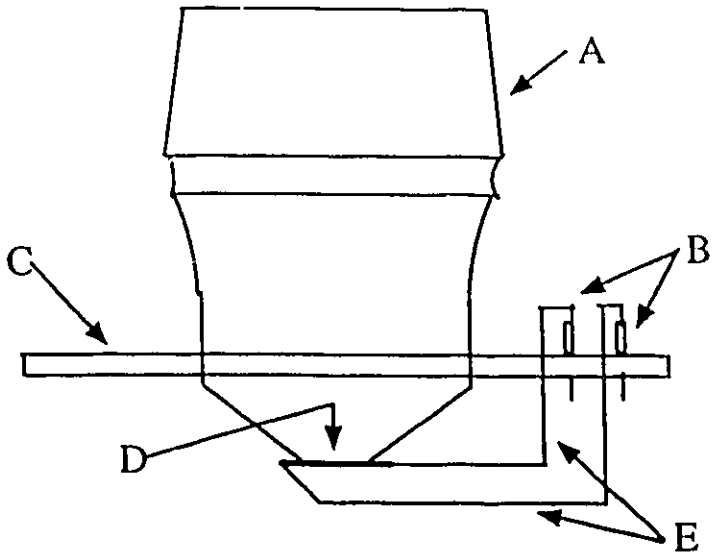

Figure 18. Lower section of electrochemical cell with attached quartz crystal. A. glass joint for connection to Luggin capillary, counter electrode chamber and solution bubbler; B. plug-jacks to connect the crystal to the oscillator circuit board; C. a plug-board affixed to the glass cell; D. quartz crystal attached to an opening of the glass cell; E. rigid leads connecting the crystal to plug-board jacks

3.3 Electrodes

Platinum working electrodes were prepared by the electrochemical deposition of Pt onto the gold substrate on the quartz crystal with the electrode potential poised at 0.350V (SCE) using a solution of hexachloroplatinic acid (2mM H_2PtCl_6 in 0.2M H_2SO_4). Prior to the deposition, gold electrodes were cleaned by oxidation/reduction cycles in 0.1M $HClO_4$. Usually 16 to 22 μg of platinum was plated on the electrode. After deposition, the electrode was cleaned by cycling it in 0.1M $HClO_4$. Electrodes prepared according to this procedure showed no influence of the gold substrate (visible from a small peak on the cathodic scan just

before the reduction of Pt oxide[194]). All electrodes were checked by voltammetry in 0.1M $HClO_4$ before each experiment of interest.

The real surface area of the Pt electrode was determined by integrating the hydrogen UPD charge (assuming that the charge of 210μC/cm^2 corresponds to a monolayer of adsorbed hydrogen on Pt[249]). The geometric surface area of the deposited Pt electrode is ca. 0.25cm^2 and thus typical roughness factors of Pt electrodes were found to be in the range 20 ~ 30.

The counter (auxiliary) electrode was a Pt wire which was put in a compartment separated by a fine glass frit from the main cell, and the reference electrode was a saturated calomel electrode (SCE) separated from the cell by a Luggin capillary. All potentials given in the present work are referred to the SCE scale unless otherwise specified.

3.4 Solutions

Solutions were prepared using water from a Millipore Milli-Q purification system (resistivity of 18 MΩcm^{-1}). 0.1M $HClO_4$ or 0.1M NaOH were used as the supporting electrolytes. Chemicals were obtained from BDH ($HClO_4$, AnalaR; H_2PtCl_6, Analytical Reagent; methanol, AnalaR; formic acid, AnalaR; and NaOH, AnalaR), Aldrich (α-D-glucose, 96%; $Pb(ClO_4)_2$, 98%; and Bi_2O_3; 99.99%), and Merck (H_2SO_4, Suprapure 96%), and were used without further purification. For the UPD and adsorption experiments with Pb^{2+} and Bi^{3+} ions, the respective metal ions were added to the electrolyte using a stock solution of 0.052M Pb^{2+} or 0.05M Bi^{3+} in $HClO_4$ (Bi^{3+} solution was made by the dissolution of Bi_2O_3 in 0.05M $HClO_4$) whilst for experiments involving the oxidation of organic molecules, a stock solution of 5.0M (methanol or formic acid) or 0.5M (glucose) was used for making additions. All experiments were performed at room temperature 22±1°C. The measurements were made in

nitrogen-saturated solutions with nitrogen (Ultra purity 99.99%, Air Products) bubbling or flowing above the solution to minimize oxygen contamination in the solution.

3.5 Oscillator Circuitry

When the crystal is placed in solution, one major problem arises, i.e. the presence of the viscous solution mechanically damps the crystal to a point where insufficient feedback exists to sustain oscillation. Thus a key point of the circuit design is to supplement the oscillator with a high-gain amplifier in its feedback loop to allow for oscillation of the crystal in the solution. Four different designs have so far been reported in the literature[60,178,250,251]. The oscillator circuit used in the present work was identical to that described by Bruckenstein and Shay[60] as shown in Figure 19. In this configuration, the oscillation frequency of the crystal is measured with respect to a reference crystal which was external to the electrochemical cell, and the difference in frequency between the two crystals was sent to a frequency-to-voltage converter. The electronic circuit for the EQCM is straightforward. It consists of (1) two oscillating circuits (U1A-C) to drive the reference and working crystals to an oscillation with the frequency of each crystal being output to separate Schmitt trigger inverters (U2B and U2C); (2) a dual D flip-flop (U3A and U3B) which is used to receive the two frequency signals from the Schmitt trigger inverters and to measure the instantaneous difference in frequency between the two frequency signals; (3) an optical isolator (U4) to receive the frequency difference from the flip-flop and isolate the common of the frequency-difference circuitry from other commons of the electrochemical, recording and monitoring circuitry.

The two oscillator circuits for the working and reference crystals are slightly different.

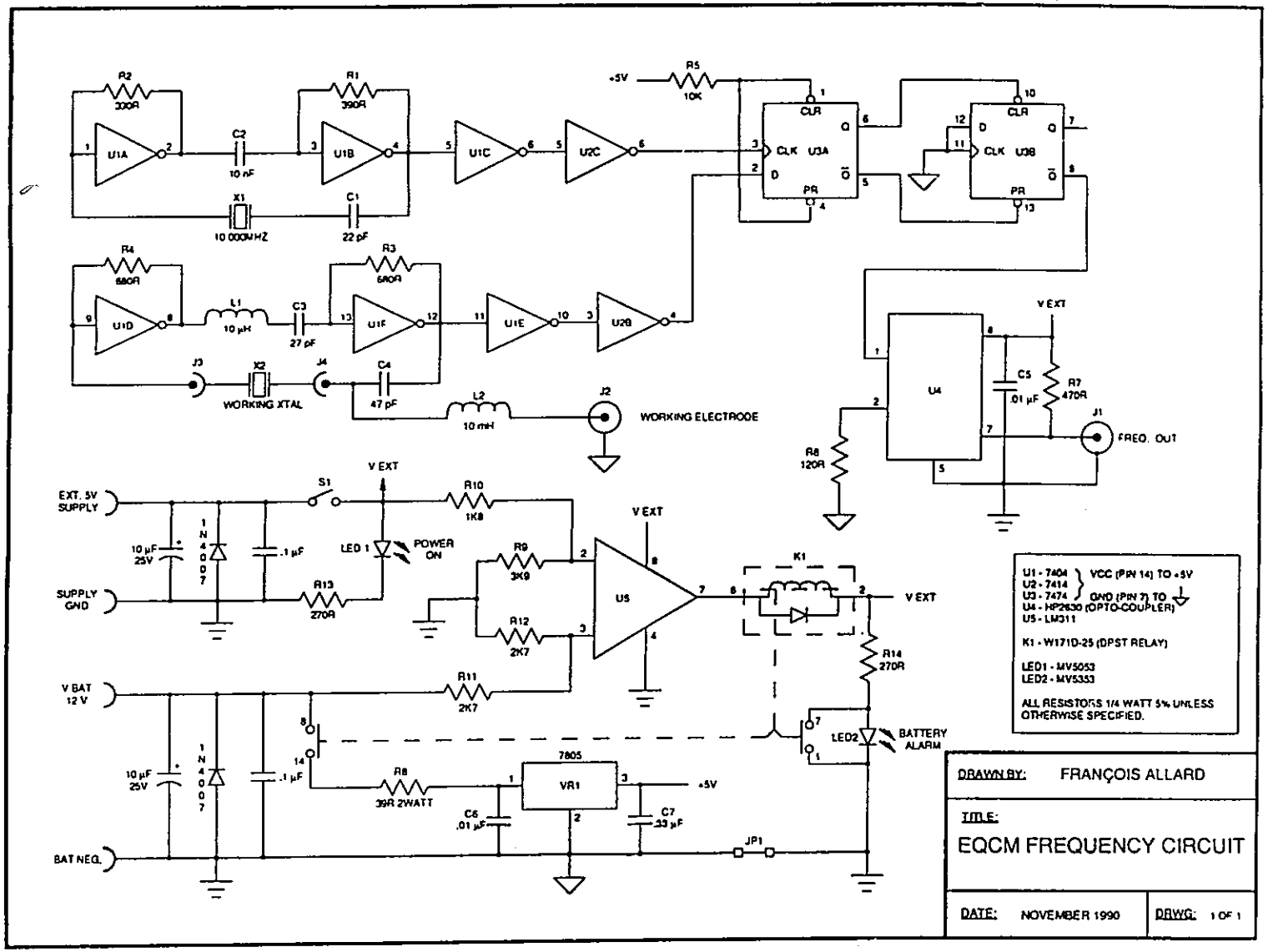

Figure 19. The EQCM circuitry with two separate reference and working oscillators. U1= 7404 HEX INVERT; U2= 7414 HEX Schmitt trigger; U3= 7474 Dual D Flip-Flop; U4= HP2630 Dual Optically Isolated Gate; Shown in the lower part of the diagram is the circuit of separate power supplies

The working crystal oscillator made use of an inductor-capacitor (LC) tuned element to provide for oscillation at 10.0MHz, while the reference crystal oscillator used capacitor coupling. The output of the reference crystal oscillator was connected to the clock pulse channel of the first flip-flop and the output of working crystal oscillator to the data channel of the first flip-flop. The second flip-flop acted as an output buffer. Thus the absolute value of the difference in frequency between the reference and working crystals was obtained from the dual flip-flop. Ideally, a minimum difference of 2 ~ 3kHz in the frequency between the two crystals was required for a desirable output. A power supply which was separate from that of the main circuit was used for the output side of the optical isolator. The output from this isolator was then sent to a frequency-to-voltage converter for analog recording of frequency difference.

All the electrical circuitry including the electrochemical cell was placed in an aluminium Faraday cage to further reduce the noise levels.

3.6 Electrochemical Apparatus

Figure 20 shows a block diagram of the EQCM instrument used in the present work. The quartz crystal was mounted to the electrochemical cell with one face exposed to solution as the working electrode. This working electrode was connected both to the potentiostat for electrochemical control and to the working crystal oscillator circuit for the frequency measurement. A 10mH inductor is placed in the connection between the crystal electrode exposed to the electrolyte and the potentiostat to further isolate the oscillator electronics from those of the potentiostat. The frequency difference between the reference and working crystals was converted to a voltage signal by a home-built frequency-to-voltage converter and

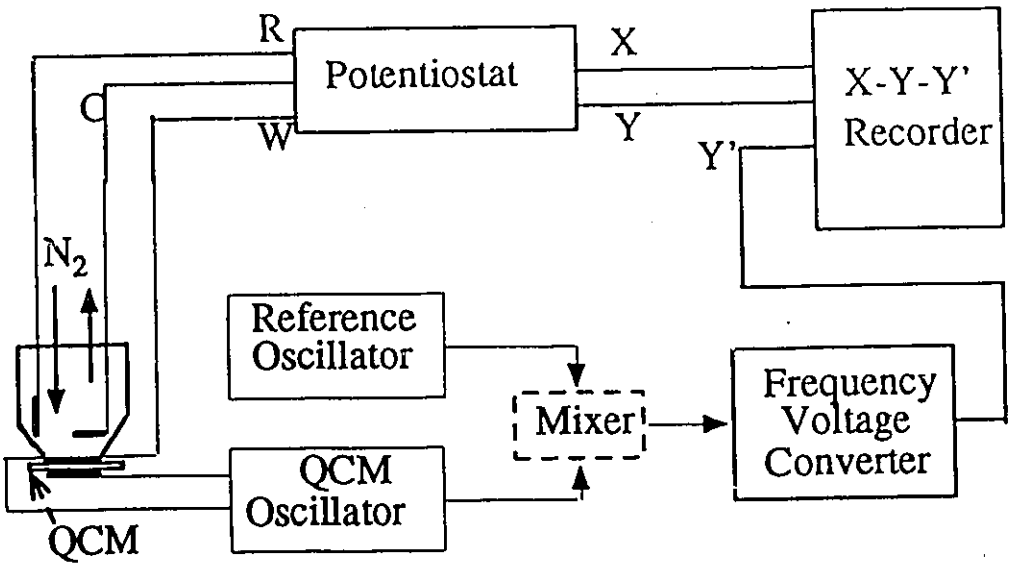

Figure 20. Block diagram of the electrochemical apparatus

displayed on either a Kipp and Zonen BD91 or Philips PM 8272 X-Y-Y' recorder, alongside the current-voltage signals from the potentiostat. Often small (mV) changes in output from the frequency-to-voltage converter are superimposed on a background level of 1 ~ 2V, thus the frequency-to-voltage converter has a voltage offset that allows such small changes to be displayed.

Potential control was accomplished by means of an Oxford Electrodes (Abingdon, UK) potentiostat. With an arrangement such as that shown in Figure 20, simultaneous measurement of both the current flowing through the electrochemical cell and the oscillation frequency of the crystal could be achieved in a typical voltammetric EQCM experiment.

3.7 Mass Sensitivity

In order to obtain accurate mass signals from the crystal, the frequency-to-voltage converter must be calibrated. This was accomplished by connecting the converter to a standard frequency generator and then measuring the corresponding voltage response. The voltage obtained was plotted as a function of frequency as shown in Figure 21. A linear relation between the voltage and the frequency was observed at up to 60 kHz used in the test. Thus the frequency sensitivity of the converter was determined to be 61.5mV/kHz or 16.2Hz/mV.

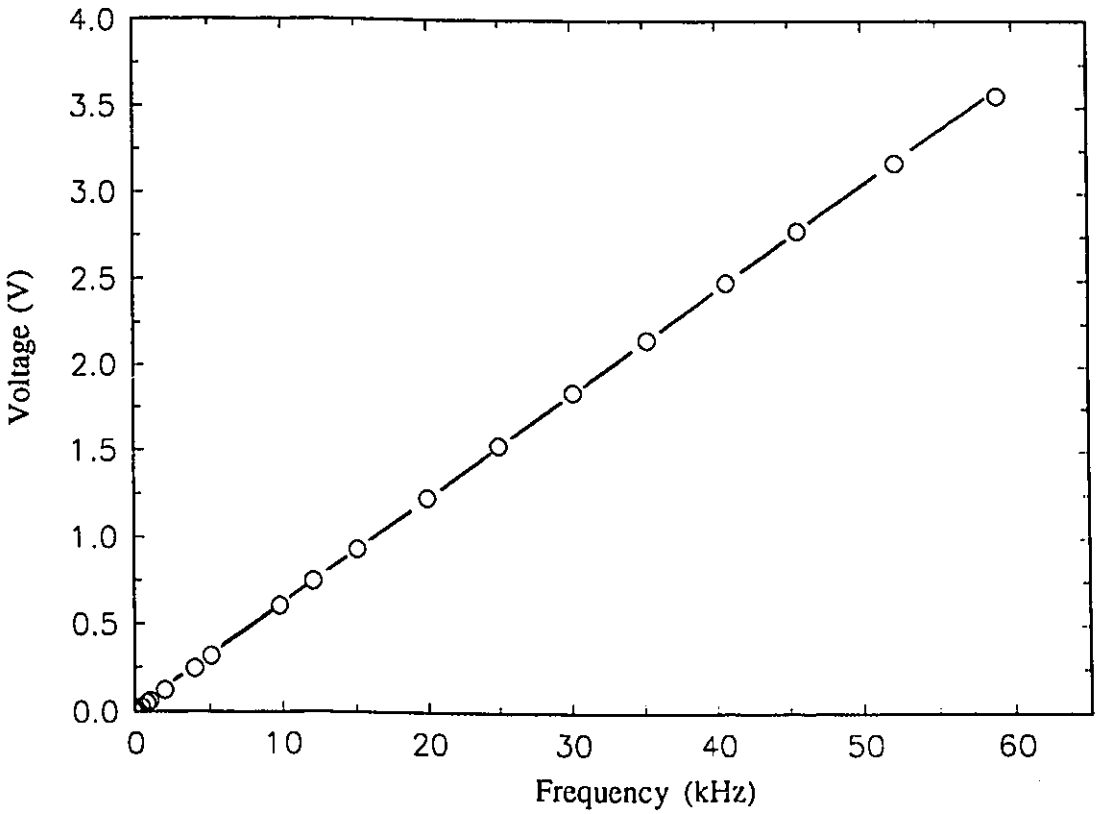

Figure 21. Correlation of voltage obtained from the frequency-to-voltage converter with the frequency for the EQCM

The mass sensitivity of the EQCM in solution was measured by galvanostatic deposition of silver onto the gold substrate from a solution of $1x10^{-3}$M $AgNO_3$ in 0.2M H_2SO_4. The reduction current was controlled at I_r = 5μA. The frequency change resulting from the deposition was recorded as a function of time and the deposited mass was estimated from the charge passed during the deposition using Faraday's Law. As only one electron transfer was involved in the reduction of Ag^+:

$$Ag^+ + e \rightleftharpoons Ag$$

the charge passed (Q), obtained as the product (I_r x t) of the deposition time (t) and the reduction current (I_r), can be related to the mass of silver deposited according to the following equation

$$m = 107.9Q/96486 \text{ (g)}$$

where 107.9 is the atomic weight of silver and 96486 (C/mol) is the Faraday constant. From the recorded frequency and charge, the relationship between mass and frequency was found as shown in Figure 22. From the slope of the line, the mass sensitivity of the EQCM was calculated to be 1.21ng/Hz. If both the piezoelectrically active area of 0.25cm^2 (i.e. the geometric area of the centre region) and the electrochemically active area of about 0.265cm^2 (including the un-insulated flag region of the crystal) of the crystal are taken into account, this value of 1.21ng/Hz corresponds to 0.219 $Hz.cm^2ng^{-1}$, which is in good agreement with the value of 0.226 $Hz.cm^2ng^{-1}$ calculated from the theory for a 10.0MHz crystal from equation (2.12) in Chapter 2. Taking the frequency sensitivity of 16.2Hz/mV for the frequency-to-voltage converter, the mass sensitivity of the EQCM can be expressed as 19.6ng/mV. Thus chart recorder settings (in mV or V) can be converted to mass values.

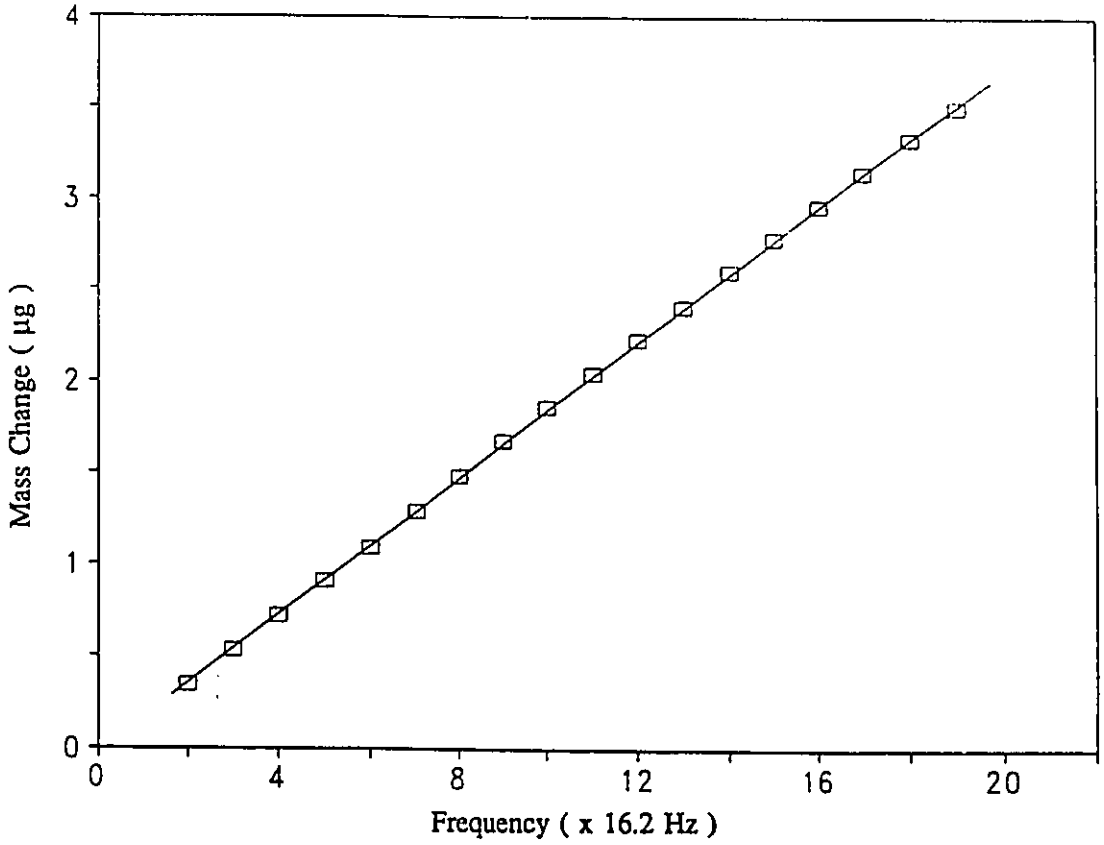

Figure 22. The relationship between mass and the frequency for the EQCM

Chapter 4

Adsorption and Underpotential Deposition of Lead and Bismuth at Platinum Electrodes

4.1 INTRODUCTION

The underpotential deposition of lead[87,252-254] and bismuth[255,256] at Pt has been studied from both fundamental and practical points of view with the area of practical interest being the effects that these UPD deposits have on a variety of electrocatalytic processes[257]. However, unlike some more widely studied systems such as lead on gold[179,180], the UPD of lead and bismuth at Pt is difficult to study. This is because for both UPD metals the peak for deposition overlaps with that for the reduction of the Pt oxide and there is also a partial overlap of the stripping peak with the onset of oxidation of platinum. Thus the currents for the two processes are superimposed. For a complete, detailed study of the UPD process, the UPD process must be separated from the reduction/oxidation of platinum. The recent advent of the Electrochemical Quartz Crystal Microbalance technique seems to allow this goal to be achieved as it can easily and reliably detect the large mass changes resulting from the UPD process. EQCM studies of UPD phenomena represent an excellent application of the technique.

In this chapter, an EQCM investigation of the underpotential deposition of the two metals at Pt in acid media is presented. These studies act as a prelude to the study of the

effect of UPD on the electrocatalytic oxidations of formic acid, methanol and glucose at Pt (the oxidations of these molecules will be described in Chapters 5, 6 and 7), and the resulting knowledge of the UPD process certainly contributes to a better understanding of the mechanism of electrocatalytic oxidations at Pt electrodes covered with underpotential deposits of the two metals.

4.2 BACKGROUND RESPONSES OF Pt ELECTRODES

In order to provide a background for consideration and discussion of the experimental results to be presented in subsequent chapters, the Pt electrode was first examined in perchloric acid alone. A typical cyclic voltammogram and mass response for a Pt electrode are shown in Figure 23 and they are described below.

4.2.1 *CYCLIC VOLTAMMOGRAM*

The cyclic voltammogram for a Pt electrode (Figure 23a) displays three different regions designated as regions A, B and C respectively. The features seen in this voltammogram are well documented[258,259]. Region A corresponds to the cathodic underpotential deposition (UPD) and anodic removal of H atoms. The resulting current peaks are known to be affected by adsorbed anions[260]. The charge obtained from the integration of the current curve in this region has been taken as a standard measure of the electrochemically active area of the electrode surface. A value of 210 $\mu C/cm^2$ for the charge (Q_H^o) corresponding to a monolayer coverage of the electrode surface by adsorbed H atoms has commonly been used as a conversion factor. The charge involved in the H UPD is also

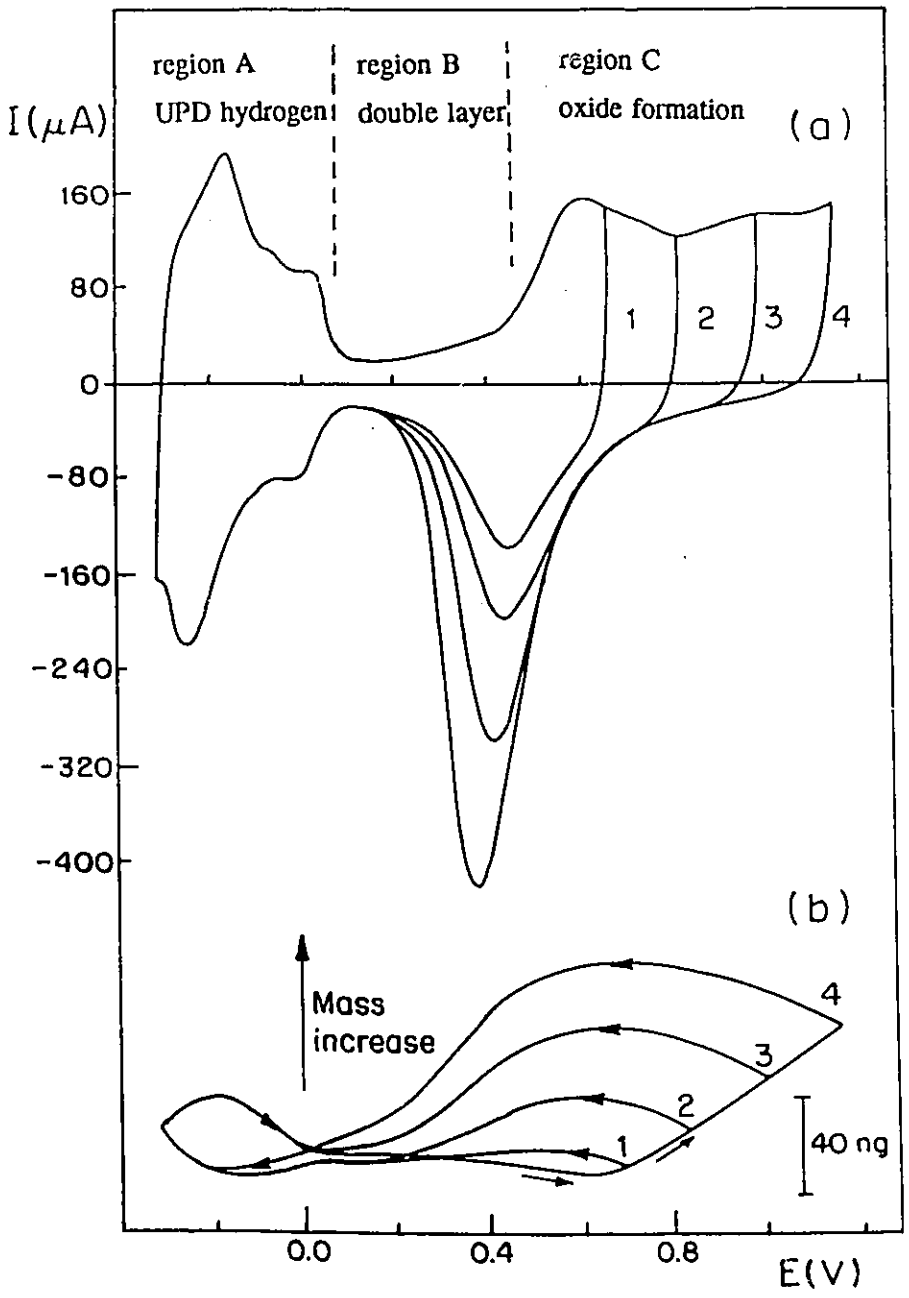

Figure 23. Cyclic voltammogram (a) and mass response (b) for an electrodeposited platinum electrode in 0.1M $HClO_4$ as the potential was taken to successively increasing upper limits. The electrode area is 4.70cm^2 and scan rate 50mV/s.

a measure of coverage of some other adsorbed species which either do not react with H atom (e.g. certain organic adsorbates) or do not adsorb H atoms (such as Pb and Bi). When these species are adsorbed on the electrode surface, the number of sites for hydrogen adsorption is decreased, and so is the charge corresponding to the monolayer coverage of the remaining sites by H atoms (Q_H). Thus the quantity

$$\theta = (Q_H^\circ - Q_H) / Q_H^\circ = 1 - Q_H/Q_H^\circ$$

is a relative measure of the number of sites not occupied by H atoms and represents the coverage of the electrode surface by other species.

Region B is the so-called double layer region where the Pt electrode behaves like a non-ideally polarized electrode (i.e. electric charge can leak across the interface). The anion adsorption is possible in this region as the potential in this region is more positive than the potential of zero charge (i.e. the potential at which the charge on the electrode is zero) (The real position of the pzc for Pt electrodes seems to be an open question with values for H_2SO_4 solutions of different concentrations ranging from 0.18 to 0.35V vs N.H.E.[261]). As the potential moves towards higher values, the charge on electrode becomes more positive and anions are expected to adsorb more strongly.

In region C, oxidation of the Pt electrode surface occurs and Pt oxide is formed. Upon scan reversal, Pt oxide is reduced. The mechanism of electrochemical oxidation and reduction of the Pt electrode surface has been discussed previously[260,262]. It involves a successive discharge of adsorbed water followed by a place exchange process, i.e.

$$Pt + H_2O \rightleftharpoons PtOH + H^+ + e \qquad (4.1)$$

$$PtOH \rightleftharpoons PtO + H^+ + e \qquad (4.2)$$

the O atom in PtO (or OH in PtOH) can insert itself into the Pt lattice (this insertion process for PtOH is schematically shown in Figure 24). This presumably leads to the mass increase observed on the anodic scan because the new Pt surface sites produced during the insertion process will be occupied by water. When the electrode surface is reduced, the inserted O or OH can re-emerge from the lattice and thus a mass decrease results. The integrated charge (Q_O) involved in the oxide formation shown in (4.1) and (4.2) is a characteristic quantity for describing the extent of Pt oxidation. It is often expressed as the ratio of Q_O/Q_H°, Q_H° is the charge required for monolayer H adsorption. A value of 1 for Q_O/Q_H° corresponds to a state where the surface is completely covered with PtOH (see (4.1)). As the potential scan proceeds to more positive values, these OH sites are replaced by O sites via electron and proton transfer (see (4.2)) and a value of 2 for Q_O/Q_H° is expected for a full monolayer of PtO.

4.2.2 *MASS RESPONSE*

In contrast to other electrodes such as Ag[186,187], the mass response of a Pt electrode in background electrolyte is not flat over the entire potential range (Figure 23b). Some mass changes are observed, which result from oxide formation/removal and some anion adsorption. However, the mass response for a Pt electrode is largely as expected from a simple consideration of the processes occurring at the surface of the electrode.

If we first consider the H UPD range (region A) as it is approached on a negative-going scan from region B, the potential proceeds through the double layer region (region B) of potential and the mass of the electrode continues to decrease until ca. -0.2V (region A). It is known that adsorbed anions are present at these potentials and a decline in anion adsorption would be expected as the potential of the electrode moves more negative of the

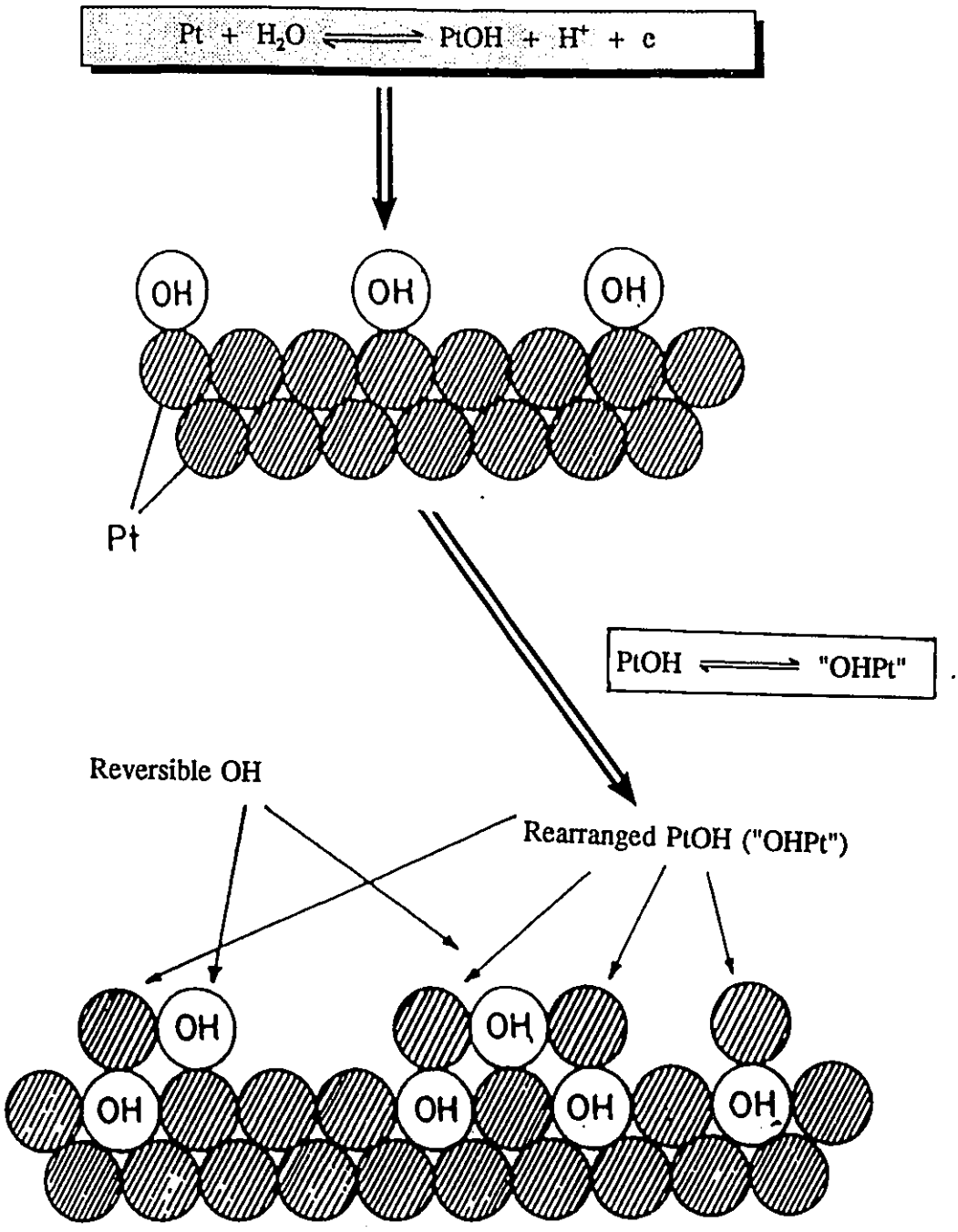

Figure 24. Schematic illustration of the formation of PtOH and the subsequent place exchange process (*from Angerstein-Kozlowska et al.*[262])

pzc. This would give rise to a mass decrease.

In the small region of potential just prior to hydrogen evolution (the negative extreme of region A) there is a mass increase observed which becomes larger at slower scan rates, and also continues during the initial stages of the anodic scan. The cause of this mass increase is not known. However, in considering the mass changes occurring over the range of potential below 0V, it is interesting to note that the presence of species that are strongly adsorbed (and not oxidised) over this potential range (such as CO[263]) influence the mass change, causing it to be drastically reduced and almost flat. Adsorption of other species which are less strongly bound and can also be oxidised over this potential range (e.g. glucose in Section 5.2.1[64]) do not alter the shape of the mass response but merely reduce it in size. Some features are more visible in the H upd region when the voltammogram and mass response is recorded at a slow scan rate (Figure 25).

a). The first feature is a decrease in mass that is observed at ca. 0.1V on the negative going scan and is indicated by the vertical arrow (a corresponding increase in mass is seen on the anodic scan) as the potential moves from the double layer region to the region of strongly bound upd hydrogen;

b). Second, at potentials below -0.05V on the negative going scan there is a mass increase which is a function of the extent of use of the electrode.

The size of this last increase is quite small for a freshly deposited electrode, increases with successive experiments to a point where it is too large to be explained by H adsorption, and is not observed in NaOH solutions (see Section 5.3). It is well known that specifically adsorbed anions are present in this potential range since the H upd peak distribution differs

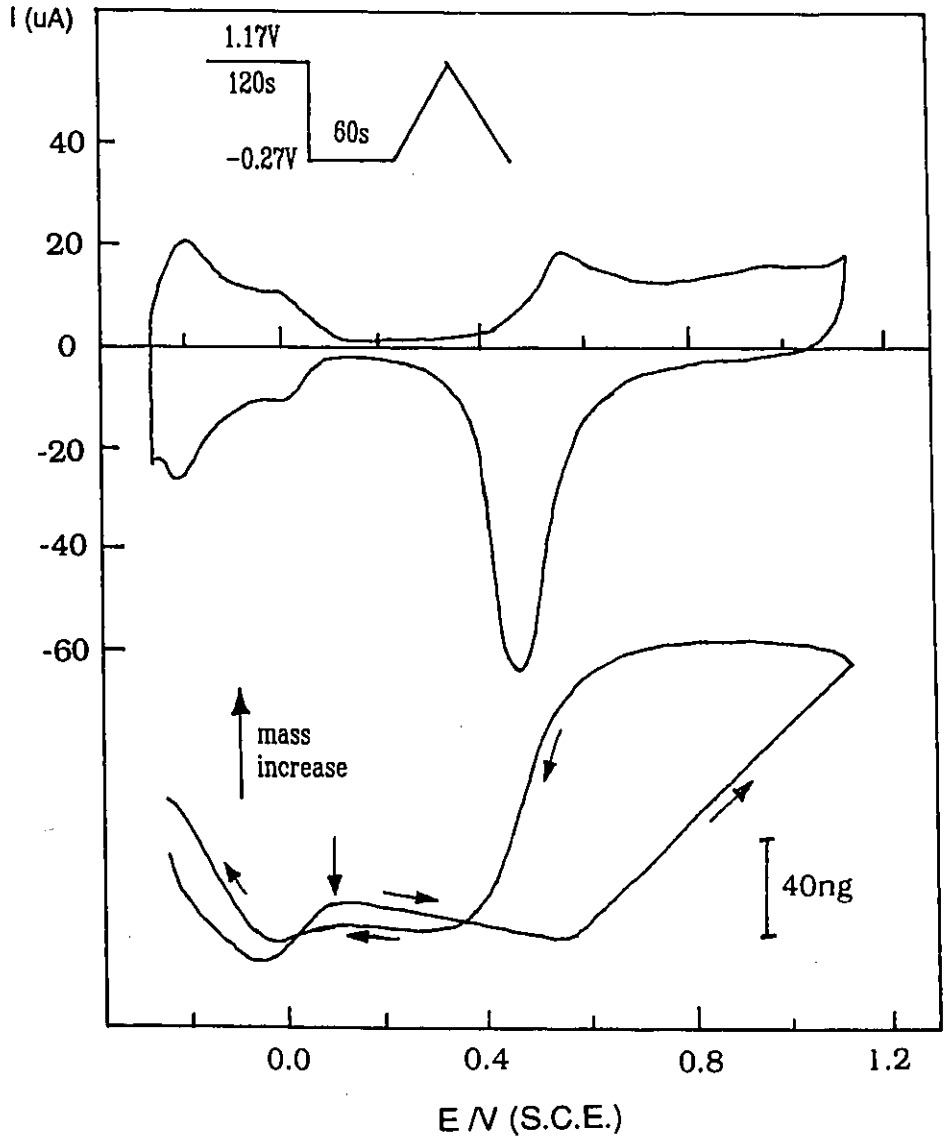

Figure 25. Cyclic voltammogram and mass response for an electrodeposited Pt electrode in 0.1M $HClO_4$. Scan rate is 5mV/s and the electrode area 4.70cm^2. The potential regime used is shown in the inset

between solutions of $HClO_4$ and H_2SO_4 of equal concentration and also changes as the concentration of H_2SO_4 is varied[260]. Thus it is most likely that these features are related to changes in anion adsorption. The changes observed with successive experiments are probably the result of varying electrode area and structure with repetitive cycling.

In the double layer region of potential (region B), the mass response is first flat and then shows a steady increase as the potential is taken more positive and the oxidation of the electrode begins. The mass increase grows as the potential limit is taken to successively more positive values reflecting the increased amount of surface oxidation (region C). Upon reversal of the potential scan there is a continued small increase in mass, perhaps resulting from continued development of oxide, followed by a larger decrease coincident with the reduction of the oxidised surface of the electrode.

In the published EQCM results of Stockel and Schumacher[247] the behaviour of platinum electrodes is unusual and shows the exact opposite of those presented here, giving a mass *decrease* (frequency increase) upon oxidation of the surface (which was not addressed in their paper) and a much larger two stage mass increase over double layer and upd H regions. This latter observation was attributed to a change in the hydrophilicity/hydrophobicity of the electrode surface influencing the coupling of the crystal oscillation to the electrolyte. It is not clear from their paper whether the platinum electrode in their study was prepared by evaporation (and therefore smooth) or by electrodeposition, as was the case here. A different electrode surface may be part of the reason for the differences between the two mass responses. Recently Randonis et al.[264] reported that the frequency response of Pt electrodes is markedly dependent on the number of oxidation-reduction cycles. They noticed that the

frequency response for an electrode obtained after a great number of cycles (i.e. 10000 cycles) is opposite to that recorded for a newly prepared electrode and a mass *decrease* accompanying the oxidation of the electrode surface is observed for the electrode with 10000 cycles. The reason for this cycling effect is unclear. However, such a phenomenon was not observed in the present work. The mass response obtained in our work always shows an increase upon the formation of oxide (as depicted in Figure 23) even after the electrode is subject to continuous use (i.e. equivalent to cycling) for several weeks.

Finally, it should be pointed out that changes in surface roughness (with possible increased solvent entrapment in pores) are not likely to play any role in the mass responses to be reported in the remainder of this thesis. This is for two reasons.

a). First, the surfaces are already rough (see Chapter 3 Experimental) and significant changes in roughness upon cycling are thus not to be expected.

b). Second, the response in the double layer region of potential in background electrolyte (Figure 25) shows no difference (within experimental error) between the mass responses accompanying the anodic-going and cathodic-going halves of the cycle. Changes in roughness upon cycling through oxidation-reduction of the electrode would not result in the mass response forming a closed loop as it does here.

4.3 LEAD

4.3.1 *LEAD UPD - CYCLIC VOLTAMMETRY*

For studies of the lead UPD process, both cyclic voltammograms and mass responses

were recorded simultaneously at a range of scan rates and concentrations of Pb^{2+} by using the EQCM technique. Figures 26 and 27 represent the corresponding results for two concentrations of 10^{-4} and $2x10^{-3}$M Pb^{2+} at a scan rate of 20mV/s. The cyclic voltammograms (Figures 26(a) and 27(a)) show that the upd of lead is not easily distinguished from the oxidation and reduction of the platinum surface, particularly at the low surface coverages that result from a low concentration of Pb^{2+} (Figure 26). The onset of upd (ca. 0.40V SCE) on the cathodic scan causes the peak current for oxide reduction (peak B) to be increased, and the peak is broadened. As the scan proceeds further negative, the presence of upd lead is apparent from the decreased current for underpotentially deposited hydrogen (UPD H) since hydrogen does not adsorb on Pb. For 2mM Pb^{2+} (Figure 27) the surface coverage is larger than for 10^{-4}M Pb^{2+} (Figure 26), and the H adsorption current is almost completely removed indicating monolayer (or greater) coverage. On the anodic scan, the removal of the upd lead (peak A) is visible just prior to, and in a slight overlap with, the onset of oxidation of the platinum surface. The peak for stripping of the deposit becomes more prominent as the bulk lead concentration increases (Figure 27). It is also noteworthy that at the highest lead concentration used (2 mM) the current on the anodic scan begins to increase at potentials significantly more negative than the upd stripping peak.

The mass responses are also shown in the Figures 26(b) and 27(b). At the highest concentration of Pb^{2+} the formation of the upd layer is clearly visible from the large increase in mass which begins at ca. 0.45V (Figure 27(b)) (RRDE experiments found that ring shielding, and hence the onset of upd, begins at a potential of 0.5V[87] and continues until the negative scan limit). The stripping process is also seen through the decrease in mass observed on the anodic scan. This decrease begins at ca. -0.05V indicating that, as noted above, the

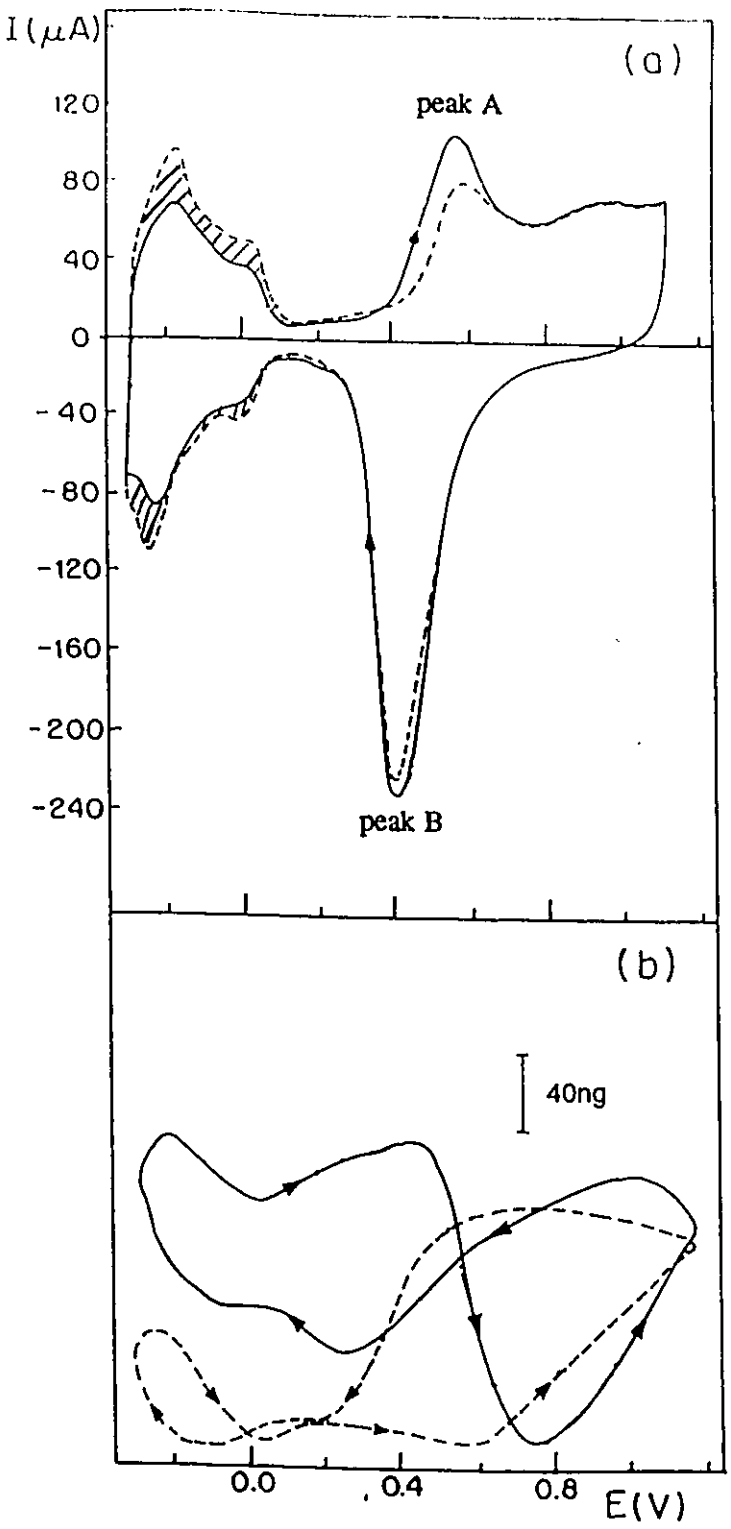

Figure 26. Cyclic voltammograms (a) and mass responses (b) for lead UPD at Pt in 0.1M $HClO_4$ for the concentration of 10^{-4}M Pb^{2+} (solid line). The response in the absence of Pb^{2+} is also shown (dashed line). The electrode area was 4.70cm^2 and scan rate 20mV/s. Mass traces for different experiments are recorded with different voltage offsets applied to the mass signal and the representation of the curve is not meant to imply that the mass of the electrode is identical where curves intersect.

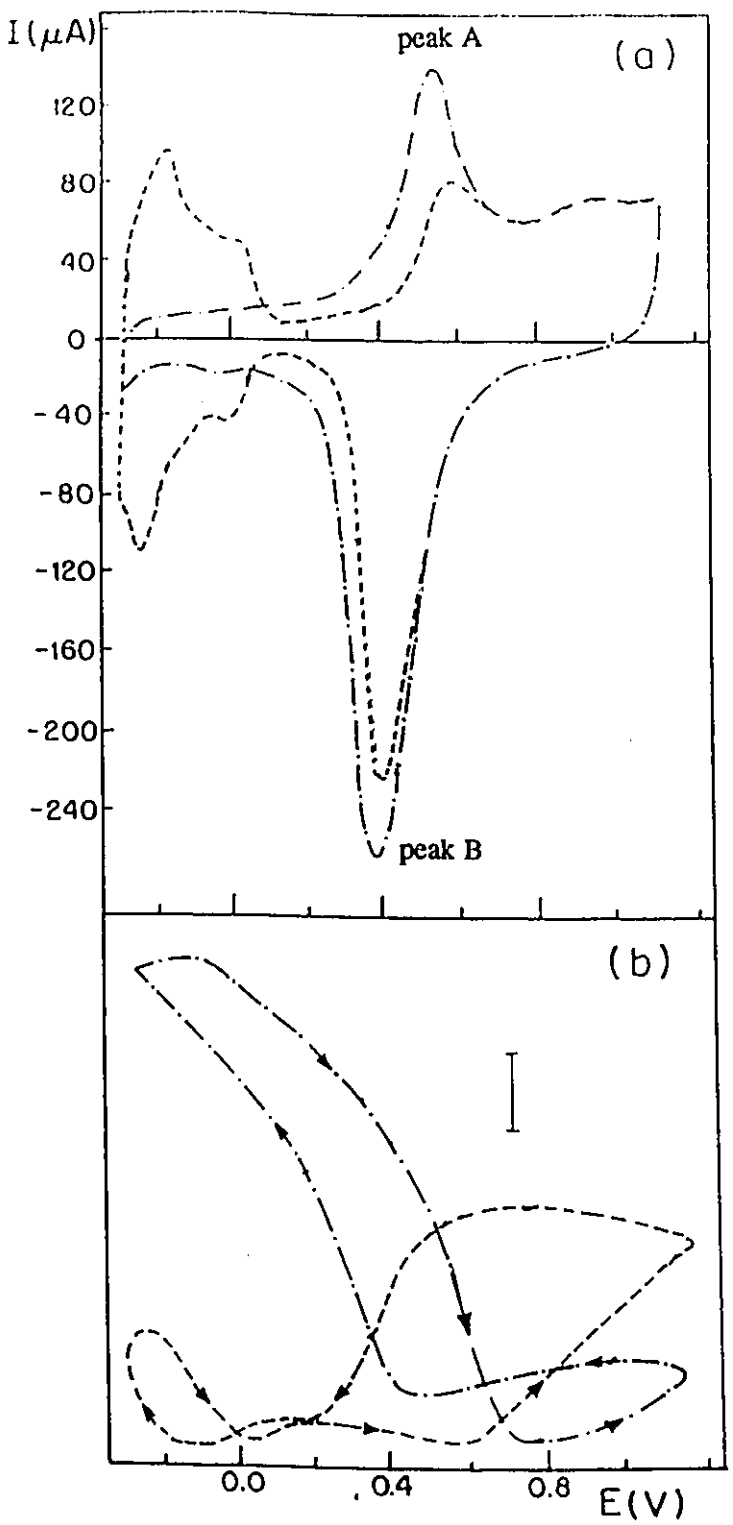

Figure 27. Cyclic voltammograms (a) and mass responses (b) for lead UPD at Pt in 0.1M $HClO_4$ for the concentration of $2x10^{-3}M$ Pb^{2+} (-.-.-.-.-). The response in the absence of Pb^{2+} is also shown (dashed line). Other conditions are the same as those in Figure 26. Note that the bar for the mass response corresponds to 40ng for a $[Pb^{2+}]$ value of 0 whereas for $[Pb^{2+}] = 2x10^{-3}M$ the bar represents 160ng.

removal of upd lead commences at lower potentials for higher coverages. There are also some kinetic effects, since the hysteresis in the mass response becomes larger as the scan rate increases.

4.3.2 *BACKGROUND SUBTRACTION OF MASS RESPONSES*

The most interesting result is the mass response recorded at 10^{-4} M Pb^{2+} (solid line in Figure 26(b)). The extent to which the H adsorption/desorption currents are suppressed in the CV (shaded area) indicates that coverage by upd lead is quite small under these conditions. The mass response for this concentration of Pb^{2+} is quite complex. Starting at the upper scan limit it is seen that the cathodic scan first gives rise to a small increase in mass and then the decrease in mass associated with the removal of the oxide begins. (There may also be some effects of the adsorption of Pb^{2+} on the oxidised surface (see Section 4.3.3)). However, before this process is complete the initial development of the upd deposit on the partially reduced Pt surface causes the net mass to begin to increase at a potential of ca. 0.3V. This increase continues until scan reversal at the cathodic limit, although it appears to involve at least two stages. There is a similarly complex response as the anodic scan begins. The mass shows an increase, then a decrease, then a further increase before the removal of the upd lead begins and causes the sharp decrease in mass that is seen at ca. 0.5V.

The mass response seen in Figure 26(b) is complicated because the mass changes resulting from the upd process are superimposed on a background that is not constant. The coverage is also low. Thus, in contrast to the higher concentrations where the lead deposition dominates the mass changes (e.g. for $[Pb^{2+}]$ = 2 mM in Figure 27(b)), there are significant

contributions to mass changes from both the upd and processes occurring at unoccupied Pt sites. Under these circumstances the mass changes taking place are revealed more clearly after a simple procedure where the mass response in the absence of Pb^{2+} was subtracted from that seen in the presence of Pb^{2+}. The result is plotted against potential for two scan rates in Figure 28. In comparing these two experiments, it is important to note that the signal displayed in the Figures is the output of a frequency to voltage (f to V) converter[60]. The device output is calibrated in mV/Hz and then the theoretical treatment of the EQCM is used to obtain a value of Hz/ng enabling the output to be represented as mass with a mV/ng factor as described in Chapter 3[60]. However, an offset voltage is added to the output to enable the signal to be displayed on a chart recorder. This offset is constant for a given experiment, but may vary between experiments. Thus ΔM represents the difference in mass between the two electrodes at a given potential *plus* a constant offset. The absolute mass difference is not measured. Nevertheless, a consideration of ΔM as a function of potential yields significant information regarding the upd process.

We first consider ΔM when the scan rate is 20 mV/s (derived from the results of Figure 26) at potentials below 0.45V. Curve 1 of figure 28 shows that ΔM increases steadily between the potentials of ca. 0.45 V and -0.30V during both cathodic *and* anodic scans. This is clearly an indication that the upd process has not reached equilibrium and that reduction of Pb^{2+} is occurring during the whole of the potential cycle in the upd region, even during the initial stages of the anodic scan. This conclusion is verified when the mass time transients (to be described in more detail later) are examined to estimate the time required to reach upd equilibrium at a variety of potentials and under the experimental conditions employed here. The mass increase is found to reach its limit after 3 and 12 minutes when the electrode

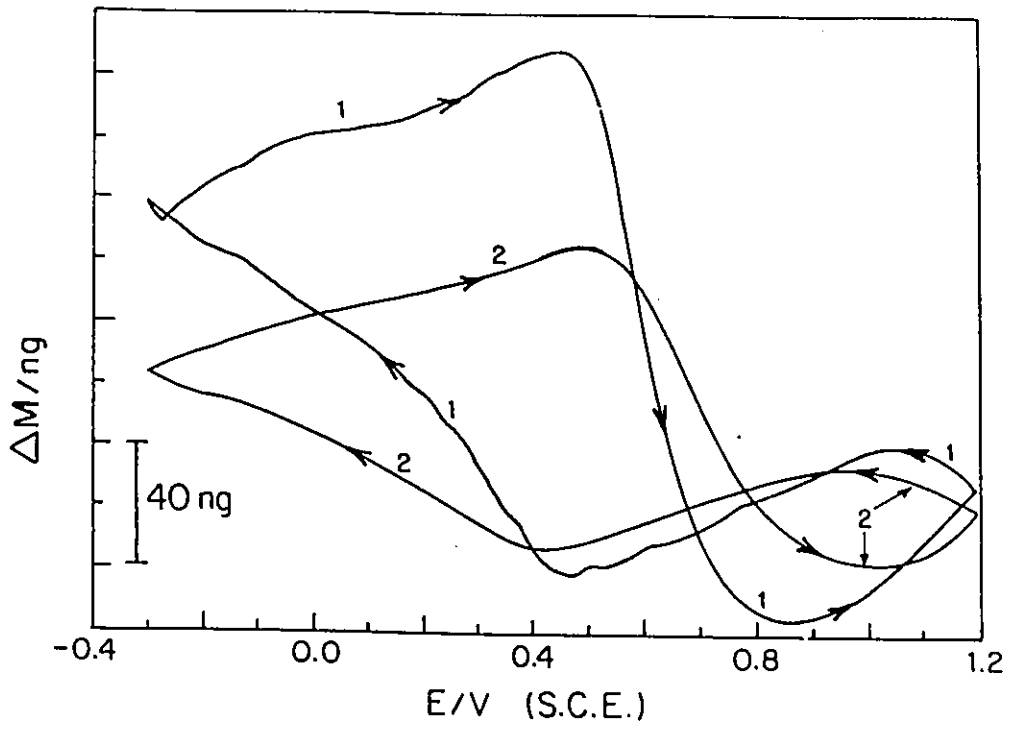

Figure 28. Mass difference (ΔM) as a function of potential for the responses 1 and 2 in Figure 26 b, $[Pb^{2+}]$ being 0 and 0.1mM respectively and scan rate = 20 mV/s (curve 1). Curve 2 was obtained from similar data recorded at a scan rate of 50 mV/s. As noted in the text the absolute value of ΔM includes a constant offset difference. Absolute mass values are not necessarily the same where curves intersect.

potential was held at 0.43V and -0.3V respectively. Thus for this value of [Pb^{2+}] and the scan rate employed, equilibrium coverage would not be reached in the above-mentioned potential range during the course of a scan. When the scan rate is 50 mV/s (curve 2 of Figure 28, which is derived from responses not shown in Figure 26) the mass increases much less over the upd region reflecting the reduced timescale of the experiment. Both curves show the removal of upd Pb beginning at ca. 0.45V on the anodic scan. The behaviour of ΔM at potentials above ca. 0.6V is discussed below.

4.3.3 *ADSORPTION OF Pb^{2+} ON OXIDISED Pt ELECTRODES*

Several previous investigations have indicated that cations such as Bi^{3+} and Tl^{+} are adsorbed on oxidised Pt and Au electrodes in acidic media. Adžić and Marković[161] studied adsorption of Bi^{3+} and Tl^{+} at Pt and Au using combined voltammetry and reflectivity/modulated reflectivity. They reported adsorption of Bi^{3+} at oxidised Pt (Cadle and Bruckenstein[256] employed the RRDE to the same end) but also commented that the experiments (for reflectivity) were difficult to perform and to interpret for Pt systems where upd begins on a partially reduced Pt surface. Although these authors showed no data for Pb^{2+} adsorption at Pt, in an earlier communication they displayed results for Cd^{2+} adsorption on Pt and reported that similar results had been obtained for Pb^{2+} and other cations[160].

To study the possibility of adsorption of Pb^{2+} on oxidised Pt we carried out some simple experiments where aliquots of Pb^{2+} were added to the $HClO_4$ electrolyte. The adsorption of Pb^{2+} on oxidised Pt electrodes in acidic solution was investigated as a function of the electrode potential and of the concentrations of Pb^{2+}, and $HClO_4$. As discussed below,

the mass is not necessarily the only factor which influences frequency in this situation. For example, any solution density or viscosity change caused by the addition of Pb^{2+} might also affect the frequency as discussed earlier in Chapter 2. However, separate experiments show that these effects can be neglected under almost all conditions used here. The relatively large frequency response resulting from the adsorption of Pb^{2+} on the electrode surface is easily detectable.

As seen from the cyclic voltammograms for Pb^{2+} shown in Figures 26 and 27, the lead upd process overlaps with the oxidation/reduction of the electrode surface. Development of the upd deposit begins at about 0.5V, a potential at which reduction of the oxidised Pt surface is not yet complete. On the anodic scan, the peak for removal of the upd deposit arises at potentials where the first stages of electrode surface oxidation occur in background electrolyte. Above 0.8V, the presence of Pb^{2+} in solution makes little difference to the voltammogram. Thus, in contrast to the situation for Pb^{2+} on Au (where there is no complication from the overlap of upd and electrode oxidation processes[160]) voltammetry offers no clear evidence for cation adsorption on the oxidised electrode surface. However, such adsorption is revealed in simple injection experiments (described above) with the potential chosen so that neither upd nor oxygen evolution processes can occur. The results of several such experiments are shown in Figure 29. The upper trace (3) shows the variation of the frequency difference (converted to mass) with time, as the concentration of Pb^{2+} is increased from 0 to 2 mM at 0.8V in 0.01 M $HClO_4$. However, before discussing these results further, it is important to eliminate the possibility that phenomena other than that of adsorption of Pb^{2+} give rise to these mass changes.

From two proposed theoretical treatments of the QCM as given in Chapter 2, it is

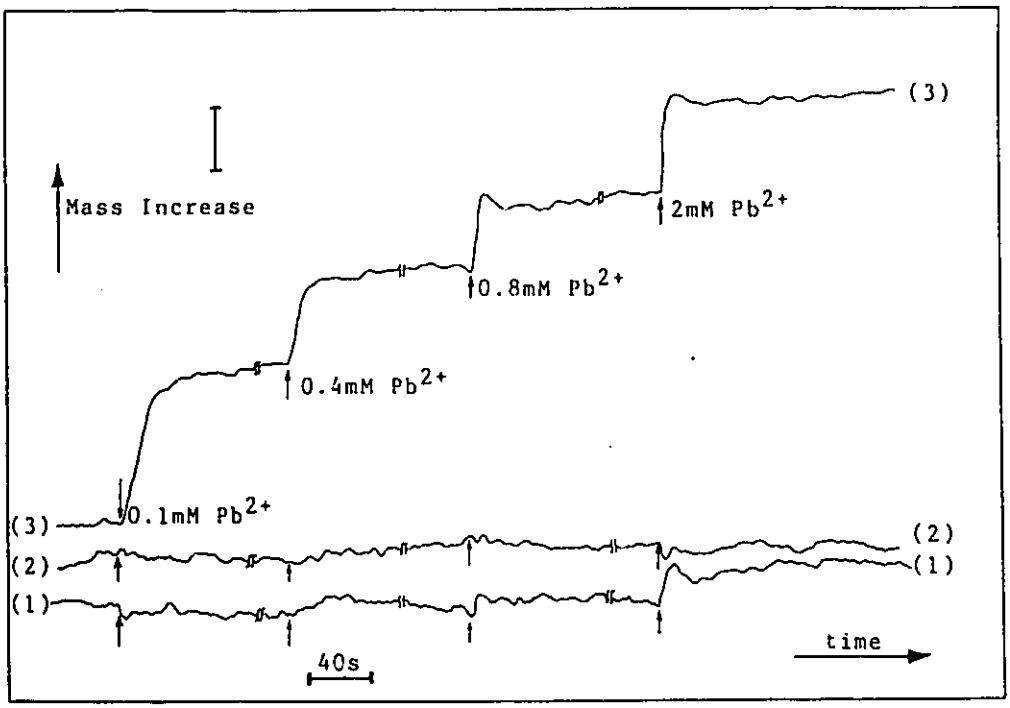

Figure 29. Mass-time transients for the successive injection of different concentrations of Pb^{2+} ions. (1). an electrode covered with a Fluoroglide layer in 0.01 M $HClO_4$; (2). as (1) except in 0.1 M $HClO_4$; (3). an oxidised platinum electrode in 0.01 M $HClO_4$ with the electrode potential held at 0.8V(SCE). Note that the vertical bar for the mass response corresponds to 20ng for (1) and (2) whereas for (3) the bar represents 32ng. Mass responses are absolute mass changes (not normalised for surface area) and are displaced vertically for reasons of clarity.

shown that when the QCM is immersed in solution, the resonant frequency is proportional to the product $(\rho_L.\eta_L)^{1/2}$, where ρ_L is the density of the solution and η_L is the viscosity[60,237]. Experiments, such as cyclic voltammetry, are normally performed in a solution of unchanging composition and constant temperature and so these effects can be neglected. However, when solution composition is changed this is not necessarily the case. Several observations support the suggestion that the mass changes seen in Figure 29 are indeed due to cation adsorption.

1. In a study of Pb upd at Ag[186], addition of 0.8 mM Pb^{2+} to 0.1 M $HClO_4$ was seen to produce no mass change at all, whereas when 0.4 mM Pb^{2+} was added to 0.1 M NaOH a large mass change was seen. These results were attributed to the different electrostatic interactions between the ions (Pb^{2+} in acid, $HPbO_2^-$ in alkaline solution) and the positively charged Ag surface at potentials positive of the upd region[186];

2. The changes observed here are potential dependent, increasing with potential between 0.8V and 1.1V (Figure 30);

3. Addition of concentrated $KClO_4$ solution to obtain a final concentration of 2mM (in an attempt to produce roughly similar viscosity and density changes) gave no mass change;

4. In order to further establish that the observed effects are due to adsorption of Pb^{2+}, a separate gold electrode which was covered with an insulating PTFE layer (formed by spraying the electrode with Fluoroglide®) was employed for injection experiments to try and eliminate effects from adsorption in the mass response.

Typical results are depicted in Figure 29, curves (1) and (2). Mass changes are very small (note that the mass scale is more sensitive for these two traces than for trace 3). Only

in 0.01 M $HClO_4$ are any changes detected and even then the addition of 2 mM Pb^{2+} led to a mass increase of just 5ng. This is further evidence for the attribution of the observed mass changes to adsorption of the cation. Small corrections were applied to adsorption data obtained in 0.01M $HClO_4$ as necessary.

Figure 30 shows the results of injection experiments in which the mass change per unit area of electrode surface (ΔM) is plotted as a function of the logarithm of the concentration of Pb^{2+} (log (c_{Pb}^{2+}/M)) for several different potentials in 0.1 M $HClO_4$. A linear relationship is seen to exist between the normalised mass change (ΔM) and log (c_{Pb}^{2+}/M), at least over the concentrations used here. Adžić and Marković found a similar relationship between the relative change of reflectivity ($\Delta R/R_o$) and log (c_{Pb}^{2+}/M) in their experiments on Au electrodes in $HClO_4$[160]. Experiments such as that shown in Figure 29, curve 3, were also performed for several concentrations of background electrolyte. The effect of perchloric acid concentration (c_{HClO_4}) on the observed mass changes is shown in Figure 31 for an electrode potential of 1.0V. At lower concentrations of $HClO_4$ larger mass changes are found. There is a linear relationship between ΔM and log (c_{HClO_4}/M). Again, this parallels previously stated results for Bi^{3+} adsorption at gold where ($\Delta R/R_o$) was found to decrease linearly with log (c_{HClO_4}/M)[161]. Evidently there is some competition between cations and anions for sites on the oxidised electrode surface. But, as we will see later, there may be some effect of solution pH on the distribution of ions present.

These EQCM results clearly show that Pb^{2+} is adsorbed on the oxidised surface of Pt electrodes in $HClO_4$ and that the extent of adsorption increases with potential and c_{Pb}^{2+} and decreases with c_{HClO_4}. The experiments are simpler and more direct than the modulated reflectivity technique used previously[161]. Although direct comparisons cannot be made, the

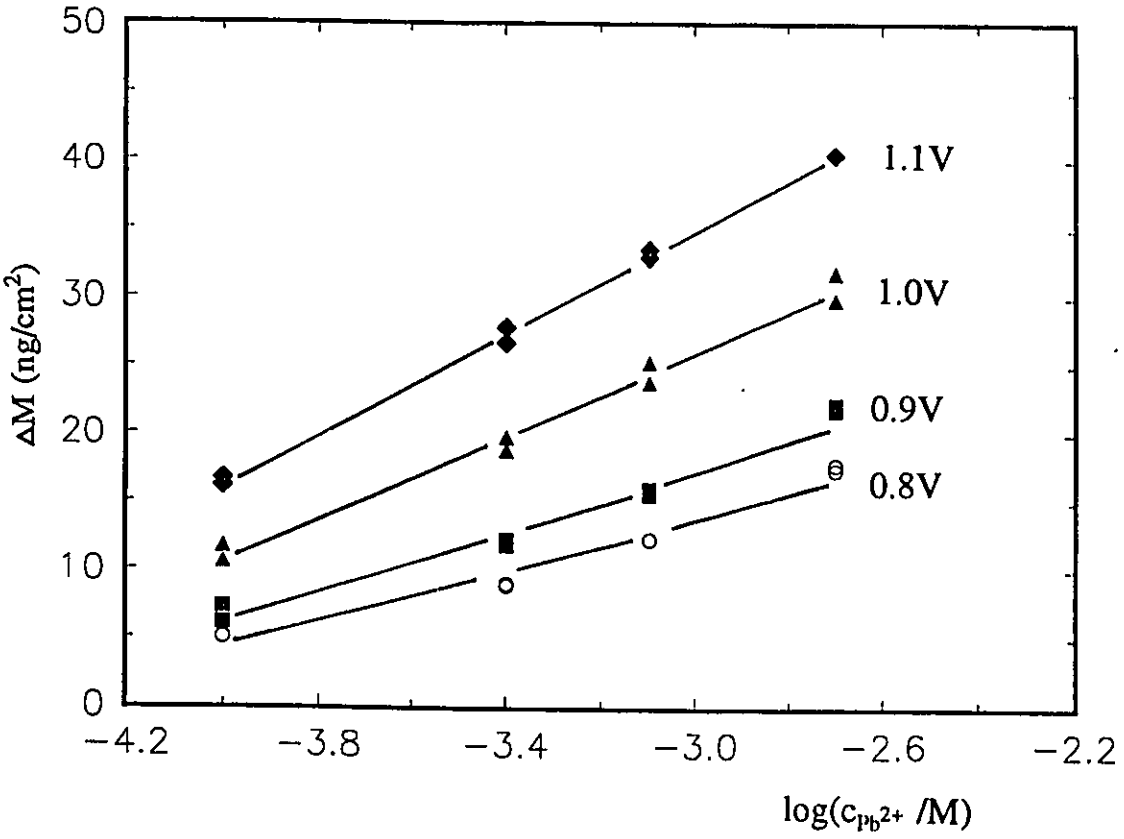

Figure 30. Normalised mass change (ΔM/ng cm^{-2}) resulting from injections of Pb^{2+} into 0.1 M $HClO_4$ at different potentials as a function of log (c_{Pb}^{2+}/M).

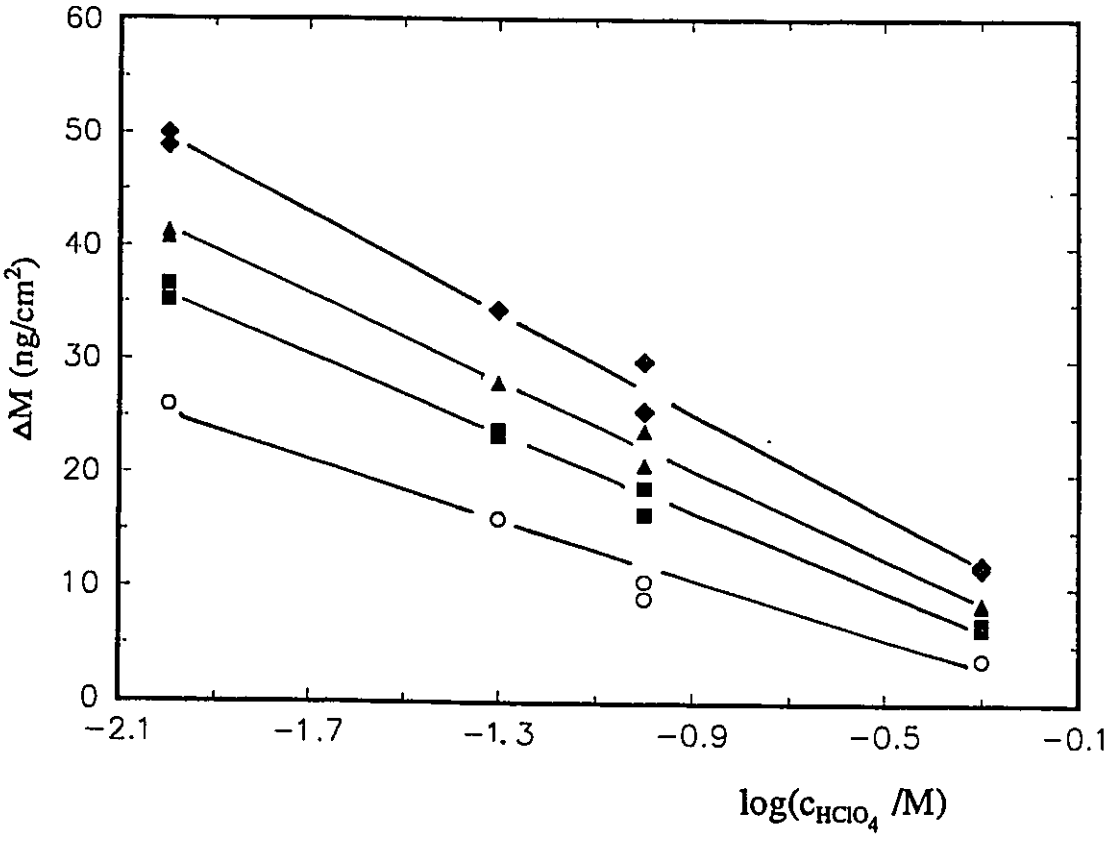

Figure 31. Normalised mass change (ΔM/ng cm^{-2}) as a function of log (c_{HClO_4}/M) at a potential of 1.0V (S.C.E.). o 0.1 mM Pb^{2+}; ■ 0.4 mM Pb^{2+}; ▲ 0.8 mM Pb^{2+}; ♦ 2 mM Pb^{2+}.

linear relationships of Figures 30 and 31 match literature results for the behaviour of $\Delta R/R_o$ for Pb^{2+} on Au[160] and Bi^{3+} on Au[161] respectively. While the presence of adsorbed Pb^{2+} on the oxidised Pt surface is established, the exact influence of these ions on the formation/removal of the oxide is not. Little information can be obtained from the cyclic voltammetry for two reasons.

First, the presence of lead makes little difference to the cyclic voltammograms above 0.8V (interestingly it was reported that for Pb^{2+} at gold, scanning into the upd region resulted in the changes in the CV and reflectivity responses arising from Pb^{2+} adsorption being diminished[160]);

Second, the overlap between oxide and upd regions obscures any effects of cation adsorption on the initial stages of oxide development (clearly visible at gold[160,161]). Stabilisation effects of the cation (resulting in a shift of the reduction peak to more negative potentials) cannot be seen for the same reason.

However, it seems likely that Pb^{2+} interacts with the dipoles of MOH or MO species as suggested previously[161] (a model of cation adsorption on oxidised metals (M) is given in Figure 32, where MOH or MO dipoles with a negative end directed to the solution side may interact with cations). The increased cation adsorption with potential might suggest that interaction is stronger with MO rather than MOH species as more MO will be formed at higher potentials, but no firm conclusions can be drawn without further work. Finally, the effect of background electrolyte seems to indicate that there is some competition for adsorption between anions and cations.

Returning to Figure 30, the amount of adsorbed Pb^{2+} at a given bulk concentration

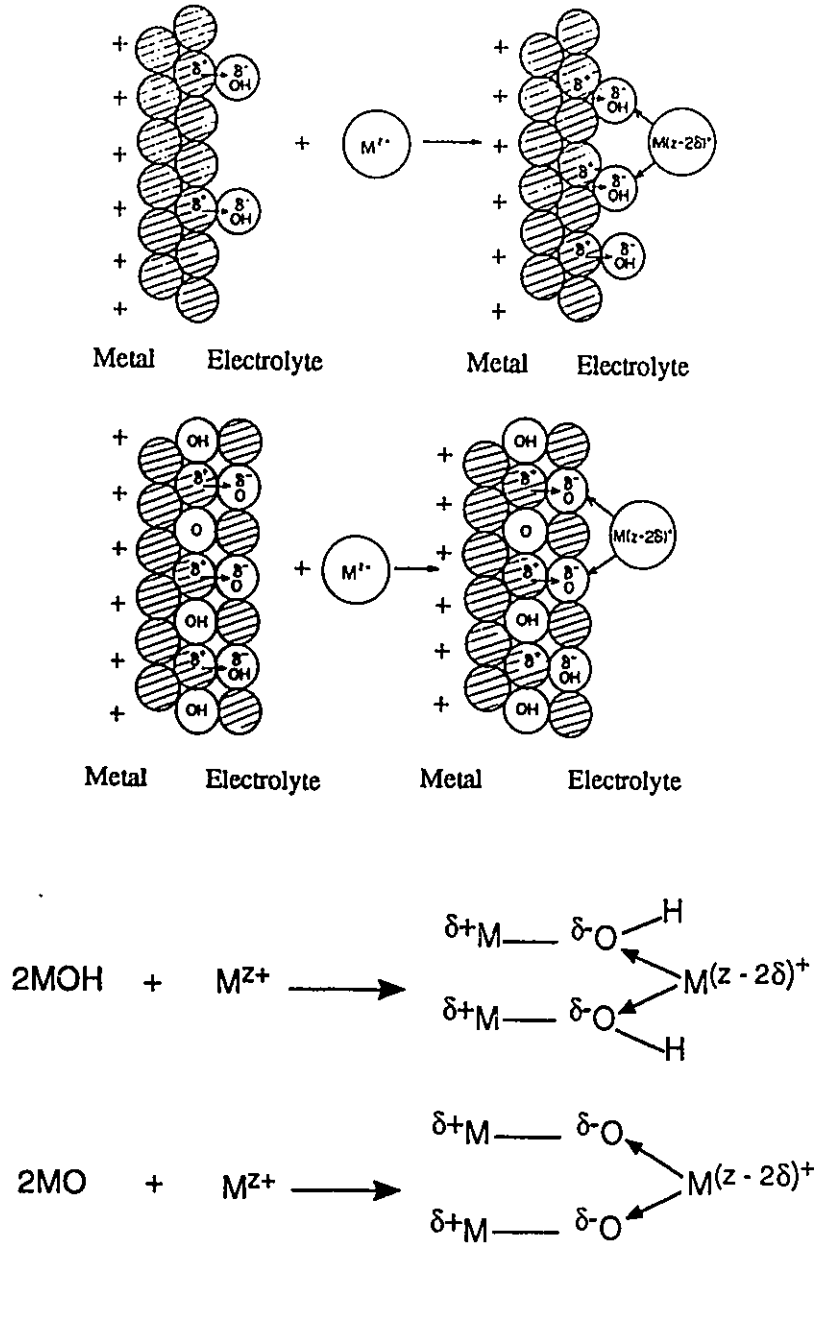

Figure 32. Model of cation adsorption on oxidised metal surface. Hydration shell of cation was not shown. (*from Adzic and Markovic*[161])

was found to increase with potential from 0.8V (the lowest potential used) to 1.1V. This explains the shape of the ΔM response in Figure 28 where ΔM becomes larger from ca. 0.8V onwards (although the increase is smaller at the higher scan rate) on the anodic scan reflecting the larger ΔM between a clean Pt electrode and an electrode where the amount of adsorbed Pb^{2+} increases with potential. These results clearly show the effectiveness of injection experiments for providing a simple, convenient method for the demonstration of adsorption processes at oxidised (and other) electrode surfaces.

The presence of Pb^{2+}_{ads} indicates that the upd process involves a contribution from the discharge of adsorbed species as well as reduction of Pb^{2+} from solution. EQCM studies of other upd systems should therefore include an investigation of the possibility of adsorption prior to discharge since the presence of undetected adsorbed species could lead to a discrepancy between charge and mass data. This is especially true for the Pb/Pt system where a mass increase is observed (as expected), in contrast to the Pb/Ag system in alkaline media where the observation of an unexpected mass decrease is a clear indication of the presence of adsorbed species[186,187].

4.3.4 *ESTIMATION OF EQUILIBRIUM UPD COVERAGE*

When a UPD process takes place, a knowledge of the corresponding equilibrium coverage is important for an understanding of the UPD mechanism. The mass change obtained from the UPD process allows the equilibrium coverage to be estimated directly. In the present work, the surface coverage (the number of upd atoms (n_{Pb}) divided by the number of substrate atoms on the surface (n_{Pt})) was calculated from the mass change using a value

for monolayer coverage of lead of 260 μC cm^{-2}[87,123,252]. For upd atoms whose atomic radius is smaller than that of Pt it is assumed that there is one upd atom per Pt and monolayer charge is the same as that for Pt i.e. 210 z μCcm^{-2}, where z is the charge on the upd ion (here taken to be completely discharged upon deposition). For Pb upd on Pt however, the atomic radius of the upd metal (r_{Pb} = 1.75Å) is greater than that for the substrate (r_{Pt} = 1.38Å)[265] and the number of upd atoms is estimated from the radii using the formula given by Bruckenstein and Swathirajan[172] after Bowles[266] where the number of surface atoms of substrate n_{Pt} is multiplied by $(r_{Pt}/r_{Pb})^2$. Based on the above considerations, the coverage of lead UPD was evaluated using the mass data obtained from two types of experiments: i.e. potential step and injection experiments. The obtained coverage data will be presented below.

4.3.4.1 *Coverages from potential step experiments*

When the potential is in the UPD region, the UPD deposit grows towards its equilibrium coverage over a given time scale. The development of the underpotential deposit and the approach toward an equilibrium coverage at a given potential and Pb^{2+} concentration can be followed by recording the transient mass response resulting from a potential step from an oxide covered surface to a potential at which upd occurs. For potential steps the initial potential was 1V. At this value the electrode potential is such that there will be no upd deposit, although there will be partial oxidation of the platinum surface, and as demonstrated earlier there will also be some adsorption of Pb^{2+}. The final potential was chosen to be in the range where upd of Pb occurs.

A series of transients were recorded first for an electrode in the absence of Pb^{2+}, and then the same experiments were repeated for a series of different concentrations of Pb^{2+}. The

mass was recorded as a function of time in both cases. A typical set of transients are shown in Figure 33. The time required to reach upd equilibrium varied from ca 20s ($[Pb^{2+}]$ = 2mM) to 12 minutes ($[Pb^{2+}]$ = 0.1 mM). The initial shape of the transient response, with an initial mass decrease followed by a mass increase, results from the competition between two processes giving rise to opposite mass changes, namely the reduction of the oxidised Pt surface and the formation of the upd deposit. The contribution of the adsorbed Pb^{2+} ions is harder to discern and could involve no mass change (simple discharge of adsorbed Pb^{2+}) or a mass decrease (ligand expulsion) assuming that the adsorbed species remain on the surface during the potential step. It was assumed here that the adsorbed ions made no contribution to the mass change. The one transient that differs from this picture of a mass decrease followed by an increase is that resulting from a step to 0.5V. A net mass decrease is seen. In fact, for potential steps from 1.0V to 0.5V there is little difference between the mass response seen in the presence and absence of Pb^{2+} and this reflects the fact that upd begins at this potential and the coverage on the surface is very low. Data such as this were not used in establishing the isotherm which is presented later.

For potential steps performed in background electrolyte there is a mass loss that corresponds to removal of surface oxide. On the other hand for experiments where Pb upd occurs, the potential step results in a mass increase as described above and shown in Figure 33. The amount of Pb deposited was thus estimated by adding the mass change observed in the absence of Pb^{2+} to that seen when upd occurs. The resulting coverage value (see below) was then further corrected by addition of the appropriate coverage resulting from reduction of Pb^{2+}_{ads} present on the surface at 1.0V (Figure 30). The coverage values obtained from these potential steps are shown in Figure 34 as a function of underpotential, E_{UPD}. E_{UPD} is

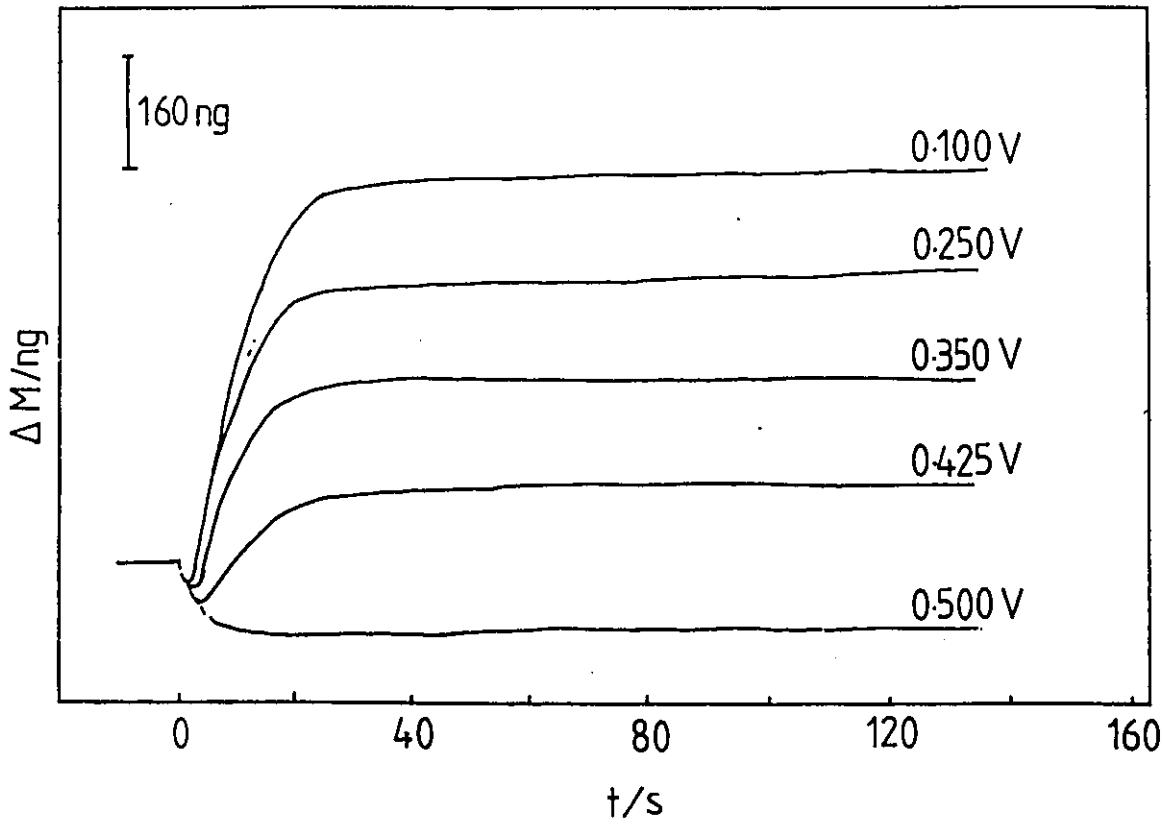

Figure 33. A typical set of mass-time transients for potential steps in the presence of 0.8 mM Pb^{2+}. Potential was stepped from 1.0V to the potential shown in the diagram.

the difference between the electrode potential (vs.S.C.E.) and the potential calculated from the Nernst equation for the appropriate value of $[Pb^{2+}]$. With values of -0.1263V for the standard potential of the Pb/Pb^{2+} couple and 0.2443V for the S.C.E (both vs. S.H.E.)[267] this yields a Nernst potential of -0.4886V for 0.1mM Pb^{2+}. Thus the E_{UPD} value of 0.0V corresponds to this point.

4.3.4.2 *UPD Coverages from injection experiments*

The transient response necessarily involves both reduction of oxide and formation of the upd deposit, so a second estimate of surface coverage was made by the injection method where mass transients were recorded after a concentrated solution of Pb^{2+} was injected into the electrolyte with the potential again held at a value where upd occurs. In this case the electrode was first subjected to oxidation/reduction cycles in 0.1M $HClO_4$ to ensure a clean reproducible surface and the potential was halted at the chosen value for injection on the anodic scan. This allows the experiments to be performed over a range of potential up to the point where surface oxidation of the platinum begins. The coverages calculated from the mass changes for the injection method are also shown in Figure 34 for Pb^{2+} concentrations of 0.1 mM and 2 mM. In this case there is no need for correction for the mass change resulting from adsorption on the oxidised surface since the transient represents the mass difference between a clean Pt surface and one with a upd deposit, whereas for the potential steps the initial surface is oxidised Pt with partial coverage of adsorbed Pb^{2+}. Inspection of Figure 34 shows that the results obtained from the two different types of transient are in reasonable agreement with each other. The combined data form a coverage/underpotential isotherm that agrees remarkably well with results obtained previously in 0.12M $HClO_4$ using an RRDE[87].

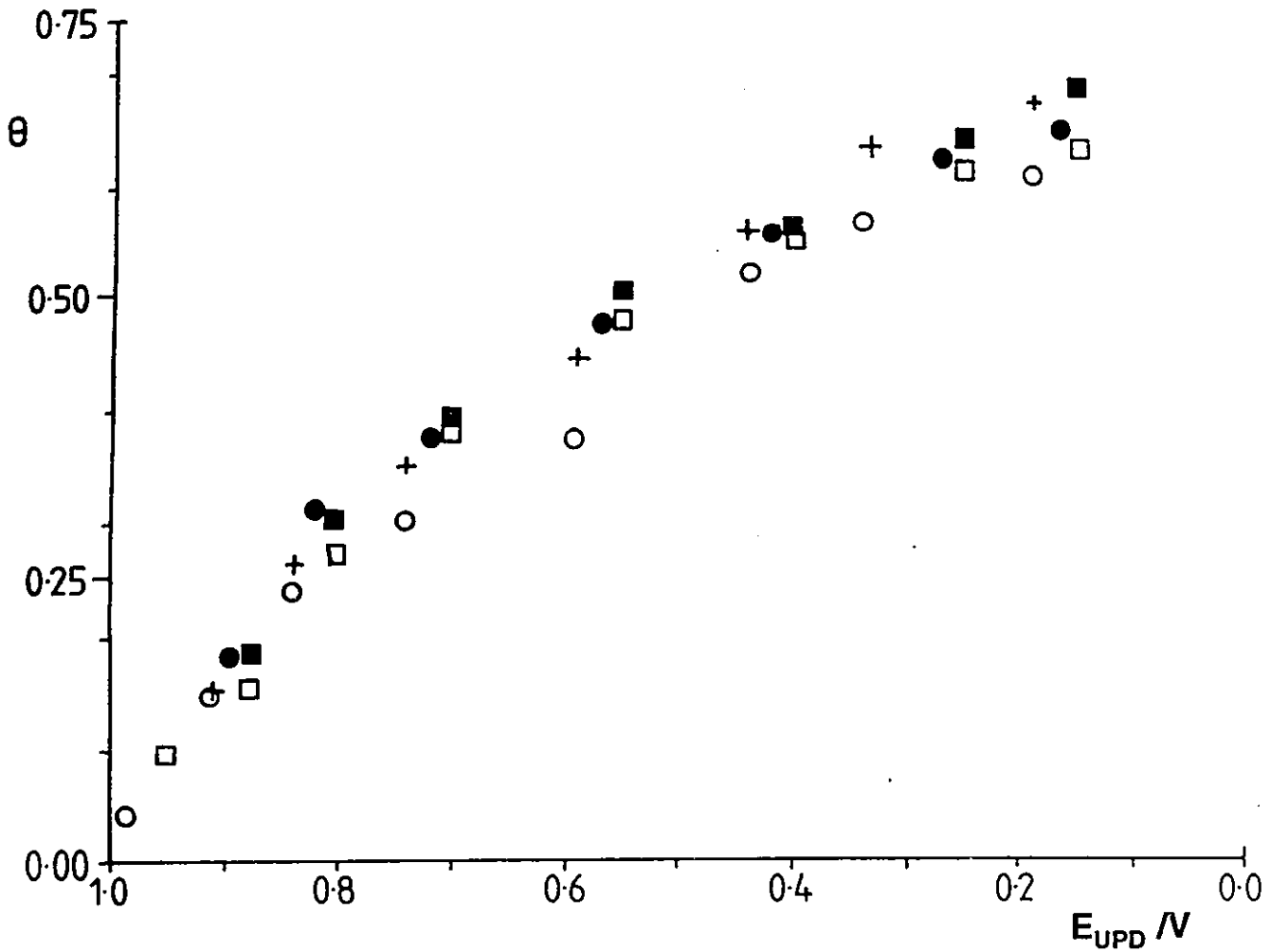

Figure 34. Coverage θ, as estimated from potential step (+,■,●) and injection (□,○) transients plotted as a function of E_{UPD}. Experiments were performed at $[Pb^{2+}] = 1 \times 10^{-4}$M (+,○), 4×10^{-4}M (●) and 2 mM (■,□).

The use of mass measurements alone for the compilation of a upd isotherm is seen to be simple and remarkably accurate. There are likely to be some errors resulting from double layer and specific adsorption differences between the platinum electrode and a partially lead covered platinum electrode as discussed earlier, but the advantage of the study of lead in this particular case is that it is a heavy metal (as are most other upd species) which produces a large mass change and this will minimise those effects. The choice of perchlorate as the anion is also important since it gives rise to less specific adsorption than bisulphate/sulphate or halides.

4.3.5 *CONCLUSIONS*

1. Cyclic voltammetric experiments with the EQCM reveal, as expected, large mass changes resulting from lead upd and the stripping process is also clearly revealed in the mass response. When the bulk lead concentration is low, comparison of the mass response with that recorded on clean Pt reveals the continued development of the upd deposit during the potential scan.

2. Simple injection experiments have revealed the presence of adsorbed Pb^{2+} on oxidised Pt as well as some competition between cations and anions for sites on the oxidised Pt surface. Thus the upd process proceeds at least partly through discharge of adsorbed ions.

3. Equilibrium upd coverage data obtained from potential step/mass transient experiments over a range of concentration agree well with those found by injection experiments after correction for adsorbed Pb^{2+} in the former. Both sets of data agree well with previously published isotherms and show that simple EQCM mass measurements can

provide good estimates of coverage data for UPD.

4.4 BISMUTH

4.4.1 *INTRODUCTION*

Compared to other UPD metals such as Pb, bismuth behaves differently in its adsorption and underpotential deposition. There are two principal differences for Bi:

i) The first is that Bi can be adsorbed, irreversibly, onto a Pt electrode by exposing an electrode to a solution of Bi^{III} at open circuit. This has been shown for polycrystalline Pt in 1.0M HCl by Szabo and Nagy[268] and for Pt single crystals by Clavilier et al.[269] using 0.6M $HClO_4$. The redox reaction of the adsorbed Bi was suggested by these latter authors to be a good probe for the detection of (111) surface domains on Pt surfaces. The fact that Bi deposits in this way at Pt electrodes at open circuit allows the preparation of electrodes with upd coverages that can be easily controlled and varied. These electrodes can then be transferred to a solution where the effect of coverage on electrocatalytic processes can be studied in the absence of Bi ions in solution. A recent example of such work is provided by a study of ethylene glycol oxidation at Pt(111) electrodes modified by bismuth[270].

ii) In addition to the irreversible adsorption of Bi the second principal difference between Bi and other upd metals is that the solution chemistry of Bi^{III} is somewhat more complicated than say, that of Pb^{II}. Bi^{III} undergoes hydrolysis[271], and in non-complexing media (such as perchloric acid) ions such as $BiOH^{2+}$, BiO^{+} ($Bi(OH)_2^{+}$) and $Bi_6(OH)_{12}^{6+}$ can be present in concentrations dependent on the pH and the bulk concentration of Bi^{III}.

The upd of Bi at Pt has been investigated previously by Bowles[255] in both HCl and $HClO_4$ and by Bruckenstein and Cadle[256] in 0.12M $HClO_4$. Bowles reported the formation of a layer of adsorbed species, postulated as being BiO derived from BiOCl, on top of the upd Bi layer in 0.1M HCl (but not in 1.0M HCl or in $HClO_4$ solutions) while Bruckenstein and Cadle used a ring-disc electrode to demonstrate that Bi species adsorb irreversibly at oxidised Pt and to formulate a model for the deposition of Bi whereby two successive monolayers of upd Bi form before two further layers, bulk Bi and a Pt-Bi alloy are deposited in a complex manner.

In this section, the adsorption of Bi species at oxidised Pt surfaces, the underpotential deposition of Bi and the behaviour of irreversibly adsorbed Bi have been studied using the electrochemical quartz crystal microbalance (EQCM) method. In particular, the role of adsorption of Bi in the upd process was assessed, taking into account the more complex solution chemistry of Bi. Finally the behaviour of adsorbed Bi in electrolytes free from the cation was also examined.

4.4.2 *ADSORPTION PRIOR TO UNDERPOTENTIAL DEPOSITION*

At Pt, the underpotential deposition of bismuth bears a strong resemblance to that of lead: i.e. the onset of the UPD coincides with the initial stages of reduction of the surface oxide film[256], and the stripping of upd Bi overlaps with the initial stages of oxidation of the surface on the positive-going half of a voltammogram. Although upd of Bi can only occur on reduced Pt, the surface is not free of bismuth at potentials outside the upd region since bismuth cations are adsorbed on the oxidised electrode surface prior to discharge[161,256]. Thus

a description of the interaction of cations with the oxidised electrode surface is presented here first. Such adsorption is easily quantified through injections of aliquots of concentrated solutions of Bi^{III} into the background electrolyte with the electrode poised at a constant potential as described in the previous section.

Figure 35 shows typical transients observed upon addition of Bi^{III} to the background electrolyte at three different potentials, two in the region where the electrode surface is oxidised (curves 1 and 2) and a third in the upd region (curve 3). Each series of additions of Bi at constant potential was performed on a clean electrode surface free from Bi. There was no observable current associated with the mass transients for potentials in the region positive of upd.

A collected set of data for experiments at oxidised electrode surfaces is shown in Figure 36 for additions of Bi^{III} to three different electrolytes (0.1M $HClO_4$, 1.0M $HClO_4$ and 0.1M $HClO_4$/0.9M $NaClO_4$). ΔM (ng cm^{-2}), the observed mass change per unit area, is shown as a function of both potential and the total concentration of Bi^{III}. We first consider the data for 0.1M $HClO_4$ (Figure 36a, open symbols). The behaviour of Bi^{III} species in this electrolyte is found to be different in two respects from that of Pb^{2+} shown in the preceding section (Figure 30).

1. For a given potential and concentration of ions, the normalised mass changes are significantly (about 5 times) larger for Bi which, given the almost identical weights of Bi and Pb indicates a much higher coverage of Bi species on the electrode surface;

2. In addition, although mass transients observed upon addition of Bi^{III} were large, it was found that the mass tended to increase very slowly with time (Figure 35) and the degree of scatter between different experiments was larger when compared to experiments with Pb^{2+}

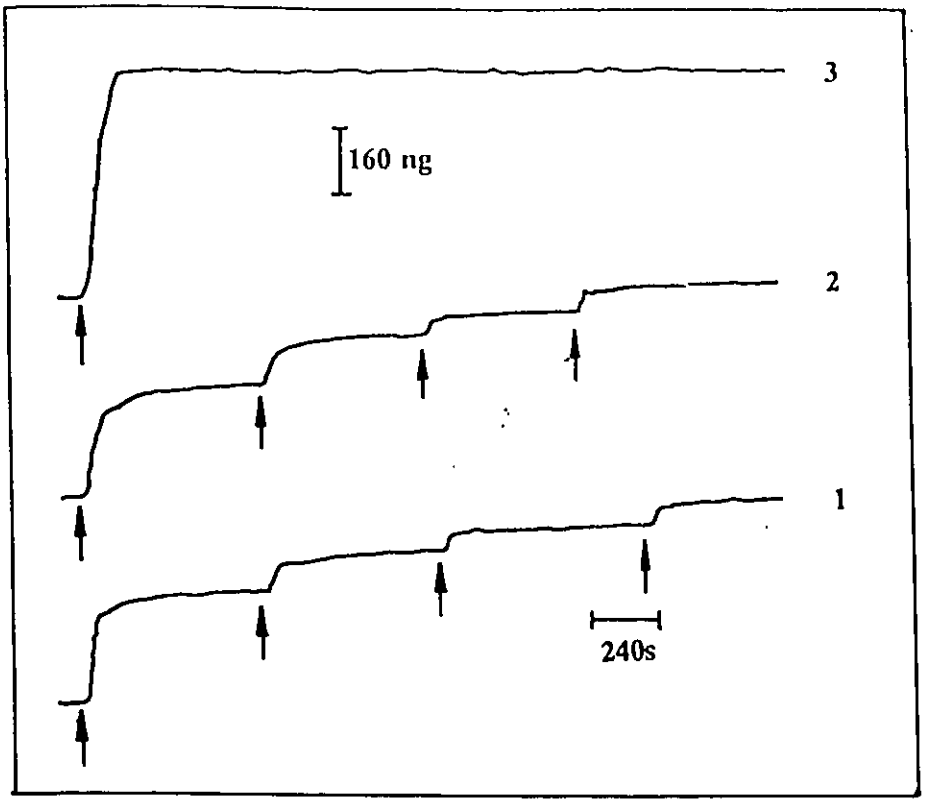

Figure 35. Mass transients observed at a Pt EQCM electrode upon addition of aliquots of Bi^{III} to 0.1M $HClO_4$. The potential was held at 1.1V (1), 0.7V (2) and 0.4V (3). The arrows indicate additions of Bi^{III} and the concentration of Bi^{III} was increased in stages from 0 mM to the following values for curves (1) and (2): 0.1 mM, 0.4 mM, 0.8 mM, 2 mM. The bulk Bi^{III} concentration for (3) was 0.1 mM. Responses are displaced for display purposes only. Electrode area was 2.5 cm^2.

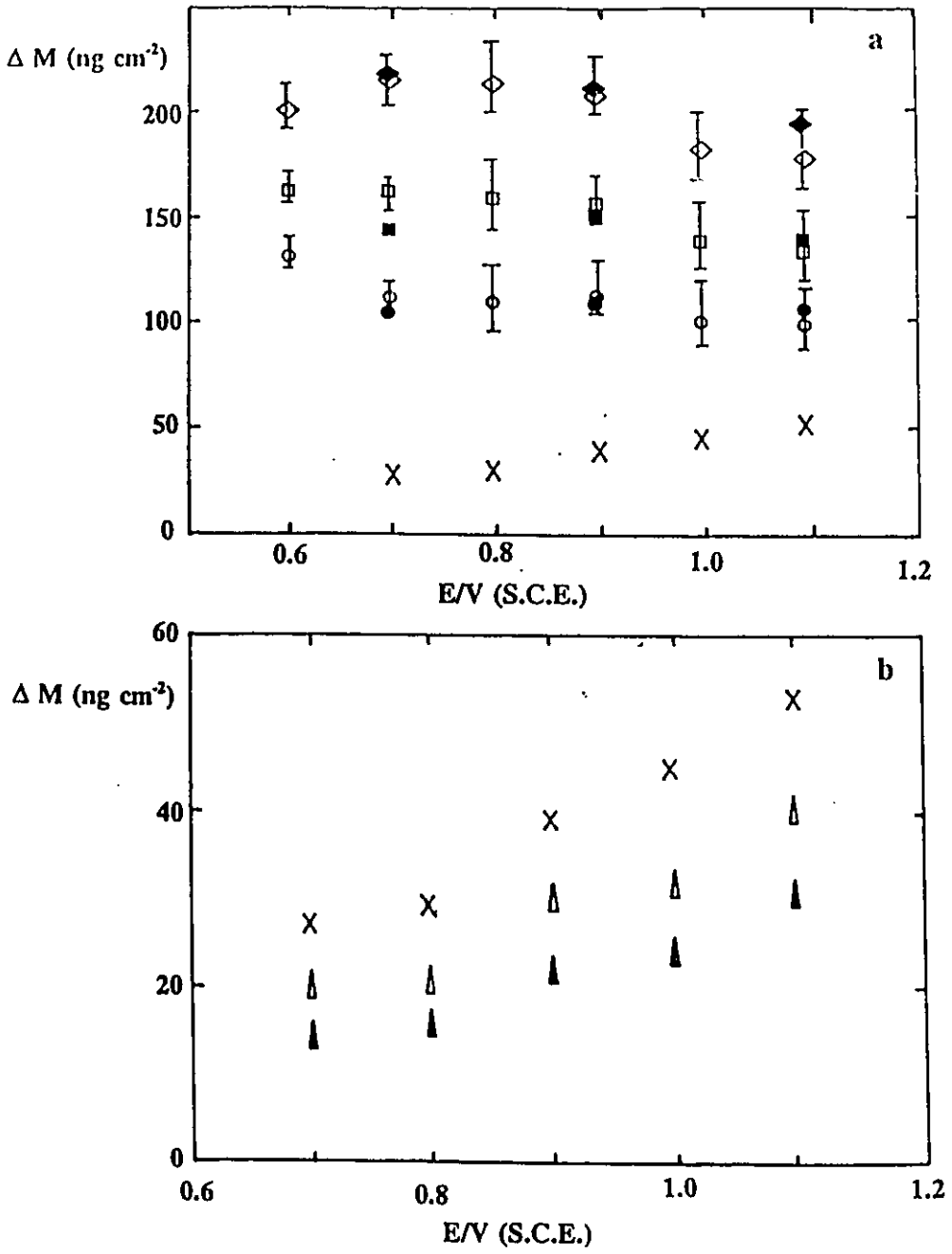

Figure 36. Normalised mass change ΔM (ng cm^{-2}) resulting from the adsorption of Bi species at an oxidised Pt electrode held at constant potential in three different electrolytes. a) Data for 0.1M $HClO_4$ are open symbols, data for 0.1M $HClO_4$/0.9M $NaClO_4$ are solid symbols. [Bi^{III}] was 2 mM (◊,♦); 0.4 mM (□, ■) ; 0.1 mM (o, o). For open symbols, the symbol represents the average value observed in several experiments, and the bar the upper and lower values observed. Also shown are data for 2 mM Bi^{III} added to 1.0M $HClO_4$ (X) for purposes of comparison. b) Data for 1.0 M $HClO_4$ with differing amounts of Bi^{III} added. [Bi^{III}] was; 2mM (X), 0.4 mM (△), 0.1 mM (▲). Note the different scales on the potential and mass axes.

in the same background electrolyte and to experiments with Bi^{III} in the other electrolytes used here.

Thus in Figure 36, each measurement in 0.1M $HClO_4$ was made 3 or 4 times. The central point represents the average value of 3-4 readings and the bars indicate the highest and lowest values obtained in a set. Given this limitation, two general conclusions emerge from the data for 0.1M $HClO_4$.

i) First, the amount of adsorbed Bi^{III} is dependent on the concentration of ions added (as for Pb^{2+});

ii) Second, in contrast to the results found for Pb^{2+}, there does not appear to be a significant effect of potential on the mass change, within experimental error, although there may be a slight decrease in the extent of adsorption at the highest potentials.

Turning now to the data for 1.0M acid (Figure 36b), the ΔM values are a fraction of those seen in the weaker acid. Furthermore, the mass transients observed in 1.0M acid were found to reach a stable plateau, and the adsorption appears to mimic that of Pb^{2+} in 0.1 M $HClO_4$, in that ΔM values are similar (implying roughly equivalent coverages since Bi and Pb have almost identical molecular weights) and increase with both potential and concentration of Bi^{III}.

These simple EQCM experiments reveal a dramatic difference in the adsorptive behaviour (as represented by ΔM values) of Bi^{III} at oxidised Pt between the two perchloric acid solutions. This could be a result of either a pH effect or an anion concentration effect, or possibly both. Consideration of the data set for injection of Bi^{III} into 0.1M $HClO_4$/0.9M

$NaClO_4$ (Figure 36 a, solid symbols) which coincides, within experimental error, with that for 0.1M $HClO_4$ indicates that the former explanation is the correct one. There is a significant effect of pH on the extent of adsorption of cationic Bi species at oxidised Pt. This is most probably derived from the influence of pH on the distribution of ions present. In aqueous perchloric acid solutions, which are non-complexing, Bi^{III} can exist in a number of forms. For example, consultation of the literature[271-273] provides stability constant values for the formation of $BiOH^{2+}$, $Bi(OH)_2^+$ (sometimes represented as BiO^+) and $Bi_6(OH)_{12}^{6+}$, although there is considerable disagreement regarding the identity and quantities of species present. Much of the discussion on this matter comes from the polarographic literature where in perchloric acid solutions at low pH only one wave is seen whereas when the pH rises above 1.2 a second wave appears. Unfortunately, there is no clear agreement on the causes of these two waves[273,274]. Taking one point of view, the potentiometric data of Olin[273] suggested the presence of Bi^{3+}, $BiOH^{2+}$ and $Bi_6(OH)_{12}^{6+}$ in 3.0 M $(Na,H)ClO_4$ as the Bi^{III} concentration was increased from 0.1 mM to 50 mM. No evidence was found for the presence of $Bi(OH)_2^+$. Moorhead and Lipcsey[275] then used the data of Olin[273] to calculate the species present in a 1 mM Bi^{III} solution in 1.0 M $(Na,H)ClO_4$ solution. Their calculations indicated that Bi^{3+} is the only species present at pH 0, while above pH 1 Bi^{3+} and $BiOH^{2+}$ are in equilibrium with the hexamer. The percentage of total Bi^{III} as Bi^{3+} is only 80% at pH 1 with the remaining 20% being almost completely $BiOH^{2+}$. Similar data for 10^{-5} molal Bi^{III} solutions show that at pH 0 the Bi^{III} present is 80% Bi^{3+} and 20% $BiOH^{2+}$ while at pH 1 the ratio is closer to 50:50 [271]. The information above leads to the suggestion that the most sensible explanation for the data of Figure 36 is that at pH 0 (1.0M $HClO_4$) the mass increases result largely from adsorption of Bi^{3+}, which is virtually the only species present under the

conditions used here. However, as the pH increases to 1, $BiOH^{2+}$ begins to be present in significant quantities (though its concentration remains substantially less than that of Bi^{3+}). This ion seems to have a higher affinity for adsorption leading to the considerable increase in the mass change as the pH increases from 0 to 1 for the same total Bi^{III} concentration. It is also quite possible that there is some adsorption of $Bi(OH)_2^+$, which may be in equilibrium with the hexamer[275]. However, given the lack of agreement on the exact nature of hydrolysed Bi^{III} species that are present it is hard to be more specific than this.

The general conclusion that the increase in ΔM with increasing pH is largely due to increased amounts of $BiOH^{2+}$ and perhaps $Bi(OH)_2^+$, together with the higher affinity of these ions for adsorption at an oxidised Pt surface, is reinforced by some preliminary data from 0.1M $NaClO_4$. In this electrolyte, addition of sufficient Bi^{III} to yield a bulk concentration of 0.1mM at a potential of 1.0 V (S.C.E.) gave a mass change of 220 ng cm^{-2}, almost double the corresponding value observed in 0.1M $HClO_4$ (see Figure 36a). This would appear to reflect the larger amount of hydrolysed Bi^{III} species present in neutral media.

The final point of discussion here is the mechanism by which the hydrolysed Bi^{III} species interact with the oxidised surface. Kozawa[276] has noted the influence of cations such as Ca^{2+}, Ba^{2+} and Sr^{2+} on oxygen evolution at Pt in 0.1M NaOH and suggested an ion exchange mechanism, but Adžić and Marković[160,161] indicated that this was unlikely to explain adsorption of cations in acidic solutions. These latter authors suggested that an interaction between cations with MO or MOH dipoles as already discussed in Section 4.3.3 (the surface will gradually change from partial coverage of PtOH through full coverage of PtOH to PtO as the potential becomes more positive) was the most likely explanation. A similar explanation could be advanced here in part, but it seems clear that the OH groups of

$BiOH^{2+}$ and $Bi(OH)_2^+$ have a strong effect on the adsorption, perhaps through hydrogen bonding interactions with the surface. While in the work presented here we are dealing with cation adsorption onto positively charged electrode surfaces, it is interesting to note a parallel situation where hydrogen bonding has also been invoked to explain adsorption where simple electrostatic considerations would suggest that it was unlikely. The example in question[277] involves the adsorption of certain organic and inorganic anions on colloidal oxides at pH values above the isoelectric point where the colloid carries a net negative charge. This adsorption was suggested to be a result of hydrogen bonding between negatively charged surface oxides and the hydroxyl functionalities of the anions. For the situation presented here there would be no surface oxide ions but one might envisage hydrogen bonding between PtO and $BiOH^{2+}$ or between PtOH and $Bi(OH)_2^+$ (BiO^+). However, despite some similarities between the two cases it is clear that further experimental evidence is needed before firm conclusions can be drawn regarding the nature of the interaction between Bi^{III} species and the oxidised Pt surface.

4.4.3 *UNDERPOTENTIAL DEPOSITION*

The adsorption phenomena reported earlier above have a significant effect on the upd response, although this is not apparent from the voltammetry alone. A typical result for the upd in 0.1M $HClO_4$ is shown in Figure 37 for a 0.1 mM solution of Bi^{III}. The mass was also recorded alongside the voltammogram, and the responses for Pt are shown for comparison. In the voltammetric response, the development of the upd Bi deposit causes the peak due to the reduction of the oxidised Pt surface to broaden and increase in size relative to the

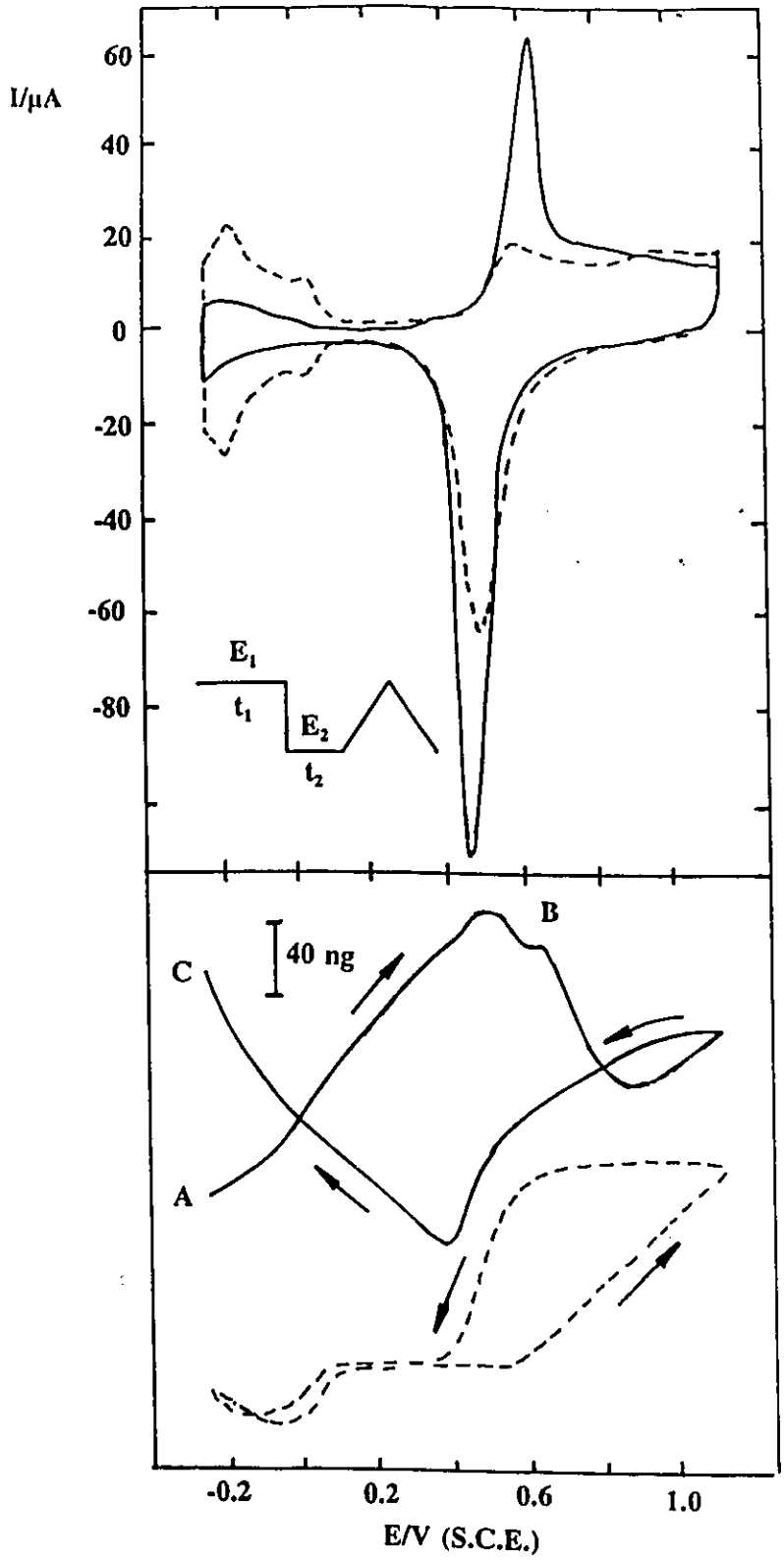

Figure 37. Cyclic voltammogram (top) and mass response for upd of 0.1 mM Bi^{III} at Pt in 0.1M $HClO_4$ (solid lines), responses for clean Pt are shown for comparison (dashed lines). The voltage programme used to record the response is shown in the inset, E_1 = 1.1V, t_1 = 120s, E_2 = -0.25V and t_2 = 60s. Note that mass increases up the page, and that the response for Bi has been shifted down by 460ng compared to that in background electrolyte alone. The electrode area was 4.01 cm^2 and the scan rate 5 mV/s.

voltammogram in the absence of Bi. Coverage of Bi may be gauged from the partial suppression of the H upd peaks, since H does not adsorb on Bi, and the sharp stripping peak is seen at ca. 0.6V as the upd deposit is removed.

In considering the accompanying changes in mass, several points are worthy of comment. First, the response for 0.1mM Bi^{3+} has been displaced by an amount equivalent to 460 ng compared to that in 0.1M $HClO_4$ alone in the figure (by means of a voltage offset as described in chapter 3). This reflects the large amount of adsorption of Bi^{III} on the oxidised surface, revealed above, and is a figure which is in accord with the ΔM data from Figure 36 for this concentration of Bi^{III} (after noting that Figure 37 shows the absolute mass change rather than the mass change per unit area). As a consequence of this extensive adsorption of Bi cations prior to discharge, the changes seen in the mass during the voltammogram are quite small, especially given the extent of coverage that is produced in the experiment (discernible from the suppression of H adsorption/desorption current). Clearly most of the upd deposit derives from reduction of adsorbed Bi species. The changes seen in the mass response thus represent, by and large, only that contribution from Bi^{III} in solution.

The anodic scan begins at point A, after the potential step from 1.1V and the pause of 60s at -0.25V. The mass increases throughout the whole of the anodic scan until stripping begins. This increase may be attributed to the fact that the deposit has not reached its equilibrium coverage value and continues to develop during the anodic scan. Similar results were observed for the upd of Pb at Pt as shown in the preceding section. As the stripping peak is seen in the voltammogram, so the mass begins to decrease, but there is an unusual arrest seen (point B) which does not appear to correspond to any feature in the voltammogram. The remainder of the mass cycle is as expected, and is broadly similar to that

seen for Pb^{2+}, with an increase as the oxidation of the surface develops, a decrease as this process is reversed on the negative going scan and then the increase in the latter stages of the cathodic scan as the upd deposit grows. The mass does not form a closed loop. At the end of the scan (point C) mass is larger than at point A. This reflects the fact that the deposit has proceeded further towards its equilibrium value after the negative going half of the scan than it had after the potential step and pause that preceded the anodic section of the curve. There may also be some subtle contributions to the mass such as possible expulsion of water or OH from adsorbed Bi^{III} species ($BiOH^{2+}$ or $Bi(OH)_2^{+}$) that are discharged to form the upd deposit. The extent of specific adsorption of anions may also vary as the Bi coverage increases and as the pzc of the surface changes with upd coverage. However, the observed response suggests that the upd deposit is derived mainly from discharge of adsorbed species with a smaller contribution from Bi^{III} diffusing from solution.

The most interesting feature of the mass response is the decrease that occurs between 0.4V and 0.9V on the anodic scan. This is presumably associated with the removal of the fraction of Bi that does not remain adsorbed on the surface following oxidation. However, it does not proceed in one smooth step. As noted above, there is an arrest at ca. 0.62 V (point B). This arrest was not seen in 1.0 M $HClO_4$, even when the coverage was increased by using a longer holding time, nor was it seen in 0.5M H_2SO_4. There is also no indication of any such feature in the stripping of upd Pb under similar circumstances. The experiment of Figure 38 provides a clearer picture of the cause of this arrest. In this experiment, the potential at which the anodic scan was started (after a step from the value of 1.1V, was gradually made more positive). The voltammetry resulting from this experiment is as expected in that the coverage (except at the most positive potential) is largely the same reflecting the same time

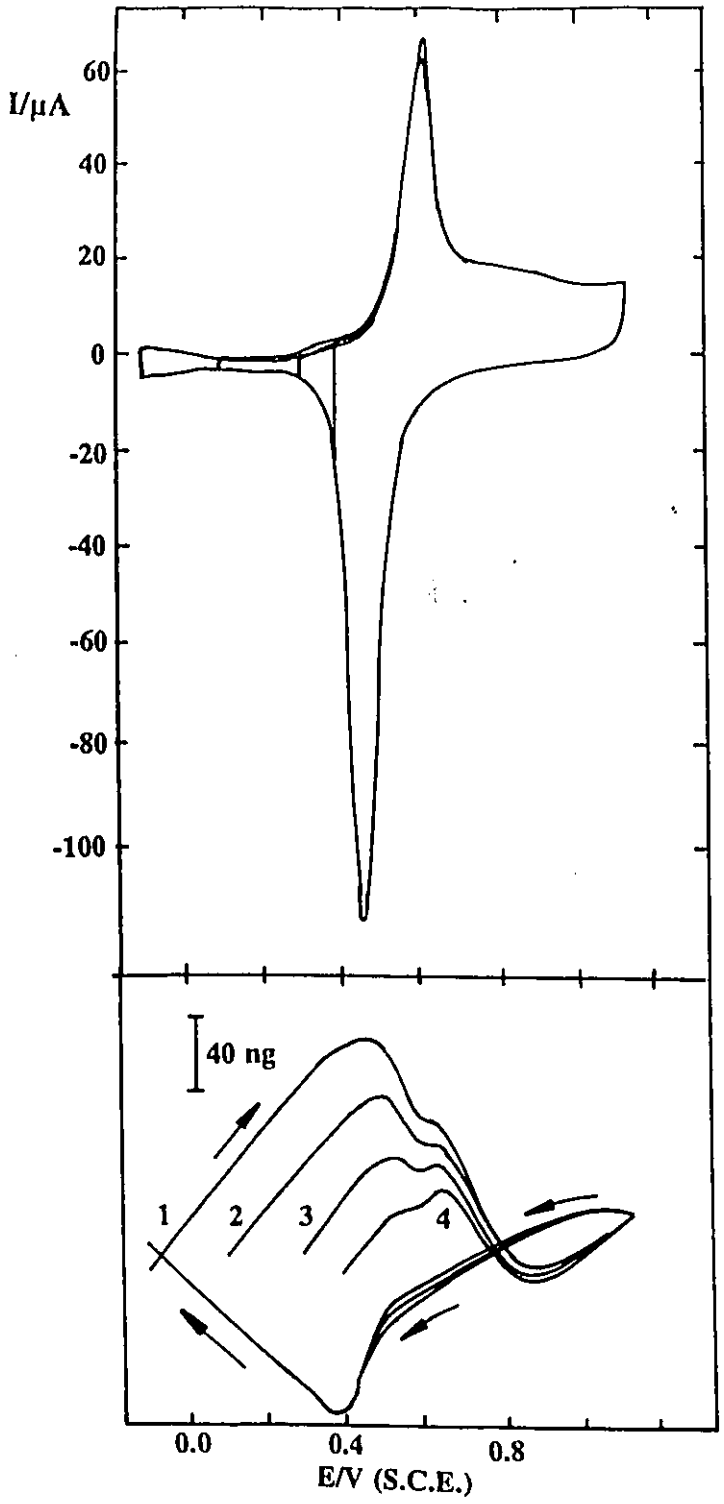

Figure 38. Cyclic voltammograms and mass responses for upd of 0.1mM Bi^{III} in 0.1M $HClO_4$. The potential programme used was as for Figure 37, with a variable E_2. Values of E_2 were : 1) -0.1V, 2) 0.1V, 3) 0.3V, 4) 0.4V. The electrode area and scan rates were as for Figure 37. Mass offset was not changed during these experiments.

of holding. The mass responses all begin at roughly the same mass for the same reason, and all increase during the initial stages of the anodic scan. However, as the holding potential becomes more positive, the increase in coverage (and hence mass) that takes place between the beginning of the anodic scan and the stripping peak is decreased and the arrest is shown to reflect a small mass increase (curve 4). The most sensible explanation for this feature is that it corresponds to conversion of some Bi^{III} on the surface to $BiOH^{2+}$ or $Bi(OH)_2^+$. These species are less likely to be present in 1.0 M $HClO_4$ (or in 0.5M H_2SO_4, as discussed above) where no arrest was seen. After this feature the mass continues to decrease, presumably as small amounts of Bi^{III} are lost into solution, before the oxidation of the electrode surface becomes the dominant process and leads to the final increase in mass as the anodic scan limit is approached.

It is important to realise that the overall mass response may represent a composite of several processes, for example as the upd Bi is oxidised there may be expulsion of Bi^{III} into solution, growth of the oxide on the electrode surface, conversion of Bi^{III} to $BiOH^{2+}$ or $Bi(OH)_2^+$, and then perhaps loss of a fraction of these last species into solution. Under these circumstances, it is difficult to make an unequivocal assignment to any feature in the mass response. However, in conclusion it may be said that the EQCM data supplements the information available from voltammetry in three important ways. First, most of the deposit is seen to derive from previously adsorbed Bi^{III} species. Second, changes in coverage during a voltammetric scan are easily visible and finally, a feature of the mass, namely the small increase indicated in Figures 37 and 38, provides information on surface processes of the adsorbed Bi^{III}. This last aspect is developed further in the following section.

4.4.4 *VOLTAMMETRIC AND MASS BEHAVIOR OF ADSORBED Bi SPECIES*

Exposure of a Pt electrode, either at open circuit or at a fixed potential, to a solution of Bi^{III} results in the irreversible adsorption of Bi species on the electrode surface[268,269]. An electrode treated in this way can then be removed from the electrolyte containing Bi ions, rinsed if desired, and immersed and examined in a background electrolyte. A typical voltammogram and two mass responses for a similar experiment are shown in Figure 39. Here the potential was poised at 1.1V in a solution of 0.1 mM Bi^{III} before the electrode was rinsed and transferred to a fresh electrolyte where the voltammogram and mass response were recorded. The adsorption step was also performed with the electrode potential in the upd region, but there was no observable difference between the results of the two experiments. The presence of adsorbed Bi species is clearly revealed in the voltammetry, particularly through the upd stripping peak (peak A). Both the voltammetry and the mass response indicated that the amount of adsorbed Bi decreased slowly with time since the extra charge was seen to decrease and the mass response showed a coincident shift to lower mass values. The data in the Figure represent a stable system which did not change further with time. The coverage of Bi species can be estimated from the suppression of the peaks due to underpotential deposition of H and is quite small in this experiment.

Upon initial inspection, the mass responses look remarkably similar (note that the offset for each response is the same and the two curves represent the absolute masses observed). However, there is a subtle difference that is revealed when the background response for Pt is subtracted from that for Pt with adsorbed Bi. (Careful inspection of the response with adsorbed Bi also shows a change in the rate of increase of mass at ca. 0.6V on the anodic scan). This data is shown in Figure 40. Two points should be noted:

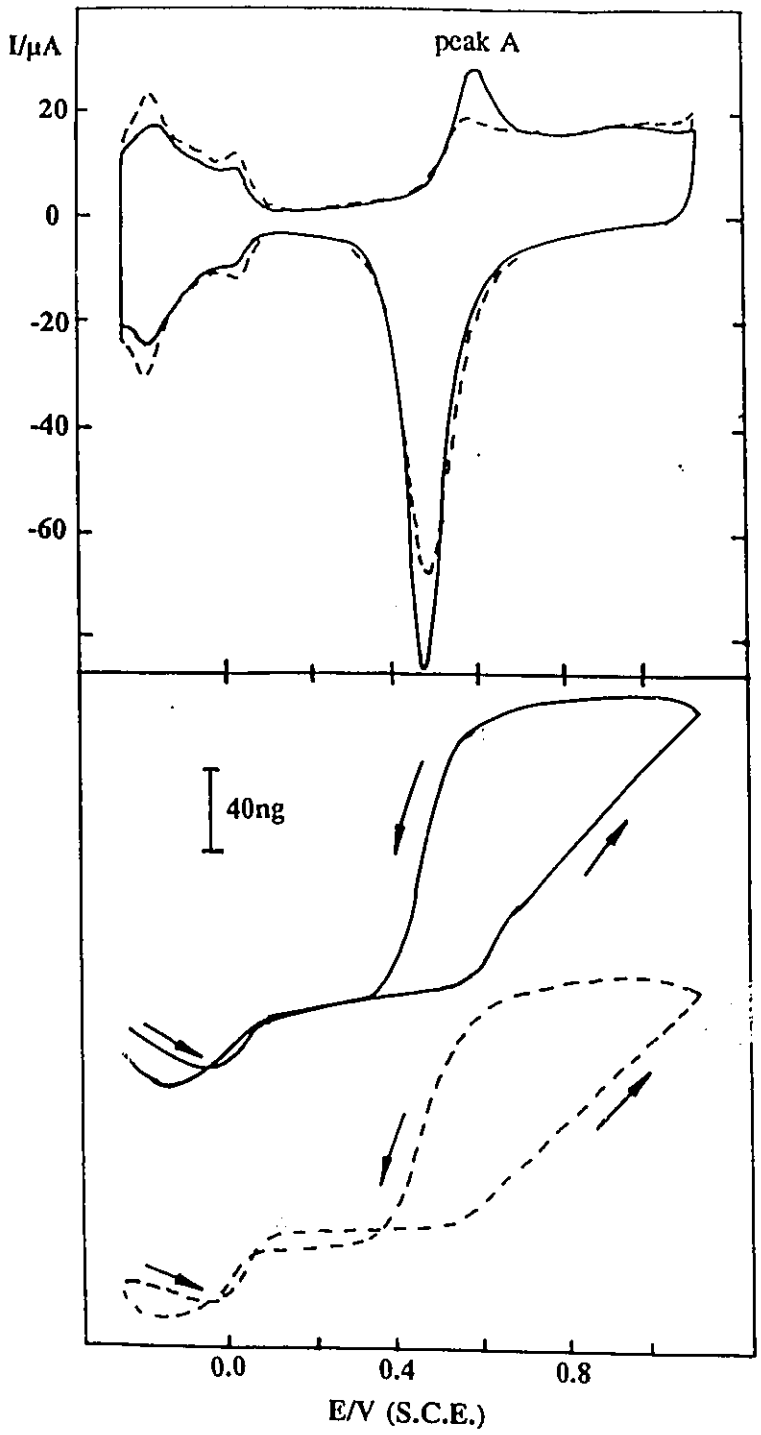

Figure 39. Cyclic voltammograms and mass responses for clean Pt in 0.1M $HClO_4$ (dashed lines) and Pt after exposure to a solution of 0.1 mM Bi^{III} for 15 minutes at 1.1V followed by transfer to a fresh 0.1 M $HClO_4$ solution. The potential programme used to record responses was exactly as shown in Figure 37. Mass responses are shown as recorded. The electrode area was 4.49 cm^2 and the scan rate 5 mV/s.

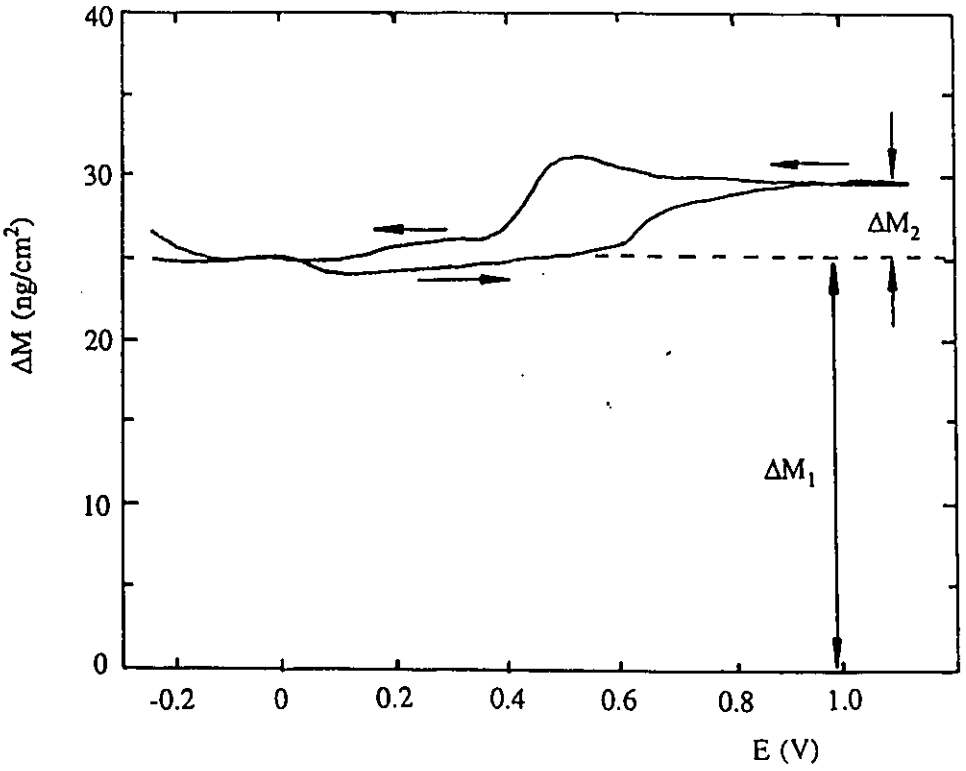

Figure 40. Mass difference (ΔM) between responses of Figure 39 plotted as a function of potential.

1. The mass difference data, as well as the original mass responses themselves, form a closed loop indicating that no material is lost from the electrode surface during the cycle;

2. A mass change occurs in parallel with the oxidation/reduction current for Bi upd.

The mass increases during the positive-going scan at ca. 0.6V and decreases in the subsequent negative-going scan at ca. 0.4V. The mass change may be attributed to the adsorbed Bi species and with the transition between upd Bi and adsorbed Bi ions.

The most obvious explanation of this phenomenon is that there is some expulsion of perhaps OH, or H_2O, from the electrode surface upon formation of the underpotential deposit. Thus we might envisage $BiOH^{2+}$ being discharged to form Bi with some expulsion of H_2O, while on oxidation of the upd Bi the process might be reversed. If ΔM_1 represents the mass difference in the upd region of potential and ΔM_2 the extra difference seen above 0.6V then the ratio of ΔM_1 to ΔM_2 is approximately 5 to 1, which would suggest that species having a molecular weight of approximately 40 was coordinated to each Bi^{III}, assuming a simple one to one relationship. This figure might suggest the presence of $Bi(OH)_2^+$ on the surface, but taking into account experimental error (at least 10%), the possible blocking of oxide formation[256] by Bi and the likelihood of differences in specific adsorption of anions and quite possibly that of water between the electrode surface in its oxidised and reduced (with partial coverage of upd Bi) states, then the safest conclusion is that the mass difference is at least of the order of magnitude to be expected for such a transition. Finally, a similar experiment where Bi was adsorbed in 0.1M $HClO_4$ but where the electrode was then transferred to 1.0M $HClO_4$ led to a mass difference that did not change with potential at all. Although the coverage was less than when the voltammetry was carried out in 0.1M $HClO_4$,

the absolute mass difference in this last experiment was still ca. 120 ng and since the sensitivity of the mass signal is of the order of a few ng, a change of ± 20% on this figure (the ratio of ΔM_1 to ΔM_2 in Figure 40) would be readily seen. This lack of an observable difference in the more concentrated electrolyte, where hydrolysed species are not expected to be present, lends support to the interpretation presented above. It is interesting to note that the work of Clavilier et al.[269] at Pt single crystals also led the conclusion that $Bi(OH_2)$ (uncharged) was present at the surface, although it was suggested to be present as Bi^{II} rather than Bi^{III} and this adsorption occurred spontaneously on non-oxide covered electrodes held at open circuit with the adsorbate being removed once the electrode surface was oxidised. There was no evidence in this work for removal of adsorbates upon oxidation of the polycrystalline electrode surface.

4.4.5 *CONCLUSIONS*

1. In perchloric acid solutions with pH values of 1 and above, extensive adsorption of Bi^{III} species is revealed through the large mass changes occurring when a concentrated solution of Bi^{III} is added to the background electrolyte. The decrease in the observed mass signal as pH is decreased, and the increase in the signal as pH is increased suggest that while there may be some adsorption of Bi^{3+}, particularly at pH 0, the majority of the Bi species are adsorbed as $BiOH^{2+}$ or $Bi(OH)_2^+$.

2. In 0.1M $HClO_4$ the large amount of adsorption of Bi leads to a small mass change when cyclic voltammetry is performed in 0.1 mM Bi^{III} solutions since most of the upd deposit develops from previously adsorbed Bi^{III} species. As upd Bi is removed from the

electrode in an anodic scan in 0.1M $HClO_4$, a small mass increase is seen which is suggested to be associated with the conversion of Bi^{3+} to $BiOH^{2+}$ or $Bi(OH)_2^+$ on the electrode surface. This increase was not seen in stronger acid solutions when Bi^{3+} is expected to be the sole ion present.

3. Finally, when Bi is deliberately adsorbed at a Pt electrode which is then transferred to a background electrolyte free of Bi^{III}, a small mass change accompanies the transition from upd Bi to Bi^{III} and this is again suggested to be due to conversion of Bi to $BiOH^{2+}$ or $Bi(OH)_2^+$.

Chapter 5

Electrocatalytic Oxidation of Glucose at Platinum Electrodes

5.1 INTRODUCTION

The electrocatalytic oxidation of glucose has been a subject of extensive investigations for the last two decades. The interest originates from the fact that glucose can be used in glucose/oxygen fuel cell as a power source for cardiac pacemakers and because of the need to develop glucose sensors for an artificial pancreas[278-282]. The overall reaction for the complete oxidation of glucose to CO_2 requires 24 electrons to be transferred.

$$C_6H_{12}O_6 + 6H_2O \rightleftharpoons 6CO_2 + 24H^+ + 24e$$

However, the reaction cannot proceed to completion as it occurs through the formation of a variety of intermediate species among which some adsorbed species may poison the electrocatalyst surface and thus prevent further oxidation of glucose. The total number of electrons involved in the overall reaction has been found to lie between 2 and 24, depending on experimental conditions such as concentration of glucose, potential and time[283-285].

5.1.1 *Reactivity and molecular structure*

The reactivity of glucose is related to the structure of the molecule. Glucose usually displays a multiplicity of chemical structures in solution, i.e. aldehydic (γ-D-glucose) and hemiacetalic ring (α, β-D-glucose) forms. The two ring forms differ from each other in the

position of the hydrogen atom attached to the anomeric C_1 atom. The hydrogen attached to the C_1 atom has an equatorial position for the α-D-glucose and an axial position for the β-D-glucose

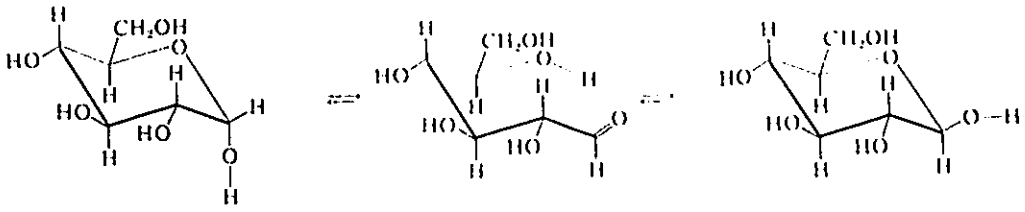

α γ β

Polarimetric measurements indicate that the active forms of glucose in solution are the α and β cyclic hemiacetalic forms and the open "aldehydic" form only exists at trace levels (ca. 0.024%) at room temperature. The two cyclic forms exhibit no difference of reactivity[286]. In addition, glucose may undergo interconversion, especially in alkaline solution, to produce D-fructose as confirmed by HPLC analysis of solution[286].

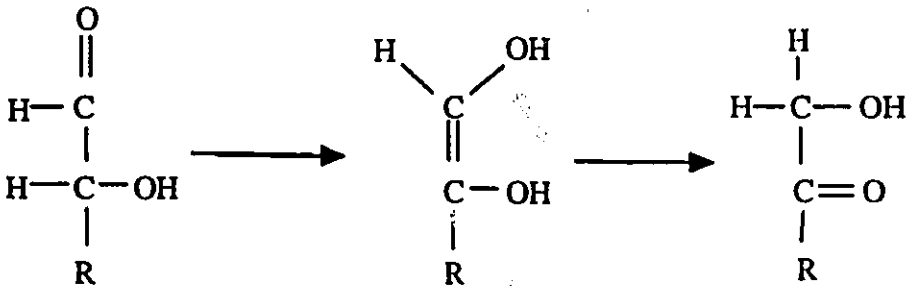

D-glucose enediol D-fructose

As a result, the reactivity of glucose may be lost gradually.

The hemiacetalic OH-group is usually considered to be a strong acid compared to the alcoholic OH-group and thus the hydrogen atom bonded to the same C_1 atom is somewhat

activated and becomes more reactive. Therefore the first stage in the oxidation of glucose is believed to be the oxidation of the hydrogen atom bound to the hemiacetalic C_1 atom. This assumption was proved by several experiments. Popovic et al.[73], in their experiments with isotopic substitution at the C_1 atom, observed a lower rate of oxidation of deuterated glucose than of protonated glucose, suggesting that the first reaction step involves the oxidation of the hydrogen bound to the C_1 atom. A comparative study of oxidation of glucose and other monosaccharides was performed to correlate the oxidation behavior with the structure of these molecules[287]. It was found that those molecules (such as D-arabinose and D-xylose) involving heterocyclic forms with hemiacetalic structure exhibit an electrochemical response similar to that of glucose, indicating that the hemiacetalic structure is responsible for the first step of glucose oxidation. Similar experimental evidence came from the analysis of a product of glucose oxidation: gluconic acid, formed through the oxidation of the hemiacetalic hydrogen, was detected as the reaction product by Ernst et al.[288] using field-desorption mass spectroscopy, and by Rao and Drake[289] using chronopotentiometry.

5.1.2 *Oxidation of glucose under various experimental conditions*

A number of electrode materials (Ag, Cu, Au, Pt, Ir and Rh)[290] have been investigated as possible electrocatalysts for glucose oxidation. Among them, Au and Pt are the two most widely employed electrodes. Pt has shown the best catalytic activity for glucose oxidation in acid solution while Au is the electrode of choice in neutral and alkaline solutions. In the case of platinum, various electrolytes have been used in a wide range of pH from acidic ($HClO_4$ or H_2SO_4)[74,290-292], through phosphate or bicarbonate buffers at the physiological pH[282,283,285,288,290-293], to alkaline media[90,286,294,295], and the oxidation of glucose

has been found to be influenced by several factors such as the nature of the anions present in the electrolyte (Cl^-, phosphate and sulphate)[282,291], pH and buffer capacity[283,296] and the ionic strength of the electrolyte[288]. Despite the different experimental conditions used, there are certain common features concerning glucose oxidation in these media at Pt electrodes. The main feature is that three current peaks appear during glucose oxidation on the positive scan (see Figure 41). The first one (peak I) is seen in the hydrogen adsorption region and this is followed by a second peak (peak II) in the double layer potential region and a third peak (peak III) in the region of Pt oxide formation. In addition, during the negative scan a very broad oxidation peak (peak IV) is seen after the reduction of Pt oxide. Peak I corresponds to the dissociative chemisorption/dehydrogenation of the hemiacetalic form of glucose[288,297] (the addition of glucose to the electrolyte causes the open circuit potential of the electrode to shift to the hydrogen adsorption region[290,291]), which leads to the formation of an adsorbed residue that poisons the electrode surface[293,294,298]. The current produced in this region is transient and the steady state current is small[290,291]. Peak II results, at least in part, from oxidation of the adsorbed residue formed in the potential range of peak I[293,298]. Peak III is generally attributed to the oxidation of glucose on an oxidized electrode surface, but it may also have contributions from oxidation of the products formed in peak II[298]. Peak IV occurs in the double layer region of potential on the cathodic half of a cycle, and is due to the oxidation of glucose at a clean Pt surface after partial reduction of the irreversibly formed Pt oxide.

5.1.3 *Nature of the adsorbed intermediates*

With respect to the nature of the adsorbed species which poison the electrode surface, there is no agreement in the literature to date. Rao and Drake[289] considered gluconic acid as

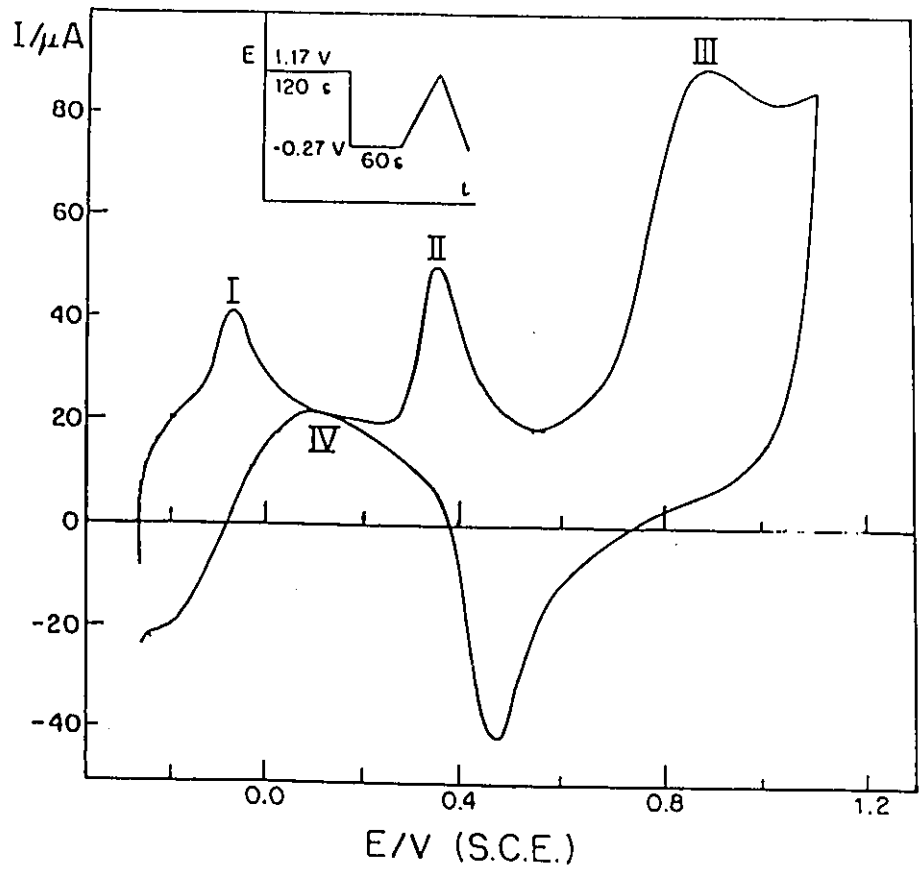

Figure 41. Cyclic voltammogram for an electrodeposited Pt electrode in 0.1M $HClO_4$ in the presence of 9mM glucose. Scan rate was 5mV/s and the electrode area 4.70cm^2. The potentail regime used is shown in the inset.

the adsorbed species. Ernst et al.[288] identified adsorbed species as glucono-δ-lactone, which is formed from the dehydrogenation of glucose molecules at the C_1 atom. This glucono-δ-lactone may further be transformed by hydrolysis into gluconic acid. Vassiliev et al.[290,291] performed kinetic measurements on glucose oxidation and concluded that the mechanism of glucose oxidation is analogous to those of elementary organic fuels such as formic acid and methanol. Kokkinidis et al.[74] also concluded from their studies of glucose oxidation at low index planes of Pt that the poisoning species are similar to those found in the oxidation of formic acid. Bolzan et al.[291] carried out on-line mass spectroscopic studies of glucose oxidation in phosphate buffer solution by examining the resulting volatile products. Their results showed that CO_2 was produced over the whole potential range, but that in the hydrogen adsorption region it is only formed from the C_1 position of glucose through decarboxylation of gluconate. Thus it was suggested that the oxidation of glucose can proceed much further than the oxidation to gluconolactone and the strongly adsorbed species formed seems to be the same as that observed in oxidation of small molecules such as methanol and formic acid.

Some other experiments gave strong evidence for the existence of CO as the adsorbed species. In-situ FTIR spectroscopic studies of glucose oxidation at Pt provided direct proof of CO as adsorbed species[294,298]. Linearly bonded CO was identified as an adsorbed species in the potential region -0.57 to 0.46V (Hg/HgO, OH^-) in alkaline solution[294], and in the potential range from -0.20 to 0.40V (SCE) in acid solution[298], respectively. This adsorbed CO is probably responsible for electrode poisoning. Recently Llorca et al.[75]investigated glucose oxidation on Pt(100) and a set of stepped surfaces containing (100) terraces. In their experiments, the adsorbed species originating from glucose oxidation were isolated by

changing the electrolyte and identified as CO by means of the electrochemical oxidation-desorption of the species. Their results indicate strongly that glucose oxidation proceeds through a "dual-pathway" mechanism, one pathway involving a reactive intermediate, allowing the reaction to continue, and the other leading to the formation of poisoning intermediates which cause the deactivation of the electrode surface. More recently, Horanyi reported, based on radiotracer studies of the adsorption of ^{14}C labelled glucose at Pt in acid solution[50], that at least two types of adsorbed species are present on the electrode surface, the behavior of adsorbed species formed in the potential range from 0 to 400mV (RHE) being significantly different from that of adsorbed species formed at higher potentials (the latter type of adsorbed species can be eliminated from the surface by reduction, and are presumably oxidation products of glucose such as carboxylic acids). Further evidence was obtained from similar experiments performed by the same author[299] with ^{36}Cl labelled Cl^- and ^{35}S labelled SO_4^{2-} as ions in the electrolytes. It was observed that the adsorbed species formed at low potentials (E < 500mV) inhibit the specific adsorption of both Cl^- and HSO_4^- while the adsorbed species formed at higher potentials only suppresses the adsorption of HSO_4^- due to its lower adsorbability compared to Cl^- ions. The former adsorbed species was suggested to be linearly bonded CO.

5.1.4 *Effect of electrode properties*

Like many other heterogeneous electrocatalytic reactions, glucose oxidation in aqueous solutions is very sensitive to the structure of electrode. Kokkinidis et al.[74] made the first attempt to investigate the role of the crystalline surface structure of Pt electrode in glucose oxidation using Pt single crystal faces as electrodes with basal orientations. The three low

index single crystal planes of Pt were found to exhibit higher activity for glucose oxidation than polycrystalline Pt, particularly the Pt(111) face which appears to be less sensitive to poison formation. Popovic et al.[73,295] studied glucose oxidation on single crystal Pt electrodes in both acidic and alkaline solution. Their results were in good agreement with those of Kokkinidis. By comparing the oxidation behavior of the adsorbed species formed during glucose oxidation with those of other similar organic molecules such as gluconolactone and gluconic acid, the former authors were able to distinguish the adsorbed species present on the three low index planes: the adsorbed species on Pt(111) appears to be of the gluconolactone type, but CO for Pt(100) and Pt(110). This probably accounts for the high activity of Pt(111) in comparison with the other two low index planes, Pt(100) and Pt(110), or polycrystalline Pt.

The oxidation of glucose on Pt has been shown to be catalyzed by foreign metal adatoms. Adatoms such as Pb[90,301,302], Bi[301,302] and Tl[90,300-302] have been found to enhance greatly the activity of Pt in both acid[300-302] and alkaline media[90]. The catalysis induced by these adatoms was recognized by the shift of the oxidation peak in the double layer region (peak II) to more negative potentials and by the increase of the peak current. The action of the adatoms has been interpreted in terms of the decrease of the electrode poisoning according to the "third body" model. The catalytic effect of adatoms Pb, Bi and Tl has also been studied using single crystal Pt electrodes[74]. In such a case, it was observed that glucose oxidation and the corresponding maximum current occurred before the beginning of desorption of the UPD layer, suggesting that direct oxidation of glucose presumably took place on surfaces covered by adatoms and that the "third body" mechanism was of minor importance. Thus the enhanced catalytic activity caused by these adatoms may be attributed

to the modification of the electronic properties of electrode substrate.

5.1.5 *Analysis of reaction products*

The reaction products, accumulated after sustained electrolysis of glucose in a wide range of pH (from acidic to alkaline medium) on pure and adatom (Pb, Bi and Tl) modified Pt electrodes, have been analyzed by "on-line" chromatographic techniques[59,303]. The main reaction product was revealed to be gluconic acid regardless of the experimental conditions. However, many other carboxylic acids such as glucaric, glucuronic, tartaric, oxalic, glycolic and formic acids were also detected in relatively small amounts. Modification of the Pt surface by UPD adatoms has been shown to affect the distribution of the reaction products, thus altering the selectivity of the electrocatalytic oxidation of glucose. For example, the presence of Bi adatoms led to an appreciable increase in the formation of glucuronic acid. Thus these results suggest that gluconic acid is not the sole and final product of glucose oxidation.

5.1.6 *Summary*

The above results demonstrate that it is difficult to find an unambiguous mechanism of glucose oxidation due to the complexity of the structure of glucose. However, certain general conclusions can be drawn: (1) the first step in glucose oxidation is the dehydrogenation of the C_1 carbon, which occurs at low potentials; (2) the main reaction product is gluconolactone, which can then hydrolyze to gluconic acid, according to the following reactions; (3) the poisoning intermediate formed during glucose oxidation is

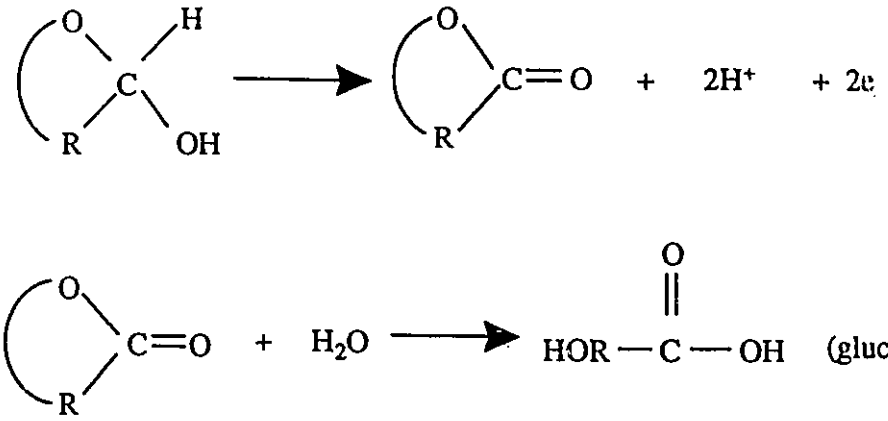

probably CO. Thus the following scheme for glucose oxidation can be postulated:

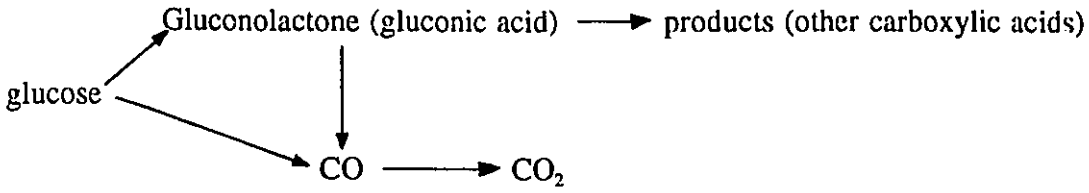

In this scheme, glucose oxidation proceeds through a dual-path mechanism to produce a reactive intermediate (gluconolactone) and a poisoning intermediate (CO). CO can also be formed from gluconic acid oxidation as a CO oxidation current was observed for gluconic acid oxidation[293]. Further oxidation of gluconic acid gives rise to various carboxylic acids, depending on experimental conditions.

Although there have been many studies of the oxidation of glucose, the investigations have not been exhaustive. For example, the nature of adsorbed intermediates in the reaction is not understood completely and the effect of UPD adatoms needs to be investigated to greater extent. This has stimulated us to study the oxidation of glucose using the electrochemical quartz crystal microbalance. In the following sections, we present an investigation of the oxidation of glucose in both acid and alkaline media as well as a study

of the influence of lead UPD adatoms on the oxidation of glucose in acid media. Especially, the utility of the EQCM technique in the study of adsorption and electrocatalytic processes has been explored and the important roles of reactant adsorption and poisoning by species in the reaction, and competition in adsorption between adsorbates from the reaction and UPD adatoms have been examined.

5.2 OXIDATION OF GLUCOSE AT Pt IN ACID MEDIA

5.2.1 *Responses in the presence of glucose*

Figure 42 shows a typical cyclic voltammogram and mass response for the oxidation of glucose (9mM) in 0.1M $HClO_4$ together with the responses found in 0.1M $HClO_4$ alone. The response was first recorded in 0.1M $HClO_4$ and then glucose added to the electrolyte to bring the concentration to 9 mM.

The four glucose oxidation peaks described previously are seen in the voltammogram recorded in Figure 42. The voltage offset (see Chapter 3 Experimental) of the frequency (mass) signal was not changed during the experiment. Thus the mass responses shown in this figure are an accurate reflection of the actual masses observed during these experiments i.e. the mass of the electrode between -0.2V and 0.4V during an anodic scan in the presence of 9 mM glucose is similar to the mass of the electrode in background electrolyte over the same potential range. The influence of glucose on the mass response is small. None of the observed changes are as large as the increase in mass that results from the oxidation of the electrode surface, but there are several subtle changes which can be discussed according to the region of potential in which they occur. We will begin at the most negative potential and describe

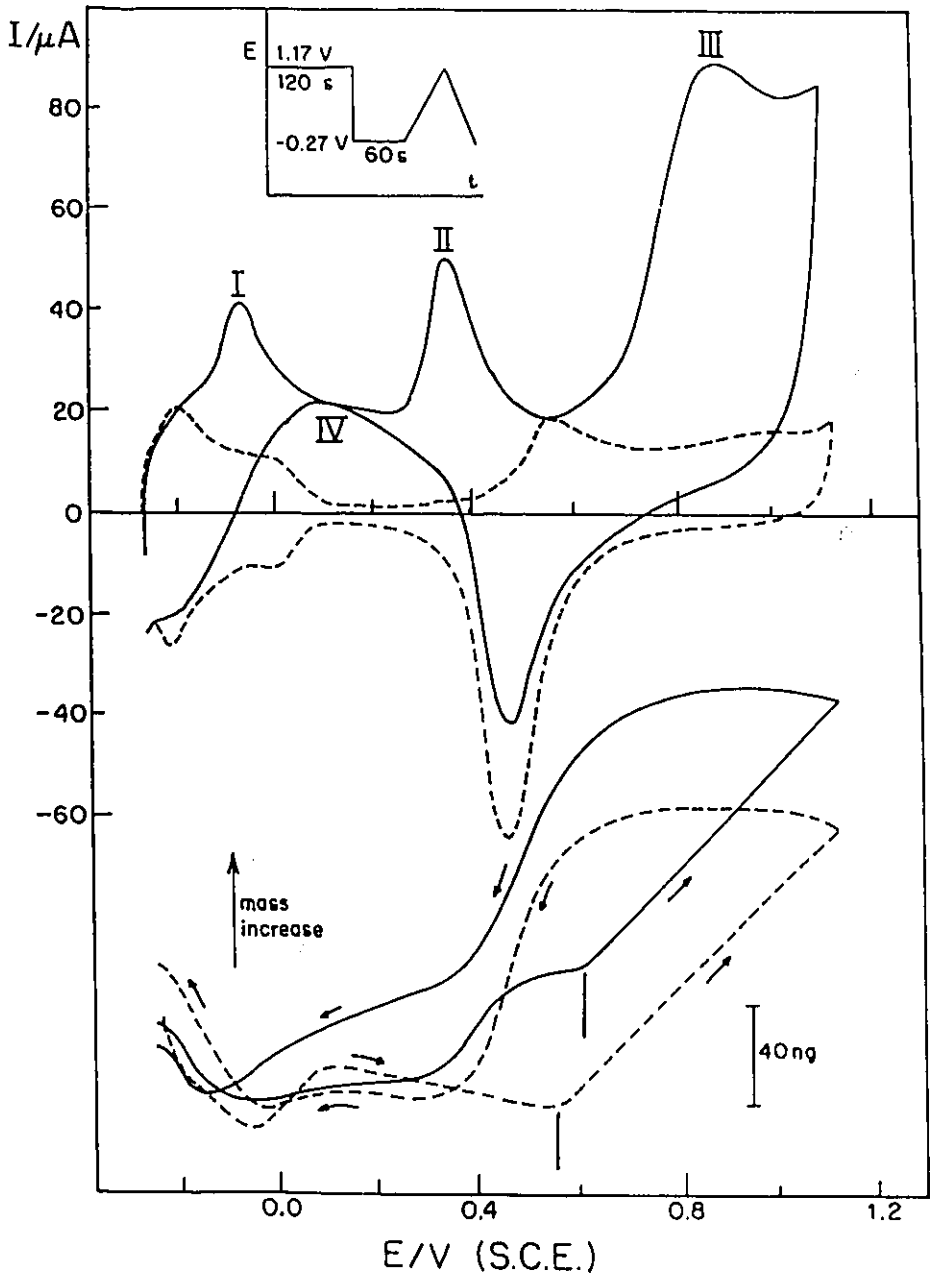

Figure 42. Cyclic voltammogram and mass response for an electrodeposited platinum electrode in 0.1M $HClO_4$ in the absence (dashed line) and presence (solid line) of glucose (9 mM). Scan rate was 5mV/s and the electrode area 4.70 cm^2. The potential regime used is shown in the inset.

the changes as the scan proceeds in the positive direction through a complete cycle.

a). First, at the negative limit of the anodic scan, the initial mass decrease is less than that seen in the absence of glucose. This is most likely to be a result of the replacement of adsorbed anions by adsorbed and perhaps partially oxidised glucose. The mass change coincident with the strongly bound UPD H (indicated by the arrow in Figure 25) is also removed so that between -0.075V and 0.3V the mass of the electrode is almost constant. It is clear from the suppression (in the presence of glucose) of features attributed to anions that there is some adsorption of glucose and/or its oxidation products in this potential range but the absolute mass of the electrode is changed very little by the presence of glucose. This is probably a result of low coverage and the fact that the observed mass change includes two contributions; an increase arising from the addition of the adsorbate to the electrode surface and a decrease attributable to species displaced from the surface.

b). The most prominent feature of the mass response is a sharp increase in mass coincident with peak II. The origin of this increase is discussed below.

c). Finally, from 0.6V onwards on the anodic scan (where the oxidation of the electrode surface begins), the mass responses in the presence and absence of glucose follow apparently parallel paths, except that the mass is larger by a roughly constant amount when glucose is oxidised in peak III. This mass difference is also observed during the first 0.5V of the cathodic scan, and indicates adsorption of glucose, or species derived from glucose, on the oxidised electrode surface. This aspect was investigated further as described below.

In addition to the voltammetry, injection experiments were performed where an aliquot of glucose was added to 0.1M $HClO_4$ to bring the concentration to 9mM with the electrode

potential poised at values between 0.62V and 1.15V. In this way the adsorption of glucose was studied as a function of the extent of oxidation of the electrode surface. A typical mass transient obtained at E= 1.05V is shown in Figure 43. For each potential, the charge required for reduction of the oxidised surface (Q_O) was estimated in background electrolyte prior to injection and is expressed here relative to the charge required to deposit a monolayer of H (Q_H°). A ratio of $Q_O/Q_H^\circ = 1$ corresponds to generation of a monolayer of PtOH, whereas when $Q_O/Q_H^\circ = 2$ a full monolayer of PtO has been produced. While Q_O/Q_H° varied from 0.6 to 2, the mass changes observed were constant (within experimental error) at 27 ± 3 ng for an electrode of 3.45 cm^2 surface area. At lower charge ratios (0.2) where only 20% of the surface is covered with PtOH, the increase is about 50% larger. Inspection of the mass responses in Figure 42 indicates that the onset of surface oxidation (indicated by vertical lines in the figure) is shifted perhaps 50 mV by the presence of glucose.

The above results show that there is clearly some glucose adsorption at the electrode during the initial stages of oxidation and this may be gradually decreased as the extent of oxidation of the electrode surface increases. The oxidation of glucose in this region has not been as extensively investigated as on the reduced surface but Skou[292] has suggested that the oxidation (in 1.0M H_2SO_4) proceeds through a rapid adsorption/oxidation mechanism and Vassilyev et al.[291] have indicated that oxidation occurs via a chemical reaction followed by electrochemical regeneration of the oxide. In addition, FTIRRAS[298] and mass spectrometry experiments[293] have shown that CO_2 is generated in this potential region. Given the complexity of the glucose oxidation reaction at the oxidised electrode surface and the fact that there may be some suppression of the oxidation of the surface by adsorbed glucose it is not possible to draw any firm conclusions regarding the mass increases observed here. However

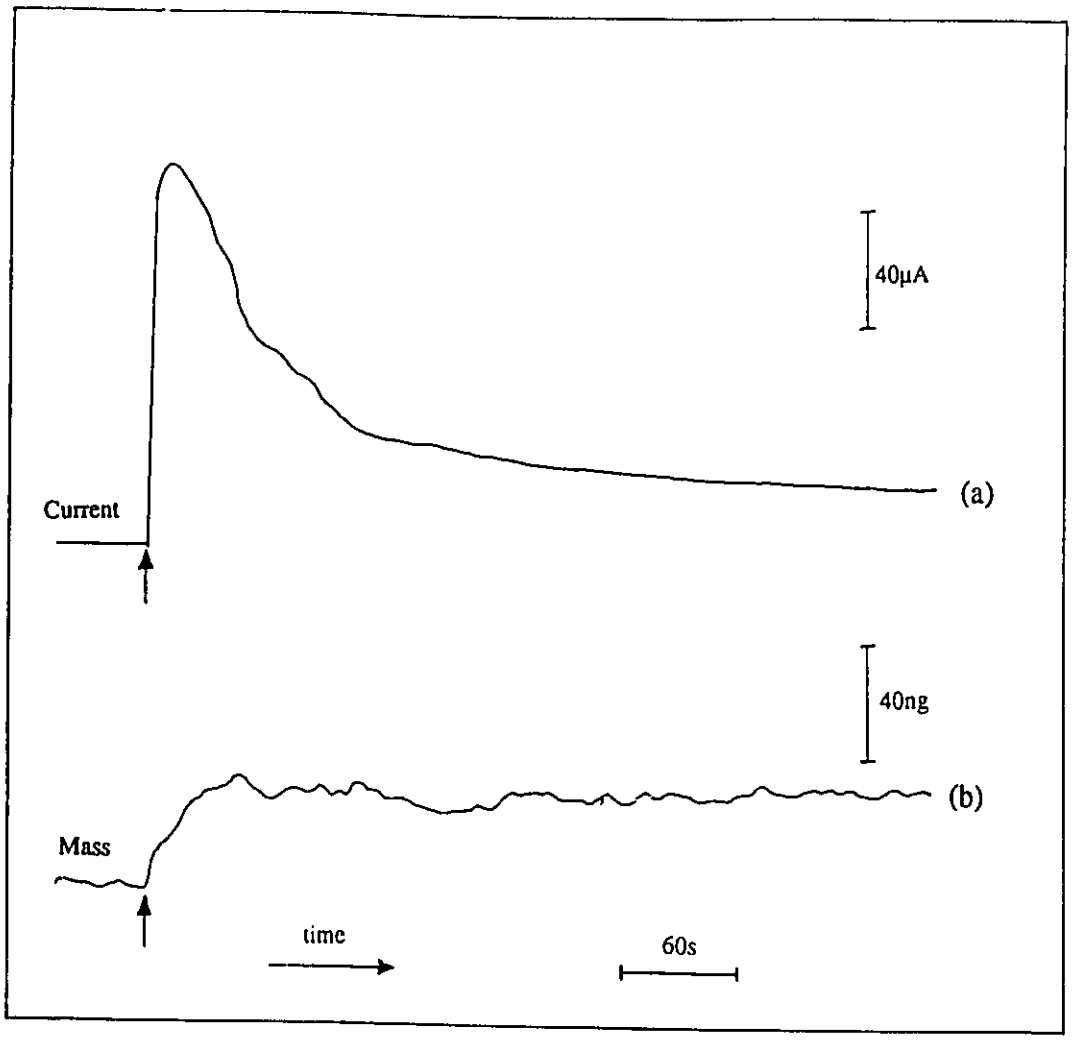

Figure 43. Current (a) and mass (b) transients resulting from the addition of glucose (to give a bulk concentration of 9 mM) to the background electrolyte (0.1M $HClO_4$) at a constant potential E = 1.05V. Electrode area is 4.58cm^2

the results do seem to indicate that an adsorbate, being either glucose or species derived from it, is present at the oxidised electrode surface.

Returning to Figure 42, on the cathodic scan, the mass difference (between the electrode in the presence and absence of glucose) becomes smaller as the irreversibly formed oxide is reduced (at ca. 0.6V). This may reflect removal of adsorbate by the reversal of the place exchange process. Such a phenomenon has been observed for 4,4'bipyridyl adsorption on gold[304]. The final broad oxidation peak (IV) begins after the reduction of irreversibly formed oxide. The mass of the electrode during peak IV is larger than it was in the same potential region on the anodic scan (where peaks I and II are seen) although it decreases steadily with potential and returns to an almost identical value at the end of a cycle. This mass change is discussed below.

5.2.2 *Origin of peak II*

It is well known that the oxidation of glucose is subject to inhibition by poisons. For example, FTIRRAS experiments have shown that oxidation of glucose at Pt produces adsorbed CO (in both acid and alkaline media)[294,298]. It has also been indicated that peak II results from the oxidation of an adsorbed residue produced by the oxidation process in peak I [293,298]. To investigate this point further, the experiment shown in Figure 44 was carried out. After recording a voltammogram by the normal method, the potential was cycled between -0.25V and 0.21V six times before a second complete scan (the eighth in all) was recorded. Repetitive cycling between -0.25V and 0.21V is seen to have two effects. First, the current for underpotentially deposited hydrogen decreases substantially with each cycle indicating that the coverage of adsorbed species is increasing. Second, (at potentials greater than -0.05V) the

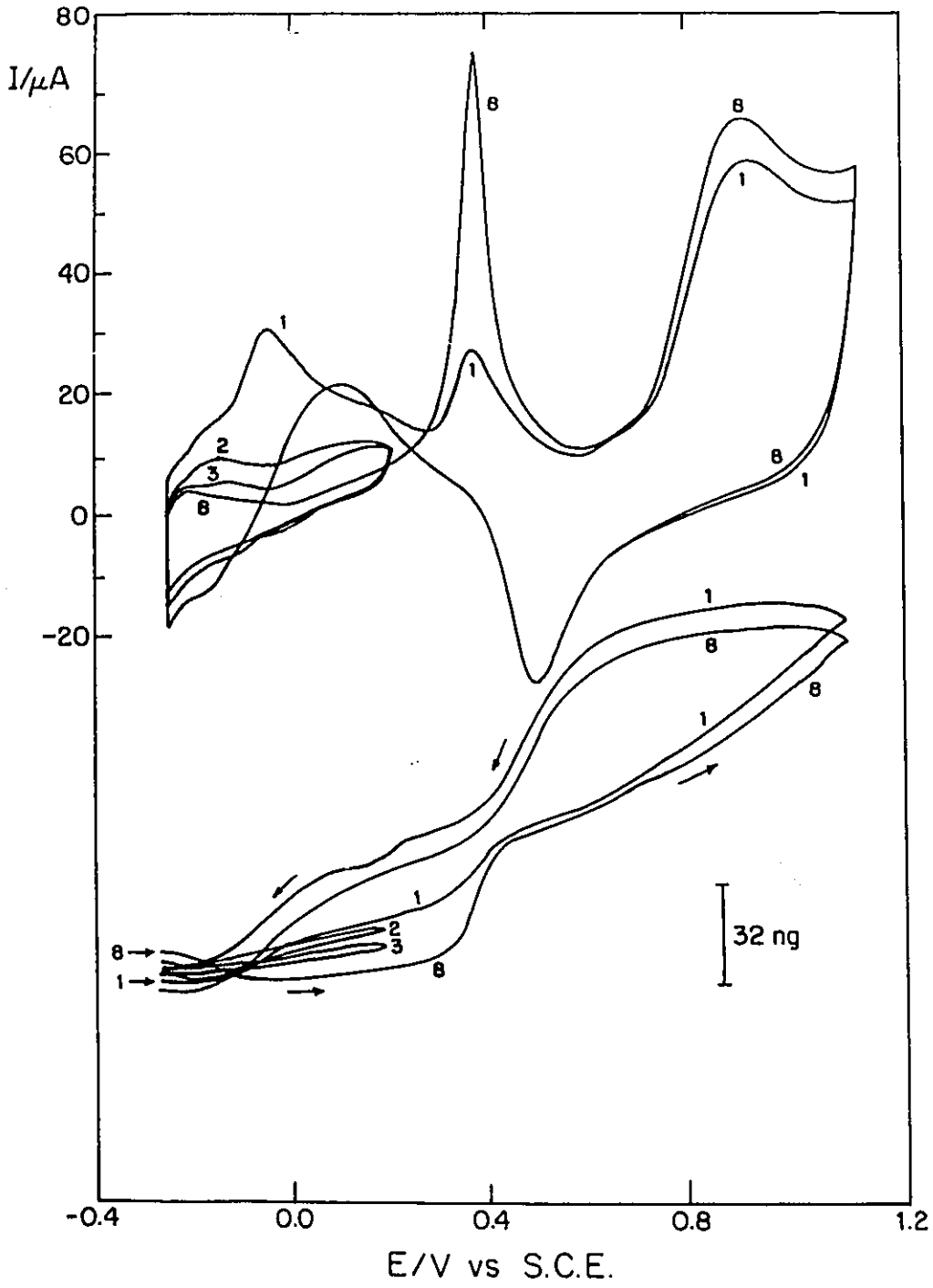

Figure 44. Cyclic voltammetry (top) and mass responses (bottom) for 9mM glucose, with two complete scans (1 and 8) separated by six cycles between -0.27V and 0.20V. Scan rate 5mV/s, electrode area was 2.6 cm^2. Potential profile prior to scan 1 was as shown in figure 41. The eighth scan begins at the cathodic limit in the anodic direction. Numbered arrows in the lower part of the figure indicate the beginning of the mass responses associated with cycles 1 and 8. Cycles 1,2 3 and 8 only are shown for clarity.

mass *decreases* with each cycle in this region. It is also noticeable that during these cycles a net oxidation current is still being passed in the potential range between 0.0 and 0.2V which is probably a result of glucose oxidation at unoccupied sites or some oxidation of the poison.

Upon extending the scan to its original limits, the current in peak II (cycle 8) is enhanced relative to cycle 1 where adsorption took place at -0.27V for 60s (the charge is roughly doubled). The mass increase that accompanies peak II becomes larger and steeper too. The current for peak III is increased a little when compared to the first complete scan but the current on the cathodic scan is unaffected.

The cyclic voltammetric data shows that a substantial part of the current in peak II results from the oxidation process in peak I. The mass *decrease* that accompanies the gradual increase in coverage of the adsorbed intermediate is a little surprising at first glance, but could result from the progressive destruction of adsorbed glucose and loss of fragments into solution, leading to species such as CO on the electrode surface. The *increase* in mass that accompanies peak II could arise from processes where the adsorbate removed from the electrode in peak II was replaced either by adsorbed anions or by adsorbed glucose or both (Further information regarding the origin of this mass increase is obtained through electrolyte exchange experiments (see the section below)). The increased current in peak III observed on the eighth cycle is likely to be a result of the further oxidation of some of the products of the oxidation in peak II arising from poor mass transport away from the electrode, because the crystal is affixed to the bottom of the electrochemical cell (see Figure 18). Bae et al. observed a similar effect in a thin layer cell designed for FTIRRAS experiments[298].

5.2.3 *Oxidation of adsorbate in the absence of glucose*

The origin of the mass increase accompanying peak II was further investigated by electrolyte exchange experiments. Here the adsorbate was formed as in Figure 44 and the glucose-containing electrolyte flushed from the cell and replaced with fresh $HClO_4$ while potential control was maintained (at either 0.1V or -0.15V). The potential was then scanned towards the cathodic limit and then a complete cycle was recorded. No difference was observed between results obtained at the two different holding potentials. The voltammogram in Figure 45 indicates the presence of adsorbate through suppression of the H upd currents (although some loss of adsorbate seems to occur during the flushing procedure) and the peak for adsorbate removal has a small shoulder and occurs at a potential 50 mV less positive than the value observed in glucose solutions. There is also some further oxidation of the products of peak II as the potential proceeds towards the upper scan limit. These results are very similar to those of Bolzan et al. for oxidation of adsorbate in phosphate buffer[293]. Once adsorbate is removed, the second complete voltammogram essentially represents a bare Pt surface.

In the mass response, the adsorbate leads to a flat signal until the oxidative removal begins, when a small increase in mass is seen. The mass of the electrode is lower in the presence of adsorbate than it is in background electrolyte alone and is almost constant at potentials below 200 mV. This experiment allows us to conclude that the mass increase that is seen to accompany peak II in a voltammogram in the presence of glucose arises from the replacement of adsorbate by both anions *and* glucose. Replacement of adsorbate by anions (Figure 45) does give an increase in mass but this merely restores the mass to its level in the background electrolyte. However, both Figure 42 and injection experiments show that at

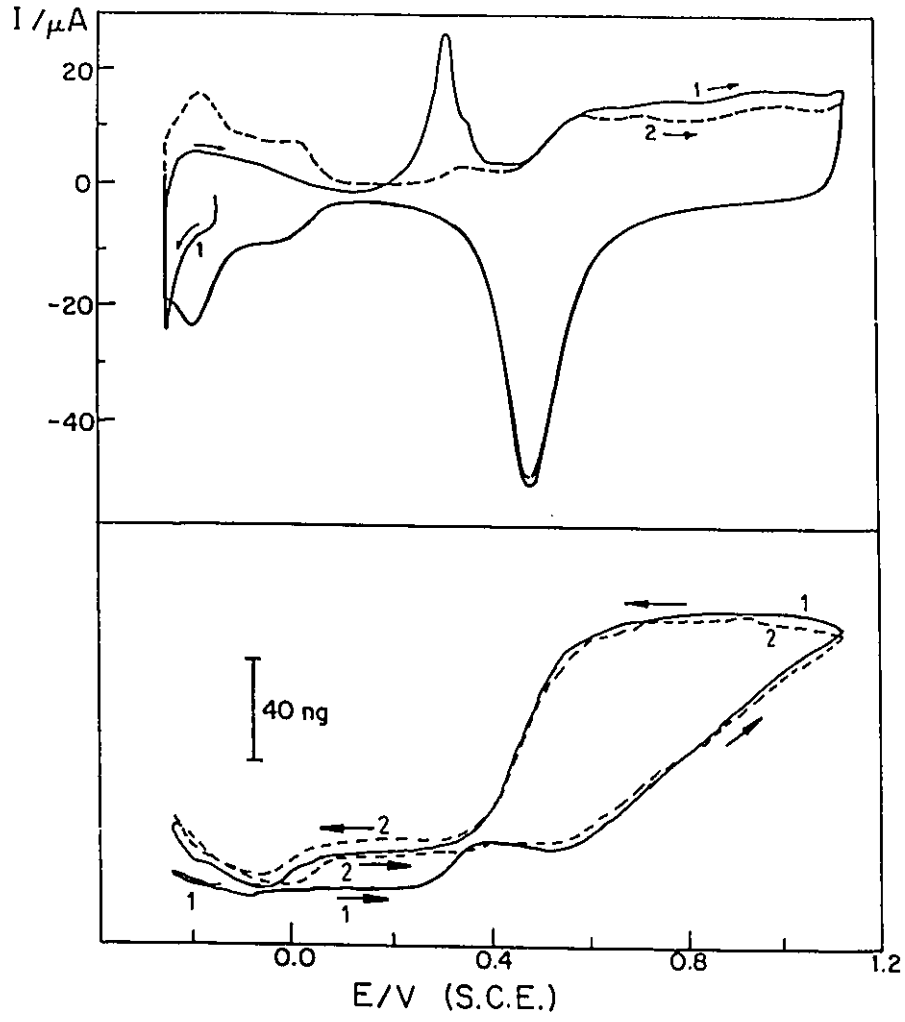

Figure 45. Cyclic voltammogram and mass response for the removal of adsorbate (formed by repetitive cycling as in Figure 44) in the absence of glucose in the electrolyte. Electrode potential held at -0.15 V while the glucose-containing electrolyte was flushed from the cell. Scan rate 5 mV/s, electrode area 3.45 cm^2.

potentials above 0.5V the mass of the electrode is heavier in the presence of glucose after adsorbate removal. This increase must arise from glucose adsorption. It is difficult to estimate the contribution of each species to the mass increase accompanying peak II but since similar increases are observed in NaOH solutions (see Section 5.3) it seems that the majority of the mass increase does result from glucose adsorption in experiments such as that shown in Figure 42. When the coverage of adsorbate is increased as in Figure 44 there may be a larger contribution from anions.

5.2.4 Cyclic voltammetry in double layer region and above

Since peak II is seen to be derived from the oxidation of a poison produced in the potential region of peak I, the mass response at potentials in the double layer region and above may also be influenced by processes occurring at lower potentials. Thus the mass behaviour of an electrode which had not been exposed to glucose in the potential region of peak I was examined. The electrode potential was poised at 0.20V (in the double layer region of potential) and glucose injected to bring the concentration to 9 mM (Figure 46). A large oxidation current was observed which gradually decayed and after a period of 12.5 minutes at 0.2V an anodic scan was begun at point A. Once the first cycle was completed the scan was reversed at 0.2V and a second cycle recorded. At the beginning of the first scan there is (even after 12.5 minutes at 0.2V) an oxidation current that is 3-4 times larger than the double layer charging current. Prior to injection of glucose at 0.2V, the electrode surface is free from both adsorbed H and oxide, and having had no contact with glucose it is also free from poisons. Thus, oxidation current passed during the holding period at 0.2V arises (at least initially) from a process that is similar to that which gives rise to peak IV (seen on the

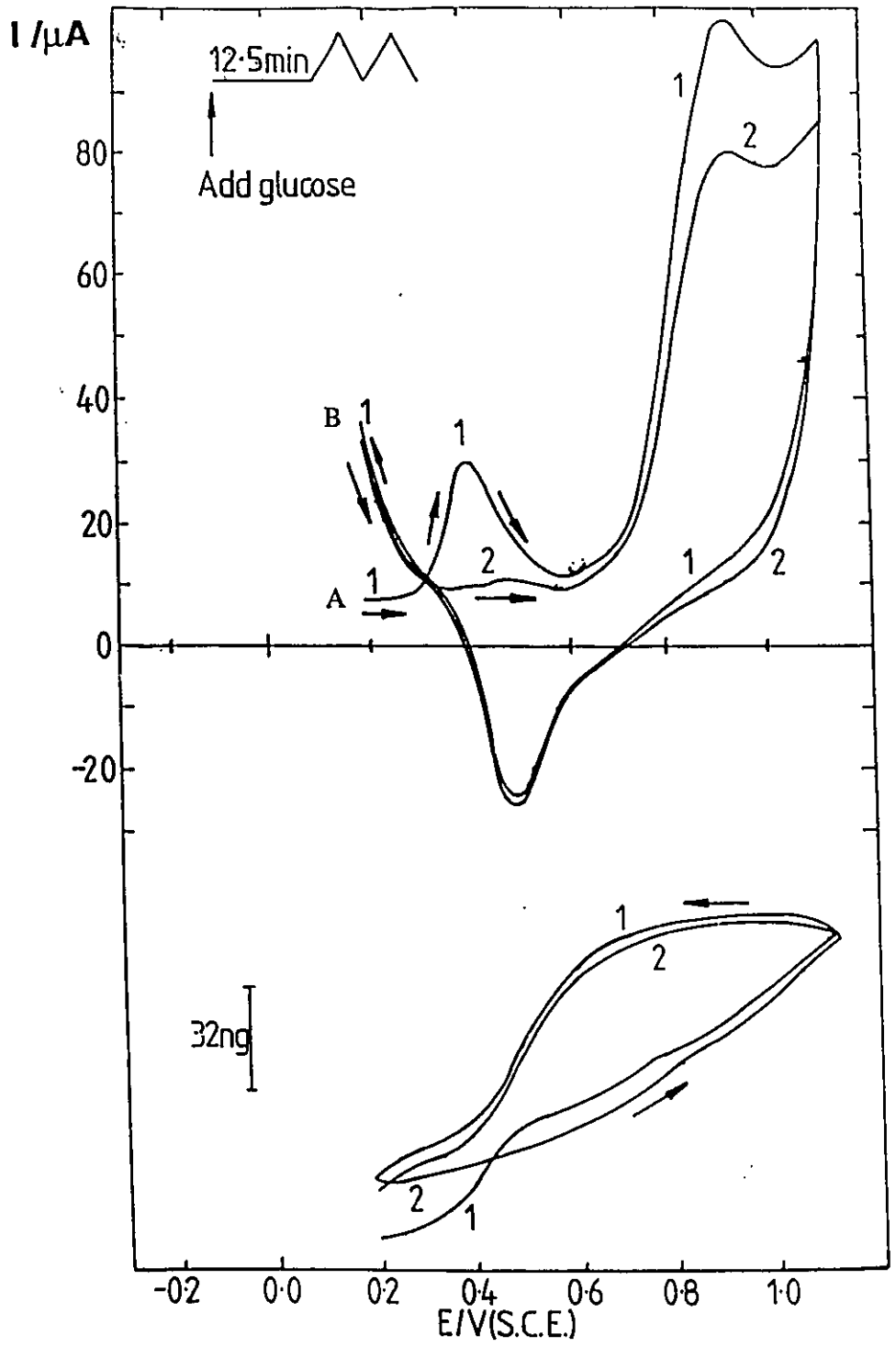

Figure 46. Voltammetry and mass responses for two complete cycles following injection of glucose and a waiting period of 12.5 minutes at 0.2V. Scan rate 5 mV/s, electrode area 3.08 cm^2. Cathodic scan limit restricted to 0.2V.

cathodic scan of a complete cycle).

The voltammogram observed after holding at 0.2V shows that poison formation does also occur at potentials outside the H adsorption/desorption region since peak II is seen. The remainder of the voltammogram is unchanged from previous examples. The large oxidation current at the end of the cathodic half of the cycle at 0.2V (point B) arises from the same process that occurs immediately after injection (described above), the difference here being that the poison is removed by oxidation (peak II) and the oxide by reduction during the cycle. On the second anodic scan, the current falls off sharply at first and peak II is barely visible and appears at a slightly more positive potential, although a significant oxidation current (relative to the double-layer charging current) still flows over the potential range from 0.3V to 0.6V. At the end of the first scan and the beginning of the second there is insufficient time for the development of significant amounts of poison and the oxidation current in this region must arise from glucose oxidation on free sites. The decreased current for peak III compared to scan 1 (where peak II was also larger) reinforces the view that the products of peak II may be oxidised further on an oxidised Pt surface.

The mass response beginning at 0.2V closely matches that in Figure 42, showing an increase in mass coincident with peak II, and at the end of the first cycle the mass of the electrode is substantially heavier than at the beginning. The mass response accompanying the second cycle shows behaviour typical of a clean Pt electrode in shape, except that it is increased in the double layer region of potential, and almost the same as the response accompanying cycle 1 thereafter.

In conclusion, it is seen that cycling at potentials below 0.2V clearly does affect the mass response at potentials greater than 0.2V. For a complete voltage cycle, the presence of

poison prevents the adsorption of glucose until the poison is removed in peak II, whereas when the lower limit of potential is set at 0.2V glucose is able to adsorb immediately, although poisoning occurs slowly. Presumably adsorbed glucose is present throughout the whole of the potential range on the second cycle in Figure 46 and thus both peak II and the mass response that accompanies it (representing the replacement of poison by glucose) are absent.

These results demonstrate the formation of a poisoning adsorbate at potentials outside the H adsorption/desorption region. The rate of formation of this adsorbate is slow but the adsorbate is oxidised in peak II, and gives rise to a decrease in mass of the electrode as it is formed and an increase in mass as it is removed. However, it may not necessarily be the same adsorbate that is formed in the potential range where adsorbed H is present on the electrode surface. Restriction of the potential to values greater than 0.2V without holding the potential does give a small oxidation current between 0.3V and 0.6V from glucose oxidation on free sites.

5.2.5 *Cyclic voltammetry in the absence of oxide formation*

In some further experiments, the current and mass data were collected with an upper potential limit being 0.6V, just after peak II, so that the electrode surface would not be subject to any significant oxidation. The results are shown in Figure 47. In background electrolyte (dotted line) the extent of oxidation of the platinum surface at the point of scan reversal (0.6V) is small. The oxidation process is reversible since the oxidation and reduction peaks appear at the same potential, gives rise to a small increase in mass and probably corresponds to development of PtOH. In the presence of glucose, peaks I, II and IV are

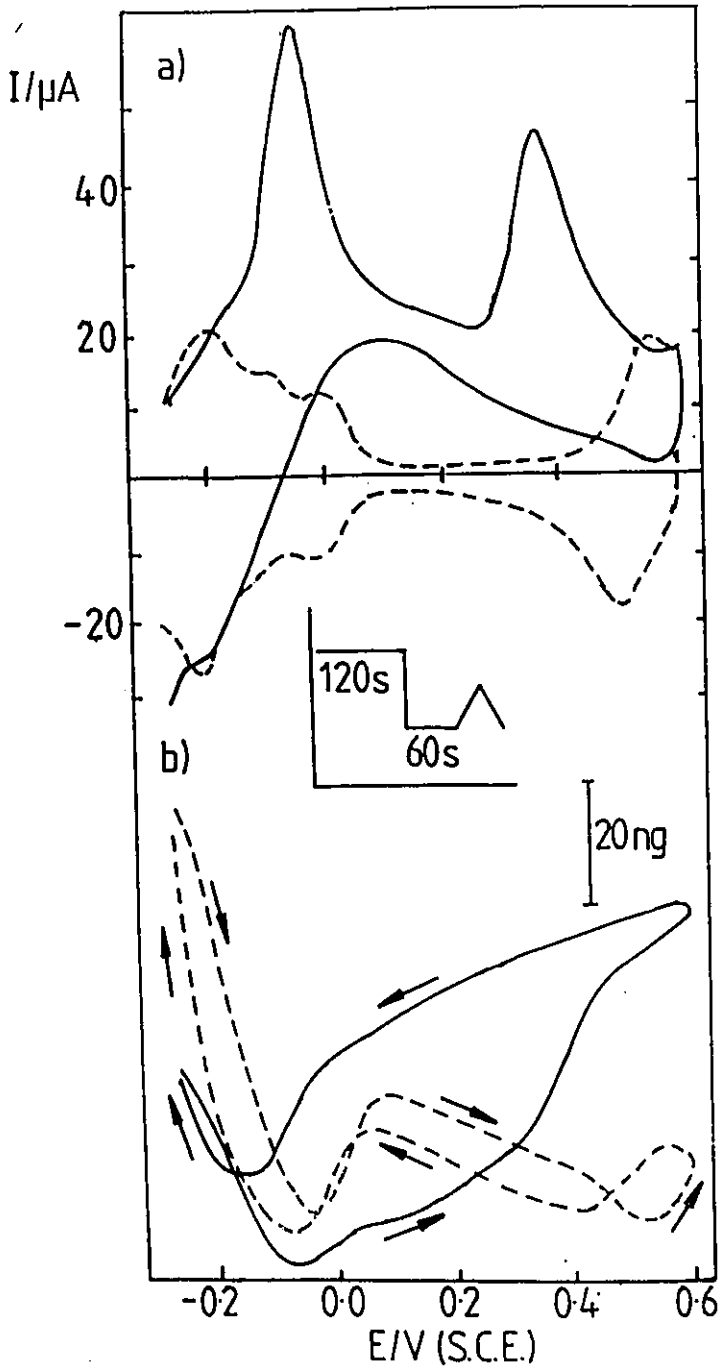

Figure 47. Cyclic voltammetry for 0.1M $HClO_4$ with varying amounts of glucose and an anodic scan limit restricted to 0.6V. [Glucose] was ; 0.0mM (dashed line), 2mM (solid line). Note that the mass scale is more sensitive than in previous diagrams. Scan rate was 5 mV/s and the electrode area, 4.70 cm^2.

visible in the voltammogram. The mass change is broadly similar to that seen in Figure 42 in this potential range (although it is on a more sensitive scale). A comparison of Figures 42 and 47 indicates that oxidation/reduction of the surface has a negligible effect on the mass response. Glucose is able to adsorb on the electrode as the adsorbate is removed in peak II thus increasing the mass of the electrode. Further evidence for the presence of glucose on the electrode at potentials positive of peak II comes from injection experiments where an aliquot of glucose was added to background electrolyte with the electrode potential poised at a potential of 0.5V. An increase in mass equivalent to that which accompanies peak II was observed.

Finally, as the cathodic scan proceeds from the point of scan reversal and glucose is oxidised in peak IV, the mass of the electrode gradually decreases and returning to its starting value at the cycle limit. This is most likely to be a result of the more rapid generation of the poison at lower potentials. There is hysteresis in the mass response from -0.1V to 0.6V which illustrates that fact that, on the anodic scan, rapid poison formation occurs at lower potentials making the mass of the electrode decrease (relative to background electrolyte). However, after peak II on the anodic scan glucose can re-adsorb and increases the electrode mass which remains higher during the negative going scan until the potential returns to the H UPD region where the poisoning process is accelerated. The data of Figures 46 and 47 clearly demonstrate that adsorption of glucose occurs at potentials in the double layer region. However for a normal voltammetric scan this adsorption is prevented by the presence of a poison and only becomes apparent (through the increase in mass accompanying peak II) when the poison is removed.

5.2.6 *Discussion and conclusions*

Discussion of the results obtained may be sensibly divided into sections related to the different oxidation processes of glucose.

1. In the potential range where peak I is observed, adsorption is apparent from the removal of mass features associated with anions but the presence of adsorbate has only a small effect on the mass of the electrode. The fact that the mass change does involve anion displacement means that it is difficult to assess the extent of coverage from the mass data. The literature does contain several estimates of coverage[290,291,293,297], mainly obtained through the usual method of measuring the decrease in H upd charge resulting from the presence of adsorbed material. Typically, the data for both acid and phosphate buffer electrolytes show a maximum coverage of ca. 0.5 at 0.2V vs. R.H.E. with a sharp decrease with potential either side of the maximum. However, most of the data are for bulk glucose concentrations higher than those used here. Coverage has been shown to be less at lower concentrations when the analysis was carried out after first allowing adsorption at 200 mV (R.H.E.) for 300s in phosphate buffer[288]. Furthermore, coverage values represent the number of sites occupied by adsorbate and not necessarily the number of glucose molecules adsorbed on the surface.

Indeed, recent mass spectrometric studies of the adsorbate formed at 0.2V (R.H.E.) in phosphate buffer indicated that nearly all the carbon atoms in the glucose molecule contributed to the formation of the adsorbate[293]. If this result applies to $HClO_4$ solutions then the coverage in terms of glucose molecules would be quite small and this together with the removal of anions from the electrode surface might account for the negligible change seen in this potential range. The fact that, for example, CO_2 has been shown to be produced during the H adsorption/desorption region (in phosphate buffers)[293] introduces a further complication

regarding the extent to which adsorbed species are oxidised as well as the number of sites occupied by the adsorbate. Thus the overall situation in this potential range is simply too complex for information regarding coverage to be extracted from the mass data.

The effect of cycling over the potential range between -0.27 and 0.2V is seen to lead to a much greater suppression of the H upd current which indicates higher surface coverage of adsorbates, although even after this treatment the current in this region is larger than the double-layer charging current and there is still oxidation occurring at potentials above 0V. This further reinforces the view that the initial extent of coverage of glucose and/or its products (under the conditions employed here) is small and does not reach a monolayer after cycling in this way. However, the increased coverage of adsorbate leads to an unexpected mass decrease probably as a result of a progressive destruction of the adsorbed glucose molecule and the loss of some fragments into solution (see below). A poisoning adsorbate, which gives similar mass behaviour to that described above, is also formed at 0.2V (S.C.E.) even when there is no adsorbed hydrogen on the electrode surface, although the rate of formation is slow. This agrees with results from experiments in phosphate buffer which showed a dramatic decline in the rate constant for adsorption at potentials above 0.2V (R.H.E.) or -0.04V (S.C.E.)[297].

2. In the double layer region of potential, interference from anions seems to be less significant (the background mass response changes much less with potential than it does in the H adsorption/desorption region), and the mass response is largely influenced by the competition for adsorption sites between poison, anions and glucose. The removal of the adsorbed material in peak II produces a mass increase arising from a reversal of the process forming the adsorbate, namely the replacement of fragments of the glucose molecule (which

might include species such as linearly adsorbed CO) by anions and glucose molecules. Mass responses from Figures 43 and 44 together with injection experiments indicate that glucose can adsorb on the electrode surface in this potential region in the absence of poison. This may be achieved *either* through oxidation of poison in peak II so that adsorption can occur at potentials greater than ca. 0.5V, giving rise to the sharp mass increase, *or* through restricting the lower range of potential to values above 0.2V. In the latter case the mass seems to be roughly constant over the double layer region of potential which seems to be an indication that the extent of adsorption of glucose is roughly constant too.

3. When the electrode surface is oxidised, voltammetric and injection experiments indicate an increase in mass of the electrode that is small and does not change significantly with potential. As discussed in the text, this is indicative of some adsorption of glucose and perhaps partially oxidised glucose but no firm conclusions can be drawn regarding the nature or coverage of the adsorbate. Inspection of Figures 42 and 43 shows (through the effect of peak II on peak III) that some of the products of the oxidation process giving rise to peak II can be oxidised in this potential range, although the majority of this oxidation arises from oxidation of bulk glucose.

EQCM experiments such as those described here provide an interesting insight into the changes in adsorption of species derived from glucose as a function of potential, despite the complexity of the system. In particular, the mass responses in the region of oxide formation and accompanying peak II provide an interesting comparison with previous work on CO oxidation at Pt[263].

a). First, the removal of adsorbed CO gives rise to a current peak similar to peak II

but produces a mass loss. In the case of glucose there is a mass gain accompanying peak II because once the adsorbate is removed, glucose (and anions) readsorb;

b). Second, the presence of CO in the electrolyte and its oxidation over the region of potential where the electrode surface is oxidised makes no difference to the mass response in this region. CO does not seem to adsorb on oxidised Pt surfaces. In contrast glucose, or species derived from it, does adsorb on the oxidised electrode as it is oxidised in peak III.

5.3 OXIDATION OF GLUCOSE AT Pt IN ALKALINE MEDIA

The oxidation of glucose in alkaline media is a much less studied reaction compared to that in acid or neutral media. This is probably due to the fact that glucose is not particularly stable in alkaline solutions as discussed in Section 5.1. However, the study of this reaction still attracts some interest because the poisoning from this reaction seems to be less significant in alkaline media and the oxidation current of glucose is higher than in either acidic or neutral media.

5.3.1 *Cyclic voltammetry of Pt in 0.1M NaOH*

A voltammogram and mass response observed for Pt in 0.1M NaOH in the absence of glucose are shown in Figure 48. The voltammetry is typical for this electrolyte. The mass response can be divided into three parts. First, in the H adsorption/desorption region there is a small increase in mass as the potential increases from the cathodic limit, this appears to be coincident with the removal of weakly adsorbed hydrogen and may correspond to the initial stages of adsorption of OH at the electrode surface. Second, the mass is constant in the double layer region of potential, and finally a steady increase in mass of the electrode is

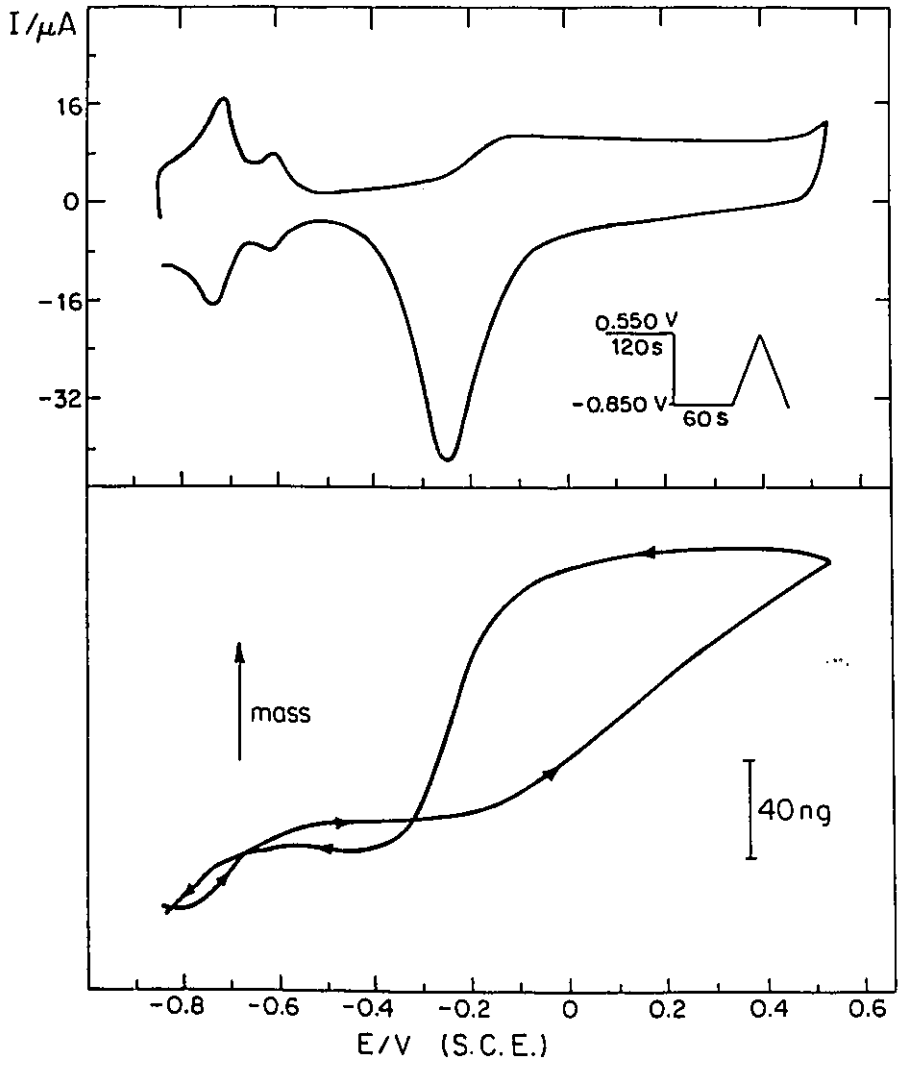

Figure 48. Cyclic voltammogram and mass response for an electrodeposited platinum electrode in 0.1M NaOH. Scan rate was 5mV/s. The potential regime used is shown in the inset.

observed as the electrode surface is oxidised. On the cathodic scan, the mass is largely unchanged until the oxide reduction begins, at which point it decreases sharply as expected. Once the potential reaches the double layer region the mass changes simply reverse those seen on the anodic scan and the mass is returned to the same value that it held at the beginning of the cycle.

5.3.2 *Experiments with glucose*

Figure 49 shows a representative voltammogram obtained using a Pt wire as the working electrode at a bulk glucose concentration of 9mM and at a scan rate of 5 mV/s. The figure illustrates characteristic features of the oxidation of glucose in alkaline media[286]. There are three peaks on an anodic scan (begun after a 60 s pause at -0.85V). The first is associated with the adsorption and dehydrogenation of glucose, and the current is generally attributed to the oxidation of the adsorbed H produced from adsorbed glucose[291]. Following peak I, there is a broad oxidation region with a sharp peak followed by a small shoulder. The complexity of the voltammogram in this so called "double-layer" region of potential has been noted by other workers[284,294]. At this bulk concentration of glucose, the third peak is the largest (it is smaller than the others at glucose concentrations below ca. 1 mM, see, for example, Figure 10 of reference 286) and occurs at potentials where the electrode surface is oxidised in the background electrolyte. This peak increases significantly when the glucose concentration increases and is most likely the result of the oxidation of bulk glucose.

On the cathodic scan, the current remains anodic throughout. The oxidation current begins to increase at ca. 0.3V and continues increasing over a broad region between 0.2 and -0.2V (potentials *positive* of the point where the reduction of irreversibly-formed oxide occurs

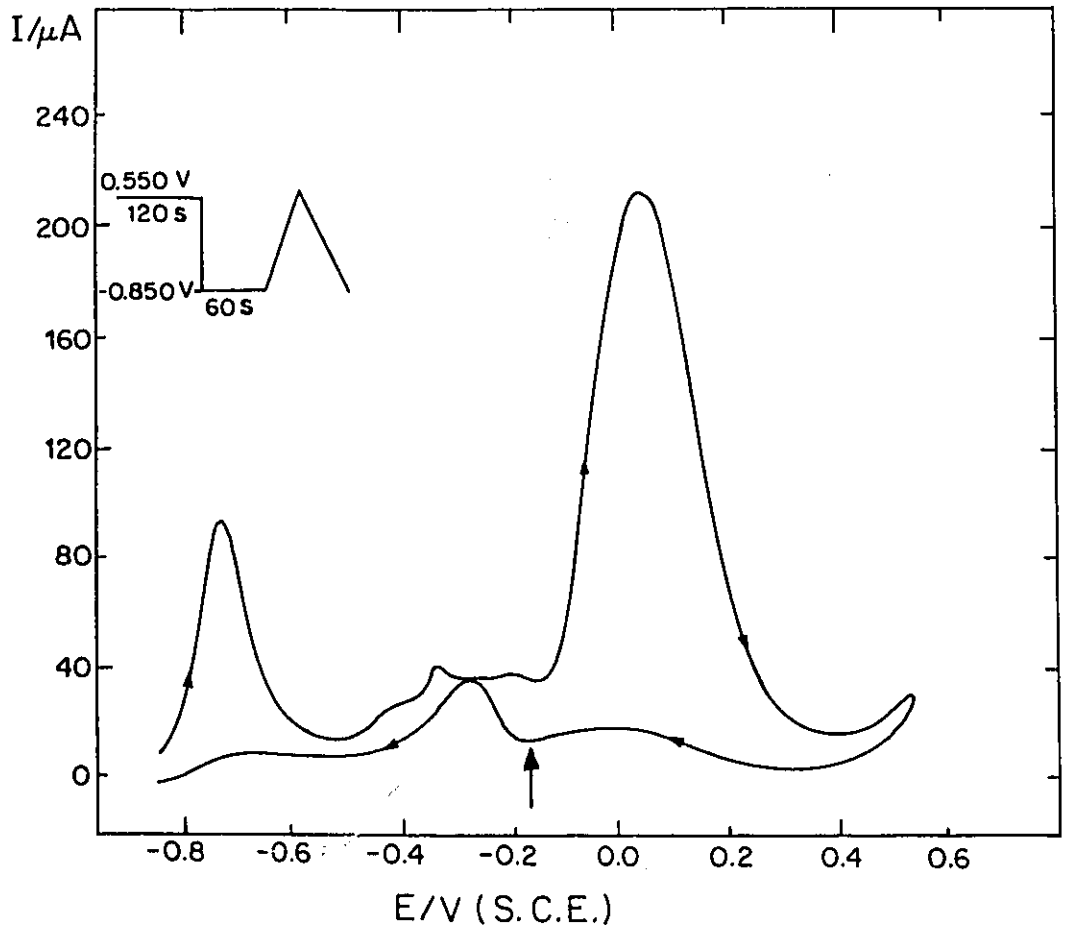

Figure 49. A typical voltammogram for a glucose oxidation (9mM) at a Pt wire in 0.1M NaOH. Scan rate was 5 mV/s. The potential regime used is shown in the inset.

in background electrolyte). The large oxidation currents observed almost obscure the reduction of oxide which is visible solely through a slight decrease in oxidation current at ca. -0.2V as indicated by the arrow in the figure. The current then rises again briefly before falling further as the potential returns to the lower scan limit.

A cyclic voltammogram and accompanying mass response obtained at the EQCM electrode are shown in Figure 50 for a bulk glucose concentration of 9mM. A comparison of the voltammograms in Figures 49 and 50 illustrates the fact that the third peak seen on the anodic scan was substantially smaller for EQCM electrodes and indeed under these experimental conditions was significantly smaller than peak II. (This was also observed for experiments at 0.5 mM and 2 mM glucose at 5 mV/s). In addition, although the peaks I and II are similar in shape for both electrodes, current densities measured for each of the three peaks were lower for the EQCM electrode (for scans at 5 mV/s). The difference was largest for peak III, and smallest for peak II (where the current density was between 1 and 2 times larger for the wire), and declined dramatically for all the peaks as the glucose concentration was increased. At all the glucose concentrations used here, experiments were carried out both at electrodeposited Pt electrodes (EQCM) and at a polycrystalline platinum wire. Results for the latter were found to give good agreement with published data over a range of concentrations. Since a platinised Pt wire gave identical results to a polycrystalline wire it appears that the differences seen between Figures 49 and 50 arise as a result of diffusional differences between the planar EQCM electrode sealed at the bottom of a cell (see Figure 18) and a Pt wire suspended in the bulk of the electrolyte.

A description of the mass response at 9 mM glucose can be divided into three sections accompanying the three voltammetric peaks.

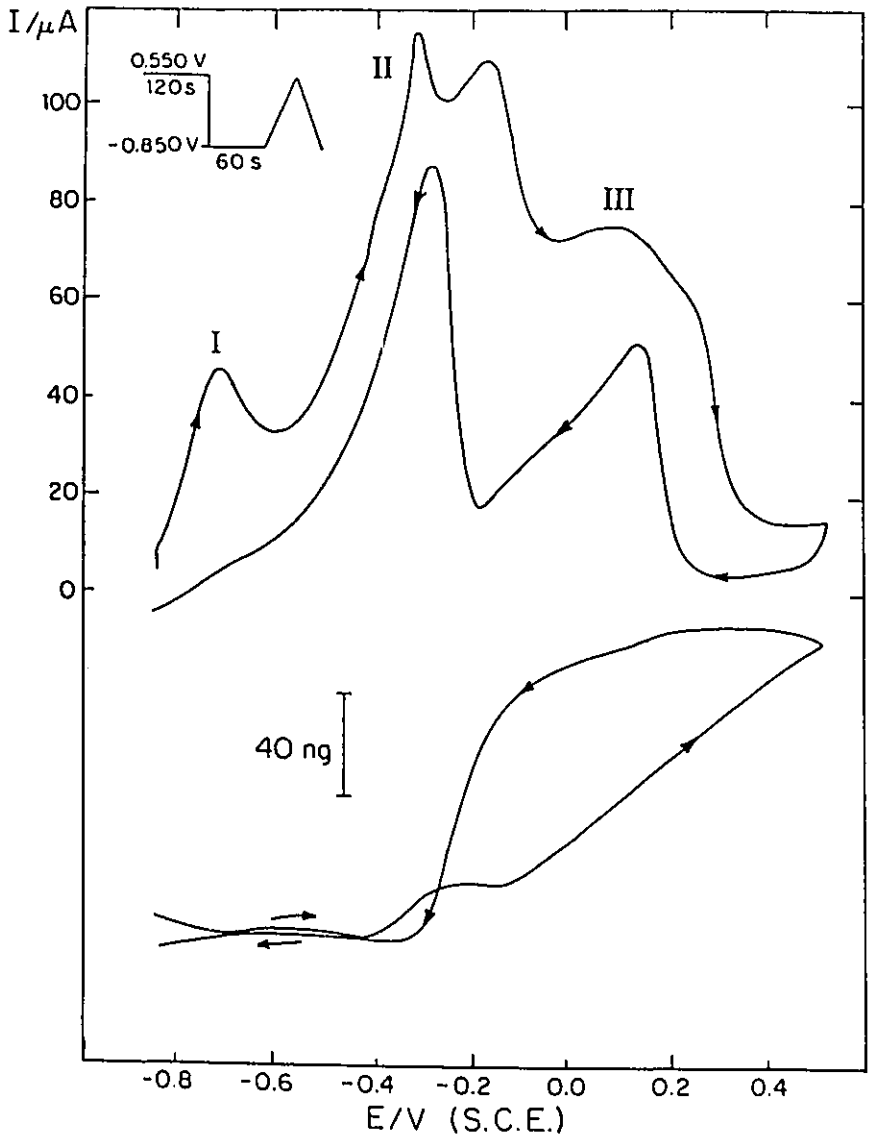

Figure 50. Voltammogram and mass response for 9 mM glucose on the electrodeposited Pt electrode of the EQCM. Scan rate was 5 mV/s. Background electrolyte is 0.1M NaOH

a). First, in the initial stages of the scan after a period of 60s at -0.85V the mass is largely constant. This may be compared with the small increase observed in this potential region in background electrolyte (Figure 45). Addition of glucose to the electrolyte with the electrode poised at a potential of -0.85V produced a mass increase of ca. 40 ng and so it is clear that there is some adsorption of glucose or its oxidation products over this potential region;

b). Secondly, over the region of potential in which peak II is seen in the voltammogram there is an increase in mass of the electrode. A similar feature was seen in 0.1M $HClO_4$ where it was suggested to be the result of the oxidative removal of partially oxidised glucose and readsorption of fresh glucose. In acid media the second oxidation peak results, for the most part, from the removal of a poison formed during the first oxidation peak[298]. Repetitive cycling over the potential range of the first peak in acid was seen to have two effects (see Figure 44), these being a small decrease in mass during cycling and then a significant increase in current for the second peak once the potential range was extended. This is not the case for alkaline solutions where we have observed that although the current decreases upon cycling over the initial stages of the scan, both the size of peak II and the mass of the electrode are largely unaffected by such cycling. Thus it seems that the oxidation current in peak II arises partly from oxidation of poison but perhaps also from some bulk oxidation. Since the mass increase that accompanies peak II is relatively small (being much less than that seen upon oxidation of the electrode) it may still be attributed to the removal of a small amount of adsorbate present on the electrode surface that is formed in the initial stages of a potential scan. Once this adsorbate is removed from the surface then glucose can re-adsorb onto freed sites thus producing the observed mass increase;

c). Finally, the mass changes accompanying the development of oxide on the electrode surface are no different from those in background electrolyte; the mass increases steadily on the anodic scan and then decreases sharply in accordance with the oxide reduction peak. There does not appear to be any significant adsorption of glucose on the oxidised surface in contrast to the situation in $HClO_4$. This conclusion is reinforced by the observation that injection of glucose (to a bulk concentration of 9 mM) with the electrode poised at 0.4V produced a negligible mass change.

In the latter half of the cathodic scan (following reduction of the oxidised Pt surface) the mass is almost unchanged between the forward and reverse scans. In acid media, the mass was actually larger on the cathodic section of the scan in this potential region. This difference arose because when this region of potential is approached in a cathodic scan the removal of oxide produces a clean electrode surface on which glucose can adsorb, whereas on the anodic scan the surface is poisoned during the initial stages of the scan (perhaps with species such as CO[294]) and this prevents adsorption of glucose in the double layer region of potential. The lack of hysteresis in the mass responses in this region in NaOH seems to indicate that in alkaline media the extent of poisoning is less than in acid, as has been suggested previously[294].

5.3.3 *Experiments in 0.1M glucose*

Figure 51 shows two voltammograms (and their accompanying mass responses) with slightly different upper scan limits for a bulk glucose concentration of 0.1M. The voltammogram changes (cf. Figure 50) compared to the lower concentrations. Peak I is less

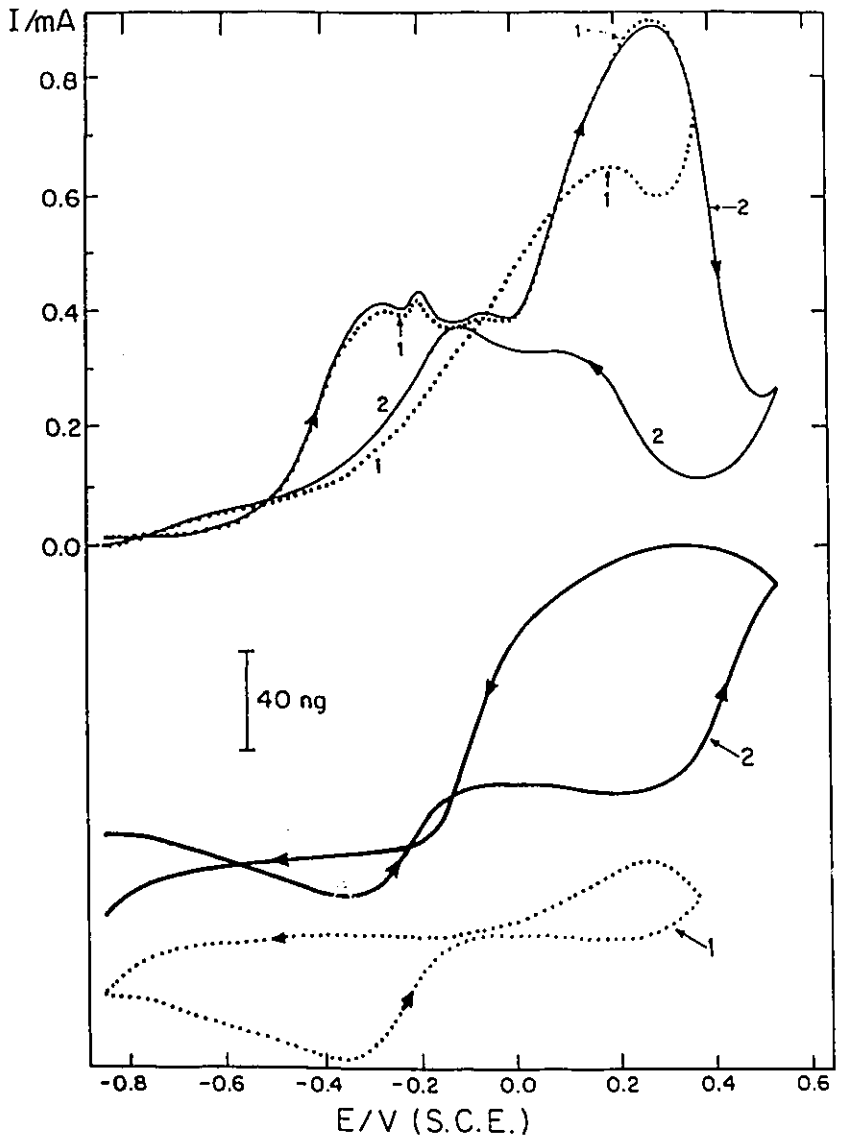

Figure 51. Two voltammograms and accompanying mass responses for a bulk glucose concentration of 0.1M. Scan rate 5 mV/s. The potential regime used for both cycles was the same as for previous figures. Mass responses are displaced for display purposes. Background electrolyte is 0.1M NaOH

prominent, peak II becomes a broad region where at least two small peaks are visible, and peak III increases so that it is larger than peak II. Although the current is anodic at all times on the cathodic scan, there is an increase in current seen at ca. 0.3V, a small dip corresponding to the reduction of irreversibly formed oxide and then a second increase in the region of potential where peak II is seen on the anodic scan. The current then falls away as the potential returns to the lower scan limit. When the upper scan limit is decreased a little (cycle 1), the glucose oxidation current begins to fall off but then rises again at 0.3V shortly after scan reversal and then falls away slowly for the remainder of the scan.

The mass responses which accompany these voltammograms provide an interesting picture of the surface processes at the electrode and specifically the growth and removal of the oxide at the electrode surface, which is largely obscured in the voltammogram because of the large currents arising from glucose oxidation. First we discuss the mass response that accompanies the full cycle (cycle 2 in the figure). A steady, but not large, decrease in mass occurs from the beginning of cycle 2 until the sharp increase that accompanies the second oxidation region in the voltammogram. The first peak in the voltammogram is also less prominent and this has been suggested to be the result of increased amounts of fructose in the solution at higher glucose concentrations, fructose being unable to undergo dehydrogenation [286]. The reason for the slow decrease in mass is not clear but this feature is typical of the mass response when the first voltammetric peak is absent, whereas when peak I is present in the voltammogram it is accompanied by a region of constant mass (Figure 50).

A similar decrease in mass over this region was observed in acid solutions particularly when the potential was cycled over the region of peak I, a process which led to increased

poisoning of the electrode surface as noted in the preceding section. This small decrease in mass thus appears to be connected with the increased poisoning of the electrode surface. As the current rises into the second broad oxidation region, the increase in mass that accompanies this peak is again evident and it is larger than at lower glucose concentrations (Figure 50). The most significant observation occurs after this mass increase because the mass does not begin to increase (as it does in Figure 50) but remains remarkably constant over a potential range of 400 mV even though large oxidation currents are passed. However, once the glucose oxidation current begins to decline at ca. 0.3V, the mass increases sharply. This behaviour would seem to be consistent with a delayed oxidation of the electrode surface caused by the presence of adsorbed glucose, so that the mass only begins to increase sharply once the glucose oxidation current falls away. On the cathodic scan, the mass increases for the first section of the scan and then begins to decrease at a point coincident with the increase in current seen at 0.3V. It then falls more sharply as the potential passes through the normal oxide reduction potential and decreases more slowly as the potential falls further through the double layer region and the hydrogen adsorption/desorption region. The mass at the end of cycle 2 is less than it was at the beginning of the scan.

For cycle 1 when the upper limit of the scan is lower, the response is a little simpler. The response for the anodic scan is largely unchanged except that the increase at the end is very small, reflecting a smaller amount of surface oxidation. There is still a small increase in mass during the initial stages of the cathodic scan, reflecting further surface oxidation, and then a slow decrease. The mass then stays fairly constant for the rest of the scan until decreasing a little in the final stages. The mass is roughly the same at the beginning and end of this shorter voltage scan. This particular difference may arise from a small amount of

dissolution of Pt when the electrode surface is oxidised (cycle 2), which leads to a lower mass at the end of this scan. When the upper voltage limit is decreased, and the extent of oxidation decreased, then the discrepancy between the mass at the beginning and end of the scan is removed. It is also noteworthy that there is now hysteresis between the mass responses in the double layer region of potential. This, together with the lack of a distinct peak I seems to be a further indication of increased poisoning of the electrode in this potential range at the higher glucose concentration (0.1M) relative to the experiment at 9 mM glucose (Figure 50). However, the constant mass signal from -0.2 to 0.2V (anodic scan) and from -0.2V to -0.7V (cathodic scan) for cycle 1, and the slight decline at the end of the scan seem to indicate that poisoning occurs primarily in the H adsorption/desorption region of potential.

The experiments shown in Figure 51 are an interesting illustration of the information that can be obtained from the EQCM. They reveal a process (or lack thereof), namely the oxidation of the Pt surface, that is not visible in the voltammogram since it is obscured by the large faradaic current arising from glucose oxidation. In the presence of 0.1M glucose, the increase in mass corresponding to surface oxidation of the electrode is delayed by ca. 0.4V (compare for example with Figure 50) but once oxidation begins the rate of increase of mass is faster in the presence of glucose. The voltammograms also give information regarding the origin of the most positive peak seen on the cathodic scan. This peak has not been discussed to any great extent in the literature but the behaviour shown in the voltammogram and the mass response strongly suggests that glucose oxidation is largely inhibited by irreversible oxidation of the electrode surface (a similar observation has been made at gold electrodes[284]), since the current falls away rapidly as the mass increases. The first increase

in current on the cathodic scan begins at a potential very close to that at which the current becomes cathodic on a cathodic scan in background electrolyte (see Figure 48) and where the mass begins to decrease slightly. Thus it appears that this current increase derives from oxidation of glucose on a small fraction of the surface at which the oxide has been removed, this current is much less than that seen on the anodic scan, reflecting the lower active area available. Furthermore, as described below, there may be a complication resulting from the catalytic reduction of the oxidised Pt surface by glucose.

5.3.4 *Catalytic reduction of an oxidised Pt surface*

It has been suggested in the literature that glucose can undergo a chemical reaction with oxidised Pt and this was proposed as the slow step in the oxidation process contributing to peak III[291]. The reaction between glucose and an oxidised Pt surface was verified here by the following experiment. An electrode was taken to the upper voltage limit in background electrolyte and then the circuit opened and the rest potential measured. Both the mass and the rest potential (ca -0.02V) of the electrode were found to be very stable over a period of many minutes. Potential control was then re-established at the rest potential and the potential scanned in the cathodic direction to confirm the presence of oxide on the surface through the observation of a reduction peak. This experiment was then repeated, except that upon establishment of the rest potential at -0.02V an aliquot of glucose sufficient to bring the bulk concentration to 9 mM was added to the electrolyte and the potential and mass were monitored with time. The results are shown in Figure 52. The potential decreased rapidly to a new rest value of -0.98 V while the mass also decreased substantially. The potential transient appears to show a slight change in slope at about -0.25V, and the changes in

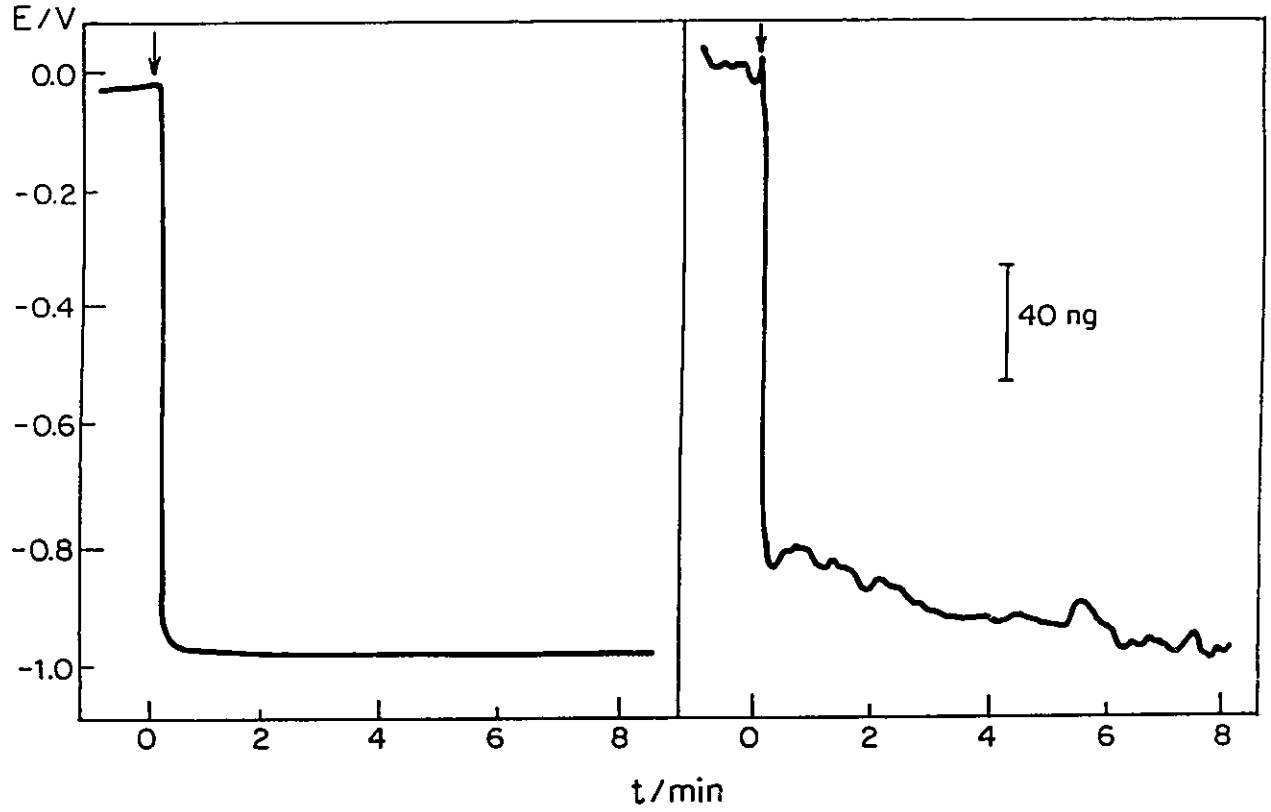

Figure 52. Simultaneous potential and mass transients resulting from the injection of an aliquot of glucose into 0.1M NaOH with the electrode initially at open circuit. The rest potential of the electrode was -0.02V. Final bulk glucose concentration was 9mM, and the arrow indicates the time at which the glucose was added to the solution.

potential and mass occur over about 15-20s. Thus at the slow scan rates used here it is certainly possible that there is some catalytic reduction of the oxidised Pt surface once the potential is such that the reduction can occur electrochemically. At potentials positive of the reduction peak, any oxide that is removed by a chemical reaction will be regenerated by electrochemical means.

5.3.5 *Conclusions*

1. Mass responses accompanying voltammograms for the oxidation of glucose (and injection experiments) indicate the adsorption of glucose or its oxidation products in the initial stages of a voltammetric scan.

2. At low glucose concentrations (9mM) there is little hysteresis in the mass response, in contrast to previous results obtained in acid media, and this seems to indicate less poisoning in alkaline electrolytes in the lower potential ranges. At higher glucose concentrations, increased poisoning of the electrode surface, perhaps because of increased amounts of fructose in solution, causes a mass decrease in this potential range and hysteresis in the mass response.

3. A mass increase accompanies the second peak in the voltammogram and this increase is larger at higher concentrations. It may reflect removal of adsorbed species, perhaps CO, which facilitates adsorption of fresh glucose molecules.

4. Mass responses reveal that the presence of 0.1M glucose is sufficient to prevent the oxidation of the electrode surface at potentials where it is normally observed and shift the onset by several hundred millivolts. However, once the oxidation begins it is rapid and the glucose oxidation falls away. This particular experiment is a further illustration of the ability

of the EQCM to reveal information about electrode processes that is not readily available through other experiments.

5.4 EFFECT OF UPD Pb ADATOMS ON THE OXIDATION OF GLUCOSE IN ACID

The previous sections in this chapter have dealt with the oxidation of glucose at Pt in acid and alkaline solutions. The following section describes a study of the effect of UPD Pb adatoms on glucose oxidation. Thus the oxidation takes place at a Pt surface partially covered with Pb. The underpotential deposit of Pb is established through the addition of Pb^{2+} to the electrolyte so that, when the potential is in the appropriate range during an experiment, Pb^{2+} will be reduced and deposited on the Pt. The extent of coverage of the Pt surface with Pb depends on a variety of factors including the Pb^{2+} concentration, time, potential and (when glucose is present) the presence of other species at the electrode surface. In the remainder of this chapter the effect of adsorbates derived from glucose on UPD (and vice versa) is studied.

5.4.1 *Choice of the potential regime*

The type of experiment performed during an examination of the effect of upd on electrocatalytic processes can have a strong influence on the results obtained. It is therefore necessary to indicate the nature of the experimental methods used in a given investigation. Unless otherwise noted, the procedure employed here involved a step from a potential E_1 (where the potential had been held for a time t_1) to a potential E_2 from where, after a period of duration t_{ads}, a voltage scan to higher potentials was begun. The value of E_1 is chosen so that the electrode surface is oxidised, and any residual adsorbates or poisons will be removed from the electrode. Then, during the period t_{ads}, the upd deposit will develop (provided E_2 is

in the appropriate region). In the absence of glucose, the extent of coverage of Pb (and whether or not equilibrium coverage is attained) depends on the value of t_{ads}, the bulk concentration of Pb^{2+}, and the potential (or more precisely the underpotential) as already described in Cnapter 4. The presence of glucose adds a further complication to this picture since during the holding period glucose can adsorb and react and will compete with Pb^{2+} for adsorption sites. Furthermore, it is clear from several studies[50,293,294,298,299] that different adsorbed species derived from glucose are present at different potentials and thus any references here to adsorbed glucose should be taken to mean adsorbed glucose and any species derived therefrom. These facts should be borne in mind when considering the results reported below.

5.4.2 *Experiments at low glucose and low Pb^{2+} concentrations*

5.4.2.1 Cyclic Voltammetry

Traditionally, examinations of the effect of upd focus on high (>0.1M) concentrations of glucose, but an examination of the effects at low concentrations provides some interesting information. Figure 53 offers a comparison of responses for clean Pt, for Pt with 50 μM Pb^{2+} and for the effect of 50 μM Pb^{2+} on the oxidation of 9 mM glucose (note that the mass traces were recorded without changing the offset of the frequency to voltage converter, and thus are shown exactly as recorded).

In the presence of Pb^{2+} but no glucose, the potential step from E_1 to E_2 provides a transition from an oxidised surface to one where underpotential deposition can take place during the holding period. The decrease in the charge for H adsorption/desorption

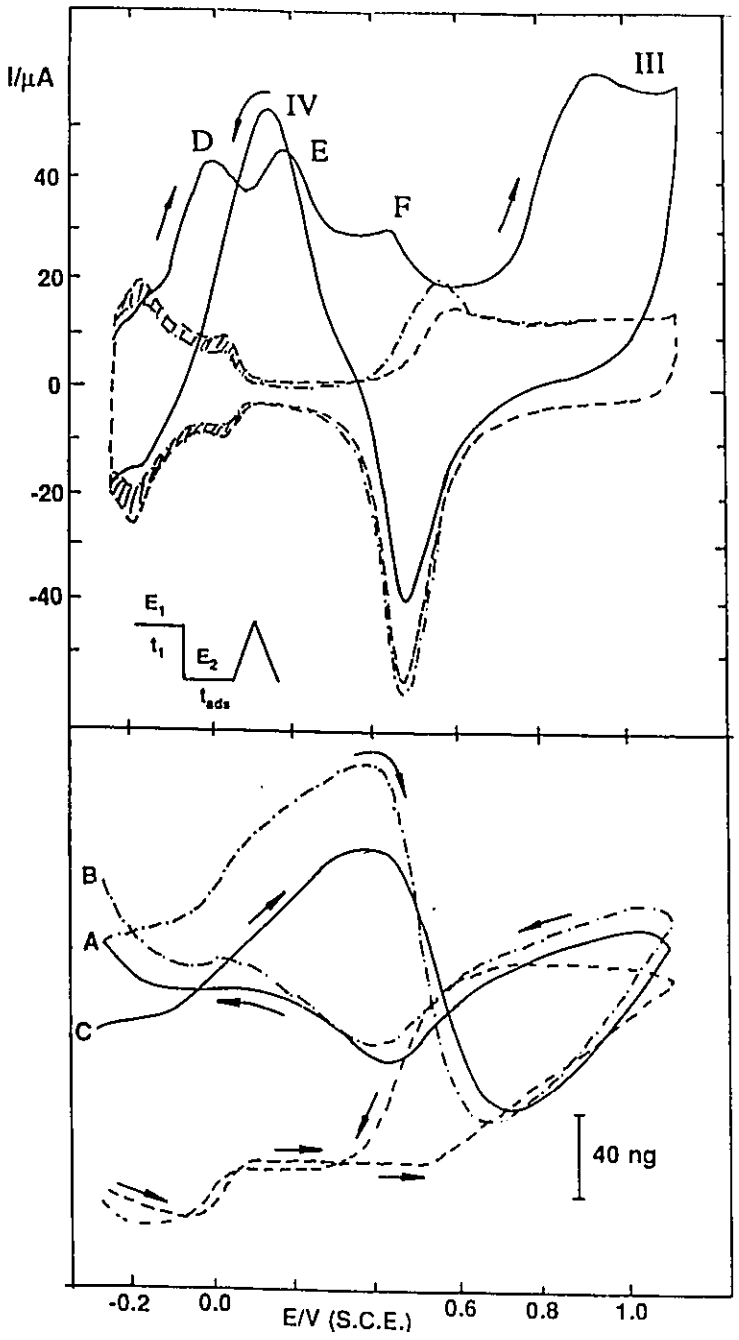

Figure 53. Cyclic voltammograms and mass responses for a Pt electrode in 0.1 M $HClO_4$ (- - -), 0.1M $HClO_4$ with 50μM Pb^{2+} (-.-.-) and 0.1M $HClO_4$ with 50μM Pb^{2+} and 9mM glucose (solid line). E_1 = 1.17V, t_1 = 120s, E_2 = -0.25V, t_{ads} = 60s, scan rate 5mV/s, electrode area = 3.90 cm^2. Mass traces are shown exactly as recorded.

(represented by the shaded area in the Figure) indicates that coverage of Pb (H does not adsorb on Pb) is low, especially since Pb, having a larger radius than Pt, may be able to block more than one Pt site.

As seen earlier, oxidation of glucose (at this concentration) in the *absence* of Pb^{2+}, (such a voltammogram is shown in Figure 41) gives rise to three peaks (designated I, II and III in order of increasing potential) on the anodic scan. In the presence of Pb^{2+} and the consequent partial coverage of the Pt with Pb, the overall enhancement of the glucose oxidation current (relative to the case where there is no upd) is small, as would be expected given the low coverage of lead. However, an interesting change in the voltammetry is observed for glucose oxidation where a broad oxidation region with three distinct peaks (D, E and F) is seen in the region of potential below 0.6V. The usual peak III is observed at higher potentials. It would seem, from a consideration of the peak potentials, that the first peak (D) corresponds to peak I (see Figure 41) which results from the oxidation of adsorbed H produced by the dehydrogenation of glucose. Even in the presence of 50 μM Pb^{2+} the coverage of Pb is small and many free Pt sites remain available for adsorption /dehydrogenation of glucose.

The subsequent peaks (E and F) in the double layer region of potential are more difficult to assign but it is interesting to note that the multiple peaks in this region are reminiscent of the response of glucose in the same potential range in alkaline solutions (Figure 49 and 50), where there is typically less poisoning[286,294]. In the absence of Pb^{2+} (Figure 41), the current falls away after peak I and the peak II, which largely corresponds to poison removal[64,298], is not observed until ca. 0.38V. However, in the region between peaks I and II an oxidation current that is substantially larger than the double layer charging current

is passed. This current must result from glucose oxidation on sites that are not blocked by a poisoning adsorbate. The presence of upd Pb enhances this current giving a peak (E) at 0.2V. From a consideration of potentials, the peak (F) at ca. 0.4V seems to be associated with glucose rather than the removal of upd lead since it is seen at a less positive potential than the UPD stripping peak. If the glucose concentration is increased from 9mM through 0.1M to 0.5M (under otherwise identical conditions to those shown in Figure 53) the broad peak structure in the double layer region remains, but this most positive peak (F) becomes more prominent. This point is of importance later in Section 5.4.3.

With regard to the remainder of the voltammogram, adsorption of Pb^{2+} on the oxidised surface does have an effect on the current of peak III causing it to diminish relative to the case where there is no Pb^{2+} in solution (as will be discussed later) and an increase in current density is observed for the oxidation peak on the cathodic scan (this is visible in Figure 54 also). This is presumably because the growth of the upd deposit also slows down poison development in this region.

5.4.2.2 Mass Responses

In turning to the mass change accompanying this voltammetry, we will first discuss the response for upd with no glucose. Both the Pt background response and the Pb upd have been described in chapter 4, and it is seen that a holding period of 60s at -0.25V is insufficient to produce an equilibrium coverage of Pb since the mass continues to increase in the first stages of the anodic scan which begins at point A. The mass at the end of this cycle (point B) is larger than at the beginning (point A) indicating that upd coverage proceeds further towards its equilibrium value during the cathodic half of the scan (under these

conditions) than it does following the potential step from 1.17V and a 60s pause.

When glucose is present, the 60s pause at E_2 allows competitive adsorption of both glucose and Pb. This is revealed through the mass at the beginning of the anodic scan (point C) being lower than it was in the absence of glucose, reflecting a slightly lower coverage of Pb. Still, the upd deposit continues to grow in the initial stages of the anodic scan here also, until stripping begins at ca. 0.4V. Clearly until this latter potential, free surface sites (either unoccupied by Pb or glucose to begin with, or freed by the oxidation of adsorbed H) are still available for the upd coverage to increase. The sharp mass decrease associated with the removal of the upd lead is smaller and less steep when there is glucose present, reflecting first the lower coverage of Pb that was developed in this experiment, and second a removal process that is extended to slightly more positive potentials when compared with the response in the absence of glucose.

This experiment at low Pb coverage and low glucose concentration thus reveals some competition for adsorption sites that leads to a slightly smaller upd coverage, but even this low coverage is sufficient to influence the oxidation of glucose, and perhaps to reduce the extent of poisoning. More importantly, the fact that (as noted earlier) glucose (alone) has little effect on the mass response is not necessarily a disadvantage in examining these systems with the EQCM since the upd lead has a large effect and the effect of glucose is revealed in the mass response through the influence it has on the upd lead coverage. Finally, the mass response allows changes in coverage of Pb, and particularly the stripping of upd lead on the anodic scan, to be followed despite the fact that they are largely obscured in the voltammetric response because the small currents associated with the UPD process are concealed by the larger current resulting from glucose oxidation.

5.4.3 *Effect of increasing coverage of UPD lead*

5.4.3.1 Influence of UPD Coverage on Voltammetry

In an experiment similar to that shown in Figure 53, the coverage of Pb was varied by increasing the time (t_{ads}) for which the electrode potential was held at -0.25V after the step from 1.17V. Increasing t_{ads} allows upd coverage to proceed further toward its equilibrium value. Figure 54 presents results for t_{ads} of 15s, 120s and 420s, and as before we shall discuss the voltammetry first.

The increasing coverage of Pb influences the oxidation in both the H upd region and the double-layer region of potential. The peak III observed on the oxidised Pt surface is not affected by t_{ads}, and neither is the oxidation peak (IV) seen on the cathodic scan to any great extent. In the latter case, as long as scan rate and the concentrations of glucose and Pb^{2+} are not changed, the coverage of Pb which can develop once the potential moves into the upd region (following partial reduction of the oxidised electrode surface) will always be the same.

In the H upd region, there is only a broad oxidation region when t_{ads} is 15s (curve 1), whereas when t_{ads} increases to 60s (curve 2) the peak is seen to have grown in size. Extension of t_{ads} to 420s then causes the peak to diminish (curve 3), so that the current is less than it was for a t_{ads} of 15s. The logical explanation of this pattern of behaviour is that adsorption/dehydrogenation of glucose is a little slow and so the current increases as t_{ads} increases from 15s to 120s (this is also seen in the absence of Pb), because there is still sufficient free Pt to allow this process to continue. However, when t_{ads} becomes 420s, the coverage of lead increases to a value where there is less Pt available for adsorption /dehydrogenation (Pb having no adsorbed H) and the current drops away. The Pb may also

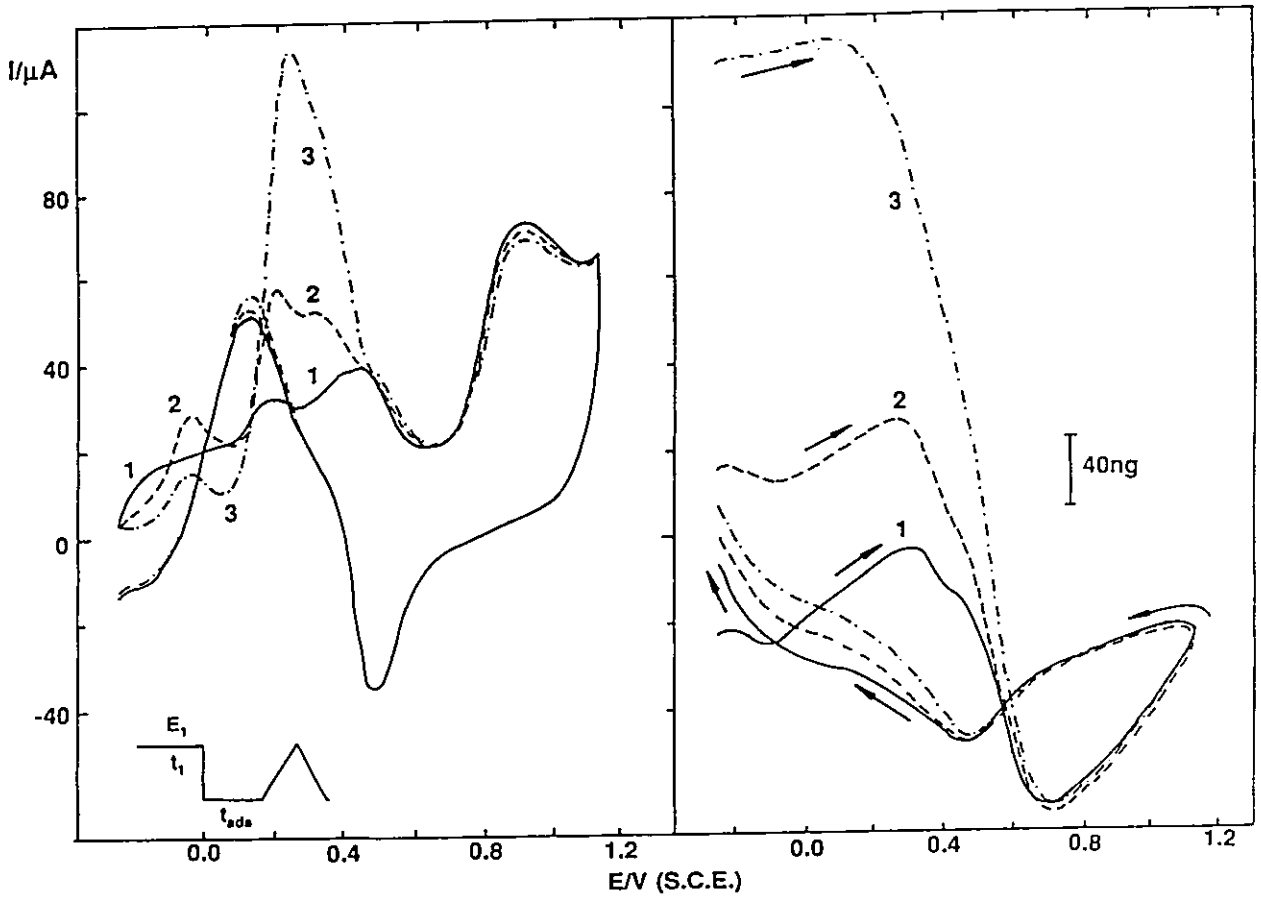

Figure 54. Cyclic voltammograms and mass responses for 0.1M $HClO_4$ with 9mM glucose and 50μM Pb^{2+}. E_1 = 1.17V, t_1 = 120s, E_2 = -0.25V, t_{ads} = 15s (1), 120s (2), 420s (3). Scan rate 5mV/s, electrode area = 3.81 cm^2.

assist somewhat in inhibiting the development of the poison in this potential range.

The increasing $t_{ads,}$ and the consequent higher coverage of Pb also influences oxidation in the double layer region of potential. For the smallest t_{ads}, and thus coverage, the response is similar to that of Figure 53 with two dominant peaks. Increasing coverage enhances both peaks, but the first peak is influenced more, so that at the highest coverage the second peak is visible only as a shoulder. The higher coverage produces a more noticeable catalytic effect on the current in this potential region. The variation of the peak structure in the double layer region of potential with concentration (described in Section 5.4.2) and with coverage (described here) seems to suggest that the oxidation at the lowest potentials (E) is that of glucose on free Pt in the absence of poisons, while that at more positive potentials (F) results from poison formation. Thus this latter peak (F) is most prominent at low coverages (t_{ads}) and high glucose concentrations, where the free Pt surface and high glucose promote the formation of poisons, whereas the current at lower potentials (E) is largest at higher Pb coverages when poisoning is inhibited by the upd coverage. Recent results from a study of glucose oxidation in alkaline solutions[58] have indicated that the product distribution from upd modified electrodes is different from that on unmodified Pt electrodes and at gold, ring disc studies have indicated that the number of electrons transferred to glucose diminishes with increasing concentration[284]. Thus it is possible that the changes in voltammetry with coverage and concentration reported here are at least in part due to changes in the extent of oxidation of glucose.

5.4.3.2 Influence of UPD Coverage on Mass Responses

The increase in t_{ads} has two effects on the mass response. First, the response in the

initial stages of the anodic scan (until stripping begins) changes from displaying an overall increase (t_{ads} = 15s, 120s) to being flat (t_{ads} = 420s), indicating that in the latter case (but not in the former) an equilibrium upd coverage is reached. Second, the increasing coverage of Pb is reflected in the dominant feature of the mass which is the decrease observed as Pb is stripped from the electrode surface. In this respect the mass provides a clear indication of the changes in coverage with time. Interestingly, for the highest coverage of Pb, stripping begins at ca. 0.2V where the oxidation current is still rising in the voltammogram. There is no variation in the mass response once the Pb deposit has been removed but the mass responses that accompany the final half of the cathodic scan do show a small variation. This may be a result of a slight increase in the interfacial concentration of Pb^{2+}, derived from the stripping of the upd deposit, giving rise to a small increase in coverage.

Comparable coverages to those of Figure 54 can also be obtained by using a higher [Pb^{2+}] and decreasing t_{ads}. In fact, the result for t_{ads} = 420s and 9 mM glucose was found to be qualitatively similar to that where a higher [Pb^{2+}] (0.4 mM) was employed with t_{ads} = 60s. The higher [Pb^{2+}] means that less time is required to obtain a coverage comparable to that obtained after 420s in Figure 54. These results highlight the importance of recognising that the upd coverage, which is a crucial factor in influencing the oxidation, is controlled by a variety of factors including the concentration of Pb^{2+} in solution, the potential (underpotential) and the time scale of the experiment (which dictates whether or not the coverage is able to reach equilibrium). Thus a maximal catalytic effect attributed to a particular concentration of upd ions may only be relevant for the experiment in question. Furthermore attribution of a maximal effect to a given coverage on the basis of a comparison of cyclic voltammetric data with an equilibrium upd isotherm alone may be misleading because of possible non-

equilibrium development of the deposit during cyclic voltammetry and also because of the fact, shown in Figure 54, that the deposit may begin to be removed before the peak current for the organic oxidation is observed.

5.4.4 *Competitive adsorption in the UPD region*

5.4.4.1 Mass transient experiments

It is well known that the oxidation of glucose leads to electrode poisoning and in a previous paper it was established that cycling the potential in the H upd region of potential in the presence of glucose led to a substantial increase in the coverage of the electrode by a poisoning adsorbate as described in Section 5.2.2. The removal of this adsorbate is effected in the double layer region of potential. Furthermore, mass transients following injections of Pb^{2+} into an electrolyte with the potential poised at a value in the upd region provide a simple means of estimating upd coverages (see chapter 4). We were therefore prompted to investigate whether such experiments could yield information regarding the coverage of adsorbates and poisons present on the electrode surface during the course of oxidation of glucose. Because of the longer time involved, these experiments are more applicable to electrolysis than to the understanding of cyclic voltammetry data. Figure 55 shows the results of two experiments. In the first, in the absence of glucose an equilibrium coverage of Pb of 0.69 was estimated from an injection of Pb^{2+} (sufficient to bring the bulk concentration to 5 x 10^{-5} M) with the potential held at 0.0V. In the second a significant coverage of poisoning species was generated by cycling the potential over the H upd region in the presence of glucose. After a period of holding at 0.0V a similar aliquot of Pb^{2+} was injected into the

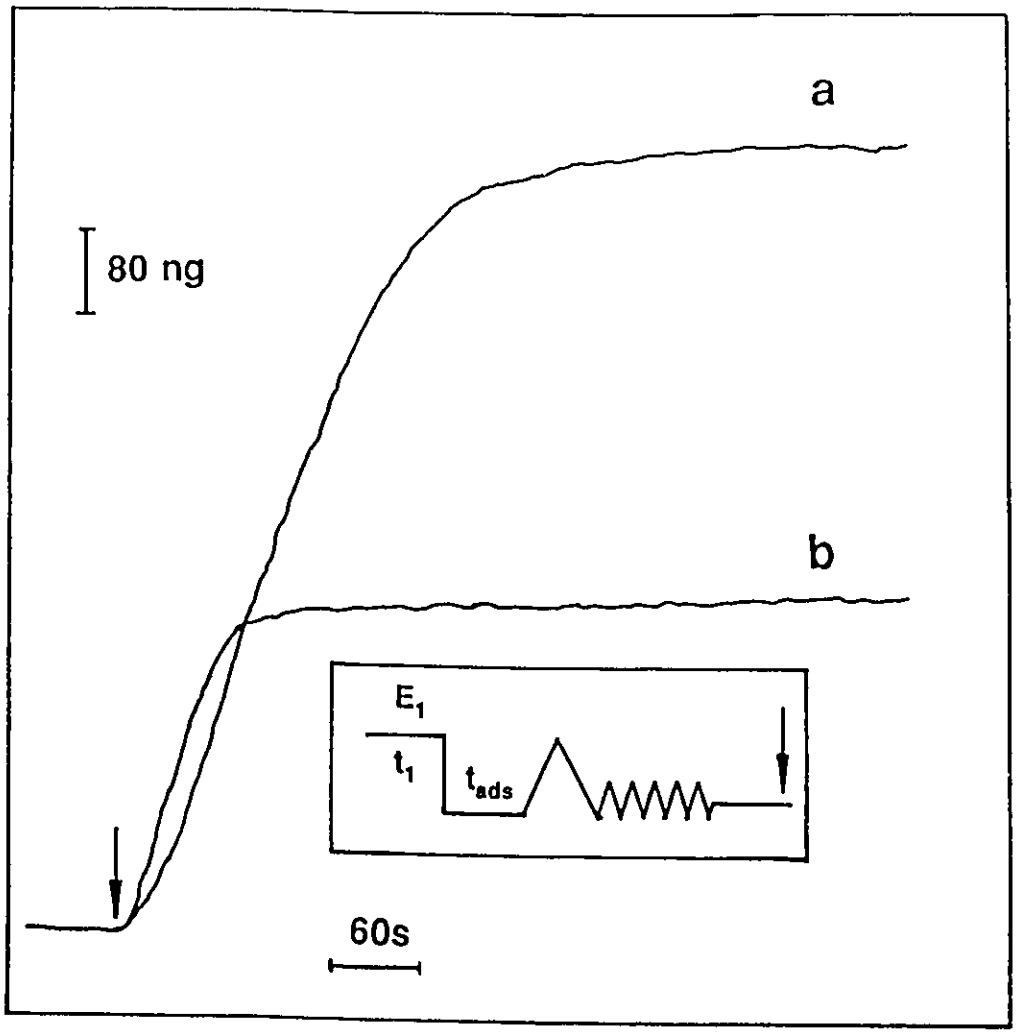

Figure 55. Mass transients resulting from injection of Pb^{2+} into 0.1M $HClO_4$ for a) a clean Pt electrode with E_1 = 1.17V, t_1 = 120s, E_2 = 0.0V, t_{ads} = 60s, b) a Pt electrode partially covered with poison derived from glucose as a result of scanning as detailed in the inset. E_1 = 1.17V, t_1 = 120s, E_2 = -0.25V, t_{ads} = 60s, and following a cycle between -0.25V and 1.17V the potential was cycled 6 times between -0.25V and 0.2V before holding at 0.0V for 180s prior to injection of Pb^{2+} to bring the bulk concentration to 50μM. Electrode area = 3.75 cm^2. The concentration of glucose was 9 mM.

electrolyte and the mass change recorded as a function of time. The observed mass change is significantly lower in this case and corresponds to a coverage of 0.29. (Coverages were calculated from mass using a value of 260 μC cm^{-2} (converted to mass) for monolayer coverage as described earlier in chapter 4). This simple experiment provides a clear indication of the extent to which the electrode surface is made inaccessible to the Pb by the adsorbate formed from glucose, although the coverage here is larger than it would be during the course of a normal voltammetric scan.

The effect of adsorbates derived from glucose was also studied as function of potential as described above. Figure 56(a) shows the equilibrium coverage of upd lead as a function of potential for two different concentrations of glucose as well as for the case where no glucose was in solution. An increase in the concentration of glucose does not have a significant effect on the results, perhaps because of the time that was allowed to elapse prior to injection of Pb^{2+}. Since equilibrium upd coverage is potential dependent, a more appropriate representation of the data is seen in Figure 56 (b), where the *decrease* in equilibrium coverage, $-\Delta\theta$, as a result of the adsorbates on the electrode surface is presented as a function of potential. Several conclusions can be drawn from this data. First, at extreme negative potentials, coverage in the absence of glucose (designated as θ_{Pb}) is high and $-\Delta\theta$ is small and it may thus be concluded that only a small fraction of the surface is covered by glucose. As the potential increases to ca. 0.1V, θ_{Pb} is still quite large (>0.6) and $-\Delta\theta$ is also significant reflecting a substantial coverage of the surface by adsorbates derived from glucose. These conclusions agree with previous estimates[291,293,297] of coverage of species derived from glucose where coverage displays a maximum of roughly 0.5 at about 0.2V (R.H.E.) and falls sharply either side of this, although it was pointed out that this profile applies where a fresh

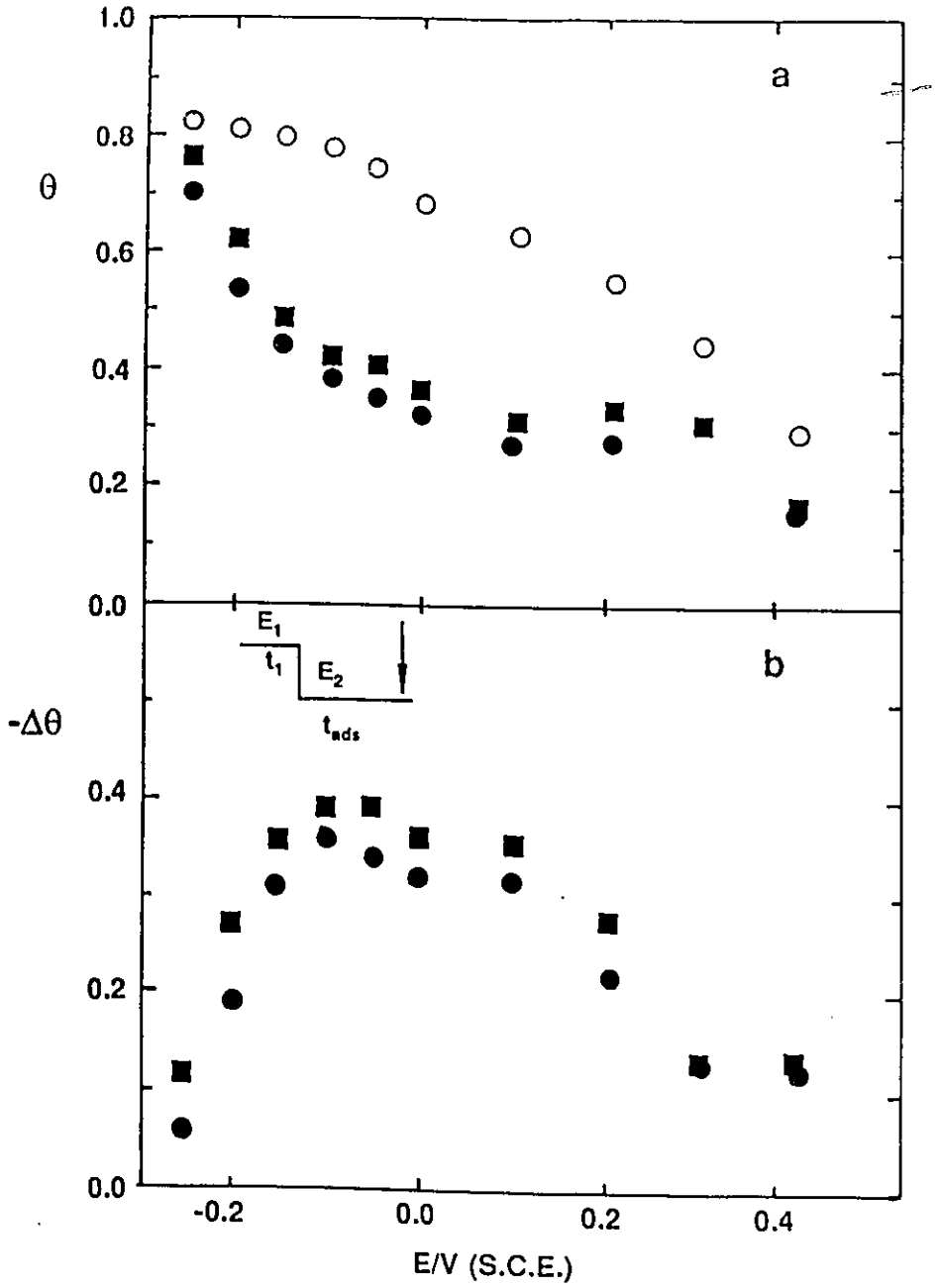

Figure 56. a) The effect of glucose concentration on the equilibrium coverage of upd Pb in 0.1M $HClO_4$. Concentrations were (o) 0 mM ; (■) 9mM ; (●) 0.1M. Coverages were obtained from mass transients recorded after the potential profile shown in the inset. E_1 =1.17V, t_1 = 120s, E_2 as indicated on the ordinate, t_{ads} = 600s. b) The decrease in equilibrium upd Pb coverage (-Δθ) as a function of potential. Data derived from Figure 56(a).

measurement was made at each potential[291]. Rate constants for adsorption (obtained in phosphate buffer solutions) also follow a similar profile[297], thus it is not unreasonable to suggest that the largest decrease in coverage seen (between -0.1V and 0.1V) is consistent with the most rapid development of poisoning of the electrode and thus highest coverage. Finally as the potential increases, both θ_{Pb} (ca. 0.3) and $-\Delta\theta$ (ca. 0.15) become small and thus it is not clear, at least from this data alone, to what extent the surface is covered by adsorbates even though there is a measurable suppression of upd. Two extreme scenarios are possible. In the first, Pb and glucose adsorb on the same sites at the surface so that at the highest potential employed in this experiment there would still be a competitive effect, even though the fraction of the surface covered by both species would be small. In the second, adsorbed species derived from glucose cover nearly all of the surface leaving only a small fraction available to Pb. Previous results indicating significant adsorbate formation at 0.2V (S.C.E.) (Section 5.2) and the data of Horanyi[50] showing coverage increasing with potential at least until 600mV (R.H.E.) indicate that this latter alternative may be the most likely.

5.4.4.2 Cyclic Voltammetry

A further interesting result is obtained if a voltammogram is recorded following an injection experiment such as that of Figure 55(b) i.e. an anodic scan is begun after the upd deposit has reached equilibrium (as indicated by the steady mass signal). Such experiments were performed for different concentrations of glucose and Pb^{2+} and a typical response is shown in Figure 57 (solid lines). However, a brief description of the two other curves will be given for clarity. These represent oxidation of 9 mM glucose (dashed line) after the standard potential programme used in Figure 53 and the voltammogram seen after a high

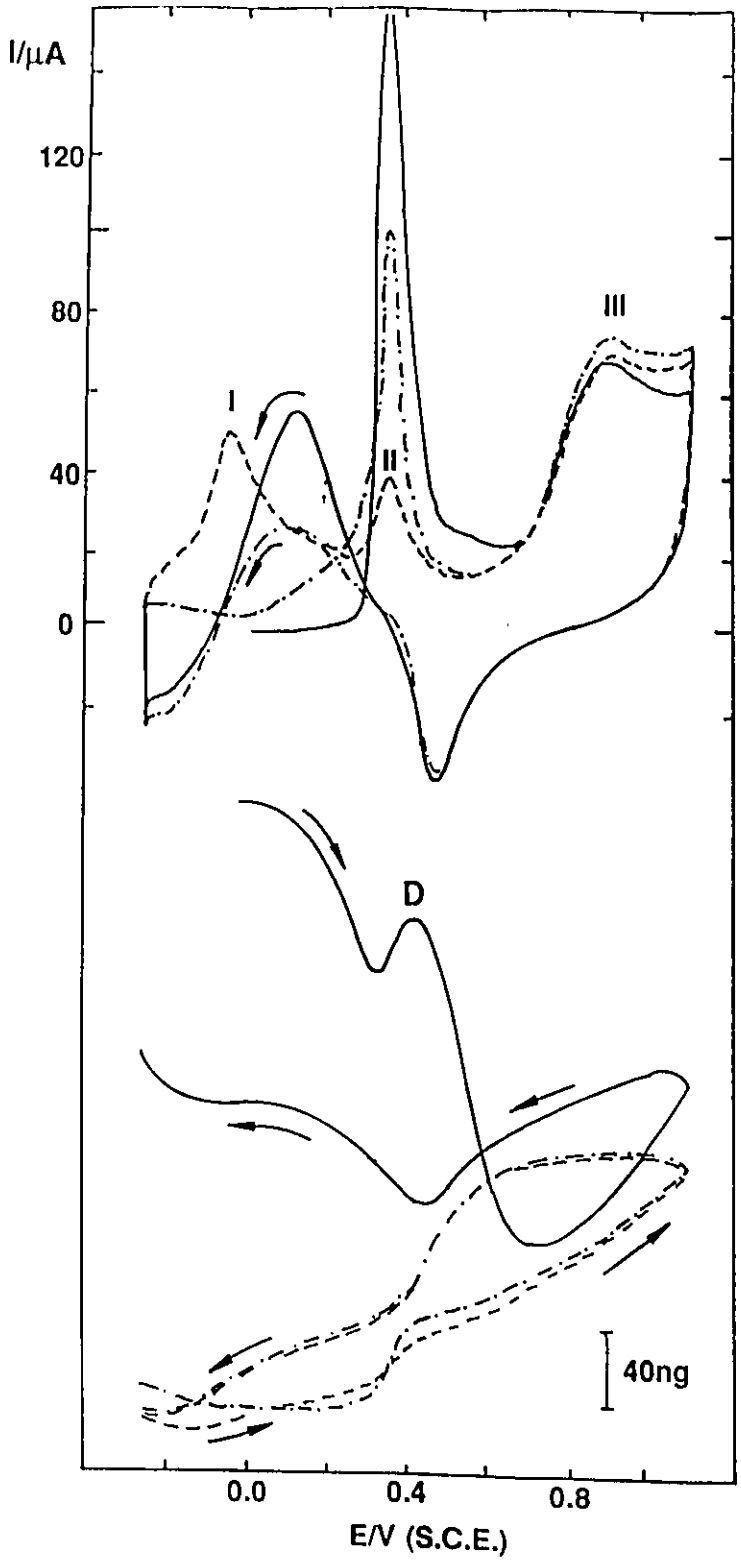

Figure 57. Cyclic voltammograms and mass responses for 9mM glucose in 0.1M $HClO_4$. (- - -) Potential profile as for Figure 53. (-.-.-.-) Following a profile like that of Figure 53, potential was cycled 5 times between -0.25V and 0.2V to develop a high coverage of poison before recording. Solid line - as for preceding response, but after cycling 5 times between -0.25 and 0.2V potential was held at 0.0V for 180s and then the concentration of Pb^{2+} was raised to 50μM and the potential held for a further 480s at 0.0V prior to recording the cycle. Scan rate 5mV/s, electrode area 3.75 cm^2.

coverage of poison is generated by cycling in the H adsorption/desorption region. Detailed descriptions are available from Section 5.2.2. The regular oxidation of glucose, (dashed line) shows the typical three peaks (I,II and III) on the anodic scan, and the final oxidation peak on the cathodic scan after surface oxide reduction. When the coverage of poison is increased prior to recording the voltammogram, peak I is suppressed because the surface is covered with poisoning adsorbates, while peak II is increased dramatically to about 100 μA, since it is largely due to poison removal[298]. The mass responses for these two cases are quite similar and do not differ significantly from that for clean Pt except in two small ways. First, there is some hysteresis in the region between 0.0 and 0.4V due to different extents of adsorption on the anodic and cathodic scans. Second, there is a small mass increase that occurs parallel with peak II. As the poison coverage grows, this mass increase becomes larger.

Turning now to the response in the presence of Pb^{2+} (solid line) the focus here is on peak II which accompanies adsorbate removal. At the starting point in the scan, the electrode surface is covered with both adsorbates derived from glucose and a (reduced) equilibrium coverage of upd lead because poison coverage was deliberately increased and then Pb^{2+} added *before* the potential scan was begun. The voltammetry displays what is a low current in the initial stages followed by a sharp oxidation peak (reaching 160 μA) as the poison is removed from the electrode surface. The remainder of the scan is reminiscent of Figure 53 although it can be seen that there is a slight enhancement of the oxidation current on the cathodic scan caused by the development of upd lead.

The mass change (solid line) that accompanies the voltammogram after addition of Pb^{2+} is initially flat and then begins to decrease. This presumably corresponds to gradual removal of Pb. However, as the potential moves further positive and the accumulated poison

begins to be removed from the electrode surface, there is an accompanying peak (labelled D) in the mass response. This peak corresponds to a mass increase and is not seen during the course of a normal voltammogram under the same conditions (i.e. 9 mM glucose, 50μM Pb^{2+}, Figure 53, solid line). In the two other mass responses shown, where Pb^{2+} is absent, removal of the adsorbate gives rise to a mass increase that is larger and steeper for the case where the higher coverage of poison was developed deliberately. This was suggested to result from the replacement of adsorbed residues (removed by oxidation) by fresh glucose as discussed in Section 5.2. Following this line of argument the peak in the mass response is most sensibly explained by some of the surface, previously blocked by adsorbate, being occupied by both glucose and Pb when sites are freed. Since glucose has a smaller influence on the mass response it is most likely that the Pb fraction of this process leads to the peak. Figures 55 and 56 show that the equilibrium coverage of Pb at 0.0V is much reduced by the adsorbate derived from glucose. The consequence of this is that as the adsorbate is removed, the coverage of Pb is still less than its true equilibrium value and so a small increase in coverage is seen. Upd is still possible in a thermodynamic sense at the potential where the adsorbate is removed. However, shortly thereafter upd removal begins and the mass response reverts to its usual form. In the region of peak III, the mass is higher in the presence of Pb^{2+} and glucose, a fact that may be attributed to the adsorption of Pb^{2+} cations on the oxidised Pt surface as described in Chapter 4. The mass data again demonstrates the ability to reveal simple information not available from voltammetry, in this instance the fact that upd can and does occur when a high surface coverage of adsorbate is removed from the electrode and secondly the presence of adsorbed cations on the oxidised electrode.

5.4.5 *Competitive adsorption at an oxidised electrode surface*

It has been noted in the literature that peak III, corresponding to the oxidation of glucose on the oxidised electrode surface, is decreased in the presence of Pb^{2+} ions in solution[302]. Although underpotential deposition is not possible at these potentials, both modulated reflectivity[161] and our EQCM experiments (chapter 4) have shown that Pb^{2+} ions are adsorbed on the electrode surface. EQCM experiments also indicated an apparent adsorption of glucose, or species derived from it, on the oxidised surface in 0.1M $HClO_4$ (Section 5.2). Possible competitive adsorption of glucose and Pb^{2+} cations was investigated by injecting Pb^{2+} into solutions containing differing concentrations of glucose at a given potential. The results are shown in Figure 58 where the electrode potential was 1.0V. There is no significant difference between the results observed in 0mM and 9mM glucose solutions, but there is an observable decrease in the mass change when the glucose concentration is increased to 0.1M (note that the actual mass changes observed (ng) are several times larger than the normalised (ng cm^{-2}) values). Unfortunately, the complementary experiment (with Pb^{2+} in solution and glucose added) is not possible for 0.1M glucose, because the difference in viscosity between 0 and 0.1M glucose leads to a frequency change not derived from mass. Nevertheless the results of Figure 58 seem to indicate that an adsorbed species derived from glucose is present at the electrode surface and inhibits cation adsorption by Pb. While Skou[292] suggested that glucose oxidation at an oxidised Pt surface proceeded through adsorption and Vassilyev et al.[291] indicated that oxidation proceeded through an interaction of glucose with the Pt oxide followed by electrochemical regeneration of the oxide, Horányi[50] concluded recently that no adsorption occurs at oxidised Pt electrodes (in 1.0M H_2SO_4) on the basis of his studies using radiolabelled glucose. These differences may result

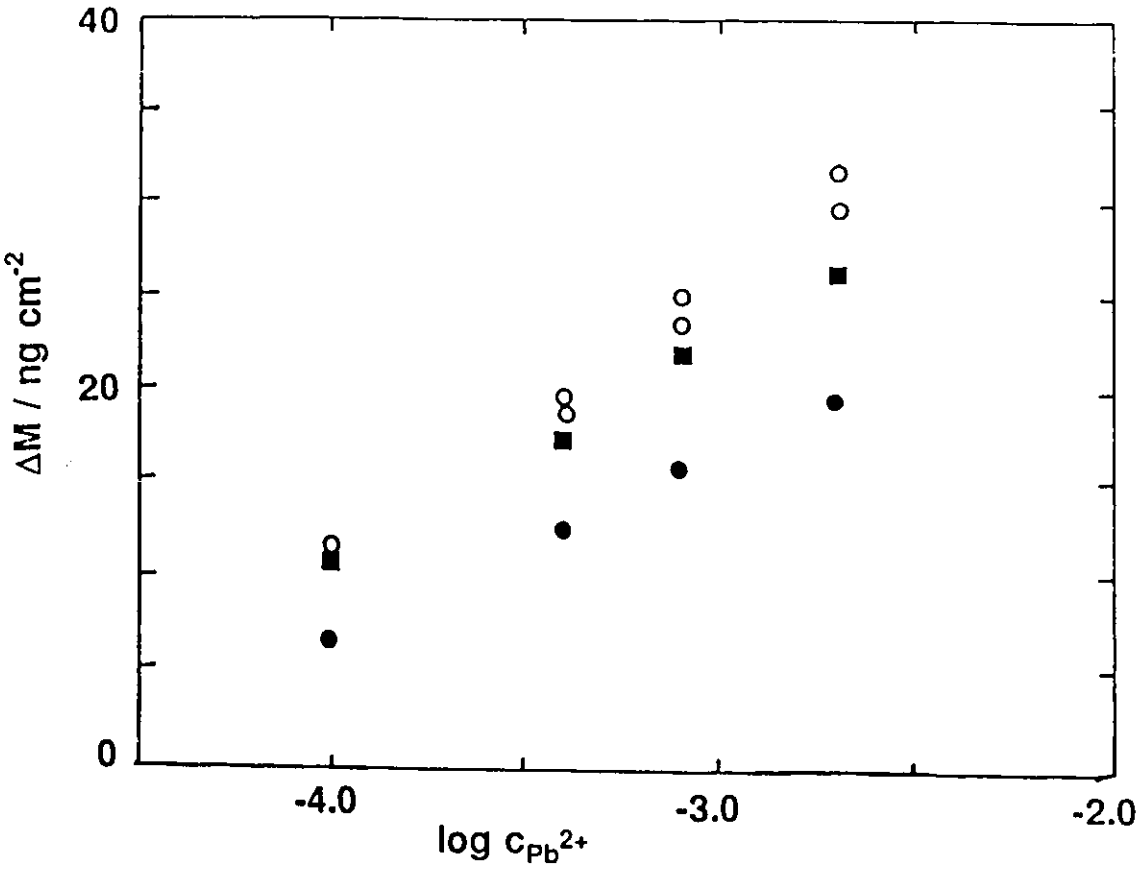

Figure 58. Mass gain (per unit area) as a function of the logarithm of the concentration of $[Pb^{2+}]$/M when Pb^{2+} is injected into 0.1M $HClO_4$ containing 0 (o), 9mM (■) and 0.1M (●) glucose. E= 1.0V. Electrode area = 2.87 cm^2.

from the fact that the radiolabelling experiment was performed beginning at a preoxidised surface at 1.4V (R.H.E.). Adsorption may well depend on the extent of oxidation of the surface and hence on the extent to which the place exchange process (where O or OH species are inserted into the metal lattice upon oxidation) has occurred. The complete two electron oxidation of the surface and place exchange may inhibit adsorption. Furthermore, the varying extents of oxidation of the glucose molecule itself and the possible presence of species such as gluconic acid and other carboxylic acids[298] could well produce adsorption of anionic species on the oxidised surface. Finally, preliminary experiments in 0.5M H_2SO_4 do not reveal the same mass increases seen in this region in 0.1M $HClO_4$ when glucose alone is added to the electrolyte. Thus the role of the anion of the background electrolyte and the strength of its adsorption may be influential.

5.4.6 *Conclusions*

1. EQCM experiments provide an interesting insight into the surface processes occurring during electrocatalytic reactions at upd modified electrodes. Despite the small changes that the presence of glucose alone has on the mass response, information about glucose adsorption is obtained through the effect it has in suppressing the upd mass response which is large.

2. EQCM data accompanying cyclic voltammetry reveals some suppression of upd, due to the presence of adsorbates derived from glucose, under the conditions used. More importantly, changes in upd coverage are apparent in the mass response even when the current associated with these changes is obscured by a glucose oxidation current. Thus it is seen to be difficult to correlate upd coverages with catalytic activity from a comparison of

cyclic voltammetric data and upd isotherms since (even at the low scan rates used here) equilibrium upd coverage is not maintained and coverage is seen to decrease even as the glucose oxidation current rises. Data from experiments where the current is sampled at a constant potential after equilibrium coverage is reached, such as those obtained for formic acid[87] are more appropriate in this respect.

3. Small upd coverages lead to a multiple peak structure in the double layer region of potential that changes to a single peak as coverage increases. This may arise in part from sufficient Pt surface being available for poison formation at low upd coverages.

4. Mass transients have been shown to be useful for the assessment of the extent of coverage of the electrode surface by adsorbates produced from glucose oxidation and it is also possible to see adsorption processes that take place upon removal of a blocking adsorbate in the mass response.

5. Finally, the adsorptive competition between the different species is also seen on an oxidised electrode surface where cation adsorption is suppressed by adsorbates derived from glucose.

Chapter 6

Electrocatalytic Oxidation of Methanol

In this chapter, we present an investigation of the oxidation of methanol using the electrochemical quartz crystal microbalance technique. Methanol has been chosen as the reactant of study because it has a rather simpler structure than glucose and fewer products/intermediates are involved in the oxidation. The main research focus is placed on the application of the EQCM to probe the extent of adsorption of organic species derived from methanol. Before proceeding to the experimental results, a short review of the literature on methanol oxidation is presented below.

6.1 INTRODUCTION

Methanol is one of the most attractive candidates as a fuel in fuel cell technology because of its simple structure, high energy density, and easy handling and storage. During methanol oxidation, six electrons are transferred per mole if the oxidation proceeds to give CO_2. In acid medium the overall reaction can be written as:

$$CH_3OH + H_2O \longrightarrow CO_2 + 6H^+ + 6e$$

Unfortunately, this reaction proceeds through a dual-path mechanism, as mentioned in Chapter 1, and poisoning intermediates can be formed on the electrode surface. Thus much work has been done in the past two decades to identify the poisoning species and to improve the catalytic activity of electrodes for methanol oxidation.

6.1.1 *Spectroscopic identification of intermediates*

The exact nature of the poisoning species has been a central point of controversy for a long time. Two types of poisons have generally been assumed: CO[305] or COH[4,9,306]. Only recently did in-situ spectroscopic measurements give new evidence for the nature of the adsorbed species. Beden et al. were the first, using the EMIRS technique, to give unambiguous proof of the presence of adsorbed CO on Pt during the oxidation of methanol[25]. Linearly adsorbed CO was found to be the main poisoning species with an IR band near 2060cm^{-1}, but bridge-bonded CO was also found to be present, with a small band at 1850-1900cm^{-1}. Similar results were reported by other authors using various IR reflectance techniques. Mundy et al. employed SNIFTIRS to study the oxidation of methanol on Pt in neutral medium[307]. Their IR spectra clearly showed the bands of adsorbed "CO" species on the surface and the reorganisation of adsorbed CO (i.e. the conversion of linear and bridged CO to triply bonded CO) was observed when the potential was stepped down from a high potential region to a low potential region, which was due to the incorporation of surface-bonded CO_2 formed at high potentials onto a poisoned surface. The presence of adsorbed CO has also been detected by Weaver et al. who used the "single-potential alteration infrared spectroscopy (SPAIRS) method coupled directly with simultaneous voltammetric measurements[33,308,309]. Bockris et al. examined the structure of intermediates of methanol oxidation on Pt in H_2SO_4 using polarization-modulation FTIR spectroscopy[310]. Their spectroscopic data also revealed the presence of both linear and bridge bonded CO during methanol oxidation over the potential range 0 - 0.8V NHE and excluded the possibility that COH was present. Recently potential-modulated reflectance spectroscopy (PMRS) was used to study the electroadsorption of methanol at Pt and Pd[311,312]. This method measures the

reflectance in the UV-visible spectral range and thus has the advantage of not requiring the thin layer cell used in IR reflectance spectroscopy. Linearly adsorbed CO was identified with a maximum band at ca. 270nm while bridge-bonded CO was also observed to give a band at 285 - 300nm.

However, the above conclusions about the nature of the adsorbed species are not in agreement with those obtained with other techniques. Electrochemical thermal desorption mass spectrometry (ECTDMS) and differential electrochemical mass spectrometry (DEMS) have been employed to investigate adsorbed species formed during methanol oxidation[13,39,41,43,313,314]. The presence of hydrogen in the adsorbate was clearly demonstrated from the detected hydrogen signal by ECTDMS, thus suggesting that either CHO or COH is an adsorbed species[48].

DEMS experiments, which were combined with isotopic labelling (D_2O was used as the supporting electrolyte), also offered evidence for CHO as the adsorbed species[38] (i.e. the hydrogen atom is attached to carbon atom). But, in further experiments using CD_3OD for methanol adsorption[39], it was concluded that the adsorbate does not contain a methylic hydrogen and that the adsorbed species was probably COH. However, it should be noted that the above conclusions obtained with isotopic labelling are mainly based on indirect observations. In addition, two assumptions are involved. First, that the adsorbate does not undergo any surface transformations and secondly, that H bonded to a carbon atom would not undergo isotopic exchange with the solvent.

6.1.2 *Electrochemical identification of intermediates*

Many electrochemical measurements have been performed to distinguish between CO

and CHO (or COH). Vielstich et al.[39,49] measured, using a flow cell technique, the charge involved in the formation and oxidation of adsorbates produced from methanol. The results suggested that three electrons were involved in adsorption and then oxidation according to the following possible reaction steps:

Adsorption: $CH_3OH \longrightarrow CHO \text{ (or COH)} + 3H^+ + 3e$

Oxidation: $CHO \text{ (or COH)} + H_2O \longrightarrow CO_2 + 3H^+ + 3e$

Results of another experiment[49], performed over a wide range of methanol concentrations, suggested that both CO and COH were the adsorbed species, depending on the concentration of methanol. It seems that a high concentration of methanol may favor the formation of CO because the formation of COH may be subject to steric hindrance under such a condition. Similar experiments have been carried out by Papoutsis et al., using programmed potential voltammetry (described in Chapter 1), to investigate the adsorption of methanol on both polycrystalline Pt[16] and a Pt(100) single crystal[15]. A constant value of N_{eps}, close to 2, was found for polycrystalline Pt, which suggested that the main adsorbed species was linearly bonded CO. However in the case of Pt(100), the N_{eps} values obtained led to the conclusions that at short adsorption times multibonded or bridged CO, along with linearly bonded CO and formyl species, exist as adsorbed species, while at long adsorption times only linear CO and formyl species are adsorbed on the electrode surface.

6.1.3 *Intermediates in methanol oxidation - summary*

In view of the above studies, it seems difficult to draw a definitive conclusion on the adsorbate composition. The most plausible one is that a mixture of CO and CHO (or COH) coexists as adsorbed species during methanol oxidation. This is supported by recent IR

reflectance measurements[71,315,316], which showed, besides bands for linear and bridged CO, weak and complex bands for CHO (around 1700cm^{-1}) and for COH (1400 - 1100cm^{-1}). If one has to make a distinction between the reactive intermediates and poisoning intermediates for the mixture of the adsorbed species, it is reasonable to think that adsorbed CO, mainly linearly bonded, acts as a poisoning intermediate while CHO or COH acts as the reactive intermediate.

6.1.4 *Oxidation of methanol at alloy and UPD modified electrodes*

In order to increase the electrocatalytic activity of the electrode, the nature of the electrode surface can be modified by metal alloying or by forming a UPD (submonolayer) deposit. Various binary alloys have been developed to act as the electrocatalysts for the oxidation of methanol. They include Pt/Sn[317], Pt/Rh[83], Pt/Pd[82] and Pt/Ru[2,53,100,318,319]. Enhanced catalytic activity has only been observed with Pt/Ru and Pt/Sn alloys. However the preferential dissolution of one metal in the alloy is a common problem encountered during long-term working conditions.

On the other hand, various metals have been used to produce underpotential deposits to try to increase the catalytic activity of Pt electrodes towards the oxidation of methanol. Only Ru[320], Bi[320], Pb[320], Sn[13,104,321,322] and Mo[106] adatoms have shown positive enhancement effects. Sn adatoms on Pt displayed the best catalytic effects while others showed slight catalytic effects only at low potentials. The high catalytic effects induced by Sn adatoms were attributed to the presence of oxygen-containing species adsorbed on Sn(II) species, which act as more effective oxygen donors more easily during the oxidation of adsorbates derived from methanol[13,42]. Compared with other fuels (such as formic acid),

methanol oxidation seems to be a special case where the electrocatalytic effect of adatoms is very limited and small. This has been assumed to be due to the fact that no direct oxidation of methanol would take place on Pt below 0.6V (RHE)[88], because OH radicals adsorbed on Pt could be required for the direct oxidation to occur since methanol only contains one oxygen atom and OH would not be present at the surface at lower potentials.

6.1.5 *Identification of products of methanol oxidation*

Reaction products derived from methanol oxidation during prolonged electrolysis have been determined by using analytical techniques (on-line mass spectrometry[41], liquid chromatography[56], colorimetry and iodometric titration[323]). The obtained results showed that CO_2 was the main reaction product and formaldehyde and formic acid were also present in relatively small amounts.

The above experimental observations suggest that the following reaction mechanism seems to be applicable to the oxidation of methanol in acid medium.

The adsorbed H_2O is discharged to produce OH_{ad} and the dissociative adsorption of methanol on Pt leads to the formation of a reactive intermediate CHO_{ad} (or COH_{ad}).

$$H_2O \longrightarrow OH_{ad} + H^+ + e \qquad (6.1)$$

$$CH_3OH \xrightarrow{\text{three steps}} CHO_{ad}\ (COH_{ad}) + 3H^+ + 3e \qquad (6.2)$$

The further oxidation of CHO_{ad} or COH_{ad} produces either the poisoning species CO or a reactive intermediate $COOH_{ad}$ or CO_2

$$CHO_{ad}\,(COH_{ad}) + OH_{ad} \longrightarrow CO_2 + 2H^+ + 2e \qquad (6.3a)$$

$$CHO_{ad}\,(COH_{ad}) \longrightarrow CO_{ad} + H^+ + e \qquad (6.3b)$$

$$CHO_{ad}\,(COH_{ad}) + OH_{ad} \longrightarrow COOH_{ad} + H^+ + e \qquad (6.3c)$$

Oxidation of CO species leads to formation of CO_2 or $COOH_{ad}$ which is then oxidized to CO_2

$$CO_{ad} + OH_{ad} \longrightarrow CO_2 + H^+ + e \qquad (6.4a)$$

$$CO_{ad} + OH_{ad} \longrightarrow COOH_{ad} \qquad (6.4b)$$

$$COOH_{ad} \longrightarrow CO_2 + H^+ + e \qquad (6.5)$$

Hence a general scheme can be expressed by

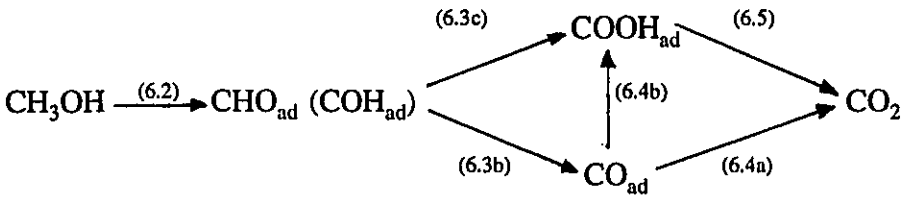

6.2 METHANOL OXIDATION IN ACID MEDIA

6.2.1 Oxidation at low concentration

Figure 59 presents typical results for the voltammetry of 0.5 mM methanol in 0.1M $HClO_4$, when the current and frequency (mass) responses are recorded after the potential

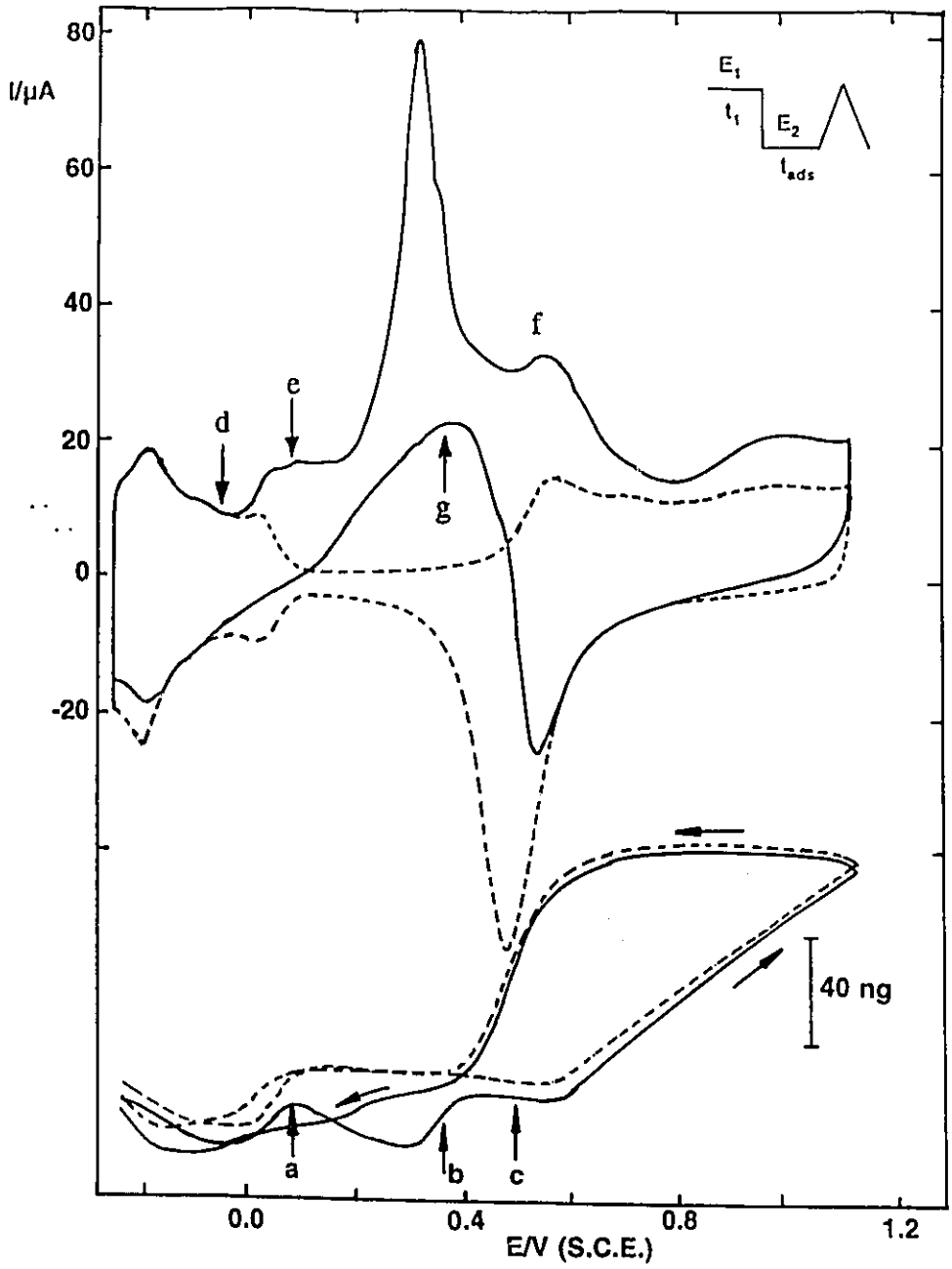

Figure 59. Cyclic voltammogram and mass response for the oxidation of 0.5 mM methanol in 0.1M $HClO_4$. For comparison the results for the background electrolyte alone are also shown (dashed lines). E_1 = 1.15V, t_1 =120s, E_2 = -0.25V and t_{ads} = 60s. The scan rate was 5 mV/s and the electrode area was 4.13 cm^2. Mass responses are shown exactly as recorded.

profile shown in the inset. At this concentration, which is significantly lower than the levels normally used (>0.1M) in studies of methanol oxidation, the first recorded voltammogram shows a multiple peak structure with the current first beginning to increase above background at the point where strongly bound hydrogen is removed from the electrode surface (point d). There are three current maxima seen, these being small peaks at 0.1V (e) and 0.55V (f) which straddle the sharpest peak at 0.32V. Finally there is a small increase in the oxidation current just prior to scan reversal. The cathodic sweep shows one oxidation peak (g) after oxide reduction and then there is a gradual decline in current towards the end of the cathodic scan. The first peak was found to be absent if a second cycle was recorded directly (not shown) and was also removed if the potential was either cycled to values greater than -0.1V, or held at such potentials for any length of time before initiating a sweep (beginning in the negative direction). Only a small degree of suppression of the H upd current (less than 10%) was sufficient to remove it. A typical result for an experiment where the potential was held at a more positive value is shown in Figure 60.

Returning to Figure 59, the first peak (e) (which almost has the form of a plateau) may be due to bulk oxidation of methanol, although there is clearly some development of strongly adsorbing species occurring in parallel. (Previously, a peak attributed to physisorbed methanol species has been reported in this potential region after adsorption at 0.07V vs. N.H.E. at smooth Pt electrodes in 0.5M $HClO_4$ [312]). These species are then removed in the second sharp peak, and once a clean electrode surface has been re-generated in this way, bulk oxidation of methanol is possible for a short time, leading to the third peak (f). The onset of irreversible oxidation of the electrode surface (i.e. of the place exchange process described in Section 4.2.1, which may be thought of as conversion of PtOH to OHPt[262]) then causes

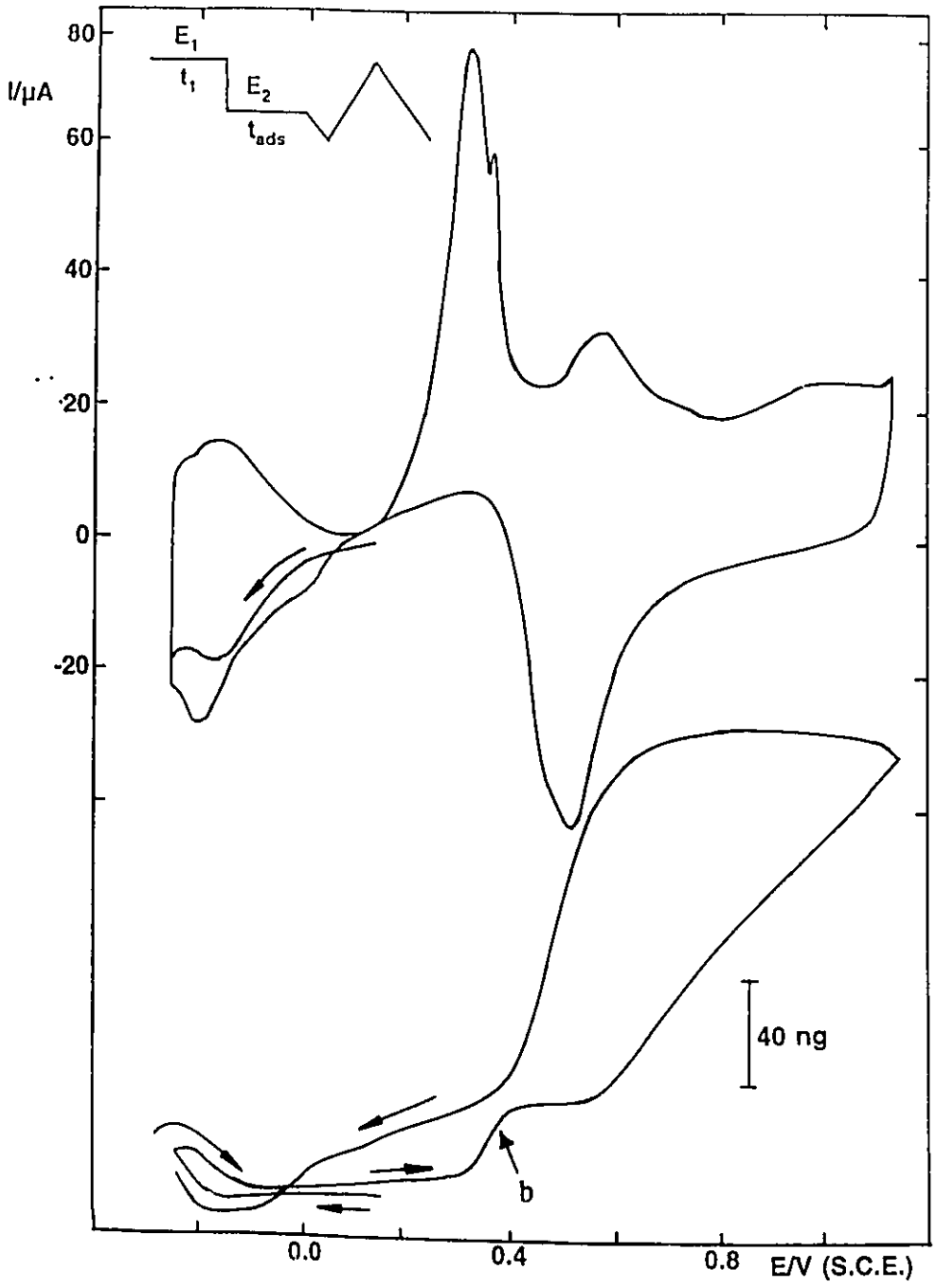

Figure 60. Details as for Figure 59 except that E_2 = 0.15V and t_{ads} = 300s. The potential was then scanned down to -0.25V before recording a complete cycle. Electrode area was 4.88 cm^2.

the current to drop away. On the cathodic scan, regeneration of the Pt surface by reversal of the place exchange process facilitates the final methanol oxidation peak (g). However, as before, the oxidation leads to accumulation of strongly adsorbing species, a gradual decline in the current and thus to some suppression of H upd coverage at the end of the cycle.

The mass responses that occur alongside the voltammetry (Figure 59) reveal several characteristic features, but before describing them it is important to note that the responses are shown exactly as recorded with no change in offset (see Section 3.6 in Chapter 3). Other responses have been recorded under the same conditions where the traces in the absence and presence of methanol were coincident in the region of surface oxidation and reduction. Thus we believe that the slight difference visible in the figure is representative of a physical effect (e.g. a small temperature drift) rather than a shift due to the presence of methanol. This conclusion is borne out by mass transient experiments, some of which are described in Section 6.2.3.

With methanol in the electrolyte, the mass response only begins to deviate from the background as the oxidation current first rises above the background current at 0V. The presence of methanol affects neither the voltammetry, nor the mass (where the features in the background response can be attributed to anion adsorption effects as discussed in Section 4.1) until this point. However, from 0V (point a) onwards there is a slow mass decrease. This can be attributed to the developing coverage of organic adsorbates which will lead to displacement of specifically adsorbed anions and water from the electrode surface. Thus it is not surprising that the adsorption leads to an overall mass decrease, particularly given the nature of the organic adsorbates and the possibility that multiple sites are occupied by CO or COH. The second mass feature occurs coincident with the sharp oxidation peak and is a

stepped increase (point b) which represents the restoration of the electrode mass to a level comparable to that seen in the background electrolyte, and of the electrode surface to a similar state. Because the concentration of methanol is so low, it is likely that after the adsorbate is removed from the electrode surface there is little further adsorption of methanol. Similar (but not identical) mass features to these were reported in the study of glucose oxidation described in Chapter 5 and have been observed in the oxidation of formic acid at Pt which will be described in the following chapter) and as such, they seem to be characteristic of the oxidations of small organic molecules at Pt.

The third small oxidation peak (f) occurs in a region of constant mass (point c) and then as the potential proceeds further positive the mass signal indicates that the oxidation/reduction of the electrode surface is largely unaffected by the presence of methanol, since it follows the background profile almost exactly. Finally, after removal of the oxide the mass decline over the potential range from 0.4V to 0.0V represents the slow build-up of strongly adsorbed species as the potential proceeds in the negative direction.

The result of increased coverage of the surface with adsorbates is seen in the mass response of Figure 60 where the potential was held at 0.15V for 5 minutes before a complete cycle was recorded, proceeding in the cathodic direction at first. Except at the negative extreme of the scan, the mass is flat as the features that are seen in the background electrolyte are removed. The subsequent mass step (feature b) that accompanies poison removal is then larger but thereafter there are no further differences.

The following general conclusions can be drawn from the data presented so far. First, at 0.5 mM methanol, there is little apparent adsorption until the region of strongly adsorbed H is reached. Second, in the double layer region of potential increased coverage of the

electrode surface by strongly adsorbing intermediates results in a mass decrease (relative to the background electrolyte), both on the positive and negative going halves of the cycle. Removal of these strongly adsorbing species gives rise to a mass step (Figure 59, point b) that is larger for an increased coverage (Figure 60, point b). Finally, some methanol oxidation can occur in a limited region of potential which arises after poison removal but before irreversible oxidation of the electrode surface, and where there is a small mass plateau. Methanol does not appear to influence the oxide formation and removal process when present at a bulk concentration of 0.5 mM.

6.2.2 Cyclic voltammograms for the oxidation of 9 mM methanol

When the bulk methanol concentration is increased to 9 mM, the voltammogram (Figure 61) takes on a more familiar shape, having one principal oxidation peak in both anodic and cathodic scans. The smaller current due to methanol oxidation on the oxidised electrode surface is also seen in the most positive regions of potential.

The twenty-fold increase in bulk methanol concentration produces only small changes in the mass response but they are, nevertheless, informative. First, following the pause at -0.25V the mass is almost constant until after 0.4V (c.f Figure 60). This suggests a relatively constant coverage of organic adsorbates giving an electrode mass that is lower than in the background electrolyte as discussed in the previous section. The mass increase that corresponds to poison removal occurs at a potential greater than 0.5V whereas at lower methanol concentration (Figures 59 and 60) it occurred at a potential below 0.4V and it is followed by a similar mass plateau which now extends over a smaller region. The small plateau is associated with the slow decline of the oxidation current that occurs after the peak

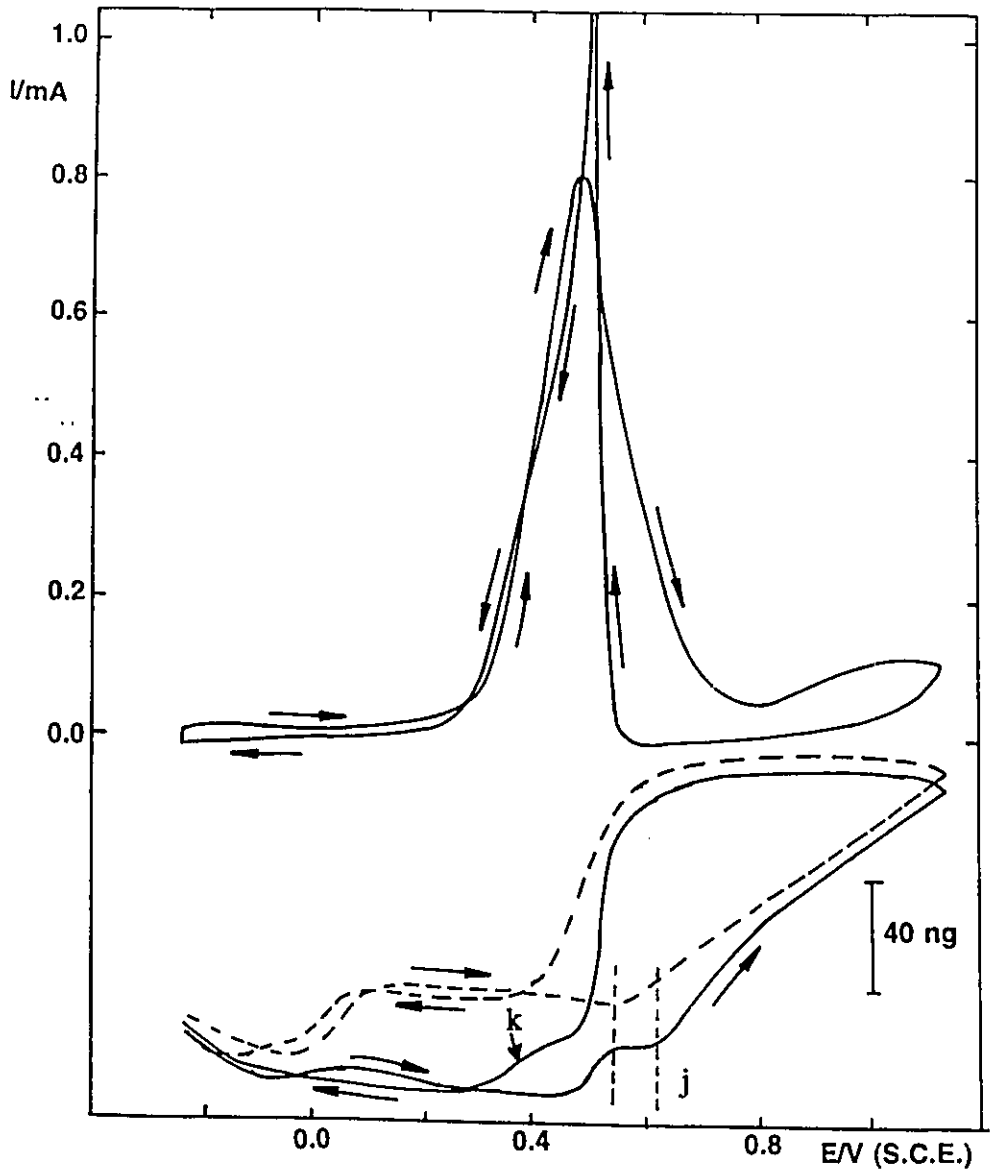

Figure 61. Cyclic voltammogram and mass response for the oxidation of 9mM methanol in 0.1M $HClO_4$. Results were recorded after a potential profile identical to that shown in Figure 59. The electrode area was 4.88 cm^2 and the scan rate was 5 mV/s. The background mass response only is shown for comparison purposes (dotted line), and the positions of the mass responses are exactly as recorded.

current is attained. It corresponds to a small region between the point where strongly adsorbed intermediates are removed from the surface and the potential where irreversible surface oxidation begins. In this region, the mass is flat but the difference between the masses of the electrode with and without methanol is now significant relative to experimental error. This may correspond to a higher level of adsorption of organic species which occurs on the electrode surface after strongly adsorbing residues are removed. The oxidation process here is presumably facilitated by the presence of OH at the electrode surface. However both a rapid decline in current, and the onset of another mass increase are produced once the field driven turnover of OH (and hence irreversible oxidation of the electrode surface) begins at point j.

Comparison of the mass responses is instructive because it reveals some inhibition of the place exchange process. The mass increase that signals the onset of irreversible oxidation of the surface (the initial stages of surface oxidation as shown in (4.1) in Section 4.2.1, namely discharge of adsorbed water and proton expulsion, will not lead to a measurable mass change) is shifted by close to 0.1V relative to the background electrolyte as revealed by the two vertical dashed lines in the figure. The rate of increase of mass here is larger than in the background electrolyte (most likely a reflection of the increased field) but after this first stage there does not seem to be any further difference until the cathodic half of the cycle.

If we now consider the reverse scan, reactivation of the electrode surface causes a sharp increase in current at 0.55V and the dramatic fall in the mass that accompanies this reactivation signals a more rapid removal of the surface oxide than is the case at 0.5 mM methanol or when the organic fuel is absent. Finally, at this higher bulk concentration there is a swift decline in the current on the cathodic scan after oxide reduction (relative to figures

59 and 60) and the mass also declines more rapidly toward the steady level developed on the anodic scan (region k). Both these phenomena would seem to be consistent with a more rapid deactivation of the electrode surface (compared to the lower methanol concentration) caused by the build-up of strongly adsorbed species.

6.2.3 *Mass transients for 9mM methanol*

The overall shape of the mass profile that is seen to accompany the oxidation of 9 mM methanol, and in particular the relative positions of the two mass responses in Figure 61, are reinforced by data from mass transients. Here, sufficient methanol to reach a bulk concentration of 9 mM was added to the background electrolyte at a series of constant potentials. The results are shown in Figure 62. At the extreme potentials used (0.0V and 1.00V, curves 1 and 5 respectively), there is little change in the mass as methanol is added to the electrolyte, but for the potentials of 0.15V, 0.3V and 0.55V, there is a mass decrease upon methanol addition. This fits the general pattern, derived from responses accompanying voltammetric data, of negligible adsorption in the H upd region and on an oxidised electrode surface and significant adsorption in the double layer region of potential. It is important to recognize, however, that for the mass transients the electrode surface was cleaned prior to each injection. This represents a difference between these experiments and the voltammetric data where the scan proceeds slowly from the negative limit so that the mass at a given potential may be dependent upon the processes that have occurred earlier in the scan. However, similar experiments were carried out at 0.5 mM and 0.1M methanol and in each case the results gave a general agreement with the relative positions of mass responses depicted in the various figures.

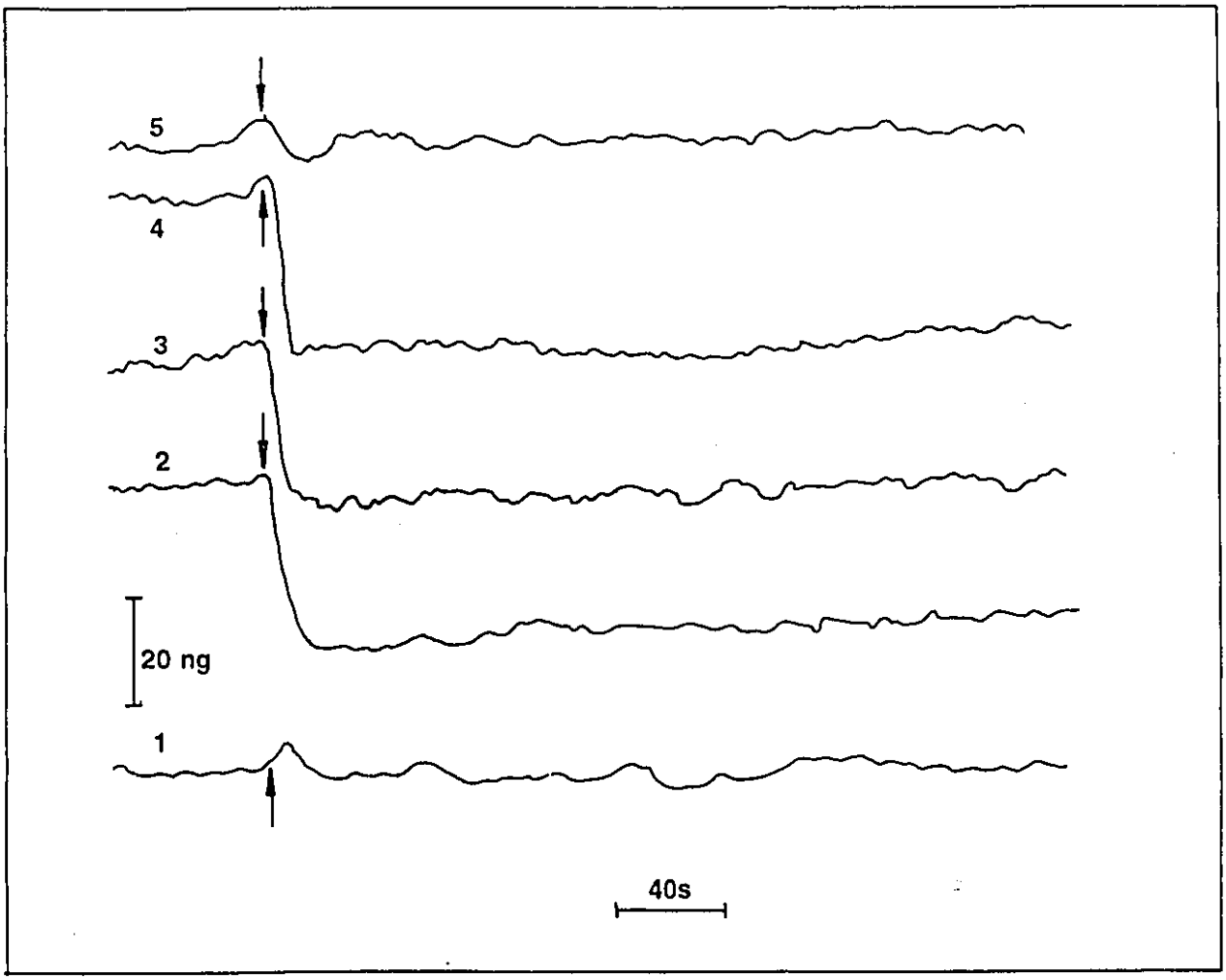

Figure 62. Mass transients resulting from the addition of methanol (sufficient to give a bulk concentration of 9 mM) to the background electrolyte at different constant potentials. Each injection was performed at a clean electrode surface. Electrode area was 4.01 cm^2. Responses are displaced for purposes of clarity and are not intended to represent relative mass values. Constant potentials used were 1, 0.0V; 2, 0.15V; 3, 0.30V; 4, 0.55V; 5, 1.0V.

In summary, the increase in the bulk concentration of methanol is seen to lead to a faster rate of poisoning in the double layer region of potential, to a higher coverage of strongly adsorbed species and to a lower electrode mass. Removal of adsorbates is shifted to more positive potentials and the accompanying mass step is larger. This latter mass feature is of great benefit in locating the point where "poisoning" adsorbates are removed, since it is no longer apparent from voltammetry because of the high oxidation currents that are passed. As for 0.5 mM methanol some oxidation can take place after strongly adsorbing species are removed and before irreversible surface oxidation. Here, there is a region of constant mass (region c in Figure 59), but this mass is low relative to the background electrolyte. This can be attributed to a more significant adsorption of organic reactants/intermediates. Such adsorption and reaction with surface OH shifts the onset of irreversible surface oxidation (the place exchange process) by ca. 0.1V (Figure 61).

6.2.4 *Oxidation of 0.1M methanol*

Concentrations such as 0.1M and higher are more commonly used in investigations of methanol oxidation because they are more appropriate for practical fuel cell operation. Figure 63 shows that the voltammogram is dominated by the large methanol oxidation currents that result, but is not significantly different from the voltammogram at 9mM methanol, except for the very sharp fall in the oxidation current on the anodic scan and the equally sharp rise on the reverse scan. This is partly due to the low scan rate used.

The accompanying mass profile shows several significant differences from that of Figure 61. First, the flat responses on the anodic scan are relatively similar for the two bulk concentrations, yet at the higher value there is no stepped mass increase which, at the lower

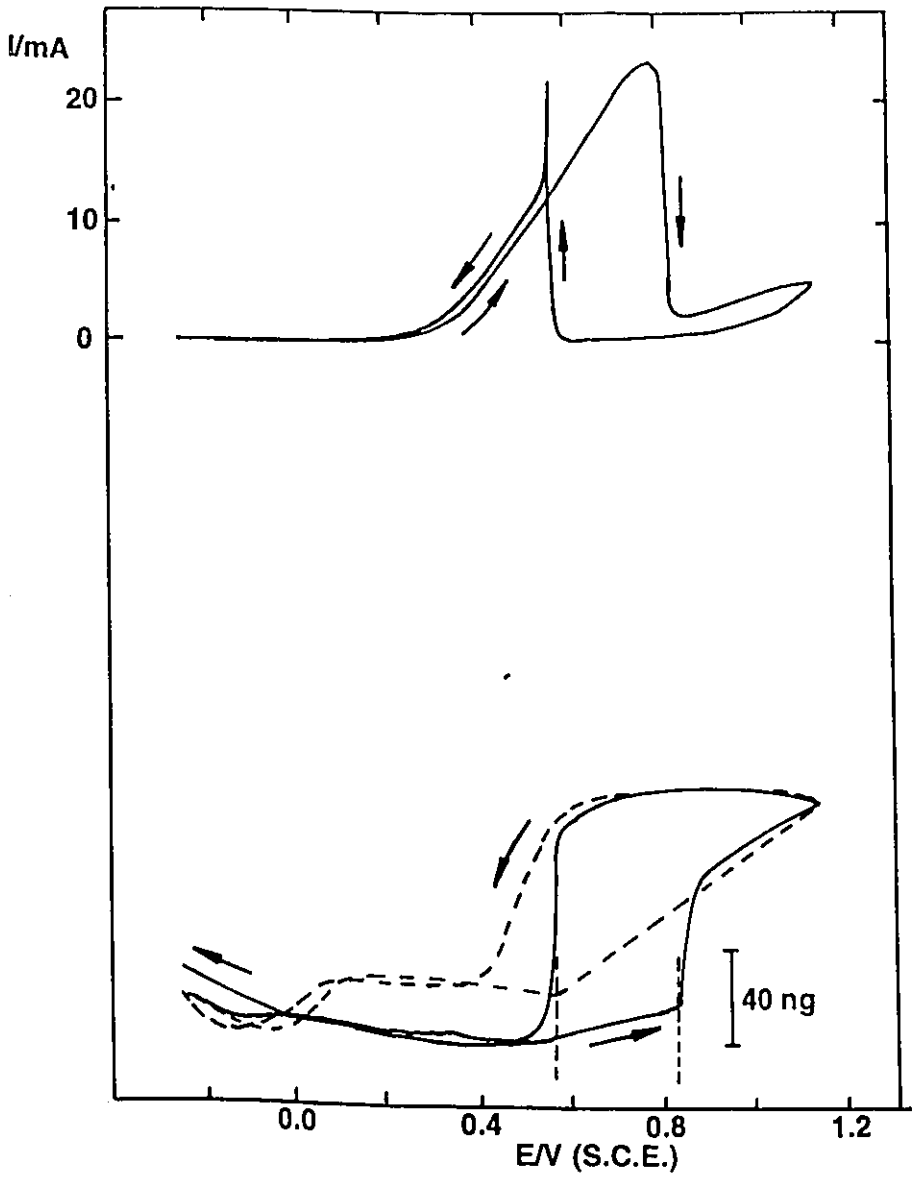

Figure 63. Cyclic voltammogram and mass response for 0.1 M methanol in 0.1M $HClO_4$. Scan rate 5 mV/s, electrode area was 3.78 cm^2. The background mass response is presented for purposes of comparison.

concentrations, coincides with the removal of the strongly adsorbed organic species. There does however seem to be a minor change in slope at ca. 0.5V followed by a slow increase over the next 0.3V. Second, the increase in mass that accompanies surface oxidation is clearly shifted by several hundred millivolts when 0.1M methanol is present (as illustrated by the dotted lines in the Figure). Finally, after the last stages of the positive-going scan and the initial stages of the negative-going scan, during which the presence of methanol makes little difference to the mass response, the dramatic rise in the current is mirrored by a steep drop in the mass. As for 9 mM methanol, the oxide surface is removed more rapidly in the presence of the alcohol. In contrast to the response of Figure 61 (region k) however, the mass then decreases immediately to the level it held on the anodic scan rather than declining more slowly.

Some of the differences in the mass behaviour at the two different concentrations are easier to explain than others. First, it seems likely that shifting of the onset of irreversible surface oxidation by several hundred mV (a phenomenon also observed for glucose oxidation in alkaline media as seen in Section 5.3) is due to rapid consumption of surface OH by reaction with methanol before it can undergo the place exchange process. At 9mM, the onset of the place exchange process (as defined by the increase in mass, point j) shows only a small shift. The consequence of increasing the concentration of methanol to 0.1M tips the balance in favour of the removal of the OH by reaction with methanol so that it is not until there is a significant increase in the potential that the larger field then favours the place exchange process leading to the sharp increase in mass as the rate of growth of the oxide is enhanced. Similarly, on the reverse scan, the initial (electrochemical) reduction of the oxidised surface probably creates some sites for the adsorption of methanol and the remainder of the oxidised

surface is then rapidly consumed in a chemical reaction with methanol. Thus the oxide is removed more rapidly (when compared to the situation in background electrolyte or at lower methanol concentrations).

The rapid reaction between methanol and the oxide surface seems to be confirmed by the mass transient experiment of Figure 64. Here the potential was first held at 0.15V in background electrolyte prior to a potential step to 0.7V. The small mass increase (ΔM_1) accompanying this process reflects the partial oxidation of the electrode surface. Once the mass had stabilised, sufficient methanol was added to the electrolyte to bring the bulk concentration to 0.1M, while the potential was maintained at 0.7V. This produced a significant decrease in mass (ΔM_2), apparently in two stages, together with a current spike that then decayed to a reasonably steady level. The final mass at 0.7V (in the presence of methanol) was less than at 0.15V (in the absence of methanol) thus supporting the validity of the relative positions of the mass responses accompanying the voltammetric data of Figure 63. When an identical experiment was carried out at 1.0V there was no change in mass. Again, this result would be predicted from an examination of Figure 63. Clearly then at 0.7V and with 0.1M methanol, the rate of the place exchange process (i.e. irreversible oxidation of Pt) is unable to compete with the rate of removal of surface OH by reaction with the alcohol, whereas at 1.0V the reverse is true. If the potential is held (in background electrolyte) at 1.0V and then the circuit opened, addition of methanol leads to a rapid removal of the oxide surface as indicated by a sharp drop in mass, and the potential drops to the region of upd H. Such results are well known[324] and indicate that a chemical reaction can take place between the oxide and methanol (the potential is then stabilised as a result of a dehydrogenation/hydrogenation equilibrium). However, when the electrode is under

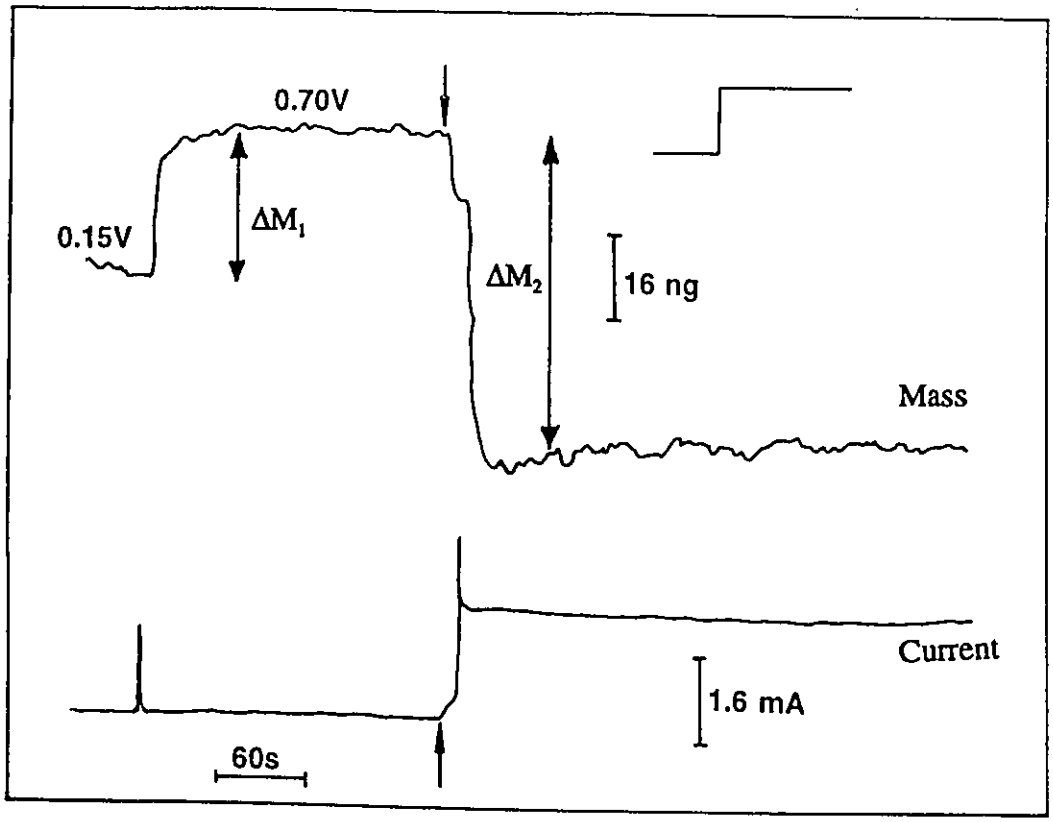

Figure 64. Mass (top) and current (bottom) transients resulting from a potential step from 0.15V to 0.7V (background electrolyte) followed by the addition of sufficient methanol to achieve a bulk concentration of 0.1M (at a point indicated by the arrows) while the potential was maintained at 0.7V. The electrode area was 3.78 cm^2.

potentiostatic control at 1.0V the oxide is regenerated electrochemically at a rate sufficient to maintain the expected oxide coverage and electrode mass.

The remaining question concerns the reason for the absence of the stepped increase in mass (point b, Figure 59) at higher methanol concentrations. This question is answered by inspection of Figure 65 which shows the evolution of the mass response with increasing methanol concentration. As the concentration is raised from 0.5 (1) to 9 mM (2), the stepped increase shifts to more positive potentials, and the subsequent plateau shortens. Then from 15 mM (3) to 30 mM (4) the step flattens further until it disappears. A subsequent increase in methanol concentration to 0.1M does not change the shape of the response but merely shifts the onset of irreversible surface oxidation to more positive values. The implication of these results is first that increased amounts of methanol in the electrolyte make the removal of strongly adsorbed species (as represented by the mass step) more difficult, causing the process to be shifted towards higher potentials. It also seems to be the case that removal of these strongly adsorbed species is followed by some new adsorption and this adsorption increases with methanol concentration. However, at methanol concentrations of 30 mM and above it is no longer possible to tell if species formed in the early stages of the scan are removed and then further adsorption occurs, or if the adsorbates are not removed at all until irreversible surface oxidation begins. Thus the suppression of oxide formation that is observed at these concentrations may result from some blockage of surface sites by adsorbates, as well as from the consumption of OH in a reaction with methanol as indicated earlier.

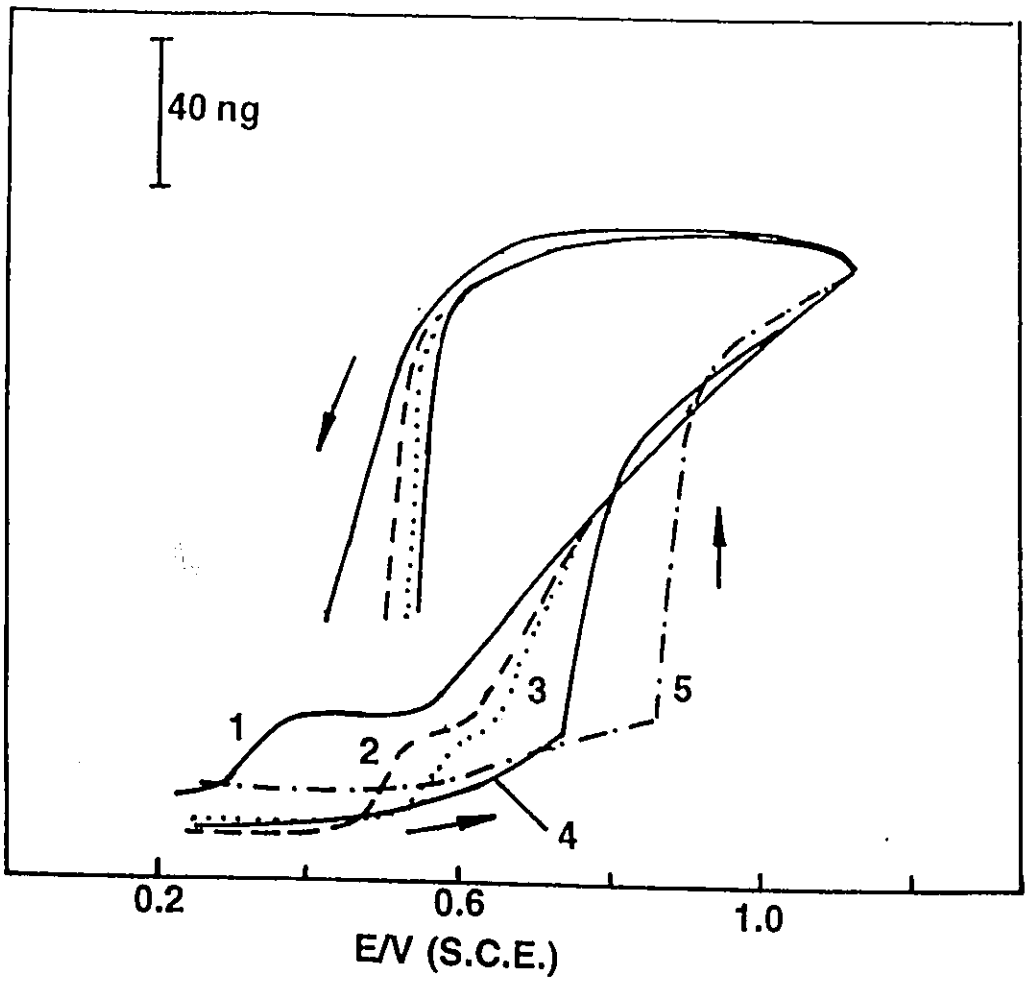

Figure 65. The influence of methanol concentration on mass response. 1. 0.5 mM, 2. 9 mM, 3. 15 mM, 4. 30 mM, 5. 0.1M. The concentration of methanol was increased in steps and then each response recorded after the potential profile shown in Figure 59 at 5mV/s. Traces are drawn aligned so that the masses were identical at the upper potential limit. At this point, the actual experimental data (recorded at constant offset) fell within a range of only 6ng for curves 1 to 4. Curve 5 was recorded 30 minutes later and differed by 20 ng. Electrode area was 4.62 cm^2.

6.2.5 *Conclusions*

Several general conclusions can be drawn from the data presented above.

1. In the H upd region, little methanol adsorption is apparent at low concentrations (0.5mM) but as the bulk concentration increases there is increased adsorption, particularly in the region of strongly adsorbed H and mass features due to anion adsorption are largely removed, except at the negative limits of the scan.

2. In the double layer region of potential, increased coverage of the electrode surface by organic adsorbates leads to a progressive decrease in the mass response, and the rate of decline of the mass as this region is approached (on either positive or negative going halves of the cycle) can be used as an indicator of the rate of development of the adsorbate coverage.

3. Oxidative removal of adsorbates formed in the first sections of an anodic scan is only visible in the voltammetry for 0.5 mM methanol but is nonetheless apparent at concentrations below 30 mM because it is accompanied by a step in the mass. Such oxidative removal is shifted towards more positive potentials at larger methanol concentrations.

4. Once the adsorbates are removed, there is (at concentrations below 15 mM) a small region of potential where the mass is flat and where methanol is oxidised at a Pt surface which is presumably covered with OH (region c in Figure 59). Adsorption also appears to take place in this region and is more significant as the amount of the alcohol in the electrolyte rises. Above 30 mM methanol it is no longer possible to distinguish the mass step and the subsequent plateau.

5. The onset of irreversible oxidation of the electrode surface is always apparent from

the mass response and is associated with the sharp decrease in the current on the positive going scan. Clearly, the onset of place exchange causes a drastic reduction in the catalytic activity of the surface toward methanol oxidation. As the methanol concentration increases, the mass can be used to monitor the progressive inhibition of the irreversible oxidation of the electrode surface, despite the fact that the currents associated with the process are swamped by large methanol oxidation currents. Mass data also show the more rapid reduction of the oxide that occurs on the cathodic scan when methanol is present in the electrolyte.

Chapter 7

Electrocatalytic Oxidation of Formic Acid

This chapter describes results of an investigation of the oxidation of formic acid using the Electrochemical Quartz Crystal Microbalance technique. The research mainly centers upon the study of adsorption phenomena observed during formic acid oxidation as deduced from the mass changes revealed with the EQCM. Before presenting the results, a general review of the oxidation of formic acid is provided below.

7.1 INTRODUCTION

As well as methanol (described in the previous chapter), formic acid has also been considered as a possible fuel for fuel cells. Its oxidation contains fewer steps than other organic fuels and therefore a knowledge of the mechanism may serve as a desirable model from which the oxidation mechanisms of other organic molecules can be elucidated. In addition, unlike other fuels, it doesn't necessarily need a source of oxygen for CO_2 production. In principle, the complete oxidation of formic acid only requires two electrons to be transferred

$$HCOOH \longrightarrow CO_2 + 2H^+ + 2e$$

However, as with other small organic molecules, poisoning intermediates can be formed during the oxidation of formic acid and this formation leads to a rapid decrease in the catalytic activity of the electrode. The generally accepted mechanism for the oxidation is that

proposed by Capon and Parsons[9,10], which includes the direct oxidation of bulk formic acid via a reactive intermediate and a parallel path involving the formation of a poisoning intermediate, i.e. the "dual-pathway" mechanism.

The first step of the oxidation is believed to be the breaking of the H-C bond to produce $COOH_{ad}$ species. This was supported by evidence from the measurement of the rates of oxidation of HCOOH and DCOOH on Pb-modified Pt where a smaller oxidation rate was observed with DCOOH[325]. The subsequent reactions follow the two parallel pathways.

7.1.1 *Identification of intermediates*

The scheme mentioned above is now widely accepted and direct evidence for such a mechanism has been obtained recently by using the technique of mass spectrometry combined with isotope labelling[43,44]. However the nature of the poisoning intermediates formed during the oxidation is still a point of discussion.

IR spectroscopic data suggested that the poisoning species is mainly CO. Beden et al.[326,327] used EMIRS to study the adsorption of formic acid and detected two IR bands which were assigned to linearly bonded CO and bridge bonded CO respectively. These bands were also observed by Kunimatsu and Kita[328] who utilized the polarization modulation IR reflectance technique (PM-IRRAS) to examine the potential-dependent CO coverage during the oxidation of formic acid on Pt. Corrigan and Weaver[308] measured the IR spectra of adsorbed species during the voltammetric oxidation of formic acid using the SPAIRS technique. Their data also showed that adsorbed CO may act as a poison species. The presence of the poisoning species, CO, was also probed by IR spectroscopies during the oxidation of formic acid on low-index Pt surfaces[70,309]. Besides the poisoning species, the

reactive intermediate, possibly $COOH_{ad}$, has also been revealed by EMIRS, which showed broad bands around 1750cm^{-1} when the potential is modulated to the region where the oxidation of the adsorbed CO occurred[70]. Similarly, the adsorbed species CO was proposed by Clavilier and Sun[67] based on a determination of the number of electrons per site, N_{eps}, required for the oxidation of the adsorbed species on a Pt single crystal electrode.

The presence of another adsorbed species, CHO, during oxidation of formic acid has also been suggested. Roch and Heitbaum[55] performed an ex-situ XPS analysis of the HCOOH adsorbate and observed a chemical shift of a carbon-containing species that lies between C and CO. Thus they concluded that the adsorbed species was probably CHO, which gives rise to the observed chemical shift. Heitbaum et al.[43,44] applied on-line MS (DEMS) to the investigation of adsorption of formic acid and the adsorbed species was characterized as CHO. As seen from the above, no consensus has been reached concerning the exact nature of the adsorbed species. The evidence for CO as the poisoning intermediate, provided by in-situ IR spectroscopic measurements, seems most conclusive and convincing, but as noted earlier, the results may be dependent on the type of spectroscopic method used.

7.1.2 *Oxidation of formic acid at alloy and UPD electrodes*

The electrooxidation of formic acid has been studied on metallic alloys such as Pt/Au[77,78], Pt/Pd[80], Pt/Rh[79] and Au/Pd[81]. The observed electrode activity was found to be higher than that of the pure metals. Such synergistic effects have been explained by similar mechanisms to those proposed for UPD-modified electrodes.

The catalytic effects resulting from the UPD of foreign metals are much more striking for oxidation of formic acid than for methanol oxidation. Significant enhancements of the

oxidation of formic acid have been observed with adatoms such as Pb, Bi, Tl and Cd. Among these adatoms, Pb has a larger effect than Bi and Tl, while Cd causes the smallest effect. However, different hypotheses have been proposed to explain the effects of such adatoms. Adzic et al.[92,93,95] attributed the effect of adatoms to the prevention of formation of the poisoning species (probably COH_{ad} as suggested by those authors and Capon and Parsons[9,10]) through suppression of the adsorbed hydrogen which was thought to be involved in the formation of the poisoning species:

$$COOH_{ad} + 2H_{ad} \longrightarrow COH_{ad} + H_2O$$

However, this model is not convincing because it cannot explain the fact that different catalytic activities are observed at electrodes having identical coverages of different adatoms.

The "third body" mechanism has been proposed to explain the catalytic effect of adatoms. Conway et al.[85] noted that formic acid oxidation was catalysed by submonolayer amounts of Hg on Pt and suggested that the role of Hg adatoms is to act as "third body" to isolate surface Pt sites and hence to slow down the formation of poisoning species because such formation requires several adjacent Pt sites. This model was adopted by several other authors: Shabrang et al.[87] investigated the catalytic effects of Bi, Pb, Ag and Cu on the oxidation of formic acid on Pt. Electrocatalysis by Bi and Pb was explained by the third body mechanism or by hydrogen inhibition while the inhibitory effects of Cu and Ag were interpreted in terms of the preferential deposition of adatoms on the Pt(111) plane which makes little contribution to the total formic acid oxidation; Clavilier and co-workers studied the effects of Bi and Sb on the direct electrocatalytic oxidation of formic acid and on the formation of poisoning intermediates at single crystals[329-331]. The oxidation of formic acid was found to be enhanced considerably by Bi and Sb adatoms according to the classic "third-

body" effect. Hartung et al. examined the effect of Hg adatoms on formic acid oxidation at Pt by means of RRDE and differential electrochemical mass spectrometry[45] and studied the interaction between adatoms and the poisoning species by measuring the adatom coverage before and after HCOOH was introduced into the solution. Their results suggested that the third body mechanism was responsible for a strong inhibition of the formation of poisoning species. However, the "third body" mechanism cannot explain the different catalytic activities obtained with different adatoms.

The bifunctional theory of electrocatalysis (described previously in Section 1.3.3) has also been proposed by Motoo and Watanabe[332] to explain the enhancement of the activity of platinum caused by Sn and Ge adatoms. However, this theory cannot explain why adatoms such as Pb and Tl which do not promote oxygen adsorption exhibit higher catalytic activity towards HCOOH oxidation than the oxygen-adsorbing adatoms.

One other theory that has been advanced to explain UPD effects is that the adatom layer itself may catalyse the direct oxidation of formic acid to CO_2[45,333]. Vielstich et al. investigated the increased activity of Pt resulting from Pb adatoms by following the co-adsorption of Pb and the poisoning species using a flow cell technique[333]. They concluded that the third body effect is of minor importance and that the bulk oxidation of formic acid takes place not only at sites free from Pb adatoms but on the surface covered by Pb adatoms as well. This idea may account for the higher catalytic effect induced by Pb adatoms relative to Tl and Cd, etc. Hartung et al.[45] observed an increase in the amount of CO_2 from direct oxidation of formic acid when they measured the oxidation of bulk HCOOH on a Pt electrode with Tl adatoms using DEMS, and therefore they assumed that Tl adatoms seem to catalyze the direct oxidation of bulk HCOOH. The same concept was used by El-Shafei et al.[334] to

explain the catalytic effects of Pb and Tl observed during the electrocatalytic oxidation of formic acid on Pt electrodes modified simultaneously by two different adatoms.

Finally, it has been suggested that the adatoms may induce an electronic interaction between the adatoms and the electrode. Xia and Iwasita used the DEMS technique with isotope-labelled ^{13}C formic acid to investigate the influence of Pb adatoms on the oxidation of both formic acid and its poisoning species on Pt[103] and measured simultaneously the rate of CO_2 production from bulk formic acid and the poisoning species. Their results indicated that the pronounced catalytic effect of Pb adatoms results from the activation of the free Pt sites through an electronic interaction between the adatoms and electrode substrate. Aldaz et al.[105,335] studied poison formation from the dissociative adsorption of formic acid on Pt(111) electrode modified with Bi and As adatoms. They found that a very small amount of adatoms (coverages less than 0.01) drastically inhibited poison formation, suggesting an electronic effect at the electrode surface induced by adatoms. This hypothesis is supported by a recent finding that Bi diminishes the value of the work function of Pt(111)[336].

7.1.3 *Summary*

It is difficult to choose one of the above theories to explain the catalytic effect of UPD adatoms because, so far, no definite experimental proof has been obtained, which may allow discrimination of one theory from the others. The accumulated experimental data only allow certain conclusions to be drawn: (1) the poisoning species is CO; (2) the reactive intermediate is of the $COOH_{ad}$ type; and (3) adatoms have a significant catalytic effect on the oxidation of formic acid, their role is presumably to occupy some specific electrode active sites necessary for the formation of poisoning species, or to modify the electronic properties

of the electrode. Moreover, the possibility of bifunctional catalysis cannot be excluded in some cases. Taking into account all the above results, an appropriate mechanism for the oxidation of formic acid can be proposed

$$H_2O \longrightarrow H^+ + OH_{ad} + e \quad (7.1)$$

$$HCOOH \longrightarrow COOH_{ad} + H^+ + e \quad (7.2)$$

$$COOH_{ad} \longrightarrow CO_2 + H^+ + e \quad (7.3a)$$

$$COOH_{ad} \longrightarrow CO_{ad} + OH_{ad} \quad (7.3b)$$

$$COOH_{ad} + H_{ad} \longrightarrow CO_{ad} + H_2O \quad (7.3c)$$

$$HCOOH \longrightarrow CO_{ad} + H_2O \quad (7.4)$$

$$CO_{ad} + OH_{ad} \longrightarrow CO_2 + H^+ + e \quad (7.5)$$

The reactive intermediate is formed in (7.2), which is then oxidized to CO_2 in (7.3a) and poisoning intermediate, CO, is produced in (7.3b, 7.3c) and (7.4). The oxidation of poisoning species occurs in (7.5). The general scheme may be written as follows:

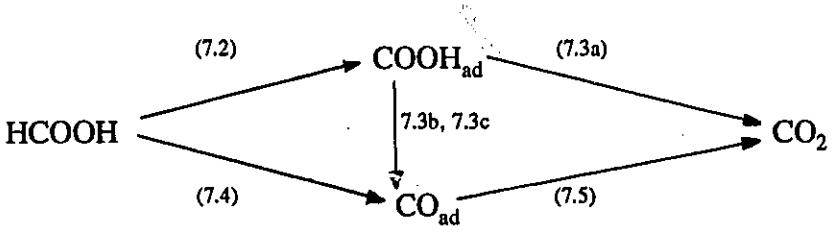

7.2 OXIDATION OF FORMIC ACID AT Pt IN ACID MEDIA

7.2.1 *Oxidation of formic acid at very low concentrations*

Figure 66 shows a voltammogram and accompanying mass response, recorded after the potential profile in the inset, for 0.5 mM formic acid. When the voltammogram is compared to the background, we can see that there is a broad oxidation of HCOOH across almost the entire potential range. This oxidation current first increases above the background at around -0.1V. Current densities are low, and the roughly constant oxidation is disturbed only by the sharp peak at 0.3V in the double layer region of potential on the anodic scan. The first stages (to -0.1V) of the mass response accompanying the anodic scan are not changed significantly by the presence of formic acid. (A discussion of the mass response in 0.1 M $HClO_4$ alone has been presented in Chapter 4). This is not unexpected, given that the value of E_2 was -0.25V where H coverage is nearly unity. Capon and Parsons[9] have shown that the reaction between H_{ads} and HCOOH (bulk) is slow at high H coverages. From -0.1V on, however, the mass response is flat and lower than in the background electrolyte over a range of nearly 400 mV (indicated as region A) until the step (feature B) that accompanies the sharp peak. The steady region of mass (A) reflects what is probably a constant (small) coverage of strongly adsorbed species, presumably developed in the earliest stages of the anodic scan and then the step (B) corresponds to their removal. These features have been observed before for glucose and methanol. The electrode surface thereafter seems to be quite similar to that seen in the background electrolyte since there is little difference in mass. In other words, after the step there is little adsorption of formic acid, and the oxidation and reduction of the surface does not seem to be affected by the presence of HCOOH. (Note that

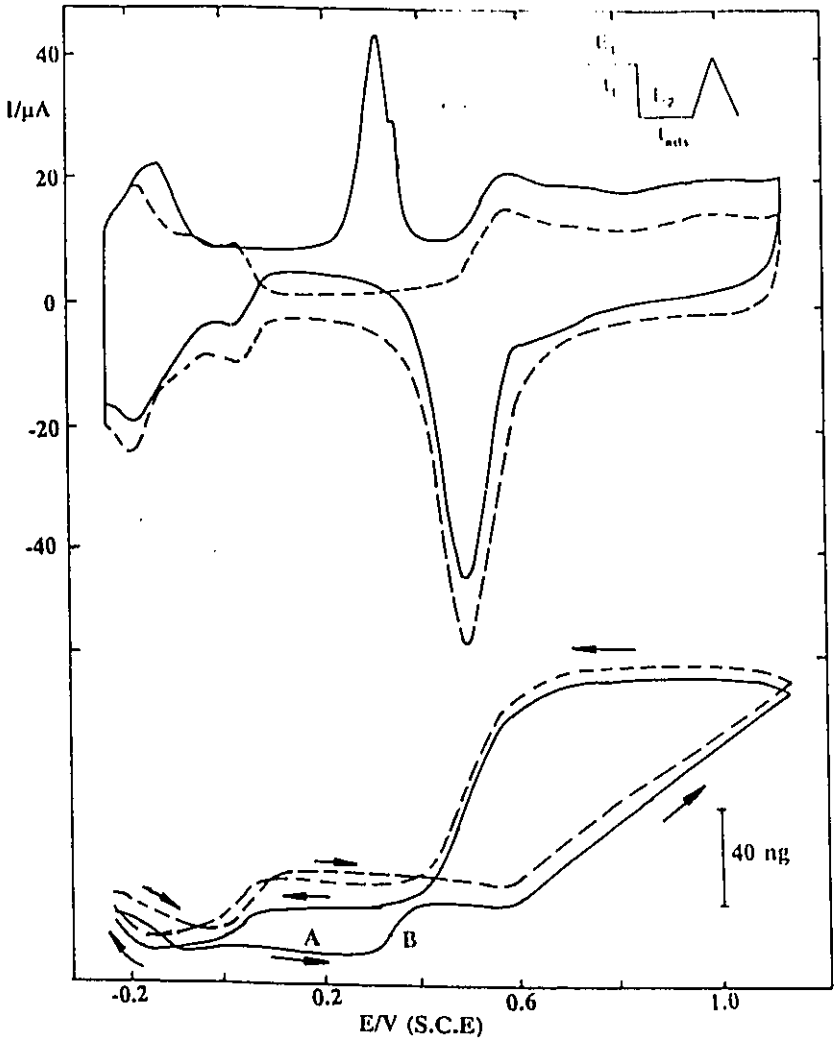

Figure 66. Cyclic voltammogram and mass response for the oxidation of 0.5 mM formic acid in 0.1 M $HClO_4$. Results for the background electrolyte alone are also shown (dotted line). E_1 = 1.15V, t_1 =120s, E_2 = -0.25V and t_{ads} = 60s. The scan rate was 5 mV/s and the electrode area was 3.82 cm^2. Mass responses are shown exactly as recorded.

the two mass traces are shown exactly as recorded and it is most likely that in fact the masses should be equal at the anodic scan limit. Some evidence for this is presented later, in the discussion of mass transients. The difference in the figure is probably a result of a small drift in the frequency between the recording of the scans). After reduction of the surface oxide, there is another flat region, yet the mass is larger than in the corresponding section of the positive going scan (indicated as region A). This difference arises because the double layer region is approached from opposite directions. On the anodic scan the initial sections involve some residue formation before the double layer region is encountered, whereas on the cathodic scan the surface in the double layer region is "clean" since it is reached directly after oxide removal. These data indicate that, under the conditions of this experiment, the formation of strongly adsorbed species occurs principally in the region of weakly adsorbed H.

Figure 67 supports this assumption. Here, the potential E_2 was increased to -0.1V and 0.1V as compared to -0.25V in Figure 66. For E_2 = -0.1V, the mass profile mirrors that of Figure 66 and the sharp current peak is seen (though there is less charge involved). For E_2 = 0.1V however, the peak is negligible (the current is constant almost throughout the double layer region) and the mass on the anodic scan actually follows the path of the signal from the cathodic scan until it merges with the mass profile from the first anodic scan at 0.4V at the beginning of the plateau region.

Under the conditions of the experiments of Figures 66 and 67, we may conclude that a small amount of adsorption occurs principally at the extreme negative limits of the scan, and there is little further adsorption in the double layer region of potential. This is not unexpected, given the small bulk concentration used. The general picture of a constant small

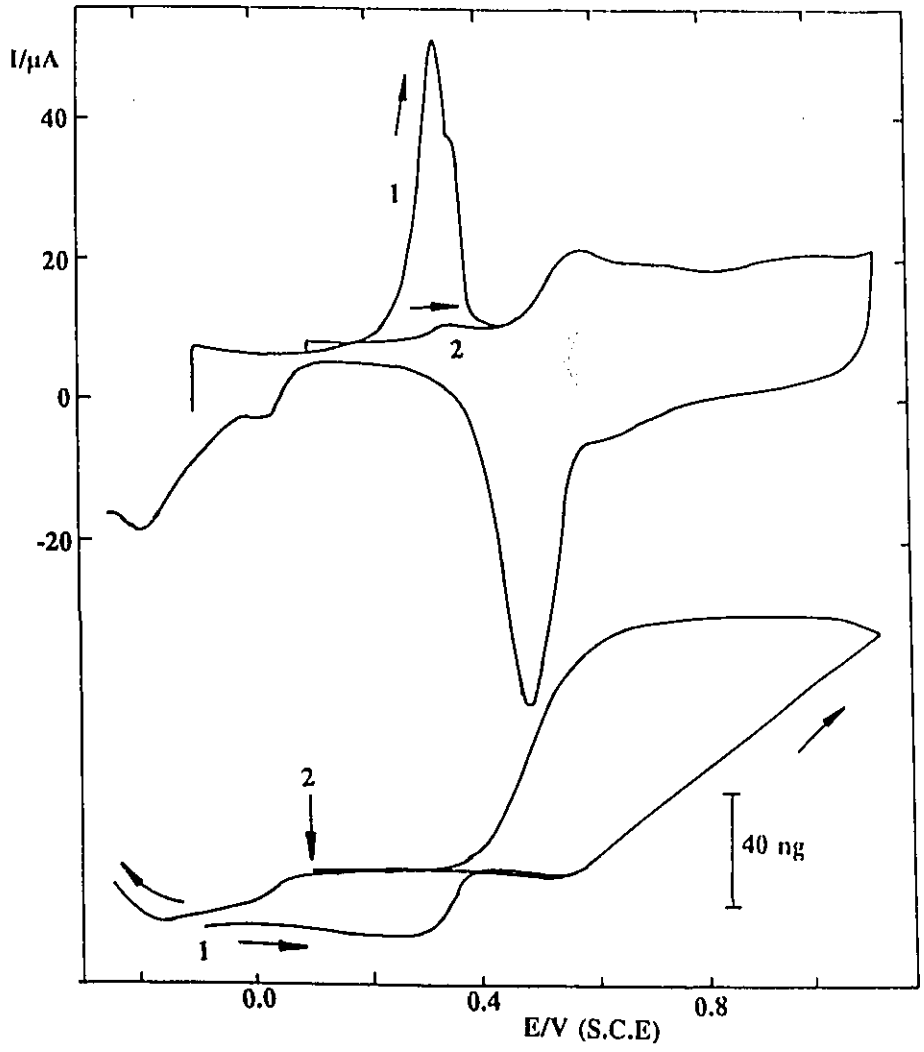

Figure 67. Details as for Figure 66 except that E_2 was -0.10V and 0.10V for curves 1 and 2 respectively. Electrode area was 4.88 cm^2. The vertical arrow labelled "2" indicates the starting point for the mass for curve 2.

oxidation current across virtually the whole potential range, together with the sharp peak, seems to fit well with the view reported earlier that the oxidation of formic acid occurs by parallel routes with a reactive intermediate and a strongly adsorbed intermediate. The differences in mass response in the double layer region of potential also illustrate the fact that increased coverage here causes the mass to decrease and a comparison of the mass responses can thus give a qualitative picture of the variation of coverage between the two scan directions.

As a final point, identical experiments to those of Figures 66 and 67 but with methanol shown in the preceding chapter (Figure 60) showed that the formation of strongly bound intermediates began at a more positive potential (than for formic acid) and continued through most of the double layer region leading to a continued decrease in mass, rather than the flat response seen here. Thus subtle differences between the behaviour of different reactants can be discerned from the mass responses.

7.2.2 *Cyclic voltammograms for the oxidation of 9mM formic acid*

When the bulk formic acid concentration is increased to 9 mM, changes in both the voltammetry and mass response can be seen (Figure 68). Currents are larger and an anodic scan is dominated by the sharp peak (E) at 0.4V with a steady increase in current prior to this and a shoulder thereafter (Note: The current *before* the sharp peak is often apparent as another peak, frequently referred to by other workers as the first anodic peak[9]). Under the conditions used here, namely slow scan rates and 0.1 M $HClO_4$ as electrolyte, this first anodic peak was not observed (c.f. reference 36, Figure 7). However, at faster scan rates in 0.5 M H_2SO_4 it was present .

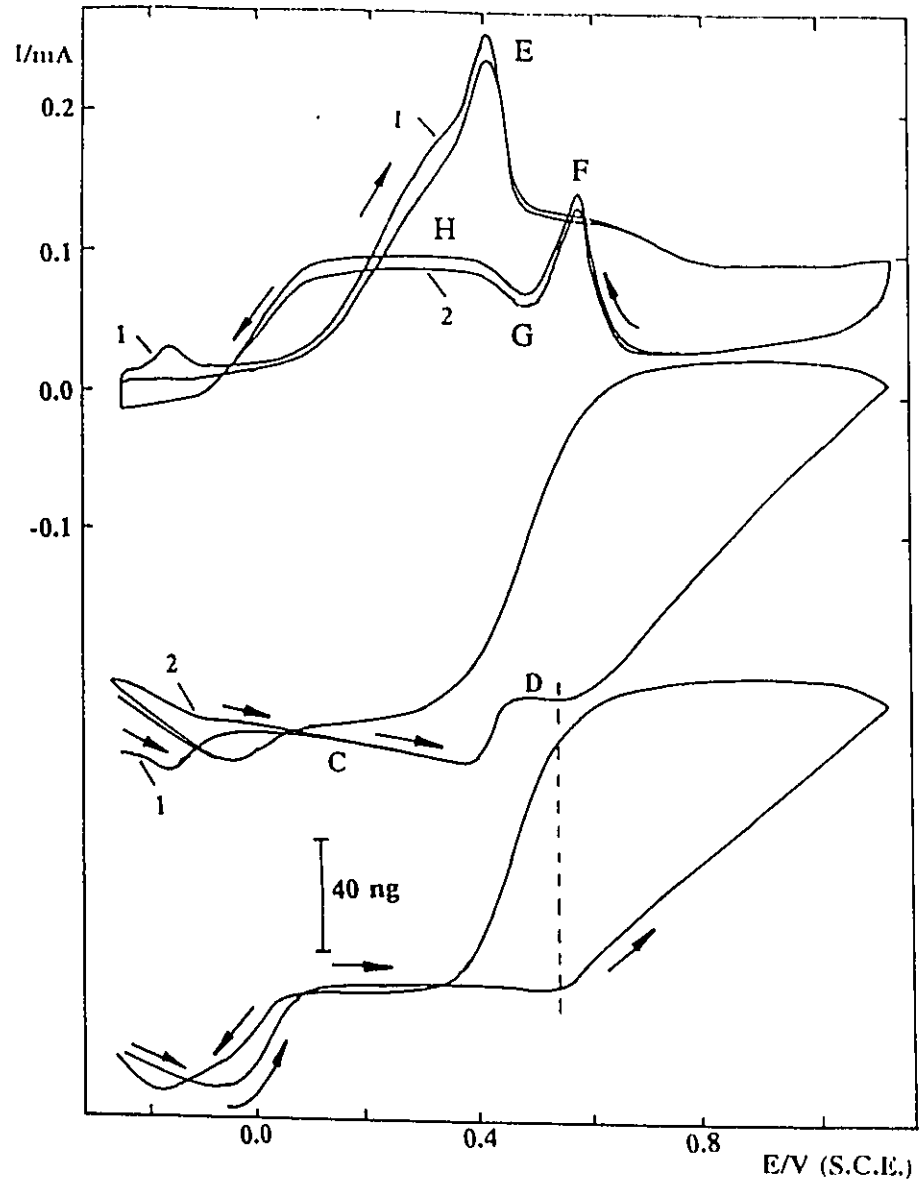

Figure 68. Cyclic voltammogram and mass response (upper mass trace) for the oxidation of 9 mM formic acid in 0.1 M $HClO_4$. Results were recorded after a potential profile like that of Figure 66. The second cycle was recorded directly after the first with no pause. The electrode area was 4.88 cm^2 and the scan rate was 5 mV/s. The background mass response only is shown for comparison purposes and is displaced downwards for purposes of clarity. The vertical dotted line is drawn to illustrate the slight shift in the point where irreversible surface oxidation begins when formic acid is present. Point C indicates where the two anodic going mass responses coincide and point D illustrates the mass plateau that follows the step.

On the cathodic scan, there is a reactivation peak (F) which is followed by a dip due to surface oxide reduction (G) and then a current plateau (H) before the final decline in current begins at 0.1V. Figure 68 also shows the second cycle recorded directly after the first. The only significant difference between the voltammograms is the suppression of the current in the region from -0.25V to -0.1V. This is a result of the higher coverage of strongly adsorbed species formed in the latter stages of the first cycle.

7.2.3 *Mass responses for 9mM formic acid*

The mass responses for the two cycles with formic acid, in the center of Figure 68, are in excellent agreement, except during the initial stages of each of the anodic halves of the two cycles (note that the lower mass response is for background electrolyte alone). The reasons for this difference will now be addressed. The state of the surface at a potential of -0.25V is affected by the potential perturbation applied to the electrode before it reaches -0.25V. In the first cycle there is a step from 1.15V and a pause of 60s at -0.25V, where some adsorption will take place. This is likely to be small as discussed above. Further adsorption can take place once the potential scan begins and adsorbed H is removed from the surface. In contrast, on the second cycle the anodic scan is preceded by a cathodic scan where, once the surface oxide is removed (G), there is a considerable time for coverage of adsorbates to develop (although this probably occurs after the plateau (H)). Comparison of current and mass in this section of the *cathodic* scan is interesting since in a general sense the two signals are similar. Thus the region of constant current (H) from 0.4V downwards is accompanied by a region of almost constant mass and as the current decreases more sharply so does the mass, at least for a short time. Finally from about 0.0V the mass increases, until it reaches -0.25V.

It is clear from a comparison of the voltammetry and mass that a higher coverage of adsorbates leads (in the H upd region) to an increase in mass, whereas the reverse is true in the double layer region of potential. However, the fact that responses for the two cycles merge at about 0.15V implies that at this point (C) there is a comparable coverage (the voltammetry is quite similar too) which is reached by different routes on the two scans. It is more difficult to explain why the mass responses take the shape they do and why an increased coverage of adsorbates leads to a mass increase in the H upd region and a mass decrease in the double layer region. Undoubtedly some of the factors described earlier in this thesis play a part. For example, the coverage of water and specifically adsorbed anions is potential dependent and thus one might not necessarily expect that the occupation of an equal number of sites by a given adsorbate results in the same net mass change at two different potentials. The roles of time and formic acid concentration are additional influences because the rate of adsorption will vary with both of these factors. Thus the scan rate and the bulk formic acid concentration will influence the mass response. Further information on this point can be obtained from mass transient experiments, but before presenting those results the remainder of the cycles of Figure 68 will be discussed.

Once the sharp peak (E) is reached in the voltammogram, the mass step is seen. There is then a plateau region (D) before the mass increases again. An interesting question is whether or not there is any adsorption in this plateau region. We know that prior to the mass step there is a significant coverage of strongly adsorbed intermediates, but does formic acid re-adsorb after these species are removed? If we choose a particular potential in the mass plateau region, say 0.5V, and then measure the mass difference between this point and the mass at the potential of scan reversal, the difference is larger than when a similar

measurement is made for the background electrolyte alone. If one assumes that the mass at scan reversal is the same in both cases (i.e. that there is a similar coverage of oxide and that there is little adsorption of organic residues; both of these points are substantiated by later results) then this implies a small amount of adsorption in the plateau region around 0.5V. This makes the electrode mass lower than in 0.1 M $HClO_4$.

It is interesting to note that the mass plateau region corresponds to a broad shoulder in the voltammogram. It may be that (some of) the oxidation here takes place with the assistance of adsorbed OH or PtOH at the electrode surface. The likelihood of adsorption in this region is also indicated by the small shift in the onset of the final mass increase of the anodic scan (refer to dotted line). This implies some blockage or shifting of the irreversible stages of surface oxidation. There is little apparent effect of formic acid on the reduction of the surface oxide, but it is interesting to note that the reactivation peak (F) on the cathodic half of the voltammogram occurs before any noticeable decrease in mass implying that no significant reduction of the oxidised surface is necessary to allow the oxidation of formic acid to begin again.

7.2.4 *Mass transient experiments*

As we have seen in previous chapters, one simple means of examining adsorption processes at the EQCM is to add a small amount of the adsorbate to the electrolyte and follow the frequency (mass) signal with time at constant potential. Thus it is possible to see whether adsorption leads to a simple mass increase or decrease relative to the background electrolyte. The progression of the mass to a steady state or pseudo steady state can also be followed. For CO adsorption, for example, initial adsorption at Pt leads to a mass decrease

but as coverage develops the mass change reverses direction and finally a net increase is seen[263]. These types of experiment thus provide further insight into adsorption processes at constant potential and to the relative positions of mass responses accompanying voltammograms for a background electrolyte containing different amounts of formic acid from zero upwards.

Results of some mass transient experiments are shown in Figure 69. Additions of formic acid were chosen to provide a final bulk concentration of 9 mM. Each experiment was carried out at a clean electrode. The results suggest the following general conclusions.

a). First, at the oxidised electrode surface (1.0V) (curve 6) there does not appear to be any significant adsorption. This was found to be true for concentrations up to 1.0 M.

b). Second, in the double layer region of potential (0.15V, 0.30V and 0.55V, curves 3, 4 and 5 respectively) there is adsorption such that the mass of the electrode is less in the presence of formic acid.

Both these conclusions agree with those derived from mass responses that accompanied the voltammetry. (The potential dependence of the mass change also reinforces the conclusion that there is no effect of the small change in solution viscosity and density on the mass response). Finally, at 0.0V (curve 2) and -0.15V (curve 1) a small increase is seen in the mass of the electrode after addition of formic acid. This too is what would be expected from the data in Figure 68, although it should be appreciated that the mass response accompanying the voltammogram is dependent upon processes occurring at lower potentials. The result at 0.0V also shows the effect of time, since the initial mass change is a decrease followed by a steady increase. Again this is most likely to be a result of the competition

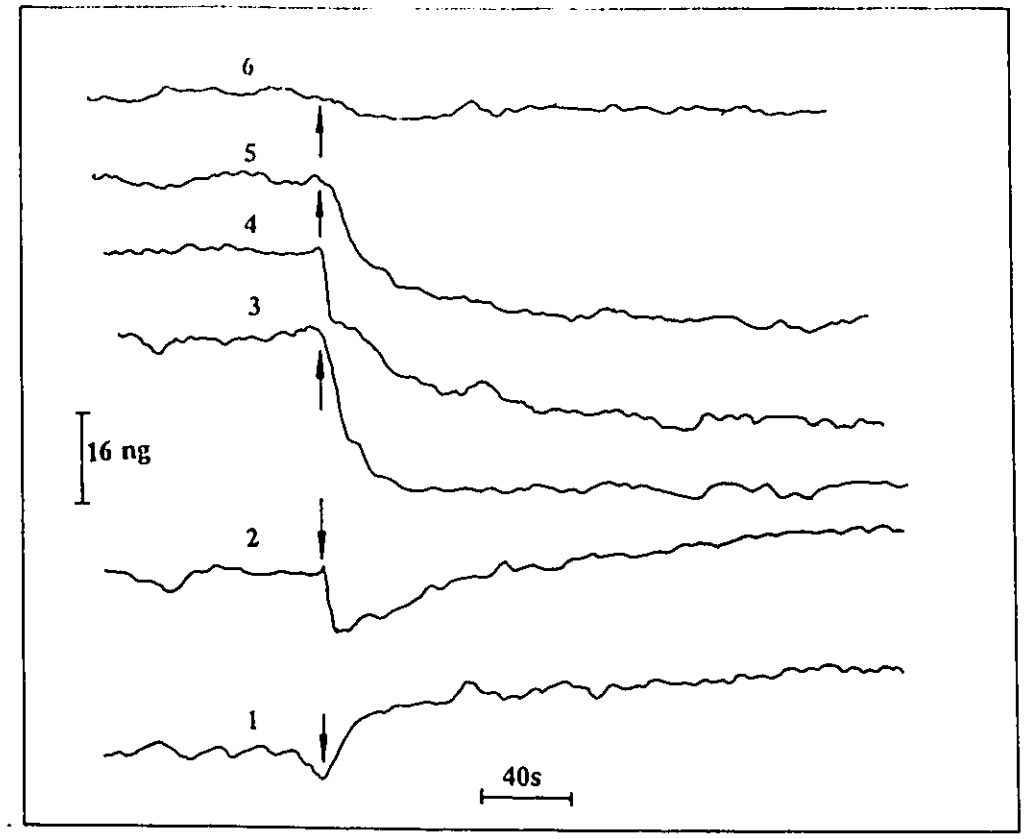

Figure 69. Mass transients resulting from the addition of formic acid (sufficient to give a bulk concentration of 9 mM) to the background electrolyte at different constant potentials. Each injection was performed at a clean electrode surface. Electrode area was 4.30 cm^2. Responses are displaced for purposes of clarity and are not intended to represent relative mass values. Constant potentials used were 1, -0.15V; 2, 0.0V; 3, 0.15V; 4, 0.30V; 5, 0.55V; 6, 1.0V. The arrows indicate when the formic acid was added to the electrolyte.

between anions and water and the adsorbate and perhaps also of the changing nature of the adsorbate with coverage (e.g. CO may shift from being multiply bound to being singly bound as coverage increases). The combined data provide a useful illustration of the fact that mass changes upon adsorption can be either positive or negative.

7.2.5 *The influence of increasing amounts of formic acid on the mass profile*

An increase in the amount of formic acid present in the electrolyte does not cause significant changes in the cyclic voltammetric response, but the following general trends are observed (when all voltammograms are recorded after a potential profile like that seen in Figure 66). First the anodic peak (peak E in Figure 68) that is associated with the mass step (and with removal of strongly adsorbed species) is shifted steadily in the positive direction from 0.42V at 20 mM to 0.70V at 0.1 M. The shoulder following the peak also gradually disappears until there is, at 0.1 M formic acid, an abrupt drop in current after the peak. At the same time the reactivation peak (peak F in Figure 68, where formic acid is oxidised on fresh sites generated by some removal of the surface oxide) becomes much sharper. It also shows a positive shift, but to a lesser extent. This data is summarised in Figure 70A. Needless to say, current densities also increase.

The evolution of the mass response is more interesting. Figure 70B shows part of the mass responses (restricted to potentials in the double layer region and above) for a series of experiments on the same electrode. There are three general effects. First the mass step shifts in a positive direction, just as the anodic current peak does. This is most clearly seen for the solid and dotted lines. It also diminishes in size and the subsequent mass plateau shortens. Second, the final mass increase of the scan is also shifted in the positive direction. Finally,

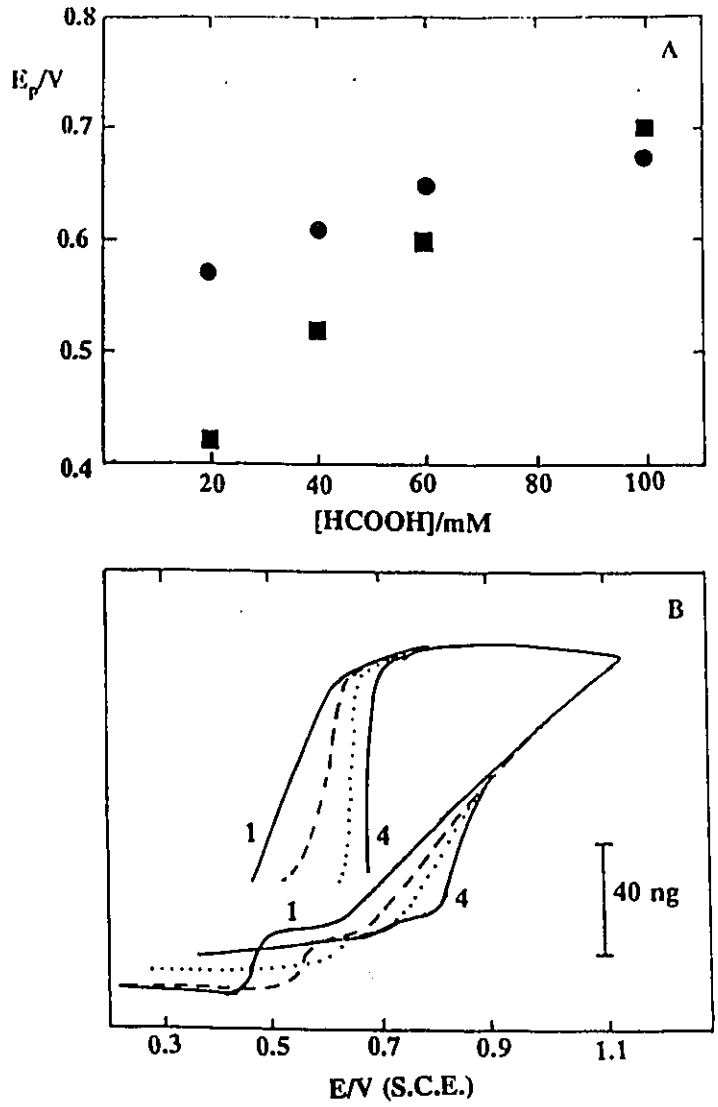

Figure 70. A: The variation of the potential (E_p) of the anodic (■) and cathodic (reactivation) peaks (o) with formic acid concentration. Scan rate was 5 mV/s and all voltammograms were recorded after a potential profile like that shown in Figure 66. B: The influence of formic acid concentration on mass response. 1. (solid line) 20 mM, 2. (dashed line) 40 mM, 3. (dotted line) 60 mM, 4. (solid line) 0.1 M. The concentration of formic acid was increased in steps and then each response recorded after the potential profile shown in Figure 66 at 5mV/s. Traces are drawn aligned so that the masses coincide at the upper potential limit. Electrode area was 4.55 cm^2.

the rate of removal of surface oxide on the cathodic scan is increased and thus the mass decreases more sharply than in the background electrolyte and at a more positive potential (compare, for example, curves 1 and 4). This behaviour is very similar to that reported earlier for methanol (Figure 65) and leads to several conclusions.

1. The removal of strongly adsorbed species is shifted towards more positive potentials as the bulk concentration increases. This results in a similar shift of both mass step and current peak. This may occur because there are less oxy-species (OH_{ads} or PtOH) at the surface to assist in oxidation of CO as a result of more extensive occupation of the surface by the reactive intermediate and possibly by CO itself.

2. There is probably more adsorption subsequent to the mass step as concentration increases, but there comes a point where the mass plateau region has almost disappeared (and so has the shoulder in the voltammogram after the peak as noted above, this will be clearly visible in the next Figure). The gradual shift in the potential at which oxidation of strongly adsorbing species occurs leads to a situation where the removal process is immediately followed by irreversible surface oxidation. This effectively "switches off" the formic acid oxidation process, although it is well known that the oxidation begins again at more positive potentials on the fully oxidised surface.

3. The more rapid reduction of the oxidised surface, illustrated by the rapid decline of the mass earlier in the cathodic scan (and the positive shift in the reactivation peak) is most likely to be associated with an increased reaction between adsorbates derived from formic acid and PtOH as concentration increases. This point is dealt with further in the next section.

A complete cycle for 0.1 M formic acid with both voltammetric and mass responses can be seen in Figure 71. A background mass response is also shown. This illustrates more clearly the changes that occur as the formic acid concentration is increased, particularly the almost complete absence of the mass step on the anodic scan and the significant shifts in the potentials of oxide formation and removal. Thus the final increase in mass, which corresponds to the beginning of irreversible surface oxidation, is shifted to 0.79 V compared to 0.57V in the background electrolyte. It is more rapid at first and then slows to a rate similar to the background response. The faster removal of the surface oxide is also seen to coincide clearly with the sharp reactivation on the negative going scan. Two further small points should be made about the response at this concentration. In the double layer region of potential the mass is flat, and there is no difference between the anodic and cathodic sections. It is likely that at this concentration the steady state coverage of adsorbates is reached rapidly (clearly this is the case after oxide removal since the mass drops sharply) and is the same on both halves of the cycle. As before, the mass increases as the potential proceeds into the H upd region (on a cathodic scan) since a higher coverage of adsorbates in this region leads to a mass increase. The slight discrepancy between the beginning and end of the mass loop may be accounted for by differing coverages. Finally the relative positions of the two mass responses are again substantiated by injection (mass transient) experiments which may be summarised thus. In the H upd region the mass of the electrode is larger than in the background. (The observed increase is in fact larger than that seen for the same potential with 9 mM formic acid). In the double layer region the mass of the electrode is less than in the background electrolyte and finally, on the oxidised electrode surface any mass difference is at the limit of experimental significance.

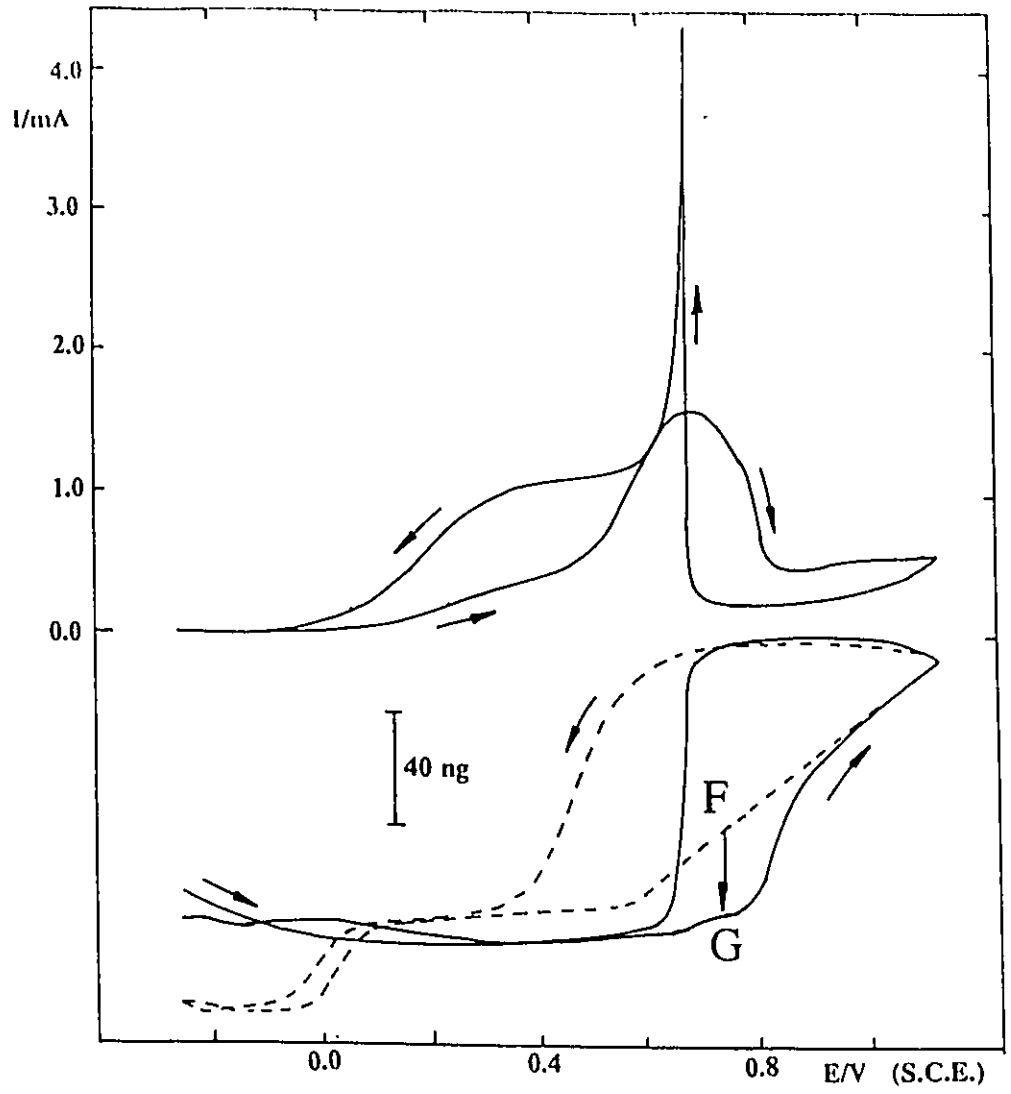

Figure 71. Cyclic voltammogram and mass response for 0.1 M formic acid in 0.1 M $HClO_4$. Scan rate 5 mV/s, electrode area was 4.55 cm^2. The background mass response (dotted line) is presented for purposes of comparison and is drawn so that masses coincide at the point of scan reversal. The vertical arrow between points F and G represents the mass change when 0.1 M formic acid is added to the electrolyte with the potential held at 0.7V. See text for details.

7.2.6 *The role of surface OH in the oxidation reaction*

Injection and open circuit potential decay experiments, where mass is recorded in parallel, provide some interesting further information regarding the interaction between formic acid and the electrode surface when it is at least partially oxidised. The injection experiment was carried out with the electrode held at 0.7V (after a step up from 0.15V) in background electrolyte. Formic acid is then added to give a final concentration of 0.1 M while the potential is maintained at 0.7V. This causes a drop in mass which is larger than could be accounted for by simple reduction of the (partially) oxidised surface alone (c.f. results reported for methanol in Figure 64). The mass decreases because the partial coverage of oxide is removed and then there is adsorption of formic acid or intermediates. This process can be represented in Figure 71 by a shift from a point at 0.7V on the background response (F) to a corresponding point on the response with 0.10 mol dm^{-3} formic acid (G). At this potential, electrochemical oxidation (turnover of PtOH to OHPt) does not appear to be able to compete effectively with removal of OH or PtOH by reaction with formic acid or intermediates. However, if the potential is increased to 1.0V and the same injection made, there is no change in mass (note that this is effectively the experiment shown in Figure 69 (curve 6) except that the bulk concentration then was 9 mM). Here, the rate of electrochemical regeneration of any oxide removed in a chemical reaction is sufficient to prevent a noticeable decrease in mass. It is also noted that at this potential there is no difference between the mass responses as drawn in Figure 71.

The chemical reaction between the oxidised surface and formic acid is well-known[324] and the results of Figure 72 illustrate this. The potential was taken to 1.0 V (in background electrolyte) and the circuit opened. Once a stable potential was attained, formic acid was

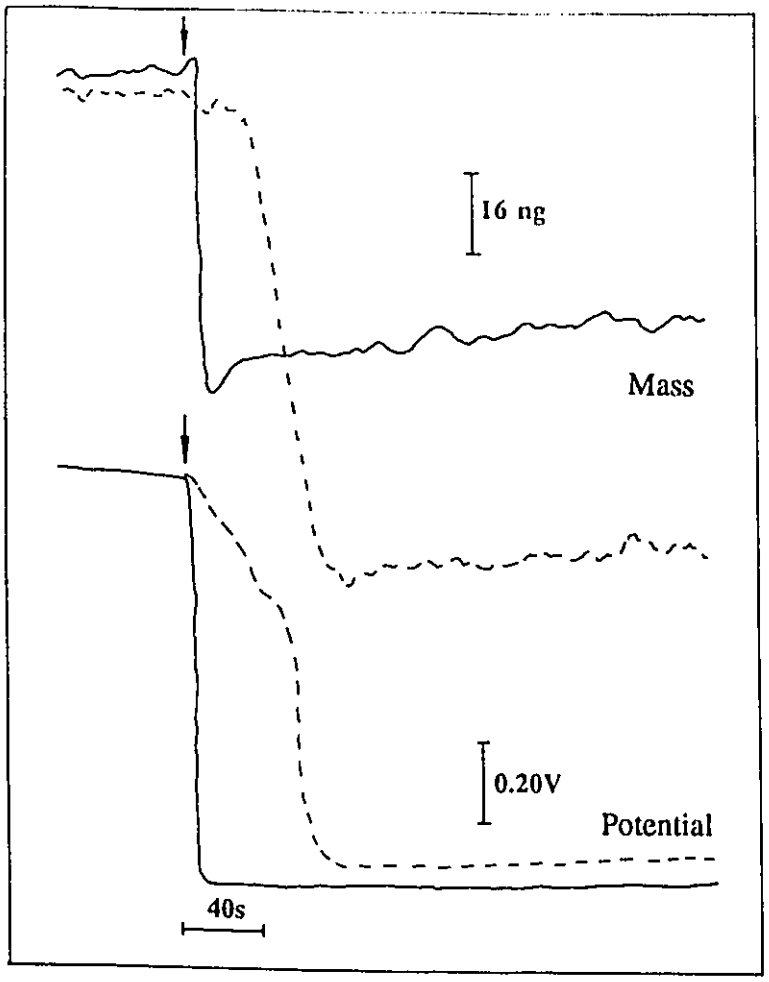

Figure 72. Mass and potential transients observed upon addition of sufficient formic acid to yield a final bulk concentration of 0.5 mM (dashed line) and 0.1 M (solid line) in 0.1M $HClO_4$. The electrode was held first at 1.0V and then the circuit opened. The starting potential was 0.8V in both cases, and the final potentials were -0.11V (0.5 mM) and -0.18V (0.1 M). The arrow indicates when formic acid was added. Electrode area was 3.50 cm^2.

added to give a chosen final concentration and the potential and mass were followed with time. Results are shown for two concentrations 0.5 mM (dashed line) and 0.1 M (solid line). Addition of formic acid in both cases leads to a shift in the potential to the region of H upd, as expected, and to a decrease in mass. Two further points emerge. The rate of decrease for both mass and potential is slower for the lowest concentration (dotted lines) as might be expected, but there is also a larger mass decrease for the lower concentration. Part of this decrease is accounted for by the removal of the oxide, but this contribution should be equal in both cases. The remainder represents the difference between the stable relative masses of the electrode surface in the presence of differing amounts of formic acid. The data suggest that at the rest potentials after injection (in the H upd region) there is a larger coverage of adsorbates developed from 0.1 M formic acid and hence the mass is larger and so the change in mass seen after the potential decay experiment is smaller for 0.1 M formic acid. It is possible to carry out an injection experiment to investigate this and indeed at a constant potential of -0.15V titration of the formic acid concentration to higher amounts leads to successive increases in mass.

7.2.7 *Conclusions*

The variations of mass seen in this chapter illustrate that interactions at the electrode surface are clearly complex and the fact that the net mass change upon adsorption depends upon the species displaced from the surface as well as those adsorbed. Thus in the H upd region of potential, increased coverage of the electrode surface by adsorbates derived from the reaction of formic acid causes an increase in the mass of the electrode. In the double layer region of potential the reverse is true and differences in the mass in this region on the two

halves of a scan can reveal the differing extents of adsorption. At low formic acid concentrations, less poisoning is seen on the cathodic scan in the double layer region and the mass is higher (Figure 60).

The mass step is found to be a feature common to several processes and is useful in locating the point where oxidative removal of strongly bound adsorbates occurs. The subsequent mass plateau region (which is visible at lower concentrations) is also informative since it can be correlated with a shoulder on the voltammogram and it is most likely that oxidation here involves consumption of surface OH, either adsorbed or as PtOH. The evolution of these two features with concentration (as seen in Figure 70) shows a shift of the step to higher potentials, and increased adsorption following the step (so that it becomes smaller in size).

Perhaps the most useful data is that furnished regarding the oxidation/reduction of the electrode surface, and how it is influenced by varying amounts of formic acid. Mass results accompanying cyclic voltammetric and data from injection experiments show that higher concentrations of formic acid appear to consume surface oxy species (perhaps PtOH) at a rapid rate in the mass plateau region so that irreversible surface oxidation is shifted towards more positive potentials until the rate of the place exchange process will have increased sufficiently to compete with consumption by formic acid (it is also possible that there is some blockage of surface sites by strongly adsorbed species). The rate of growth of the oxide (as represented by the rate of increase of mass) is then faster than usual when it does occur because of the higher field (curve 4 in Figure 70). In addition, removal of the oxide occurs at a more positive potential too. This is also a result of the swift consumption of PtOH and PtO by formic acid.

7.3 Review of conclusions from chapters 4 - 7

Despite the most obvious drawback of the technique, namely the inability to identify adsorbed species present at the electrode surface, significant information can be obtained through the careful application of the EQCM to electrocatalytic reactions. There are several common traits in the oxidation processes of small organic molecules such as glucose, methanol and formic acid at platinum electrodes as we have seen in the past few chapters. Thus it is not surprising to find that when these processes are studied with the microbalance technique some similar mass features are to be found too. These latter are presented here to provide an overview of the work carried out in this thesis.

1. In general, the presence of organic adsorbates at the electrode surface causes only small differences in mass profiles (relative to those of the background electrolyte). This is because of factors such as the small molecular weight of most organic fragments (for example CO and CHO), submonolayer coverages, and the fact that adsorption will involve displacement of adsorbed water and specifically adsorbed anions (typically perchlorate and sulphate/bisulphate). Furthermore, one CO, for example, may occupy one, two or three surface sites. In fact, for Pt electrodes in $HClO_4$, it has been found that coverage of the electrode surface with poisoning adsorbates in the double layer region of potential (whether they be derived from glucose, methanol or formic acid) leads to a mass *decrease*. It should also be noted here that because of the factors mentioned above, together with the difficulty in obtaining an exact indication of the nature and distribution of species adsorbed at the surface as a function of potential, the extraction of coverage values for adsorbates from mass data is exceptionally difficult.

2. At low ($< 10^{-2}$ M) concentrations of the organic fuel, the oxidative removal of

strongly adsorbing species or poisons (which is often associated with a sharp peak in the voltammogram) leads to a transition between a surface that is largely covered with organic adsorbates and one that is largely free from such adsorption. As a consequence, a mass step that corresponds to a mass increase is often observed to accompany the removal process because the mass is (as noted above) lower when the surface is covered with poisons. However, the likelihood of adsorption subsequent to the removal of the strongly adsorbing intermediates increases with the concentration of the organic reactant. Thus the mass step diminishes in size as concentration increases.

3. For the oxidations of 0.1 M glucose in alkaline media (presented in Section 6.2), of 0.1 M methanol in perchloric acid solutions, and of 0.1 M formic acid, the mass responses reveal a significant positive shift in the point at which irreversible oxidation of the electrode surface begins. (The large current due to organic oxidation prevents detection of this phenomenon in the voltammogram). In both background electrolyte and when organic fuels are present, there is a region of constant mass before the onset of irreversible surface oxidation. The mass increases again only when the place exchange process (insertion of OH (and O) into the Pt lattice[262,337]) starts, because the initial stages of oxidation of the surface, where PtOH is produced from adsorbed water, do not lead to a mass change. The point where mass begins to increase again after the double layer region of potential, and its variation with increasing amounts of organic fuel in the electrolyte are thus easily identified. Finally, a related item of interest is that the rate of increase of mass (and hence oxide growth) is more rapid when shifted towards more positive potentials, presumably because of the increased field at the higher onset potential.

REFERENCES

1. J. O'M. Bockris and S. Srinivasan, "Fuel Cells: Their Electrochemistry", McGraw-Hill, New York, p289, 1969
2. B. D. McNicol, "Power Sources for Electric Vehicles", (B. D. McNicol and D. A. J. Rand, eds.), Vol.11, Elsevier, Amsterdam, 1984
3. N. A. Hampson and M. J. Willars, J. Power Sources, 4, 191, 1979
4. V. S. Bagotsky and Yu. B. Vassil'ev, Electrochim. Acta, 12, 1323, 1967
5. B. D. McNicol, J. Electroanal. Chem., 118, 71, 1981
6. A. J. Appleby, J. Electroanal. Chem., 118, 31, 1981
7. S. Srinivasan, J. Electroanal. Chem., 118, 51, 1981
8. J. O'M. Bockris, B. E. Conway, E. Yeager and R. E. White, "Comprehensive Treatise of Electrochemisty", Vol.3, Plenum Press, New York, 1981
9. A. Capon and R. Parsons, J. Electroanal. Chem., 45, 205, 1973
10. A. Capon and R. Parsons, J. Electroanal. Chem., 44, 239, 1973
11. R. Parsons and T. VanderNoot, J. Electroanal. Chem., 257, 9, 1988
12. J. M. Leger and C. Lamy, Ber. Bunsenges. Phys. Chem., 94, 1021, 1990
13. T. Iwasita-Vielstich, "Advances in Electrochemical Science and Engineering", (H. Gerisher and C. W. Tobias, eds.), Vol.1, VCH, D-6940 Weimheim, p127, 1990
14. B. Beden, J. M. Leger and C. Lamy, "Modern Aspects of Electrochemistry", (R. E. White, J. O'M. Bockris, and B. E. Conway, eds.), Vol.22, Plenum Press, New York, p97, 1992

15. A. Papoutsis, J. M. Leger and C. Lamy, J. Electroanal. Chem., 359, 141, 1993

16. A. Papoutsis, J. M. Leger and C. Lamy, J. Electroanal. Chem., 234, 315, 1987

17. J. M. Leger, B. Beden and C. Lamy, Ber. Bunsenges. Phys. Chem., 91, 336, 1987

18. B. Beden, S. Bilmos, C. Lamy and J. M. Leger, J. Electroanal. Chem., 149, 295, 1983

19. J. M. Leger, B. Beden, C. Lamy and S. Bilmes, J. Electroanal. Chem., 170, 307, 1984

20. C. Lang, F. Hahn and B. Beden, Portugaliæ Electrochim. Acta, 7, 435, 1989

21. A. Hamnett P.A. Christensen and S.J. Higgins, Portugaliæ Electrochim. Acta, 7, 591, 1989

22. A. Bewick, "Trends in Interfacial Electrochemistry", (A. F. Silva, ed.), D. Reidel Publishing Company, p331, 1986

23. B. Beden, NATO ASI Ser., Ser. C, 320, 103, 1990

24. A. Bewick and S. Pons, "Advances in Infrared and Raman Spectroscopy", (R. S. H. Clark and M. E. Hester, eds.), vol.12, Heyden, London, Chap.1, p1, 1985

25. B. Beden, C. Lamy, A. Bewick and K. Kunimatsu, J. Electroanal. Chem., 121, 343, 1981

26. S. Chang and M. J. Weaver, J. Phys. Chem., 94, 1034, 1990

27. I. T. Bae, X. Xing, C. C. Liu and E. Yeager, J. Electroanal. Chem., 284, 335, 1990

28. R. G. Greenler and T. L. Slager, Spectrochim. Acta, 29A, 193, 1973

29. A. Bewick, K. Kunimatsu, B. S. Pons and J. W. Russell, J. Electroanal. Chem., 160, 381, 1984

30. J. W. Russell, J. Overend, K. Scanlon, M. W. Severson and A. Bewick, J. Phys. Chem., 86, 205, 1982

31. K. Kunimatsu, J. Electroanal. Chem., 140, 205, 1982

32. S. Pons, T. Davidson and A. Bewick, J. Electroanal. Chem., 160, 369, 1984

33. D. S. Corrigan, L. W. H. Leung and M. J. Weaver, Anal. Chem., 59, 2252, 1987

34. D. S. Corrigan and M. J. Weaver, J. Phys. Chem., 90, 5300, 1986

35. W. G. Golden, K. Kunimatsu and H. Seki, J. Phys. Chem., 88, 1275, 1984

36. D. S. Corrigan and M. J. Weaver, J. Electroanal. Chem., 241, 143, 1988

37. O. Wolter and J. Heitbaum, Ber. Bunsenges. Phys. Chem., 88, 2, 1984

38. J. Willsau and J. Heitbaum, J. Electroanal. Chem., 185, 181, 1985

39. T. Iwasita, W. Vielseich and E. Santos, J. Electroanal. Chem., 229, 367, 1987

40. S. Bruckenstein and J. Comeau, Faraday Disc. Chem. Soc., 56, 285, 1974

41. T. Iwasita and W. Vielstich, J. Electroanal. Chem., 201, 403, 1986

42. B. Bittins-Cattaneo and T. Twasita, J. Electroanal. Chem., 238, 151, 1987

43. J. Willsau and J. Heitbaum, Electrochim. Acta, 31, 943, 1986

44. O. Wolter, J. Willsau and J. Heitbaum, J. Electrochem. Soc., 132, 1635, 1985

45. T. Hartung, J. Willsau and J. Heitbaum, J. Electroanal. Chem., 205, 135, 1986

46. S. Wasmus and W. Vielstich, Electrochim. Acta, 38, 185, 1993

47. A. E. Bolzan, T. Iwasita and W. Vielstich, J. Electrochem. Soc., 134, 3052, 1987

48. S. Wilhelm, W. Vielstich, H. W. Buschmann and T. Iwasita, J. Electroanal. Chem., 229, 377, 1987

49. S. Wilhelm, T. Iwasita and W. Vielstich, J. Electroanal. Chem., 238, 383, 1987

50. G. Horanyi, Electrochim. Acta, 37, 2443, 1992

51. L. W. H. Leung and M. J. Weaver, Langmuir, 6, 323, 1990

52. K. V. Ramesh, P. R. Sarode, S. Vasudevan and A. K. Shulka, J. Electroanal. Chem., 223, 91, 1987

53. M. Watanabe, M. Uchida and S. Motoo, J. Electroanal. Chem., 229, 395, 1987

54. J. B. Goodenough, A. Hamnett, B. J. Kennedy and S. A. Weeks, Electrochim. Acta, 32, 1233, 1987

55. E. Roch and J. Heitbaum, J. Electroanal. Chem., 205, 151, 1986

56. E. M. Belgsir, H. Huser, J. M. Leger and C. Lamy, J. Electroanal. Chem., 225, 281, 1987

57. M. Shibata and S. Motoo, J. Electroanal. Chem., 209, 151, 1986

58. K. B. Kokoh, J. M. Leger, B. Beden, H. Huser and C. Lamy, Electrochim. Acta, 37, 1909, 1992

59. K. B. Kokoh, P. Parpot, E. M. Belgsir, J. M. Leger, B. Beden and C. Lamy, Electrochim. Acta, 38, 1359, 1993

60. S. Bruckenstein and M. Shay, Electrochim. Acta, 30, 1295, 1985

61. J. H. Kaufman, K. K. Kanazawa and G. B. Street, Phys. Rev. Lett., 53, 2461, 1984

62. C. P. Wilde and M. Zhang, Electrochim. Acta, 39, 347, 1994

63. C. P. Wilde and M. Zhang, J. Chem. Soc., Faraday Transaction, 89, 385, 1993

64. C. P. Wilde and M. Zhang, J. Electroanal. Chem., 340, 241, 1992

65. J. Clavilier, R. Parsons, R. Durand, C. Lamy and J. M. Leger, J. Electroanal. Chem., 124, 321, 1981

66. S. Motoo and N. Furuya, J. Electroanal. Chem., 184, 303, 1985

67. J. Clavilier and S. G. Sun, J. Electroanal. Chem., 199, 471, 1986

68. R. R. Adzic, A. V. Tripkovic and V. B. Vesovic, J. Electroanal. Chem., 204, 329, 1986

69. R. R. Adzic, A. V. Tripkovic and W. O'Grady, Nature, 296, 137, 1982

70. S. G. Sun, J. Clavilier and A. Bewick, J. Electroanal. Chem., 240, 147, 1988

71. S. Juanto, B. Beden, F. Hahn, J. M. Leger and C. Lamy, J. Electroanal. Chem., 237, 119, 1987

72. M. I. Lopes and I. Fonseca, P. Olivi, B. Beden, F. Hahn, L. M. Leger and C. Lamy, J. Electroanal. Chem., 346, 415, 1993

73. K. D. Popovic, A. V. Tripkovic and R. R. Adzic, J. Electroanal. Chem., 339, 227, 1992

74. G. Kokkinidis, J. M. Leger and C. Lamy, J. Electroanal. Chem., 242, 221, 1988

75. M. J. Llorca, J. M. Feliu, A. Aldaz , J. Clavilier and A. Rodes, J. Electroanal. Chem., 316, 175, 1991

76. S. Motoo and N. Furuya, J. Electroanal. Chem., 197, 209, 1986

77. B. E. Conway, H. Angerstein-Kozlowska and G. Czartoryska, Z. Phys. Chem. N.F., 112, 195, 1978

78. E. Rach and J. Heitbaum, Electrochim. Acta, 32, 1173, 1987

79. N. R. de Tacconi, J. M. Leger, B. Beden and C. Lamy, J. Electroanal. Chem., 134, 117, 1982

80. A. Capon and R. Parsons, J. Electroanal. Chem., 65, 285, 1975

81. B. Beden, C. Lamy and J. M. Leger, Electrochim. Acta, 24, 1157, 1979

82. F. Kadirgan, B. Beden, J. M. Leger and C. Lamy, J. Electroanal. Chem., 125, 89, 1981

83. D. F. A. Koch, D. A. J. Rand and R. Woods, J. Electroanal. Chem., 70, 73, 1976

84. K. Shimazu, D. Weisshaar and T. Kuwana, J. Electroanal. Chem., 223, 223, 1987

85. B. E. Conway, H. Angerstein-Kozlowska and B. MacDougall, J. Electrochem. Soc., 120, 756, 1973

86. V. B. Hughes and R. Miles, J. Electroanal. Chem., 145, 87, 1983

87. M. Shabrang, H. Mizota and S. Bruckenstein, J. Electrochem. Soc., 131, 306, 1984

88. M. Beltowska-Brezezinska, J. Heitbaum and W. Vielstich, Electrochim. Acta, 30, 1465, 1985

89. E. P. M. Levia and M. C. Giordano, J. Electrochem. Soc., 130, 1305, 1983

90. N. Xonoglou, I. Moumtzis and G. Kokinidis, J. Electroanal. Chem., 237, 93, 1987

91. M. Shao, X. Xing and C. C. Liu, Bioelectrochem. Bioenerg., 17, 59, 1987

92. R. R. Adzic, W. E. O'Grady and S. Srinivasan, J. Electrochem. Soc., 128, 1913, 1981

93. R. R. Adzic, Israel J. Chem., 18, 166, 1979

94. R. R. Adzic, D. N. Simic, A. R. Despic and D. M. Drazic, J. Electroanal. Chem., 65, 587, 1975; 61, 117, 1975

95. R. R. Adzic, D. M. Simic, A. R. Despic and D. M. Drazic, J. Electroanal. Chem., 80, 81, 1977

96. D. Pletcher and V. Solis, J. Electroanal. Chem., 131, 309, 1982

97. M. Watanabe and S. Motoo, J. Electroanal. Chem., 60, 275, 1975

98. S. Motoo and M. Watanabe, J. Electroanal. Chem., 98, 203, 1979

99. M. Shibata and S. Motoo, J. Electroanal. Chem., 187, 151, 1985

100. M. Watanabe, Y. Furuuchi and S. Motoo, J. Electroanal. Chem., 191, 367, 1985

101. M. Watanabe, M. Shibata and S. Motoo, J. Electroanal. Chem., 187, 161, 1985

102. S. Trasatti, Materials Chemistry and Physics, 16, 157, 1987

103. X. H. Xia and T. Iwasita, J. Electrochem. Soc., 140, 2559, 1993

104. M. M. P. Janssen and J. Moolhuysen, J. Catal. 46, 289, 1976

105. E. Herero, A. Fernandez-Vega, J. M. Feliu and A. Aldaz, J. Electroanal. Chem., 350,

73, 1993

106. H. Kita, H. Nakajima and K. Shimazu, J. Electroanal. Chem., 248, 181, 1988

107. W. J. Lorenz, H. D. Hermann, N. Wüthrich and F. Hilbert, J. Electrochem. Soc., 121, 1167, 1974

108. E. Bosco and S. K. Rangarajan, J. Electroanal. Chem., 129, 25, 1981

109. K. Jütter and W. J. Lorenz, Z. Phys. Chem. N.F, 122, 163, 1980

110. N. Pangarov, Electrochim. Acta, 28, 763, 1983

111. S. Trasatti, Z. Phys. Chem. N.F., 98, 75, 1975

112 D. M. Kolb, "Advances in Electrochemisty and Electrochemical Engineering", (H. Gerischer and C. W. Tobias, eds.), John Wiley, New York, Vol.11, p25, 1978

113. S. Swathirajan and S. Bruckenstein, Electrochim. Acta, 28, 865, 1983

114. S. Szabo, Intern. Rev. Phys. Chem., 10, 207, 1991

115. D. M. Kolb, M. Przasnyski and H. Gerischer, J. Electroanal. Chem., 54, 25, 1974

116. G. V. Hevesy, Physik. Z., 13, 715, 1912

117. K. F. Herzfeld, Physik. Z., 14, 29, 1913

118. L. B. Rogers, D. P. Krause, J. C. Griess, Jr. and D. B. Ehrlinger, J. Electrochem. Soc., 95, 33, 1949

119. R. C. De Geiso and L. B. Rogers, J. Electrochem. Soc., 106, 433, 1959

120. L. B. Rogers and A. F. Stehney, J. Electrochem. Soc., 95, 25, 1949

121. M. Haissinsky, J. Chim. Phys., 43, 21, 1946

122. M. Haissinsky, Experientia, 8, 125, 1952

123. M. M. Nicholson, J. Am. Chem. Soc., 79, 7, 1957

124. M. M. Nicholson, Anal. Chem., 32, 1058, 1960

125. T. Mills and G. M. Willis, J. Electrochem. Soc., 100, 452, 1953

126. R. R. Adzic, "Advances in Electrochemistry and Electrochemical Engineering", (H. Gerischer, C. W. Tobias, eds.), John Wiley & Sons, New York, Vol.13, p159, 1984

127. W. Gordy and W. J. O. Thomas, J. Chem. Phys., 24, 439, 1956

128. S. Trasatti, J. Electroanal. Chem., 33, 351, 1971

129. K. Englesmann, W. J. Lorenz and E. Schmidt, J. Electroanal. Chem., 114, 11, 1980

130. A. Bewick and B. Thomas, J. Electroanal. Chem., 65, 911, 1975; 84, 127, 1977;

131. J. W. Schultze and D. Dickertmann, Surf. Sci., 54, 489, 1976

132. M. Boudart, J. Am. Chem. Soc., 72, 3556, 1958

133. J. W. Schultze and K. J. Vetter, J. Electroanal. Chem., 44, 63, 1973

134. J. W. Schultze and F. D. Koppitz, Electrochim. Acta, 21, 327, 1976

135. K. J. Vetter and J. W. Schultze, Ber. Bunsenges. Phys. Chem., 76, 920, 1972

136. K. J. Vetter and J. W. Schultze, Ber. Bunsenges. Phys. Chem., 76, 927, 1972

137. G. Horanyi and G. Vertes, J. Electroanal. Chem., 45, 295, 1973

138. G. Horanyi, J. Electroanal. Chem., 55, 45, 1974

139. E. Schmidt, H. R. Gygax and P. Bohlen, Helv. Chim. Acta, 49, 733, 1966

140. J. N. Jovicevic, V. D. Jovic and A. R. Despic, Electrochim. Acta, 29, 1625, 1984; 30, 1455, 1985

141. E. Schmidt and N. Wuthrich, J. Electroanal. Chem., 28, 349, 1970

142. G. Horanyi, J. Solt and G. Vertes, J. Electroanal. Chem., 32, 271, 1971

143. V. A. Vicente and S. Bruckenstein, Anal. Chem., 45, 2036, 1973

144. H. D. Abruna, "Electrochemical Interfaces: Modern Techniques for In-situ Interface Characterization", VCH, New York, 1991

145. H. D. Abruna, J. H. White, M. J. Albarelli, G. M. Bommarito, M. J. Bedzyk and M. J. McMillan, J. Phys. Chem., 92, 7045, 1988

146. M. G. Samant, G. L. Borges, J. G. Gordon, O. R. Melroy and L. Blum, J. Am. Chem. Soc., 109, 5970, 1987

147. A. Tadjeddine, A. Lahrichi and G. Tourillon, J. Electroanal. Chem., 360, 261, 1993

148. M. G. Samant, M. F. Toney, G. L. Borges, L. Blum and O. R. Melroy, J. Phys. Chem., 92, 220, 1988

149. M. F. Toney, J. G. Gordon, M. G. Samant, G. L. Borges, D. G. Wiesler, D. Yee and L. B. Sorensen, Langmuir, 7, 796, 1991

150. G. Materlik, J. Zegenhagen and W. Uelhoff, Phys. Rev., B32, 5502, 1985

151. J. Zegenhagen, G. Materlik and W. Uelhoff, J. X-ray Sci. Tech., 2, 214, 1990

152. G. M. Bommarito, J. H. White and H. D. Abruna, J. Phys. Chem., 94, 8280, 1990

153. H. D. Abruna, T. Gog, G. Materlik and W. Uelhoff, J. Electroanal. Chem., 360, 315, 1993

154. O. M. Magnussen, J. Hotlos, R. J. Nichols, D. M. Kolb and R. J. Behm, Phys. Rev. Lett., 60, 2929, 1990

155. S. Maune, P. K. Hansma, J. Massie, V. B. Elings and A. A. Gewirth, Science, 251, 183, 1991

156. C-H. Chen, S. M. Vesecky and A. A. Gewirth, J. Am. Chem. Soc., 114, 451, 1992

157. T. Hachiya, H. Honbo and K. Itaya, J. Electroanal. Chem., 315, 275, 1991

158. A. Bewick and B. Thomas, J. Electroanal. Chem., 85, 329, 1977

159. R. R. Adzic, E. Yeager and B. D. Cahan, J. Electrochem. Soc., 121, 476, 1974

160. R. R. Adzic and N. M. Markovic, J. Electroanal. Chem., 102, 263, 1979

161. R. R. Adzic and N. M. Markovic, Electrochim. Acta, 30, 1473, 1985

162. J. D. E. McIntyre, "Advances in Electrochemisty and Electrochemical Engineering", (R. H. Muller, eds.), Vol.9, Wiley-Interscience, New York, p61, 1973

163. J. D. E. McIntyre, Surf. Sci., 37, 658, 1973

164. J. Anderson, G. W. Rubloff and P. J. Stiles, Surf. Sci., 37, 75, 1973

165. T. Takamura, K. Takamura, W. Nippe and E. Yeager, J. Electrochem. Soc., 117, 626, 1970

166. D. M. Kolb, D. Leutloff and M. Przasnyski, Surf. Sci., 47, 622, 1975

167. T. Takamura, K. Takamura and F. Wantanabe, Surf. Sci., 44, 93, 1974

168. T. Takamura, K. Takamura and E. Yeager, J. Electroanal. Chem., 29, 279, 1971

169. T. Takamura, F. Wantanabe and K. Takamura, Electrochim. Acta, 19, 933, 1974

170. T. Takamura and Y. Sato, J. Electroanal. Chem., 47, 245, 1973

171. S. Swathirajan and S. Bruckenstein, J. Electrochem. Soc., 129, 1202, 1982

172. S. Swathirajan and S. Bruckenstein, Electrochim. Acta, 28, 865, 1983

173. T. M. Riedhammer, L. S. Melnicki and S. Bruckenstein, Z. Phys. Chem., N.F., 111, 177, 1978

174. S. Bruckenstein and B. Miller, Accts. Chem. Rev., 10, 54, 1977

175. E. Schmidt and H. Siegenhaler, Helv. Chim. Acta, 52, 2245, 1969

176. H. Bort, K. Jutter, W. J. Lorenz and E. Schmidt, J. Electroanal. Chem., 90, 413, 1978

177. H. D. Hermann, N. Wuthrich, W. J. Lorenz and E. Schmidt, J. Electroanal. Chem., 68, 273, 1976; 68, 289, 1976

178. S. Bruckenstein and S. Swathirajan, Electrochim. Acta, 30, 851, 1985

179. O. R. Melroy, K. K. Kanazawa, J. G. Gordon II and D. Buttry, Langmuir, 2, 697,

1986

180. M. R. Deakin and O. Melroy, J. Electroanal. Chem., 239, 321, 1988

181. S. Lakkaraju, M. J. Bennahmias, G. L. Borges, J. G. Gordon II et al., Applied Optics, 29, 4943, 1990

182. Y. Tang and T. E. Furtak, Electrochim. Acta, 36, 1873, 1991

183. C. P. Wilde and M. Zhang, J. Electroanal. Chem., 327, 307, 1992

184. C. P. Wilde and M. Zhang, Langmuir, 10, 1600, 1994

185. C. P. Wilde and M. Zhang, J. Electroanal. Chem., 338, 359, 1992

186. M. Hepel, K. Kanige and S. Bruckenstein, J. Electroanal. chem., 266, 409, 1989

187. M. Hepel and S. Bruckenstein, Electrochim. Acta, 34, 1499, 1989

188. M. Hepel, K. Kanige and S. Bruckenstein, Langmuir, 6, 1063, 1990

189. M. Hepel, S. Bruckenstein and K. Kanige, J. Chem. Soc., Faraday Trans., 89, 251, 1993

190. H. Abruna, In situ studies of electrochemical interfaces, VCH Chemicals, New York, 1991

191. C. Lu and A. W. Czanderna, "Applications of piezoelectric quartz crystal microbalance", Elsevier, 1984

192. S. Bruckenstein and M. Shay, J. Electroanal. Chem., 188, 131, 1985

193. M. R. Deakin, T. T. Li and O. R. Melroy, J. Electroanal. Chem., 243, 343, 1988

194. Z. Shu and S. Bruckenstein, J. Electroanal. Chem., 317, 263, 1991

195. H. E. Hager, R. D. Ruedisueli and M. E. Buehler, Corrosion, 42, 345, 1986

196. W. D. Hinsberg, C. G. Willson and K. K. Kanazawa, J. Electrochem. Soc., 133, 1448, 1986

197. C. Gabrielli, M. Keddam and H. Takenouti, Corrosion Science, 31, 129, 1990

198. H. J. Schmit, Anal. Chim. Acta, 273, 561, 1993

199. C. K. Baker and J. R. Reynolds, Synth. Met., 28, C21, 1989

200. C. K. Baker and J. R. Reynolds, J. Electroanal. Chem., 251, 307, 1988

201. P. T. Varineau and D. A. Buttry, J. Phys. Chem., 91, 1292, 1987

202. D. Orata and D. A. Buttry, J. Am. Chem. Soc., 109, 3574, 1987

203. M. R. Deakin and H. Byrd, Anal. Chem., 61, 290, 1989

204. R. R. McCaffrey, S. Bruckenstein and P. Prasad, Langmuir, 2, 228, 1986

205. G. G. Guilbault, Anal. Chem., 55, 1682, 1983

206. M. Thompson, C. L. Arthur and K. D. Gurbaksh, Anal. Chem., 58, 1206, 1986

207. H. Muramatsu, K. Kajiwara, E. Tamiya and I. Karube, Anal. Chim. Acta, 188, 257, 1986

208. E. S. Grabbe, R. P. Buck and O. R. Melroy, J. Electroanal. Chem., 223, 67, 1987

209. S. Z. Yao and Z. H. Mo, Anal. Chim. Acta, 193, 97, 1987

210. W. Z. Wei, L. H. Nie and S. Z. Yao, Anal. Chim. Acta, 269, 149, 1992

211. G. Guilbault, Ion Selective Electrode Reviews, 2, 3, 1980

212. J. F. Alder and J. J. McCallum, Analyst, 108, 1169, 1983

213. P. L. Konash and G. J. Bastiaans, Anal. Chim., 52, 1929, 1980

214. T. Nomura, Anal. Chim. Acta, 124, 81, 1981

215. T. Nomura, T. Nagamune, K. Izutsu and T. S. West, Bunseki Kagaku, 30, 494, 1981

216. T. Nomura and M. Iijima, Anal. Chim. Acta, 131, 97, 1981

217. R. Schumacher, Angew. Chem. Int. Ed. Engl., 29, 329, 1990

218. D. A. Buttry, in "Electroanalytical Chemistry", (A. J. Bard, ed.), Marcel Dekker, New

York, Vol.17, 1, 1991

219. M. D. Ward and D. A. Buttry, Science, 249, 1000, 1990

220. J. F. Alder and J. J. McCallum, Analyst, 108, 1169, 1983

221. D. A. Buttry and M. D. Ward, Chem. Rev., 92, 1355, 1992

222. M. Thompson, A. L. Kipling, W. C. Duncan-Hewitt, L. V. Rajakovic and B. A. Cavic-Vlasak, Analyst, 116, 881, 1991

223. F. W. Maarsen, M. C. Smit and J. Martz, Rev. Trav. Chim. Pays-Bas, 76, 713, 1957

224. G. Z. Sauerbrey, Phys. Verhandl, 8, 113, 1957

225. G. Z. Sauerbrey, Z. Phys., 115, 206, 1959

226. Z. Lin, C. M. Yip, I. S. Joseph and M. D. Ward, Anal. Chem., 65, 1546, 1993

227. C. S. Lu and O. Lewis, J. Appl. Phys., 43, 4385, 1972

228. B. Parzen, Design of Crystal and Other Harmonic Oscillators, Wiley-Interscience, New York, 1983

229. T. Okajima, H. Sakurai, N. Oyama, K. Tokuda and T. Ohsaka, Electrochim. Acta, 38, 747, 1993

230. H. E. Hager, Chem. Eng. Commun., 43, 25, 1986

231. S. J. Martin, V. E. Granstaff and G. C. Frye, Anal. Chem., 63, 2272, 1991

232. H. Muramatsu, X. Ye, M. Suda, T. Sakuhara and T. Ataka, J. Electroanal. Chem., 322, 311, 1992

233. W. G. Cady, Piezoelectricity, McGraw-Hill, New York, 1964

234. H. Muramatsu, E. Tamiya and I. Karube, Anal. Chem., 60, 2141, 1988

235. M. R. Deakin and D. A. Buttry, Anal. Chem., 61, 1147A, 1989

236. T. Zhou, L. Nie and S. Yao, J. Electroanal. Chem., 293, 1, 1990

237. K. K. Kanazawa and J. G. Gordon, Anal. Chim. Acta, 175, 99, 1985

238. S. J. Lasky and D. A. Buttry, J. Am. Chem. Soc., 110, 6258, 1988

239. S. J. Martin and G. C. Frye, Appl. Phys. Lett., 57, 1867, 1990

240. R. Schumacher, G. Borges and K. Kanazawa, Surf. Sci., 163, L621, 1985

241. R. Schumacher, J. Gordon and O. Melroy, J. Electroanal. Chem., 216, 127, 1987

242. K. E. Heusler, A. Grezegorzewski, L. Jackel and J. Pietrucha, Ber. Bunsen-Ges. Phys. Chem., 92, 1218, 1988

243. S. Bruckenstein and M. Shay, Electrochim. Acta, 30, 851, 1985

244. E. P. EerNisse, J. Appl. Phys., 44, 4482, 1973

245. G. T. Cheek and W. E. O'Grady, J. Electroanal. Chem., 277, 341, 1990

246. L. V. Rajakovic, B. A. Cavic-Vlasak, V. Ghaemmaghami, K. M. R. Kallury, A. L. Kipling and M. Thompson, Anal. Chem., 63, 615, 1992

247. W. Stockel and R. Schumacher, Ber. Bunsen-Ges. Phys. Chem., 345, 91, 1987

248. J. Wang, L. M. Frostman and M. D. Ward, J. Phys. Chem., 96, 5224, 1992

249. H. Angerstein-Kozlowska, "Comprehensive Treatise of Electrochemistry", (E. Yeager, J. O'M. Bockris, B. E. Conway and S. Sarangapani, eds.), Vol.9, Plenum Press, New York, p15, 1984

250. M. Benje, M. Eiermann, U. Pittermann and K. G. Weil, Ber. Bunsen. Phys. Chem., 90, 435, 1986

251. G. C. Komplin, F. Schleifer and W. J. Pietro, Rev. Sci. Instrum., 64, 1530, 1993

252. A. R. Nisbet and A. J. Bard, J. Electroanal. Chem., 6, 332, 1963

253. E. Schmidt and N. Wüthrich, J. Electroanal. Chem., 40, 399, 1972

254. R. R. Adzic and Lj. V. Minevski, Electrochim. Acta, 32, 125, 1987

255. B. J. Bowles, Electrochim. Acta, 15, 737, 1970

256. S. H. Cadle and S. Bruckenstein, Anal. Chem., 44, 1993, 1972

257. G. Kokkinidis, J. Electroanal. Chem., 201, 217, 1986

258. M. W. Breiter, Electrochemical Process in Fuel Cells, Springer, New York, 1969

259. H. Angerstein-Kozlowska, W. B. A. Sharp and B. E. Conway, Proceedings of The Symposium on Electrocatalysis, (M. W. Breiter, ed.), The Electrochemical Society, New Jersey, p94, 1974

260. B. E. Conway, H. Angerstein-Kozlowska and F. C. Ho, J. Vac. Sci. Technol., 14, 351, 1977

261. J. F. Llopis and F. Colom, "Encyclopædia of Electrochemistry of the Elements", (A. J. Bard, ed.), Vol VI, Dekker, New York, 1973

262. H. Angerstein-Kozlowska, B. E. Conway and W. B. A. Sharp, J. Electroanal. Chem., 43, 9, 1973

263. S. Bruckenstein and C. P. Wilde, Ext. Abs. 116, 198th ACS National Meeting, Miami Beach, Florida, 1989

264. R. Randonis, D. Plaušinaitis and V. Daujotis, J. Electroanal. Chem., 358, 351, 1993

265. J. A. Dean (ed.), Lange's Handbook of Chemistry, McGraw-Hill, New York, 13th edition, 1985

266. B. J. Bowles, Nature (London), 212, 1456, 1966

267. D. R. Lide (ed.), CRC Handbook of Physics and Chemistry, CRC Press, Inc., Florida, 73rd edition, 1992-1993

268. S. Szabo and F. Nagy, J. Electroanal. Chem., 87, 261, 1978

269. J. Clavilier, J. M. Feliu and A. Aldaz, J. Electroanal. Chem., 243, 419, 1988

270. X. Jiang, S. -C. Chang and M. J. Weaver, J. Chem. Soc., Faraday Trans., 89, 223, 1993

271. C. F. Baes and R. E. Mesmer, The Hydrolysis of Cations, R. E. Krieger, 1986

272. "Stability Constants of Metal-Ion Complexes"; The Chemical Society, London, 1964

273. A. Olin, Acta. Chem. Scand., 11, 1445, 1957

274. B. Lovrecek, M. Metikos-Hukovic and I. Mekajavic, "Encyclopedia of the Electrochemistry of the Elements", (A. J. Bard, ed.), Vol IX Part B, Marcel Dekker, p92-93, 1986

275. E. D. Moorhead and S. Lipscey, J. Electroanal. Chem., 26, 27, 1970

276. A. Kozawa, J. Electroanal. Chem., 8, 20, 1964

277. W. H. Morrison, J. Colloid Interface Sci., 100, 121, 1984

278. J. J. Yao, A. J. Appleby, A. Geisel, H. R. Cash and S. K. Wolfson, Nature, 224, 921, 1969

279. U. Gebhardt, G. Luft, G. J. Richter and F. von Sturm, Bioelectrochem. Bioenerg. 5, 607, 1978

280. J. Giner, L. Marincic, J. S. Soeldner and C. K. Colton, J. Electrochem. Soc., 128, 2105, 1981

281. L. Marincic, J. S. Soeldner, J. Giner and C. K. Colton, J. Electrochem. Soc., 126, 1687, 1979

282. L. Marincic, J. S. Soeldner, C. K. Colton, J. Giner and S. Morris, J. Electrochem. Soc., 126, 43, 1979

283. M. F. L. de Mele, H. A. Videla and A. J. Arvia, J. Electrochem. Soc., 129, 2207, 1982

284. L. A. Larew and D. C. Johnson, J. Electroanal. Chem., 262, 167, 1989

285. H. Lerner, J. Giner, J. S. Soeldner and C. K Colton, J. Electrochem. Soc., 126, 237, 1979

286. L. H. Essis Yei, B. Beden and C. Lamy, J. Electroanal. Chem., 246, 349, 1988

287. M. F. L. de Mele, H. A. Videla and A. J. Arvia, Bioelectrochem. Bioenerg., 9, 469, 1982

288. S. Enst, J. Heitbaum and C. H. Hamann, Ber. Bunsenges. Phys. Chem., 84, 50, 1980

289. M. L. B. Rao and R. F. Drake, J. Electrochem. Soc., 116, 334, 1969

290. Yu. B. Vassilyev, O. A. Khazova and N. N. Nikolaeva, J. Electroanal. Chem., 196, 127, 1985

291. Yu. B. Vassilyev, O. A. Khazova and N. N. Nikolaeva, J. Electroanal. Chem., 196, 105, 1985

292. E. Skou, Electrochim. Acta, 22, 313, 1977

293. A. E. Bolzan, T. Iwasita and W. Vielstich, J. Electrochem. Soc., 134, 3052, 1987

294. I. T. Bae, E. Yeager, X. Xing and C. C. Liu, J. Electroanal. Chem., 309, 131, 1991

295. K. D. Popovc, N. M. Markovic, A. V. Tripkovic and R. R. Adzic, J. Electroanal. Chem., 313, 181, 1991

296. M. F. L. de Mele, H. A. Videla and A. J. Arvia, Bioelectrochem. Bioenerg., 10, 239, 1983

297. S. Ernst, J. Heitbaum and C. H. Hamman, J. Electroanal. Chem., 100, 173, 1979

298. I. T. Bae, X. Xing, C. C. Liu and E. Yeager, J. Electroanal. Chem., 284, 335, 1990

299. G. Horanyi, J. Electroanal. Chem., 344, 335, 1993

300. M. Shao, X. Xing and C. C. Liu, Bioelectrochem. Bioenerg., 17, 59, 1987

301. M. Sakamoto and K. Takamura, Bioelectrochem. Bioenerg., 9, 571, 1982

302. N. Xonoglou and G. Kokkinidis, Bioelectrochem. Bioenerg., 12, 485, 1984

303. K. B. Kokoh, J. M. Leger, B. Beden and C. Lamy, Electrochim. Acta, 37, 1333, 1992

304. C. P. Wilde and T. Ding, J. Electroanal. Chem., 327, 279, 1992

305. E. P. Lieiva and M. C. Giordano, J. Electroanal. Chem., 158, 158, 1983

306. V. S. Bagotsky, Yu. B. Vassiliev and O. A. Khazova, J. Electroanal. Chem., 81, 229, 1977

307. G. R. Mundy, R. J. Potter, P. A. Christensen and A. Hamnett, J. Electroanal. Chem., 279, 257, 1990

308. D. S. Corrigan and M. J. Weaver, J. Electroanal. Chem., 241, 143, 1988

309. S. Chang, L. H. Leung and M. J. Weaver, J. Phys. Chem., 94, 6013, 1990

310. K. Chandrasekaran, J. C. Wass and J. O'M. Bockris, J. Electrochem. Soc., 137, 518, 1990

311. J. A. Caram and C. Gutierrez, J. Electroanal. Chem., 344, 313, 1993

312. J. A. Caram and C. Gutierrez, J. Electroanal. Chem., 323, 213, 1992

313. J. Willsau, O. Wolter and J. Heitbaum, J. Electroanal. Chem., 185, 163, 1985

314. B. Beden, M. -C. Morin, F. Hahn and C. Lamy, J. Electroanal. Chem., 229, 119, 1987

315. B. Beden, F.Hahn, S. Juanto, C. Lamy and J. M. Leger, J. Electroanal. Chem., 225, 215, 1987

316. T. Iwasita and F. C. Nart, J. Electroanal. Chem., 317, 291, 1991

317. M. R. Andrew, J. S. Drury, B. D. McNicol, C. Pinnington and R. T. Short, J. Appl. Electrochem., 6, 93, 1976

318. J. B. Goodenough, A. Hamnett, B. J. Kennedy, R. Manoharan and S. A. Weeks, J. Electroanal. Chem., 240, 133, 1988

319. A. Hamnett and B. J. Kennedy, Electrochim. Acta, 33, 1613, 1988

320. B. Beden, F. Kadirgan, C. Lamy and J. M. Leger, J. Electroanal. Chem., 127, 75, 1981

321. J. Clavilier, C. Lamy and J. M. Leger, J. Electroanal. Chem., 125, 249, 1981

322. M. M. P. Janssen and J. Moolhuysen, Electrochim. Acta, 21, 869, 1976

323. K. Ota, Y. Nakagawa and M. Takahashi, J. Electroanal. Chem., 179, 179, 1984

324. W. Vielstich, "Fuel Cells", Wiley, New York, 1970

325. A. Razaq and D. Pletcher, J. Electrochem. Soc., 131, 957, 1984

326. B. Beden, A. Bewick and C. Lamy, J. Electroanal. Chem., 148, 147, 1983

327. B. Beden, A. Bewick and C. Lamy, J. Electroanal. Chem., 150, 505, 1983

328. K. Kunimatsu and H. Kita, J. Electroanal. Chem., 218, 155, 1987

329. J. Clavilier, A. Fernandez-Vega, J. M. Feliu and A. Aldaz, J. Electroanal. Chem., 258, 89, 1989

330. A. Fernandez-Vega, J. M. Feliu, A. Aldaz and J. Clavilier, J. Electroanal. Chem., 258, 101, 1989

331. J. Clavilier, A. Fernandez-Vega, J. M. Feliu and A. Aldaz, J. Electroananl. Chem., 261, 113, 1989

332. S. Motoo and M. Watanabe, J. Electroanal. Chem., 69, 429, 1976

333. A. Castro Luna, T. Twasita and W. Vielstich, J. Electroanal. Chem., 196, 301, 1985

334. A. A. El-Shafei, H. M. Shabanah and M. N. H. Moussa, J. Electroanal. Chem., 362, 159, 1993

335. A. Fernandez-Vega, J. M. Feliu, A. Aldaz and J. Clavilier, J. Electroanal. Chem., 305, 229, 1991

336. S. A. Campbell and R. Parsons, J. Chem. Soc. Faraday Trans., 88, 833, 1992

337. B. E. Conway, Prog. Surf. Sci., 16, 113, 1984